UNIVERSITY OF READING

Department of Meteorology

Boundary Layer Ventilation and Moisture Transports

DAVID JOHN MCNAMARA

A thesis submitted for the degree of Doctor of Philosophy

[November 2015]

DECLARATION

I confirm that this is my own work and the use of all material from other sources has been properly and fully acknowledged.

David McNamara

ABSTRACT

The atmospheric boundary layer is the layer of air closest to the Earth's surface which is separated from the free troposphere by an inversion in the potential temperature profile. Moisture sourced from the Earth's surface has to penetrate this temperature inversion in order to be ventilated to the free troposphere. Moisture is important for the production of rain and the transfer of energy from the tropics to the poles. Here we explore the role of the atmospheric boundary layer in the transport of moisture and tracers.

This thesis presents for the first time a climatology of boundary layer mass ventilation. Areas of high boundary layer ventilation are found in the tropics, over the major mountain ranges and in the storm tracks. Storm track ventilation is investigated by looking at a case study of a mid latitude cyclone using the Eulerian boundary layer moisture budget equation and Lagrangian trajectories whose paths are perturbed stochastically in order to mimic the turbulent atmosphere. Turbulence within the boundary layer is found to be responsible for the widespread distribution of moisture within the warm conveyor belt. It is found that the majority of ventilation occurs due to unresolved turbulent process to the east of the cold front. Convection does not play an important role in this location.

Moist static energy transports are important for the climate. It is demonstrated that large poleward transports in moist static energy are accompanied by a large proportion of the available moisture. In order to investigate the moisture source regions, two climatologies were produced for events dominated by moisture transported from the tropics and moisture ventilated by the local boundary layer. It is shown that poleward moisture transports are limited and are thus critically supported by moisture which is ventilated from the local boundary layer. Representative climatological patterns in mean sea level pressure for each type of event are presented.

ACKNOWLEDGEMENTS

I would like to thank my supervisors; Bob Plant and Stephen Belcher for helping me to think through my ideas, being critical when it was necessary but also supportive when I have needed the support. In particular I am very grateful for any time that they have been able to spare over the last year. I would also like to thank my monitoring committee; Len Shaffrey, Helen Dacre and Daniel Kirshbaum for testing my knowledge over the course of the PhD and making me stop and think about things before diving straight into the work.

I would also like to acknowledge my fellow PhD students, past and present, who have provided me with the inspiration necessary to keep going during the tough periods over the last couple of years. In particular, special thanks go to Robert Warren who sat next to me for nearly four years and thus bore the brunt of my frustrations with boundary layer mass / moisture budgets. You have always been willing to share your time and for that I am grateful. I am also very grateful to Sian Lane who has given me the strength to continue my studies through my 5th year. Without your help I would have surely given up.

I would like to thank Andrew Allen and James Padfield for their support at the start of my PhD. I probably wouldn't have made it this far if you guys hadn't encouraged me. Thanks also to Sebastien Perceau Wells for popping into Reading every now and again in order to make sure that I ate.

Finally, I would like to thank my parents and family for their support over the last couple of years. I must also acknowledge Mia and Andy who have provided me (unknowingly) with a sense of perspective throughout my PhD studies.

David McNamara - November 2015

Contents

Chapter 1:
Introduction

1.1 Introduction

The atmospheric boundary layer is a very well studied feature of the Earth's atmosphere (e.g. Monin, 1970 and Carson, 1973) with many text books being devoted to the subject of how boundary layers form and the transports of material that take place within them (Stull, 1989 and Garratt, 1994). The interactions that take place between the boundary layer and the free atmosphere above it are extremely important in terms of defining the characteristics of the boundary layer (Sinclair *et al.*, 2009) and in defining the constituent make up of the free atmosphere above (Monin, 1970). Whilst many researchers have studied the interaction of the boundary layer with the free atmosphere in case studies (e.g. Henne *et al.*, 2004a and Alizadeh Choobari *et al.*, 2012) and idealised modelling studies (e.g. Sinclair *et al.*, 2009 and Boutle *et al.*, 2010), only a very limited number of studies have looked at these interactions on the climatological scale (e.g. Cotton *et al.*, 1995).

The ability of the boundary layer to determine both the amount of various materials and their spatial distribution in the free atmosphere above is of interest to researchers of a diverse set of issues including; the distribution of aerosols which can effect the Earth's climate (Akimoto, 2003), the distribution of latent heating within a mid latitude cyclone (Ahmadi-Givi *et al.*, 2004) due to the increase in the ventilation of moisture (Boutle *et al.*, 2010), the modification of Rossby waves in the atmosphere (Martinez-Alvarado *et al.*, 2015) and the amount of precipitation produced by extratropical cyclones (Eckhardt *et al.*, 2004). The ventilation of moisture from the boundary layer is also an important process to study when considering the poleward transport of energy (Oort, 1971), a transport process that can be split up into parts that are associated with the flow of sensible and latent heat.

The remainder of this chapter will focus on discussing the existing literature relevant to this

thesis, starting off with an introduction to the types of mixing processes within the boundary layer and a discussion of the role of large scale transports of energy in the atmosphere of which moisture is an important variable. Then a review of some of the literature concerning boundary layer ventilation will be undertaken in order to provide motivation for the work in chapter 2. Chapter 3 concerns the turbulent redistribution of moisture within the boundary layer and a section reviewing past literature relevant to this topic is presented in Section 1.4.2. This will be followed by a review of the current literature describing the redistribution of moisture on large scales in the atmosphere and how the boundary layer plays an important part. The specific aims of this thesis will then be described and some questions posed which this thesis will try to address.

1.2 The boundary layer

The atmospheric boundary layer is loosely defined by Stull (1989) as being "the layer of air in the lower troposphere that is directly affected, on timescales of 1 hour or less, by the forcing at its lower boundary, the Earth's surface". The boundary layer can be categorised into two separate types based upon the stability of the air within the boundary layer and the flux of heat into the boundary layer from the surface. In an unstable layer of air with a positive heat flux from the surface, the boundary layer is categorised as being convective. Whilst in stable air with a negative heat flux from the surface, the boundary layer is determined by wind shear. However, the formation of cloud within the boundary layer can complicate the mixing patterns seen within the boundary layer. Six different boundary layer types are shown in Figure 1.1. Each of these will now be explained in turn.

Figure 1.1a represents the dry convective boundary layer. Heating from the surface induces large turbulent eddies which mix the air up to the temperature inversion. Whilst the boundary layer is growing in the daytime some of these thermals will overshoot the boundary layer. These eddies will now be negatively buoyant and drop back down into the boundary layer bringing with them some warmer air which allows the boundary layer to grow. This process is known as encroachment (Carson, 1973).

A well mixed boundary layer that has formed a layer of stratocumulus on the top is represented in Figure 1.1b. Air at the top of the stratocumulus layer cools radiatively and as such becomes

negatively buoyant and sinks. This sinking air is replaced by air within the cloud in a form of reverse convection (Lock *et al.*, 2000). Figure 1.1c represents an unstable boundary layer that has been capped by cumulus cloud. Cumulus cloud forms as thermals rise in the mixed layer until a point is reached where moisture starts to condense. This point is known as the lifting condensation level and is marked LCL in 1.1c. Once moisture starts to condense out the air is heated by the release of latent heat, which causes air parcels to rise until they reach the capping inversion. A strong updraft is maintained within the centre of the cloud with strong subsidence occurring within about 600 m of the cloud edge (Chen *et al.*, 2012b).

The case when only a very weak temperature inversion exists above the well mixed layer and convection forms which is capable of mixing boundary layer air up to high altitudes within the troposphere is represented by Figure 1.1d. Air ascends the cloud in a step like motion being continually detrained and re-entrained through the edges of the cloud (Yin *et al.*, 2005).

Figure 1.1e represents the case when the boundary layer is stable near the surface. This causes the mixed layer to collapse and a stable layer to form near the surface. Above the stable layer, but below the inversion a residual layer remains until surface heating can reform the well mixed layer again. For strong stability the wind flows in laminar sheets until the shear forces cause intermittent bursts of turbulence that act to temporarily mix the air for a short time before the laminar flow reforms. The wind profile can, as in Figure 1.1e, form a low level jet at the top of the stable layer which can cause an increase in the shear stress experienced between the laminar layers and thus promote more frequent turbulent mixing (Thorpe and Guymer, 1977). Figure 1.1f shows the situation where a layer of stratocumulus is present over the stable boundary layer. As in Figure 1.1b this decoupled layer of stratocumulus promotes mixing within the top of the residual layer.

1.3 Large scale atmospheric circulation

The poleward transport of energy (F) as described by Oort (1971) is given by

$$F = F_{PE} + F_{SH} + F_{LH} + F_{KE} \tag{1.1}$$

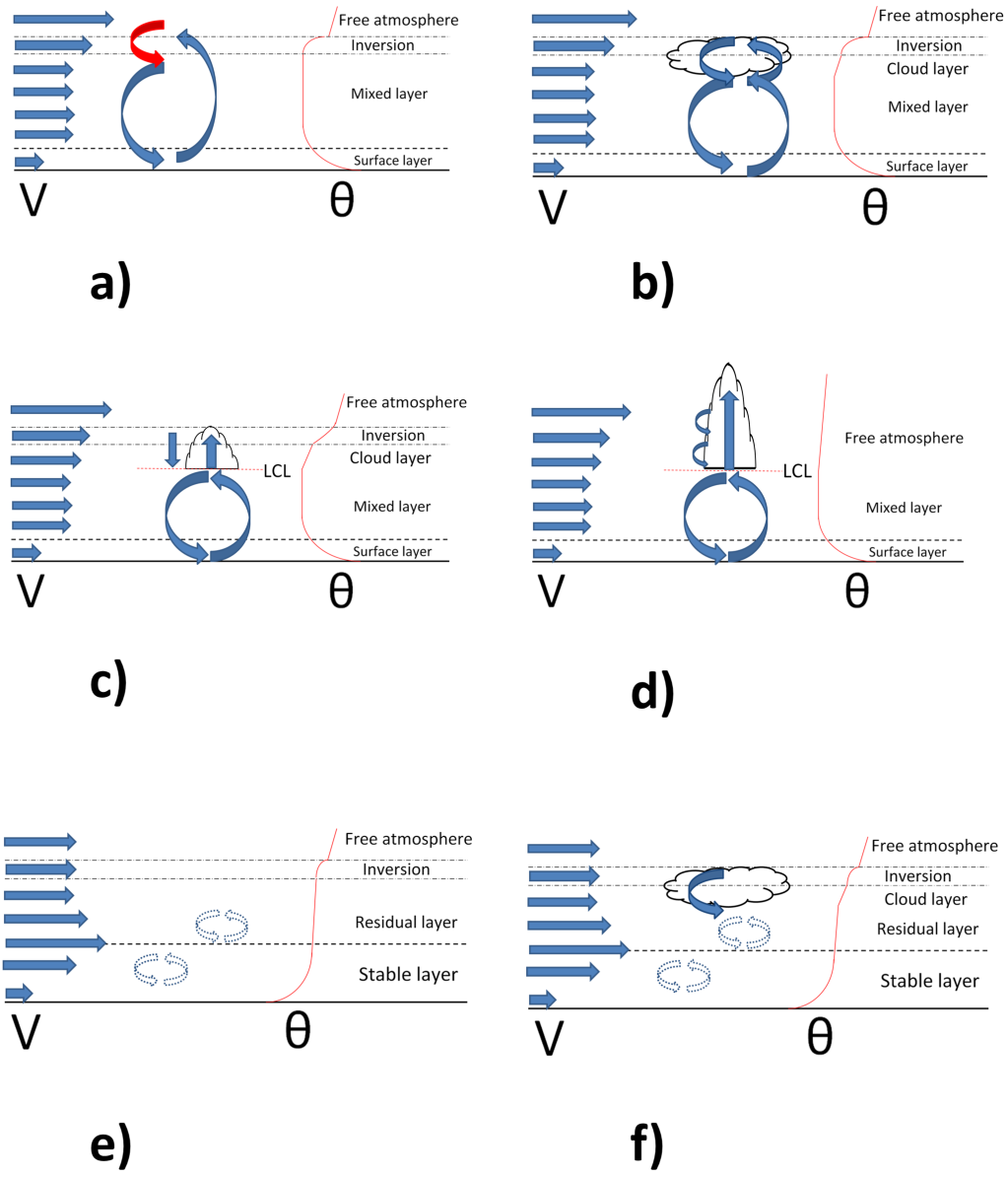

Figure 1.1: a) The dry convective boundary layer. b) Stratocumulus capped unstable boundary layer. c) Cumulus capped boundary layer. d) Mid/Deep convection capped boundary layer. e) Stable boundary layer. f) Stratocumulus capped stable boundary layer. The blue horizontal arrows represent the environmental wind and the red line represents the change in potential temperature with height. The red arrow represents warm air entrained from the free troposphere above. Blue curved arrows represent thermally driven turbulence whilst the dashed blue lines represent intermittent turbulence.

where each of the terms represent the flux of potential energy (F_{PE}), sensible heat (F_{SH}), latent heat (F_{LH}) and kinetic energy (F_{KE}) through a latitudinal band. The study demonstrated that the transports of potential energy, sensible heat and latent heat were the dominant factors and that these could be split up into three basics modes of transport. For example, the transport by latent heat can thus be described by

$$F_{LH} = F_M + F_S + F_T \tag{1.2}$$

where F_M is the transport by the mean circulation, F_S is the transport by the stationary eddies and F_T is the transport by the transient eddies. Each of these terms is now described.

1.3.1 The mean circulation

The mean circulation of the atmosphere has been demonstrated by Oort and Rasmusson (1970) and Trenberth *et al.* (2000) to consist of three circulations of air in each hemisphere. The strongest of these circulations is a thermally direct cell which rises in the tropics and descends in the sub tropics. This cell is commonly known as the Hadley cell. A weaker, thermally indirect, cell is incumbent in the middle latitudes which is named the Ferrell cell and a very weak thermal circulation resides in the polar regions known as the polar cell. The strength of these circulations are regulated by the changing of the seasons.

1.3.2 Stationary and transitory Rossby waves

The existence of upper level troughs in the atmosphere and their correlation to rainfall patterns (Wexler and Namias, 1938) were the motivation for the study by Rossby *et al.* (1939) who used means of isentropic charts (surfaces of constant entropy) in order to show that a series of semi permanent perturbations in the flow aloft were set up over the United States of America. In order to explain these perturbations Rossby introduced the idea of the β parameter as a means of simplifying the calculation of the change in Coriolis parameter ($f = 2\Omega sin\phi$, where Ω is the rotation rate of the earth and ϕ is the latitude) with latitude such that

$$\beta = \frac{2\Omega cos\phi}{r} \tag{1.3}$$

where r is the radius of the Earth. Using this concept Rossby introduced the analytically defined "trough formula" which relates the velocity of the waves (c) to the wavelength (L) and the gradient wind (U) such that

$$c = U - \frac{\beta L^2}{4\pi^2} \tag{1.4}$$

Equation 1.4 can be solved for stationary waves (i.e. $c = 0$) to give a length scale L_s which if exceeded allows waves to propagate westward whilst waves that are of shorter wavelengths propagate eastwards. In another study Rossby (1940) went on to address the conditions necessary for the stationary wave to remain in the atmosphere and the conditions under which the flow pattern starts to change. The paper is important, not least because he introduces the idea of potential vorticity, but also because he notes the importance of orography and the influence of surface temperature contrasts in the development of wave patterns in the upper troposphere. These wave patterns have been shown to exist in computer simulations by including orography (Grose and Hoskins, 1979) and sources of thermal forcing (Hoskins and Karoly, 1981).

The ways in which low frequency Rossby waves are controlled is a current area of research (see Domeisen and Plumb, 2012 and Grazzini and Vitart, 2015). However, the implications of variability exhibited by these waves are much better known. One of the most prominent indicators is the NAO which is determined by the difference in pressure between the regions of the Azores and Iceland (Pinto and Raible, 2012). A schematic illustrating the effect of the NAO on wind and pressure patterns in the Atlantic is given in Figure 1.2. The phase of the NAO is known to be instrumental in determining the position of the storm track and thus the amount of rain that is received at any particular location. The NAO acts on timescales that range from days to centuries (Pinto and Raible, 2012). In particular the positive NAO conditions have been linked to the occurrence of extreme cyclones (Pinto *et al.*, 2008) and have been shown to be linked to a similar pattern in the Pacific ocean called the PNA (see Croci-Maspoli *et al.*, 2007 and Pinto *et al.*, 2011).

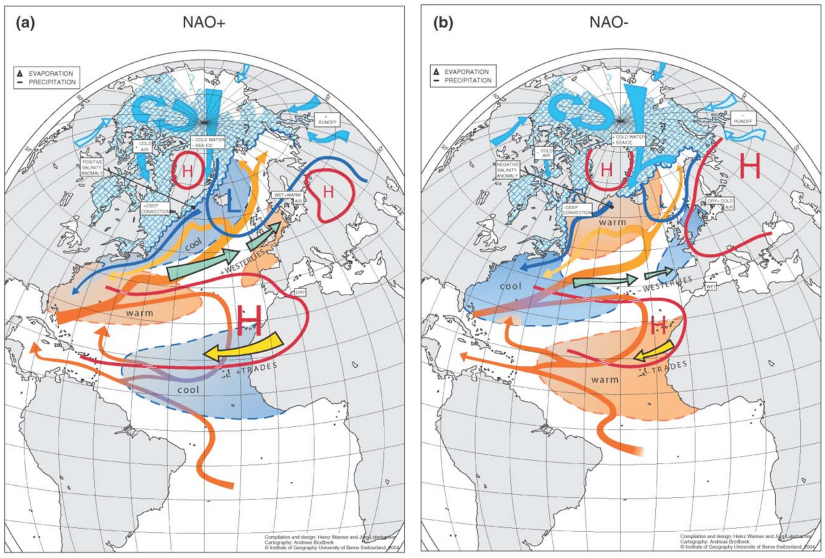

Figure 1.2: The positive (a) and negative phases of the NAO. The arrows represent flows in the oceans, atmosphere and rivers. Shaded areas represent sea surface temperatures when surrounded by dashed lines and sea ice extent when cross hatched. Climatic processes are described within boxes whilst the mean sea level pressure anomalies are indicated by red (H, high) and blue (L, low) contours. From Wanner *et al.* (2001).

1.3.3 High frequency transients and baroclinic instability

The process of baroclinic instability may be initiated by a perturbation in the upper level contours of geopotential height. Geopotential height (Z) is defined to be

$$Z = \frac{\int_0^h g(\phi, z)dz}{g_0} \tag{1.5}$$

where g_0 is the gravitational acceleration at the surface and $g(\phi, z)$ is the gravitational acceleration determined by the height (z) and latitude (ϕ). The perturbation in geopotential height in the form of a trough on an isentropic surface from the north is accompanied by the advection of high values of positive potential vorticity see (Figure 5.5 in Hoskins, 1990). Ertel potential vorticity is defined to be

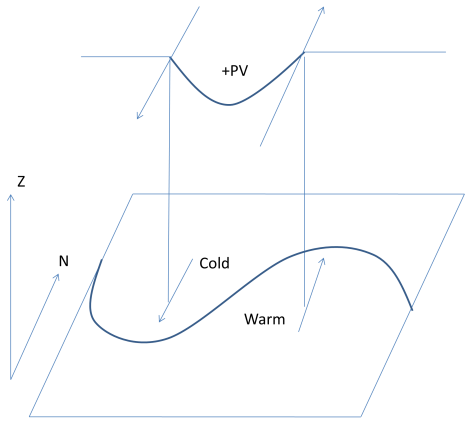

Figure 1.3: Schematic showing the influence of an upper level positive potential vorticity (+PV) anomaly on the low level temperature field. The diagram is orientated in the north (N) south direction and indicates the difference in height (Z). Arrows indicate the direction of the wind. Adapted from Sinclair (2008).

$$PV = \frac{1}{\rho}\zeta.\nabla\theta \tag{1.6}$$

where θ is the potential temperature, ζ is the absolute vorticity and ρ is the density of the air. An example of this occurring would be in a trough associated with a Rossby wave. The rotation of the air around the anomalous values of PV in the upper atmosphere is counter clockwise and thus causes the air below it to rotate in the same direction. This in turn causes a wave like structure to develop in the field of potential temperature at the surface. This situation is depicted in Figure 1.3. The developing thermal wave near to the surface transports heat from regions to the south into the northern latitudes and also has an influence on the perturbation in geopotential height aloft. Thus the two anomalies act to reinforce each other. This reinforcement of the upper and lower anomalies is the process known as baroclinic instability and the developing wave is known as a baroclinic wave.

Baroclinic instability is represented analytically by the Eady (Eady, 1949) and Charney (Charney, 1947) models. A good description of the Eady model is given by Gill (1982) and Vallis (2006). A summary of the Eady model, which is less mathematically complex than the Charney model is presented in Section 1.3.3.1.

1.3.3.1 The Eady model

Baroclinic instability can be represented analytically by the Eady model (Eady, 1949). The model describes a zonal flow between two rigid surfaces. It simplifies the analysis of the problem by assuming that all motion occurs on a plane (f-plane) tangential to the model's central point. The Coriolis parameter is assumed to be fixed and as such does not vary with latitude. It is assumed that the atmosphere is uniformly stratified and that a linear gradient exists in the zonal wind profile, starting at the lower surface where the wind speed is zero up to the upper surface where it is given a positive value. It is assumed that the mean flow in the meridional direction is zero. A temperature gradient is included with warmer air to the south of the domain and colder air to the north. The change in temperature is assumed to be smooth, so that the change in buoyancy in the meridional direction is constant. Baroclinic instability is shown occur spontaneously given these conditions, as discussed further in Appendix C.

Solutions to the Eady model reveal that for the most unstable wave the growth rate is given by

$$\sigma = 0.31 \frac{1}{fN} \frac{\partial U}{\partial z} \tag{1.7}$$

which demonstrates that the growth rate of the wave is directly proportional to the gradient in horizontal wind speeds ($\frac{\partial U}{\partial z}$) and inversely proportional to the static stability (N). The static stability is defined to be

$$N = \left[\frac{g}{\bar{\theta}} \left(\frac{\partial \bar{\theta}}{\partial z} \right) \right]^{1/2} \tag{1.8}$$

and thus altering the profile of $\frac{\partial \bar{\theta}}{\partial z}$ will have an impact on any developing waves. Since the gradient in horizontal wind is directly proportional to the meridional temperature gradient, the growth rate is also known to be a function of the meridional temperature gradient.

1.3.4 Conceptual models describing cyclogenesis and the airflows within mid latitude cyclones

Mid latitude cyclones, their corresponding patterns of precipitation and cloud and the processes by which they form (cyclogenesis) have been studied for a long time (e.g. Bjerknes (1919)). In order to visualise the structure of a mid-latitude cyclone conceptual models have been developed for the movement of air throughout each stage of development.

1.3.4.1 The Norwegian model

The Norwegian model was developed within the Bergen school of Meteorology in Norway during the early part of the twentieth century (see Bjerknes and Solberg, 1922). The model uses as its basis the concept of an air mass. An air mass can be described as a large body of air which exhibits homogeneous properties of both temperature and moisture. The meeting of two air masses of dissimilar properties occurs at what is commonly known as a front, a name borrowed from the time of the first world war in an attempt to conjure up the meeting of two great armies as a visual metaphor for the orientation of the two air masses. In the atmosphere, such a discontinuity occurs at the boundary between the polar regions to the north and the air which normally resides in the extratropics. Typically air to the north has the properties of being relatively cold and of low moisture content, whilst air that resides within the extratropics is relatively moist and warm. Air masses to the south of this boundary are classified as being either tropical maritime or continental maritime, whilst air masses to the north are termed polar maritime, polar continental or arctic maritime in order to distinguish the place of origin.

The Norwegian cyclone model assumes that an initial perturbation in the zonal flow will induce cyclogenesis. A pictorial depiction of a cyclone developing in the Norwegian model is illustrated in Figure 1.4a. In the Norwegian model the individual air masses are assumed to be static but the fronts move at differing speeds with the cold front moving faster than the warm front. The occlusion is therefore formed as the tropical maritime is lifted up over the occluded front in a region where the cold and warm fronts meet. A cross section depicting the relative positions of each air mass is shown in Figure 1.4b in the occluded front. The location of this cross section is given in Figure 1.4a.

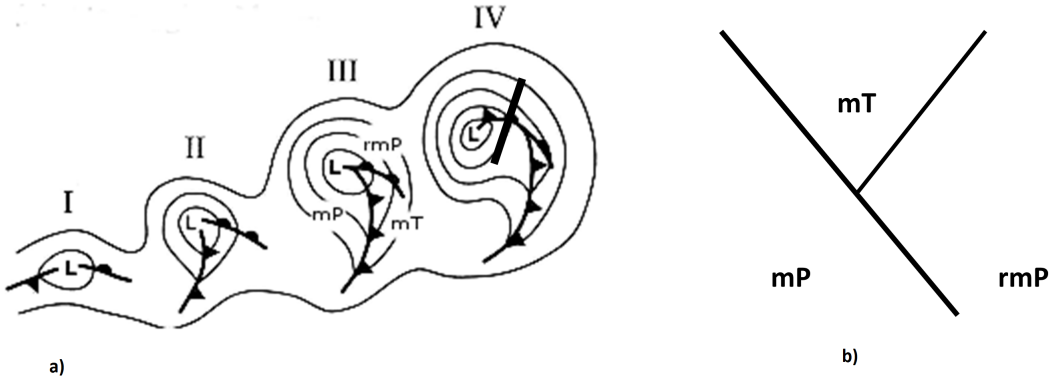

Figure 1.4: a) The lifecycle of a mid latitude cyclone (I-IV) according to the Norwegian model. Air masses are labelled Polar maritime (mP), Tropical maritime (mT) and Returning polar maritime (rmP). Standard meteorological symbols are used for isobars, the warm front, the cold front and the occlusion. The low pressure centre is indicated by an L. The location of the cross section depicted in b is marked by a strong black line cutting through the occlusion in stage IV. b) A cross section through stage IV of the occlusion indicating the relative locations of each air mass. Adapted from Schultz *et al.* (1998)

1.3.4.2 The conveyor belt model

The conveyor belt model of mid latitude cyclones was developed as a pictorial representation of the air flows around the low pressure centre. These pictures were obtained by subtracting the translational speed of the moving cyclone from its wind fields in order to reveal the system relative wind flow within the cyclone. A graphical representation of these wind patterns is given in Figure 1.5. The warm conveyor belt starts off within the boundary layer and ascends up on an isentropic surface over the warm front. In the conceptual model described by Carlson (1980) the flow then turns anticyclonically and merges with the westerly flow of air associated with the jet stream. This corresponds to the situation depicted in Figure 1.5a which shows the flow of two branches of the warm conveyor belt flowing in the same direction but with the second branch (W2) on a slightly lower isentropic surface to the upper branch (W1). In the work of Martínez-Alvarado *et al.* (2014) the warm conveyor belt is shown to have a branch that ascends up and over the warm front, turning cyclonically and a branch that, after partially ascending turns anticyclonically around the low centre. This second situation is depicted in Figure 1.5b.

The second type of air flow shown in Figure 1.5a is known as the cold conveyor belt (Schultz,

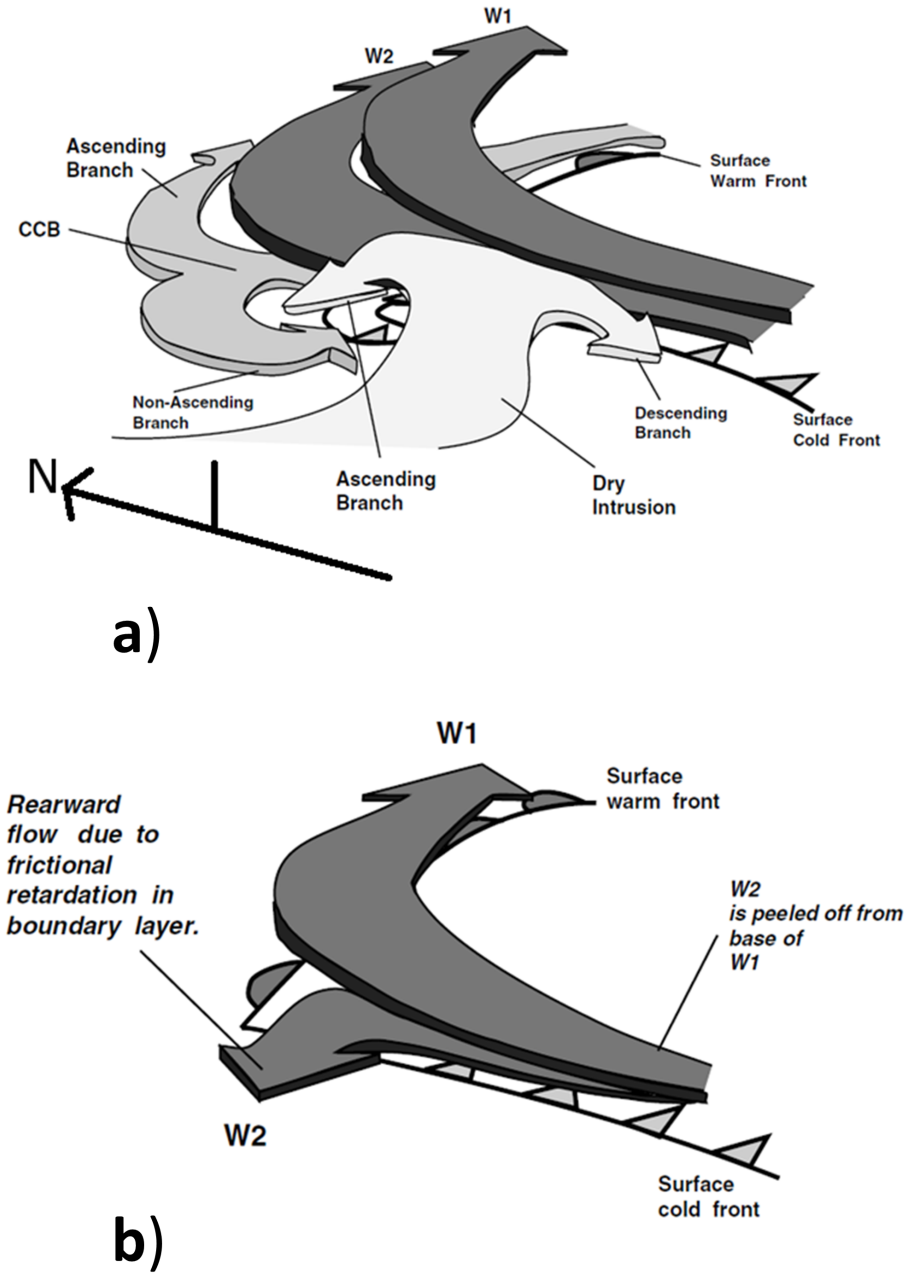

Figure 1.5: The air flow through a mid latitude cyclone describing two different possible flows associated with the warm conveyor belt (w1, w2), the cold conveyor belt (CCB) and the dry intrusion relative to the surface frontal locations. The two depictions represent two different times in the cyclones lifecycle, Figure a being earlier than Figure b. The orientation of both Figures is given by the directional arrow in Figure b which is pointing north (N). Adapted from Semple (2003)

2001). Air within this flow originates poleward of the warm front (i.e. within the airmass designated as returning polar maritime in the Norwegian model of cyclogenesis). This air stream flows from east to west around the warm front and then turns either anticyclonically (Carlson, 1980) or cyclonically (Schultz, 2001) as described in Figure 1.5a.

The dry intrusion originates from the upper troposphere (Carlson, 1980) or from within the stratosphere (Cooper *et al.*, 1998) and descends down upon an isentropic surface to within middle or low levels behind the cold front. The descent of this air allows it to warm adiabatically and causes air parcels to have a very low relative humidity. This region of air can be detected in water vapour imagery as a dry slot close to the low pressure centre of the cyclone (Browning, 1997).

1.3.4.3 The Shapiro-Keyser model

Given the view that cyclones consisted of large masses of air that were moving relative to each other, a new model of cyclone development was devised which suggested that the branch of the warm conveyor belt labelled W2 in Figure 1.5b fractured the cold front and moved air from the warm conveyor belt into the region of air between the occluded front and the cold front. This new model of cyclone development is known as the Shapiro-Keyser cyclone model. Shapiro and Keyser (1990) developed the model in order to explain observations of cyclone development which did not conform to the classical Norwegian model of cyclone development. Unlike the time at which the Norwegian model was developed, numerical simulations of cyclones were now available which the researchers utilised in order to construct the new conceptual picture of cyclone development. The model is described in Figure 1.6.

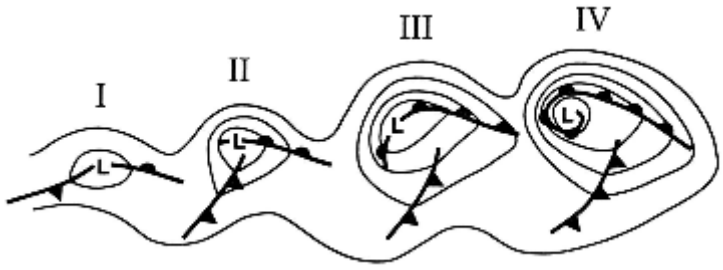

Figure 1.6: The lifecycle of a mid latitude cyclone (I-IV) according to the Shapiro Keyser model of cyclogenesis. Adapted from Schultz *et al.* (1998)

In stages I and II the lifecycle is very similar to that of the Norwegian model depicted in Figure 1.4a, although the angle of the cold front to the warm front is no longer oblique but perpendicular. By stage III the process of frontal fracture has begun with a definite area of separation of the two fronts. The orientation of the fronts can now be described as a T-bone structure with the air between the warm front and the rear of the cold front having an unusually large moisture content (if compared with the standard Norwegian model). The later stages of cyclone development are depicted in stage IV with the occlusion wrapping around the centre of the cyclone and thus encircling the seclusion within the centre of the cyclone.

1.3.5 Transport by transient eddies

Although this thesis is primarily concerned with the transport of moisture and the role that the boundary layer plays in this transport it should be stressed that moisture is an important part of the global atmospheric energy cycle (see Equation 1.1). The role that transient eddies have in transporting energy from the tropics to the polar regions was investigated in a recent study by Messori and Czaja (2013). They found that a large proportion of the moist static energy, approximately 57 - 60%, (Equation 1.1 - F_{KE}) was transported by the top 10% of events. This agreed with and extended the work previously done by Swanson and Pierrehumbert (1997) who found a similar result by looking at three locations in the Pacific ocean.

1.4 Previous research attempts

1.4.1 Boundary layer ventilation

1.4.1.1 Introduction

The boundary layer is an important interface between the Earth's surface and the free troposphere above (Monks *et al.*, 2009). The ability of the boundary layer to ventilate pollutants, moisture and air on a range of scales can be described in terms of the mechanisms by which this ventilation occurs. There is a broad range of literature which discusses the transport of material out of the boundary layer and into the free troposphere however, relatively little attention has been paid to

the concept of mass. The following section reviews some of this material and in some cases uses variables such as moisture in order to track the movement of air. The movement of moisture has been suggested to be a good proxy with which to track air parcels (Siebesma *et al.*, 2003).

1.4.1.2 Ventilation by synoptic scale systems

Advection of material out of the boundary layer by synoptic scale systems is a major contributor to the overall rate at which the boundary layer is ventilated (Monks *et al.*, 2009). In the study by Cotton *et al.* (1995) the overall contribution to ventilation by individual systems was estimated from results of numerical weather prediction models and then scaled up by the number of occurrences of each system per year. It was estimated that mid-latitude cyclones were the number one ventilator of material out of the boundary layer followed by Mesoscale convective systems, Ordinary thunderstorms, Tropical cyclones and Mesoscale convective complexes. The study assumed a fixed boundary layer height of 900 hPa in all systems.

The removal of trace gasses from the planetary boundary layer by the warm conveyor belt within a mid latitude cyclone was demonstrated in Grant *et al.* (2000) who from the analysis of air samples obtained during the Subsonic Assessment, Ozone and Nitrogen Oxide Experiment (SONEX) experiment determined that regions of low ozone concentration were present in the upper troposphere. These regions were subsequently traced back using back trajectories for 10 days which showed the source region of the air mass to be within the tropical marine boundary layer and that they had come into contact with the ITCZ. However, analysis of satellite derived water vapour imagery overlayed with numerical weather prediction fields indicated that the trajectories coincided with the location of a warm conveyor belt (Harrold, 1973 and Carlson, 1980).

Several other studies have also associated the atmospheric properties of the warm conveyor belt with those of the source region within the boundary layer (e.g.Stohl, 2001, Hess and Vukicevic, 2003 and Brown-Steiner and Hess, 2011). Cooper *et al.* (2002) constructed a conceptual model describing the transport of trace gasses within the air streams of a mid latitude cyclone. This was achieved by taking air samples from different altitudes within each of the major airstreams belonging to 8 mid latitude cyclones, during 11 flights, and analysing them for their chemical composition. The study showed that ozone was increased within the flow of a warm

conveyor belt. These increased ozone concentrations were attributed to the fact that the warm conveyor belts originated within the continental boundary as opposed to those which were analysed by Grant *et al.* (2000) and originated in the marine boundary layer.

The importance of mid latitude cyclones in ventilating the boundary layer was confirmed in a study by Hess (2005) who used a global chemical transport model in order to separate out regimes which were dominated by convective transport from those dominated by large scale advection. The chemical transport model was driven by NCEP/NCAR reanalysis data fields. Boundary layer and convective transports were parameterised (see Hess, 2005 for details). The conclusions to this study were that both convective and non convective transport regimes were important for the transport of material out of the boundary layer but that seasonal cycles exist which determine the importance of each of these two regimes. Many other studies have investigated the ventilation of the boundary layer by the warm conveyor belt in detail e.g. Donnell *et al.* (2001), Agustí-Panareda *et al.* (2005), Sinclair *et al.* (2008) and Boutle *et al.* (2010). Each of these studies will be reviewed in detail in Section 1.4.2.4.

The conditions under which boundary layer ventilation is increased were investigated in the study by Sinclair *et al.* (2010). Sinclair *et al.* (2010) simulated some idealised dry baroclinic waves using the Met Offices Unified Model. Simulations were started by adding a small temperature perturbation to a north south temperature gradient within a zonal flow field. Sensitivity studies were then performed, first by altering the drag co-efficient in order to investigate how different boundary layer regimes might affect the results and secondly by altering the speed of the jet stream in order change the amount of vertical wind shear. The results showed that the rate of boundary layer ventilation was controlled by the jet stream. This dependance on the jet stream suggests that a climatology of boundary layer ventilation should produce a region of ventilation that is coincident with the position of the storm tracks.

1.4.1.3 Convective ventilation

The ability of convection to ventilate the boundary layer is due to the fact that when air is raised cloud condensate forms just above the lifting condensation level and an associated release of latent heat occurs. This heat warms the surrounding air parcels and transports air across the inversion

which separates the convective boundary layer from the free troposphere. In order to demonstrate this fact, several studies demonstrating the ability of convection to ventilate the boundary layer will now be reviewed.

Flossmann and Wobrock (1996) used a two dimensional model which included the micro-physical representation of clouds in order to investigate the redistribution of a tracer from the boundary layer into the free troposphere. The model was set up in order to mimic the conditions found within the tropics (9°N 23°W) on the 18th September 1984. Southerly winds prevailed below 2 km and above 6km whilst northerly winds prevailed in the levels between. The model was run and a convective cloud aloud to form with a maximum depth of 2.4 km. The largest flux of mass was found to be through the cloud base at 35 minutes into the simulation. Only small amounts of mass were transported through the cloud top and the horizontal cloud boundaries. The mass of tracer was found to be reduced within the boundary layer and increased within the region of cloud. Similar studies have confirmed the ability of convective cloud to ventilate large amounts of tracer from the boundary layer (e.g. Flossmann, 1998, Mari *et al.*, 2000, Yin *et al.*, 2001, Yin *et al.*, 2005 and Barthe *et al.*, 2011). It has further been shown that transport of tracer from the boundary layer and into the upper troposphere has been shown to take place via an indirect route (Mari *et al.*, 2000 and Yin *et al.*, 2005), whereby it is detrained from the middle of the cloud before being re-entrained and subsequently transported to the cloud top.

The ventilation of the boundary layer by shallow cumulus cloud has been investigated by Chen *et al.* (2012b). Chen *et al.* (2012b) used a large eddy simulation model in order to represent the cloud layer, the mixed layer below and an inversion which capped the cloud layer. Two experiments were performed, one with tracer initialised near to the surface and one with tracer initialised within the atmospheric inversion. The purpose of this experiment was to investigate the occurrence of cumulus induced downdraughts close to the cloud edges and asses the ability of the cloud to transport material across the capping inversion. The experiments showed that over a period of 24 hours tracer that was released from the surface mixed throughout the atmospheric column whilst tracer that was released within the inversion layer mixed throughout the cloud layer with a smaller amount mixing down to the sub cloud layer. The strongest downward transport of tracer was found to occur within 600 m of the cloud centre and just below the top of the cloud whilst no tracer was found to penetrate the overlying capping inversion. The impenetrability

of the capping inversion has previously been suggested by Cotton *et al.* (1995) and agrees with figures found in Stull (1989) and the results of Siebesma *et al.* (2003) who compared the results of 10 different LES experiments run by different research groups in order to show that the upward flux of moisture tends to zero near to the height of the capping inversion.

On larger scales ventilation of the atmospheric boundary layer by convection has also been shown to be a significant mechanism for the removal of pollutants. Hov and Flatøy (1997) investigated the transport and production of ozone out of the continental boundary layer during two ten day periods in the summer and autumn of 1994. The study was conducted using the combination of a chemistry transport model coupled with a numerical weather prediction model. The study used a rather simplistic definition of the boundary layer which it defined as being the three lowest model layers which gave a height of approximately 1250 m above the Earths surface. It's conclusions were that convection dominates the removal of pollutants during the summer months whilst in the autumnal season the synoptic scale vertical advection was the dominant mechanism. Other studies using improved representation of the boundary layer have also concluded that convection is an important process in removing pollutants from the boundary layer on the large scale (e.g. Hess, 2005 and Li *et al.*, 2005). In particular convection has been shown to been shown to be important during the summer months (Hess, 2005).

Observational studies have also found evidence for the ventilation of the boundary layer by convection. Dickerson *et al.* (1987) used aircraft measurements of the chemical composition of the atmosphere between the surface and 10 km. Using the fact that CO generally decreases in concentration as you ascend in the atmosphere, flights measured the atmospheric profile of CO both outside and within a cumulonimbus cloud. The presence of increased CO within the cloud suggested that the gas had been brought up from the boundary layer. Other chemical signatures within the cloud supported the hypothesis that large convective clouds could transport boundary layer air into the upper troposphere. Similar observational studies have been carried out more recently and have each reached similar conclusions (e.g. Huntrieser *et al.*, 2002, Bertram *et al.*, 2007 and Huntrieser *et al.*, 2011) thus validating the results obtained from numerical modelling experiments.

Both convection and the warm conveyor belt are capable of ventilating the boundary layer and lofting pollutants to high levels. However, ventilation can also be achieved by processes

that remove materials from the boundary layer to shallower regions of the atmosphere where the ambient winds are not as strong and as such confine such pollutants to thin layers, their vertical motion inhibited by the stratified nature of the free troposphere (Schneider, 2004). Some of these known processes will know be reviewed.

1.4.1.4 Orographic ventilation and entrainment

The study of Lu and Turco (1994) investigated the production of elevated layers of pollution which occur within the vicinity of the coast and in the presence of orographic features. The study was motivated by several previous studies which hypothesised the production of these layers to be due to the formation of convergence zones in concurrence with sea breezes which, due to their influence on vertical motion, act to lift pollutants up into the region of the overlying temperature inversion by means of:

- The removal of pollutants by air parcels which are heated by the slopes of a mountain.
- The horizontal advection of pollutants away from the mountain and into the temperature inversion.
- The lifting of air parcels by an inland propagating sea breeze front and a combination of topographic forcing along with the action of convective mixing

(see references in Lu and Turco, 1994). In order to investigate the dynamical mechanisms by which elevated pollution layers occur, Lu and Turco (1994) used a two dimensional numerical weather prediction model in order to isolate the individual effects. Four model configurations were chosen in order to represent; the effect of a sea / land breeze in the presence of flat terrain, the effect of orography on its own, and both the presence of orography (situated inland and near to the coast) with the formation of a sea breeze. The study concluded that pollutants formed discreet layers in the atmosphere by:

- The formation of a sea breeze which undercuts the polluted air inland and thus lifts it up into the overlying inversion.

- The inland propagation of marine air which allows the displacement of air near the elevated slopes of a mountain into the surface inversion.
- The combination of anabatically forced winds with a sea breeze which subsequently allow air to be advected into the inversion.
- The venting of pollutants above the top of a mountain range due to the convergence of anabatic flows which force pollutants through the overlying temperature inversion.

The increase in temperature required to overcome the stratification of the atmosphere in the region of the temperature inversion was attributed to the diabatic heating (mountain chimney effect) of the air by the surface. In a follow up study Lu and Turco (1995) used a fully three dimensional numerical weather prediction model of the Los Angeles basin in order to show that the results of the idealised simulations were robust to a more complicated terrain environment.

The role of mountainous topography in isolation has also been studied in relation to its role in controlling exports of mass through the boundary layer top. In the study of Kossmann *et al.* (2000) it was shown by the use of lidar measurements that katabatic winds were present within the boundary layer over glacial regions in the European Alps. These katabatic winds had the effect of sucking down air from the free troposphere into the boundary layer . Although, it was also noted that analysis of surface station data indicated that this was not a common occurrence.

The use of the term ”topographic venting” in order to describe the sole effects of orography on the venting of the boundary layer was first coined by Henne *et al.* (2004b) in order to describe the influence of orography as an independent exporter of mass. The study aimed to quantify the amount of ventilation taking place over a region of the European Alps in order to document the process so that suitable parameterisations could be developed for mountainous regions in numerical models. The study constructed box models around alpine valleys taking into account the flow into and out of the valley and the changing valley wind speeds in order to calculate a net residual vertical flux of mass out of the top of the valley (Any valley subsidence was assumed to be close to zero). The wind measurements were taken from surface observations and data retrieved from the flight of a meteorological observation aircraft. lidars were used in order to understand the 2D structure and aerosol layers present in transects cut through each valley. Using these methods it was determined that the up-slope winds were the most important mechanism for exporting air

from the valley into the free troposphere. The study did not however, try to resolve the boundary layer height due to a lack of suitable data and as such could only provide a description of the large scale flows of air in relation to the large scale topography.

A study which did explicitly take into account the height of the boundary layer was that of De Wekker *et al.* (2004) who used aircraft lidar measurements of aerosols in conjunction with a numerical weather prediction model in order to describe the mechanisms by which air was released from the boundary layer. The boundary layer was represented by a bulk Richardson number method and distinguished from a layer above termed the aerosol layer which formed due to the venting of boundary layer air from below. The conceptual model consisted of three independent mechanisms by which air was removed from the convective boundary layer during day time. These included:

- Mountain venting; which involves air being heated up on the slopes of mountains and continues to rise up out of the boundary layer after it reaches the mountain top. This is the same mechanism described by Lu and Turco (1994) and represents the mountain chimney effect.
- Cloud venting; which involves the formation of (convective) cloud within the boundary layer which transports air parcels above the boundary layer by the addition of heat through the process of latent heating. (note that cloud venting does not have to have mountainous terrain present in order for it to occur.)
- Advective venting; which involves air parcels being advected horizontally through the boundary layer which has been warmed by the surface into the cooler air (potential temperature) of the surrounding free troposphere.

A conceptual diagram describing the mechanisms of boundary layer ventilation in the region of orography as described by De Wekker *et al.* (2004) is presented in Figure 1.7.

The study also noted that if the models were re-run and the mountainous terrain was taken away that the aerosol layer was co-incident with the boundary layer as described by the Richardson number method. This led the study to conclude that the height of the aerosol layer over mountainous terrain was distinct from the boundary layer height and was more representative of

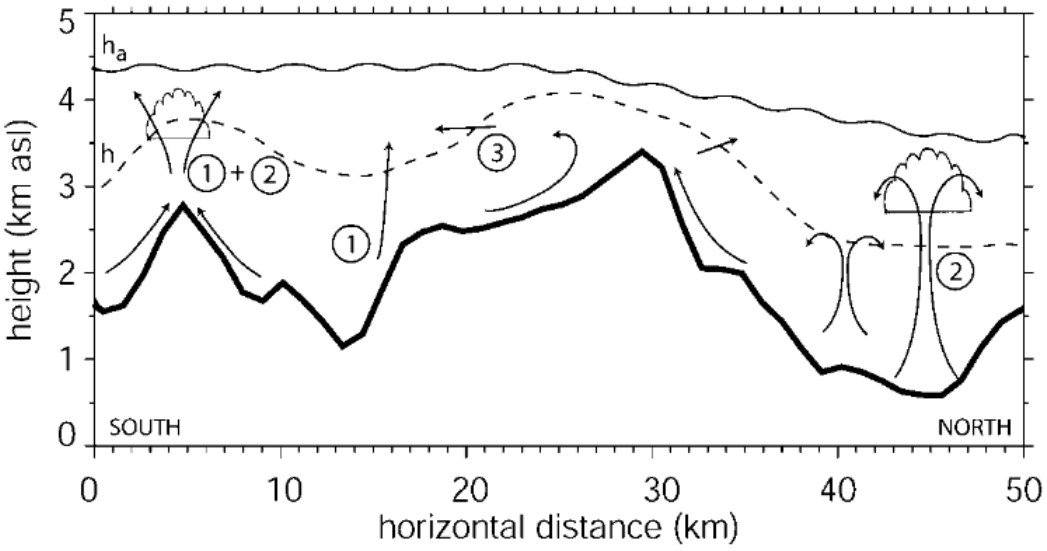

Figure 1.7: A conceptual diagram describing the ventilation mechanisms of the atmospheric boundary layer in the presence of topography. h represent the boundary layer height (as derived by the bulk Richardson number), $h_a$represents a layer of aerosols that has formed above the boundary layer. The mountain range is depicted by the thick solid black line and airflows are represented by arrows. The diagram shows ventilation due to the processes of 1) Mountain chimney effect, 2) Cloud ventilation, 3) Advective ventilation. Adapted from De Wekker *et al.* (2004).

the ”mixing height”.

The role of orography in removing pollutants is now an established area of research with studies devoted to each of the individual mechanisms described above (e.g. Chen *et al.*, 2009, Langford *et al.*, 2010 and Kirshbaum and Wang, 2014). In addition the important role that topographic elevations have in exporting moisture into the free troposphere from the boundary layer is also recognised (Weigel *et al.*, 2007).

1.4.1.5 Coastal ventilation

Ventilation of the boundary layer in the region of the coast line has been shown, due to the disparity in height of the boundary layer over the sea and land surfaces, to contribute significant amounts of ventilation (Dacre *et al.*, 2007). The study by Dacre *et al.* (2007) used the Met Offices Unified Model (UM) in order to simulate boundary layer ventilation of passive tracers during a

period where convection was being stymied by an area of high pressure that was moving in from the west. The study showed a region of boundary layer ventilation over the coast of southern England and Ireland and studied the effects of advection, turbulent mixing and convection on the rate at which tracer was being exported from the boundary layer. Cross sections were produced which cut perpendicularly through the southern coast line and the changes in boundary layer height across the coast line were described. The study demonstrated that due to higher boundary layer heights over the land than the sea horizontal advection through the boundary layer top in the vicinity of the coast could occur and be enhanced by the presence of a sea breeze front. A pictorial representation of this process is given in Figure 1.8. The study further showed that ventilation could be greatly enhanced by the additional mechanisms of turbulent mixing and convection. Similar instances of pollutants being removed from the boundary layer have also been documented in the literature (e.g. Loughner *et al.*, 2011,Davis *et al.*, 2012 and Loughner *et al.*, 2014).

In order to try and extend the results of Dacre *et al.* (2007) to a much wider area, Peake *et al.* (2014) used a box model which was set up as a series of six boxes, three over land and three over the sea. The intersections between the three boxes in the vertical represented the height of the boundary layer and the height of the residual layer above. The region studied was over the eastern coast of continental North America. The meteorological conditions were supplied by an NWP model over the course of a 4 week period in the summer of 2004. The study derived analytical equations in order to describe the rate of change in tracer mass in each of the boxes. By altering the size of the land boxes it was shown that using larger boxes allowed a better representation of the variability in tracer concentration on the synoptic scale whilst smaller boxes over land better showed the diurnal variation in tracer concentrations. The study concluded that coastal outflow was as important to boundary layer ventilation as large scale advection and convection.

1.4.1.6 Outstanding issues in the literature

The only global estimates of boundary layer ventilation are the original review paper by Cotton *et al.* (1995) and the two dimensional analysis performed by Hess (2005). No study so far has produced a full three dimensional representation of the boundary layer ventilation and entrainment rate. The production of such a map would be useful to researchers in order that future research into

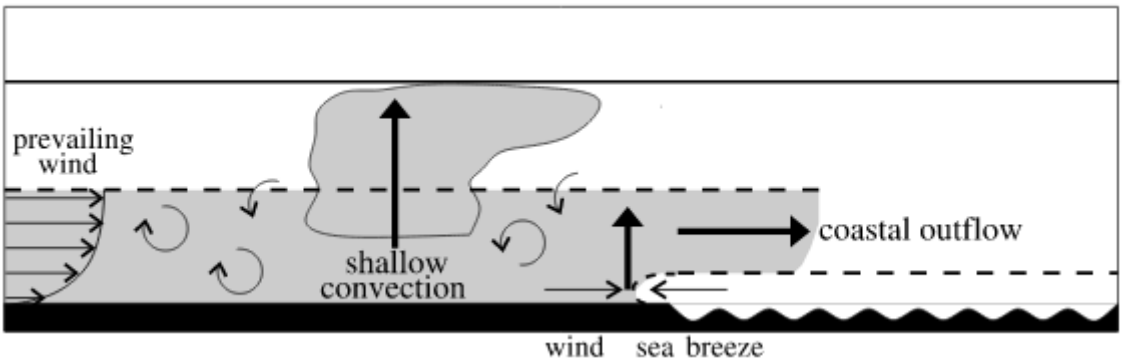

Figure 1.8: The ventilation of the boundary layer in the region of a coast line. Large arrows show the large scale transport of air-masses whilst the small curly arrows represent the turbulent overturning of the atmosphere. The dashed line represent the boundary layer height over land and over the ocean. The figure represents the time during the afternoon when the convective boundary layer over the land is at its maximum. Adapted from Dacre *et al.* (2007).

boundary layer ventilation regimes can be prioritised. The identification of the mass flux through the top of the boundary layer is also the first step on the way to comparing boundary layer sources of moisture to tropical moisture exports and assessing the relevance of each in terms of their precipitation patterns. In order to achieve this we first need to answer the question:

- Can global data sets with limited temporal resolution, be used to accurately represent the process of boundary layer ventilation?

A good way to test whether or not the processes are adequately represented will be to compare the results of boundary layer ventilation with suitable studies provided in the literature. These assessments will be done on the timescale of an individual system and in terms of a longer climatology.

1.4.2 The redistribution of moisture by the turbulent boundary layer

1.4.2.1 Introduction

Mid latitude cyclones are one of the most studied aspects of extratropical weather. Partly because of their ability to bring about large changes to the weather but also because of the large amounts of damage that they can cause (e.g. Leckebusch *et al.*, 2007, Fink *et al.*, 2009 and Donat *et al.*, 2011).

It is therefore extremely important that knowledge about how these systems develop and intensify is gained. In this section we will review a classification system which splits storms up into three types and describe how the addition of latent heating in the centre of the storm is important. Some Lagrangian methods will then be described in order to detail how researchers have previously investigated this topic. We also highlight the importance of boundary layer ventilation. A review of the current literature on boundary layer ventilation within baroclinic waves will highlight what is known about the topic and where further investigation is required.

1.4.2.2 A cyclone classification system

The mechanism of baroclinic instability presented in Section 1.3.3 is an idealisation of the many different ways in which a baroclinic wave might develop in the real world. These different manifestations of a developing baroclinic wave can categorised into three different classes (Deveson *et al.*, 2002, Plant *et al.*, 2003). The first two classes were initially described by Petterssen and Smebye (1971) and were labelled as type A and type B. Type A baroclinic waves were defined by the atmosphere having an initial high degree of baroclinicity in the lower troposphere and a zonal flow aloft. As the cyclone develops an upper level trough forms in the upper atmosphere which is driven by the low level thermal advection. These two features remain separated until the cyclone reaches peak intensity. In comparison Petterssen and Smebye (1971) hypothesised that type B cyclones could form as the result of a pre-existing upper level trough in the overlying Rossby wave pattern advecting over an area of low level baroclinicity. This upper level trough would induce thermal advection and increase baroclinity at low levels. The upper level trough would continue to advect eastwards (in the northern hemisphere) at a rate greater than the low level feature and as such be positioned directly over the low level thermal structure when the system reached its peak intensity. The study by Petterssen and Smebye (1971) used analysed fields taken from radiosonde soundings at the standard pressure levels (i.e 850 - 100 hPa). In order to quantify the properties of type B events Petterssen and Smebye (1971) described the evolution of kinetic energy at different levels inside a theoretical box surrounding two cyclones that had developed over the north American continent. The first of these cyclones conformed exclusively to the description of a type B event whilst the second cyclone was a mixed type A / type B but with a tendency towards becoming more type B than type A. The study showed that the net generation

of kinetic energy in type B events was greatest in the upper layer (400 - 100 hPa), whilst being deficient in the middle and lower layers. Kinetic energy was thus transferred down from the top of the storm to the bottom.

One limitation of the Petterssen and Smebye scheme of cyclone classification is that it only considers the effects of the large scale dynamics on cyclone development and does not incorporate the role of moisture, which through the process of releasing heat as water vapour condenses can instigate changes in the development of the cyclone (e.g. Whittaker and Horn, 1984,Emanuel, 1988, Davis and Emanuel, 1991 and Heo *et al.*, 2015). (The process by which water vapour can release heat through condensation in a mid latitude cyclone due to the lifting of air parcels is an example of diabatic heating. The term diabatic represents the fact that changes in the temperature of an air parcel occur because of the heat that is released due to the formation of intermolecular bonds.) The classification scheme also has the disadvantage of being highly subjective as illustrated by the second case study in Petterssen and Smebye (1971) which is described as ”acquiring the trappings of a typical frontal wave (Type A)”.

In order to address the problems identified above with the Petterssen and Smebye (1971) scheme, Deveson *et al.* (2002) tried to objectively categorise 16 cyclones observed during a field campaign, during January and February in 1997 (named FASTEX), into type A or type B based upon output from a numerical weather prediction (NWP) model. By using an omega equation to calculate the vertical velocities at 700 hPa which were forced by the layers above and below the 700 hPa mark, statistics were produced which allowed cyclones that were forced by upper level (U) vorticity advection (type B) to be distinguished from those that were forced by low level (L) thermal advection (type A). Another set of cyclones, type C, were also classified. These exhibited high levels of forcing by upper level vorticity advection but did not show any correlation between their relative vorticity and the separation between the upper level trough and the cyclone centre. In Deveson *et al.* (2002) the 3 cyclones that were identified as type C were found to occur at high latitudes and initially had properties that closely resembled polar lows although it was noted that the transition to full blown baroclinic waves was possible.

In the study by Ahmadi-Givi *et al.* (2004) a single cyclone was selected in order to investigate the effects of diabatic heating on the overall development of the baroclinic wave. The study used the technique of potential vorticity inversion (see Griffiths *et al.*, 2000 for details of the technique)

in order to attribute changes in the wind field of the cyclone to changes in the field of potential vorticity. In order to investigate the effect of latent heating on cyclone development, a case study was chosen in which latent heating was known to be exceptionally strong. Several numerical sensitivity experiments were performed in which the role of potential vorticity anomalies were isolated as a function of height, as well as sensitivity tests to latent heating and the addition of surface fluxes. The results of these experiments showed that the development of a low level potential vorticity anomaly acted to enhance the originally weak surface cyclone whilst simultaneously weakening the upper level potential vorticity anomaly. The development of this storm closely resembled those described as type C in the paper by Deveson *et al.* (2002),

In a follow up paper (see Plant *et al.*, 2003) the classification of cyclones based upon the method described by Deveson *et al.* (2002) was used and extended to include all cyclones that occurred in the year 2000 which had been collated onto an offline database by Tim Hewson whilst working at the Joint Centre for Mesoscale Meteorology at Reading University (we label this database as DAT1). Cyclones were classified as a function of their average ratio U/L and segregated based on the thresholds originally defined by Deveson *et al.* (2002). Roughly half of the events were shown to correspond to type C cyclogenesis even when taking into account the fact that some clear type B events initially demonstrate U/L values which are higher than the type C threshold and removing any events which had been classified as non frontal low pressure systems. By applying the anomalous PV inversion techniques to a typical type B cyclone, the study of Plant *et al.* (2003) were able to show that the main dynamical features of a type B system were captured by this technique. The technique was then applied to two other cyclones that were defined to be type C in DAT1 and the results were contrasted with those of the system studied by Ahmadi-Givi *et al.* (2004). The results showed that for one of the systems it was demonstrated that latent heating played a similar role in storm development to that found by Ahmadi-Givi *et al.* (2004) but that for the other system latent heating did not play an important role. The second cyclone's evolution was almost entirely dominated by the upper level dynamics. The study by Plant *et al.* (2003) concluded that type C might form an important class of cyclone events.

Gray and Dacre (2006) also looked at the occurrence of cyclones which had characteristics similar to those described by Petterssen and Smebye (1971) (type A and B) and Plant *et al.* (2003) (type C) in the region of 30°- 60° North in an attempt to define regions in which each category of

cyclogenesis takes place. The study utilised data obtained from the database used by Plant *et al.* (2003) but with the application of a cyclone tracking algorithm (Hodges *et al.*, 1994) in order to eliminate the multiple occurrence of cyclones that may have biased the results of the Plant *et al.* (2003) study (i.e cyclones that initially demonstrate type C characteristics before becoming a type B cyclone). Using a similar set of diagnostics to the studies of Deveson *et al.* (2002) and Plant *et al.* (2003) the genesis regions of individual cyclones were plotted and percentages of the occurrence of each cyclone type computed. The study concluded that 30%, 38% and 32% of cyclones were associated with cyclone types A, B and C respectively. Type A cyclones were found to preferentially form to the east of the Rocky mountains, type B cyclones were found to form near the gulf stream whilst type C cyclones were found to form preferentially over oceanic regions. It was also noted that a large number of type C cyclones died out in their early stages of development and failed to reach maturity.

A more detailed study of DAT1 combined with the tracking algorithm of Hodges *et al.* (1994) but restricted to the Atlantic ocean (Dacre and Gray, 2009) over a period of 6 years performed compositing of the characteristics of cyclones. It was shown that type C cyclones were preferentially found in the eastern regions of the Atlantic ocean where low level baroclinicity was minimised due to the absence of strong currents such as the Gulf stream in the western Atlantic. The relative distributions of cyclone type (A,B and C) for the west and east Atlantic were reported to be 24%, 51% and 25% compared with 11%, 50% and 39% respectively. The results of the analysis done by Dacre and Gray (2009) have been further confirmed by Dacre and Gray (2013) who studied a twenty year period utilizing the ERA-interim dataset to composite cyclones in the western and eastern Atlantic. The study considered a sensitivity parameter in order to assess the sensitivity of cyclone development to potential vorticity at 700 hPa. Only cyclones in the eastern Atlantic showed an increased sensitivity in cyclone development to potential vorticity at these levels. The study suggested that this was due to the higher proportion of type C cyclogenesis events found in the eastern Atlantic by Dacre and Gray (2009).

The combined studies of Plant *et al.* (2003), Dacre and Gray (2009) and Dacre and Gray (2013) suggest that the increased presence of moisture at mid levels in a cyclone affects the development of a large number of cyclones. It has also been shown that the distribution of this moisture can influence cyclone development. Smith (2000) showed how the surface vorticity in

a cyclone is dependent on the horizontal distribution of moisture. This was achieved by using an analytical model which described the effect of different latent heat distributions on the development of surface vorticity. The results demonstrated that distributions could be found that not only increased cyclone development but that it was also possible to find distributions that weaken the cyclone.

In addition to the changes in cyclone intensity that can occur due to the horizontal distribution of latent heating, differences in the pattern of latent heating in the vertical direction have also been shown to cause a change in the behavior of individual cyclones (e.g Chang *et al.*, 1982,Davis *et al.*, 1993 and Lapeyre and Held, 2004) and on the dynamics of the storm track as a whole (Chang *et al.*, 2002).

Moisture that is advected into a storm can be tracked by a trajectory model. A brief review of this approach is presented next. However, the tracking is complicated by the underlying boundary layer which acts to initialise the trajectories with moisture through the process of boundary layer ventilation. A review of recent studies into the detailed analysis of boundary layer ventilation by fronts and mid latitude cyclones is therefore also given.

1.4.2.3 Trajectory analysis of mid latitude cyclones

The flow patterns and the paths that air parcels take through a mid latitude cyclone have been studied for a long time. A frequently used conceptual model to describe this flow has been presented by Carlson (1980) and a review of conceptual models is provided by Semple (2003). These models are based upon the large scale uplift of air on surfaces of constant entropy (isentropic uplift). In order to analyse the flow of individual air parcels, trajectories are used which demonstrate the flow of an air parcel as experienced by an observer moving with the air parcel in question (Lagrangian flow).

It has been shown by analysing the Lagrangian flow of air that trajectories can be grouped together in order to represent coherent air streams which do not resemble the flow of air represented by standard conveyor belt models (Mass and Schultz, 1993). In order to analyse the Lagrangian track of air parcels through a synoptic system Wernli and Davies (1996) used a numerical weather prediction model in order to supply the meteorological fields necessary in order to construct the

Lagrangian trajectories. This study demonstrated that trajectories could be used to examine the existence of anomalous potential vorticity at mid levels within the centre of the cyclone and provide a means of tracking such anomalies through to the outflow region of the warm conveyor belt (Carlson, 1980). Although the study initialised trajectories within the boundary layer no attempt was made to account for the mixing of air parcels by boundary layer turbulence (e.g. Lock *et al.*, 2000) prior to boundary layer ventilation.

One study which used back trajectories to explicitly study boundary layer ventilation was that of Hannan *et al.* (2003) which assumed a boundary layer height of 850 hPa across the domain. This ignores the synoptically-driven changes in boundary layer height which can occur within a mid latitude cyclone (Sinclair *et al.*, 2009). Despite this limitation the study did indicate that in one case examined air can be drawn in from many regions before assembling into a coherent air stream to be uplifted on the warm conveyor belt. This was shown to be dependent upon the exact synoptic conditions present at the time of analysis with another case being made up of air flows more consistent with the traditional view obtained from isentropic analysis (Carlson, 1980). Using atmospheric pollution measures it was verified that layers of pollution had their origin within the boundary layer and over continental land masses. In some cases these polluted areas were initially behind the cold front. This was seen to justify the use of back trajectories.

The analysis of trajectories has been further used to directly investigate the three dimensional potential vorticity structure at the centre of a cyclone (Rossa *et al.*, 2000). The structure of a ”tower” of potential vorticity within the cyclone was shown to match an area of condensation-induced latent heating. Parcels from this area were tracked back using Lagrangian trajectories to the low level warm sector confirming that the air which produced the mid level latent heating was of low level origin. However, by using a standard Lagrangian trajectory the turbulent transports within the boundary layer were not represented. A true source region for the trajectories could therefore not be determined. Many other studies have also followed similar approaches (e.g. Joos and Wernli, 2012, Schemm *et al.*, 2013 and Chagnon *et al.*, 2013).

In the study of Martínez-Alvarado *et al.* (2014) trajectories were released at many points across the domain and it was shown that the warm conveyor belt can be separated into two distinct branches based upon the change in potential temperature of each parcel of air as it rises up along the warm conveyor belt. It was further shown that these distinct branches of the warm conveyor

belt underwent changes in potential vorticity which it was hypothesised could lead to changes in the down stream Rossby wave amplitude, and so would have an impact on the forecast produced by a numerical weather prediction model. The study further demonstrated that it was the micro-physical processes associated with the large scale cloud scheme that provided the largest changes to the heating rates within the simulated storm. The smaller contribution by convection was shown to be inconsistent between two different NWP models which were used to independently model the storm. This difference was attributed to the different convection schemes used.

The usefulness of back trajectories for studying pollution transports has been confirmed by many authors in the past (e.g. Cape *et al.*, 2000,Stohl *et al.*, 2003 and Freitag *et al.*, 2014) although mixing of air parcels is recognised to be an important process (Pugh *et al.*, 2012) which some current models attempt to replicate. However, moisture is a unique variable as it undergoes phase changes during its transport along any one individual trajectory. This fact along with the role of turbulent mixing within the boundary layer which is constantly perturbing the parcel height means that we have to be very careful when using standard deterministic trajectory models to interpret water vapour transport pathways. Using a trajectory model which also simulates the dispersive elements of the boundary layer in order to show how the boundary layer turbulence affects parcel trajectories would make a useful and unique contribution to the growing literature on trajectory models in mid latitude cyclones.

1.4.2.4 Boundary layer ventilation by mid latitude cyclones

One of the first detailed studies of boundary layer ventilation was conducted by Donnell *et al.* (2001). The study investigated the ventilation of a passive tracer in terms of three mechanistic pathways out of the boundary layer; turbulent mixing, convection and advection, using the Met Office's Unified Model. Three case studies were chosen over the United Kingdom, two of which featured fronts and one which was dominated by high pressure. The boundary layer top was defined by the use of a moist Richardson number and each simulation was run for 24 hours. The results of these experiments demonstrated that advection transported the tracer to the highest altitudes and that this height was increased on the days in which frontal systems were present. It was also determined that mixing was important in order to bring pollutants up to a region where advection could transport it out of the boundary layer. Convection was shown to be important at

transporting material out of the boundary layer behind the surface front.

In a similar study, Kowol-Santen *et al.* (2001) investigated the amount of tracer that was removed from the boundary layer by the warm conveyor belt. It was shown that 70% of the passive tracer released into the boundary layer was removed in the region of the warm conveyor belt. This study was very limited in terms of its investigation into the mechanisms by which the boundary layer is ventilated. However, it does indicate that the warm conveyor belt is especially adept at ventilating material into the free troposphere.

In the field study by Purvis *et al.* (2003) the role of the kata (forward sloping) cold front was investigated in order to understand the role of convection compared with that of advection out of the boundary layer and along the warm conveyor belt. In order to do this samples of air were taken at various points along the warm conveyor belt and analysed for the presence and concentration of non-methane hydrocarbons which are relatively short lived within the atmosphere. The concentrations of these hydrocarbons were compared with concentrations observed within the boundary layer and it was shown that these were consistent with rapid uplift in the atmosphere which may be attributed to transport by convection as opposed to advection along the warm conveyor belt. Convection was thus determined to be a major factor in the ventilation of the boundary layer air.

Whilst the numerical modelling study of Donnell *et al.* (2001) had shown that advection was the dominant mechanism for ventilation of boundary layer air in a frontal system the result of Purvis *et al.* (2003) had shown by observational methods that convection could also play an important role. In order to separate out these processes the study by Agustí-Panareda *et al.* (2005) looked in more detail at the ventilation by a kata cold front over the European continent. The experiment involved the numerical modelling of the cold front with the inclusion of tracers that were released within the boundary layer. The age of the air mass since leaving its source region within the boundary layer was then calculated using the respective mixing ratios and source strengths of two tracers with different life times. Additionally, different tracers represented the different transport mechanisms out of the boundary layer (e.g. a tracer subject to advection only or a tracer subject to advection and convection). The study showed that convection was an important mechanism for ventilating the boundary layer and that the combination of mixing, convection and advection was more important than the roles of each process separately. In a follow up study, Agustí-Panareda *et al.* (2009) used the same methods to describe and contrast the ventilation of

boundary layer air in an ana (rearward sloping) cold front with that occurring in a kata (forward sloping) cold front. Ventilation rates between the two systems were found to be very similar and followed the air flows represented in the conceptual models describing these systems. Convection behind the cold front was also shown to contribute to the amount of ventilation.

In order to obtain results that would be representative of mid latitude cyclones in general the use of idealised NWP models became important for the study of boundary layer ventilation. In the idealised setup a meridional temperature gradient along with a zonal jet stream in thermal wind balance are pre-specified over a limited domain. Perturbations are then induced (e.g. to the potential temperature field in Boutle *et al.*, 2010) in order to initiate baroclinic instability. The simulation can then be run for a number of days during which a series of baroclinic waves will develop.

This approach was used in a dry baroclinic atmosphere in order to simulate the ventilation of tracers in a study by Sinclair *et al.* (2008). In this study two systems were generated in order to recreate the two life cycles first described by Thorncroft *et al.* (1993) (denoted LC1 and LC2). LC1 lifecycles are characterised by equatorward moving anticyclones whilst the cyclone moves poleward and becomes confined in the zonal direction. LC2 cyclones remain roughly at the same latitude and are characterised by much broader baroclinic waves. The warm conveyor belt was identified by using a threshold in the vertical velocity which was dependent upon the model resolution used. The study concluded that both the processes of mixing and horizontal advection of material within the boundary layer were important for the ventilation by the warm conveyor belt. Since this study was performed in a dry atmosphere transport by convection was not available. Another study by Polvani and Esler (2007) also looked at transport out of the boundary layer in similar idealised cyclones although the main focus of that study was troposphere - stratosphere exchange of air and as such the simulations did not explicitly include a dynamical boundary layer scheme. The amount of tracer ventilated by the boundary layer was roughly half that calculated by Sinclair *et al.* (2008) thus proving the importance of including a boundary layer scheme when estimating boundary layer ventilation rates.

In Sinclair *et al.* (2009) the mass budget equation for the boundary layer was derived and the terms were diagnosed from the idealised simulations of Sinclair *et al.* (2008). This demonstrated quantitatively the pattern of boundary layer ventilation in the region of the warm conveyor belt

and also boundary layer entrainment behind the cold front. These areas of mass gain and mass loss were related to the convergence of boundary layer air in the warm conveyor belt and divergence of boundary layer air in the two anticyclones to the east and west of the cold front.

The study by Sinclair *et al.* (2009) led the way for two additional studies which adapted the boundary layer mass budget equation to consider the moisture budget. The first of these studies (Boutle *et al.*, 2010) described the evolution of an idealised cyclone wave including a full set of dynamical parameterisations including boundary layer processes and convection. The study showed that high evaporation rates found in the anticyclones to the east and west of the cold front were maintained by divergence within the boundary layer which produced a saturation deficit in the boundary layer moisture content directly above the point over which evaporation was taking place. Conversely large areas of boundary layer moisture convergence were found to occur in a region of strong boundary layer ventilation above the warm front. The study concludes that the ultimate source region of moisture for the strong ventilation rates must be the areas of high evaporation. The divergence and convergence of the flow was attributed to the large scale ageostrophic flow of the air. However, the study does not actually demonstrate any of the pathways that the moisture follows during its journey and as such does not provide a complete picture of the boundary layer moisture cycle. The second study (Boutle *et al.*, 2011) showed that the ventilation of moisture by the boundary layer was roughly equal in magnitude to the rate of precipitation produced within the region identified as the warm conveyor belt by the method of Sinclair *et al.* (2008). This is suggestive of a rapid conversion of moisture to cloud and then to precipitation once it has been ventilated by the warm conveyor belt. It was additionally shown that convection outside of the warm conveyor belt ventilated a similar amount of moisture.

1.4.2.5 Outstanding issues in the literature

All of the reviewed studies have provided information relating to the question:

- How does the turbulent boundary layer redistribute moisture within a mid latitude cyclone?

The current body of knowledge provides partial answers to many aspects of this question . For example the study of Boutle *et al.* (2010) associates the large sources of moisture in the anti-

cyclones to the high ventilation rates observed in the warm conveyor belt and thus to the large amounts of precipitation falling within the warm conveyor belt region. However, no direct link in terms of the transport of moisture was shown as all of the results were presented in the Eulerian framework. On the other hand in the Lagrangian framework, the effect of boundary layer turbulence on the possible trajectories has been neglected in the literature reviewed in Section 1.4.2.3. Therefore, a useful addition to the literature on this subject would be to test the hypothesis that sources of evaporation are directly linked through lagrangian pathways with areas that produce the precipitation in a mid latitude cyclone passing through areas that exhibit high ventilation rates within the warm conveyor belt. It would also be useful to look at the mechanism of boundary layer ventilation in more detail and discover what new insights might be gained by combing both the techniques of Eulerian and Lagrangian analysis. In particular it would be interesting to look at the question

- By what mechanism or mechanisms does the boundary layer ventilate air parcels?

with particular emphasis placed upon the question

- Does convection play an important role in the ventilation of particles?

Such a framework would also enable a more direct comparrison of the results with those provided by the study of Purvis *et al.* (2003). In addition the role of the boundary layer in redistributing moisture over the whole scale of the cyclone wave requires further investigation. For example, if flows within the boundary layer promote a wide dispersion of moisture this will demonstrate that it is critical to ensure that the detailed boundary layer scheme employed by a model is capable of redistributing moisture into the middle of the cyclone in a physically accurate way in order that the large scale dynamics of the system can be accurately forecasted (Smith, 2000).

1.4.3 The redistribution of moisture by the free atmosphere

1.4.3.1 Introduction

The study of moisture and in particular the study of the hydrological cycle has received a lot of attention as a key component of the Earth's climatic system (Bengtsson, 2010, Su *et al.*, 2010 and Allan *et al.*, 2014). However the role of the boundary layer within the hydrological cycle on a global scale has yet to be shown. In order to provide the motivation for the work done in chapter 4 a review of two strands of the literature has been undertaken. Firstly a historical look at the history of precipitation recycling has been provided in order to highlight some very old problems which occur within the literature to this day. Secondly the subject of atmospheric rivers is discussed in order to provide a more direct introduction to the topic at hand. Finally some questions are posed which still need to be answered and a link will be drawn between the two separate strands of literature.

1.4.3.2 Precipitation recycling

In the early part of the twentieth century all moisture that precipitated over the continental land masses was assumed to be a consequence of local evapotranspiration (see Mead, 1919, Zon *et al.*, 1927 and Meyer, 1928). This preconception led to the speculation that the local precipitation rates were determined by local sources of moisture (Schwarz, 1921).

In the 1930's Jensen conducted a series of experiments (Jensen, 1936, Jensen, 1938) in which an attempt was made to link the patterns of precipitation with those of evaporation. This was achieved by obtaining rainfall amounts from rain gauges in the region of North west Minnesota, a region which is populated by numerous lakes. Computation of the evaporation of moisture from the lake was done by the use of an empirical formula, which took into account the wind speed over the water and the difference in vapour pressure from the saturated vapour pressure of the air. Large amounts of evaporation were calculated which Jenson assumed contributed to the total amounts of rainfall whilst also acknowledging the fact that it is likely that large amounts of moisture must have been sourced from the Gulf of Mexico.

Theorists also took the view that large amounts of precipitation could be sourced from the local area and therefore moisture could be ”recycled” on a continual basis. The study by McNish (1936) suggested that patterns in precipitation recurrence could be used by forecasters in predicting future events. A few years later in the study by Bernard (1938) another theory was introduced by equating local evaporation moisture sources, which were due to the delay and storage of runoff water, with the loading of moisture into the overlying air masses. The theory then suggested that this moisture was advected away from the continents and precipitated out over the oceans. In the study of Bernard (1938) it was recognised that it was important to combine the study of hydrology with that of meteorology and the new term hydro-meteorology was introduced.

In the early 1940's a study by Horton (1943) looked at the the concentration of chlorine in the surface water runoff. Using the fact that oceanic moisture sources contain large amounts of chlorine due to the occurrence of sodium chloride as a cloud condensation nuclei, Horton was able to show that only runoff originating within 300 miles of the coastline contained large amounts of chlorine in solution. He thus concluded that oceanic moisture sources only had an influence on these coastal regions with the majority of inland precipitation being derived from local evaporative sources. The study did not take into account the possibility that chlorine may have been deposited during its time in transit from inland regions to the ocean.

During the late 1930's and early 1940's an alternative point of view to that of Horton was beginning to be seen in the literature of the time. In 1937 a paper written by Holzman *et al.* (1937) was published which used the theory of airmasses as described by Willett (1933) (who attributes the initial work on airmass theory to Bergeron (1930)) to describe the overall moisture content of air which is advected over the continents from oceanic regions. In the paper by Holzman *et al.* (1937) and the subsequent paper by Thornthwaite and Holzman (1938) it was asserted that it is the properties of these air masses which determine the continental precipitation rates and that the small amount of moisture which is evaporated over the land has very little bearing on precipitation. Holzman *et al.* (1937) argued that in order to prove the theory pertaining to the ”cycling of air masses” more upper air monitoring stations were needed in order to measure the total moisture content of the air.

Benton *et al.* (1950) sought to provide quantitative proof that through the movement of air masses large amounts of ocean-derived water vapour were advected over the continents and were

thus responsible for the majority of precipitation over continental land masses. This was attempted by using data derived from 35 radiosonde stations situated in and around an area known as the Mississippi watershed. In order to determine whether or not a maritime air mass was responsible for the observed precipitation at an individual location, cross sections were produced and precipitating clouds were assigned to individual air masses. The results of this extensive study were that the majority of precipitation produced over land was of maritime origin. An attempt was made to quantify the amount of precipitation produced by moisture sourced from evapotranspiration. This was done by analysing records of pan evaporation alongside records of precipitation and information on air mass occurrence. It was shown that approximately 85 % and 35 % of precipitated water was returned to the atmosphere in the summer time and the wintertime respectively and that roughly equal amounts were returned to maritime and continental air masses. The cycle was then completed by the use of radiosonde stations situated at the border of the Mississippi watershed which showed that the majority of moisture entering the region was of maritime origin. Using this data Benton *et al.* (1950) were able to construct a complete picture of the hydrological cycle over the Mississippi watershed and conclude that large volumes of water are transported over the area, mostly from oceanic sources. Only a fraction of this moisture is precipitated out but that this accounts for over 90 % of the precipitation occurring over the Mississippi watershed. This result agreed with a similar study conducted over the town of Huntington in west Virginia at the eastern extent of the Mississippi watershed which found that between 85 and 90 % of precipitation received over that area could be traced back to maritime air (Benton and Blackburn, 1950).

In 1954 a follow up study by Benton and Estoque (1954) was undertaken which extended the area of interest to include the entire North American continent and split up the contributions of moisture transport into those associated with the mean meridional flow and those associated with meridional atmospheric eddies. This was achieved by calculating the time mean flow component and then subtracting this from the total meridional water vapour transport. The transports were calculated at radiosonde stations and interpolation routines used for regions in between. It was shown that a large proportion of moisture transport in the meridional direction was the result of these eddies. The theory of mass continuity was used in order to reconstruct the hydrological cycle over the United States of America. The amounts obtained for evapotranspiration were shown to agree well with those obtained by theoretical arguments and as such the paper cemented

the relationship between the hydrological and meteorological sciences.

The results of the work done by Benton and Blackburn (1950), Benton *et al.* (1950) and Benton and Estoque (1954) implied that after being evaporated moisture remained in the atmosphere for a considerable amount of time. This was confirmed by the work of Sutcliffe (1956) who showed by some simple calculations involving the estimated global precipitation rate and the estimated amount of moisture in the air that the air contained 10 days worth of precipitation. If we assume that all of the moisture within the air is continually circulated due to the process of evaporation and precipitation this implies a residence time of 10 days.

In 1962 the view that precipitation was produced by the large scale transports of moisture was presented in McDonald (1962). The article, by the use of some simple calculations, clearly demonstrates the infeasibility of using areas of water in order to enhance local precipitation levels. Instead it was proposed that precipitation is due to a process of uplifting air masses which allows water to condense out and form rain droplets. In his calculations, McDonald demonstrated that lakes would have to be 100's of kilometers in diameter in order to produce any noticeable effect on American statewide precipitation levels.

Despite the evidence provided by Benton *et al.* (1950) and McDonald (1962) arguments over the importance of local sources of moisture continued to be represented in the scientific literature. One such example is the controversy published by two sets of researchers in Science magazine (Eddy *et al.*, 1975). The article was focused on the effect that irrigation had on the local levels of precipitation. In order to prove that irrigation was responsible for precipitation trends. Stidd chose to examine two periods of rain gauge data. The first period represented data that preceded construction of a local dam, whilst the second period was post construction of the dam. In addition the data set was further split up into stations that were close to the dam and the second set which were further away. By use of a significance test Stidd was able to show that the stations close to the dam did not belong to the same population as the stations further away. He thus concluded that the construction of the dam was responsible for an increase in rainfall experienced at stations located close to the dam when compared with rainfall that fell at the same stations prior to the dam's construction. In the same article however, Fowler and Helvey disputed these results and argued, by the use of double mass plots (see Eddy *et al.*, 1975), that the increase in rainfall was not due to the dam's construction.

In Barnston and Schickedanz (1984) the technique of separating out precipitation patterns, by the use of empirical orthogonal functions, was used in order to identify periods when irrigation had affected the precipitation patterns in the Great Plains region of North America. These time periods were then also shown to coincide with stationary weather fronts being present in the area. The study concluded that irrigation played a minor but detectable role in influencing local precipitation but that it was the convergence and subsequent uplift of moisture on the frontal surfaces that was responsible for these increases. However, another study by Moore and Rojstaczer (2001) used an alternative time period in order to question the original results presented by the Barnston and Schickedanz (1984) study. Their conclusion was that irrigation had only a slight effect on the local precipitation pattern. The debate over how much irrigation and local evaporation affect precipitation over the local area continues in the scientific literature (e.g. Trenberth, 1999, Segal *et al.*, 1998, Harding and Snyder, 2012, Huber *et al.*, 2014) and it is now recognised that in order to observe changes in precipitation large areas of land need to be taken into account (Harding and Snyder, 2012) in order to account for both the mesoscale and synoptic scale variability with the local sources of evaporation.

Some of the aforementioned studies (Trenberth, 1999, Harding and Snyder, 2012) use the concept of precipitation recycling in order to obtain their results. In order to quantify the amount of precipitation produced over an area in comparison to the amount of precipitation that is produced by moisture being advected into the area the precipitation recycling ratio (ρ) is used and is defined to be

$$\rho = \frac{P_e}{P} \tag{1.9}$$

(see Eltahir and Bras, 1996) where P_e is the amount of precipitation produced by surface evaporation and P is the total amount of precipitation. If we take these values for the entire globe then the value of ρ is equal to one as all of the moisture that is evaporated must eventually return to the surface as precipitation (assuming that the global atmosphere is not rapidly warming or cooling). Smaller areas produce values of ρ that are less than one. One of the earliest methods for determing ρ was described by a Russian scientist named Mikhail Ivanovich Budkyo (Eltahir and Bras, 1996) and is credited with being used as the basis for the formulation of many current precipitation recycling models (Burde, 2006).

The Budkyo model is based upon the formula

$$\beta = 1 + \frac{EL}{2F_{in}} \tag{1.10}$$

where β is the ratio of precipitation produced by an influx of moisture into an area to the total amount of precipitation over that area (i.e $\beta = 1 - \rho$). F_{in} is the flux of moisture (integrated from the surface to the top of the atmosphere) into the area along the path of a stream line. E is the average evaporation rate within the area and L is a length scale which defines the area of interest. The Budkyo model relies upon F_{in} being parallel to the stream line of flow into the area and the assumption that the atmosphere is well mixed within the area of interest.

Trenberth (1999) derived a relationship between precipitation sourced from moisture advected into an area to precipitation sourced from local evaporative sources in a similar fashion to the Budkyo model. Trenberth then applied his recycling formula to data from the NCEP-NCAR reanalysis data project (Kalnay *et al.*, 1996) in order to obtain recycling ratios for land areas across the globe. The results of this study were that for length scales of 500 km the recycling ratio was 9.6% whilst for length scales of 1000 km the recycling ratio was just under 20 %. The study then went on to look at the different recycling ratios over different drainage basins across the globe focusing specifically on the Mississippi basin and the Amazon basin.

The precipitation recycling model has been used in various forms over different drainage basins over the globe in order to understand the differences in hydrological cycle over these regions (e.g. Eltahir and Bras, 1994, Bosilovich and Chern, 2006, Martinez and Dominguez, 2014). Each of these studies concentrate on specific regions of the globe but in recent years the topic of advective verses locally evaporative precipitation has once again become an important one albeit on a much larger scale. This is related to the topic of atmospheric rivers which is described in the next section.

1.4.3.3 The concept of an atmospheric river

The concept of an atmospheric river has been around since the early 1990's when two studies (Newell *et al.*, 1992 and Newell and Zhu, 1994) described the occurrence of strong water vapour

fluxes (integrated from the bottom to the top of the atmosphere) which were concentrated into filaments in which the along stream to cross stream dimension ratio was approximately five to one. These filaments were identified using ECMWF analysis data and supported by observations using the Total Ozone Mapping Spectrometer. In these early studies, this filament of high moisture was termed a tropospheric river due to the fact that the majority of the transported moisture vapour was below 500 hPa (Newell *et al.*, 1992). The study of Newell *et al.* (1992), noted in the discussion that the observed filaments were not always associated with a cold front, despite some of the filaments being seen to be made up of middle and high level cloud.

The study of Newell and Zhu (1994) had shown that the transient eddy component of the moisture vapour flow could be further split up, by the process of harmonic analysis, into high frequency perturbations of less than three days and low frequency perturbations of greater than three days. By splitting the perturbations up in this way it was shown that the high frequency perturbations correlated well with the position of the storm tracks. However, the total eddy perturbation was uncorrelated with the storm tracks and thus the idea of an atmospheric river being a separate entity to the mid latitude cyclone was born (although the high frequency link between the two was also confirmed).

Ralph *et al.* (2004) used dropsondes in order to document the structure of a frontal system. In particular the researchers focused their attention on the low level poleward moisture flux, just east of the surface cold front and parallel to the low level jet. It was shown that the frontal system contributed 20% of the hemispheric total poleward moisture flux at $35^{\circ}N$ and they described the spatial characteristics of this flow of moisture. These observations were then compared with instantaneous water vapour (IWV) data from the special sensor microwave imaging instrument on polar orbiting satellites. This comparison showed that the features exhibited in the case study matched those seen in the satellite data, associated with atmospheric rivers. The study concluded by suggesting that further work needed to be done on atmospheric rivers in order to provide a link between short term climate variability and the occurrence of extreme precipitation events and flooding.

1.4.3.4 Atmospheric rivers and flooding

An established link between the presence of an atmospheric river and large amounts of precipitation which lead to flooding events has been evident in the scientific literature over the last decade. Ralph *et al.* (2006) established the link between atmospheric rivers and flooding by looking at seven different flood events on the Russian river in northern California. It was found that six of the seven events shared features in common with the definition of an atmospheric river which was previously documented by Ralph *et al.* (2004). The remaining event did show areas of column integrated water vapour in excess of 2cm but did not show that these areas were contiguous in nature and as such only partially met the criteria for an atmospheric river. In addition to the presence of an atmospheric river it was determined that the influence of the local orography in enhancing precipitation was an important factor in the flooding which occurred in all seven of the documented cases.

In 2008 two observational and modelling studies were performed by Neiman *et al.* (2008a) and Neiman *et al.* (2008b). These focused upon the impact of atmospheric rivers on the western coast of the USA. Neiman *et al.* (2008b) focused on the link between atmospheric rivers and heavy precipitation events concluding that in the winter the presence of atmospheric rivers strongly increases the amount of precipitation falling over particular regions and thus tied the link between atmospheric rivers and the potential for flooding. Neiman *et al.* (2008a) showed that a satellite system, using the global positioning system radio occultation technique (Kuo *et al.*, 1999) , was able to accurately detect the large amounts of moisture within the lower levels of the atmosphere associated with the atmospheric river and show that this agreed with both reanalysis products and dropsondes which were dropped within the same region. However, neither of these studies showed any direct link between the large areas of moisture near the surface and the flooding events on the western coast. They also failed to directly connect the transport of tropical moisture into these regions with any flooding that occurred. The only evidence was provided by the presence of an atmospheric river, which does not imply any dynamic movement of moisture but merely shows that moisture exists in that particular place. More recently over the river basins of western North America various other studies have further demonstrated the link between atmospheric rivers and large precipitation events (e.g. Dettinger, 2013, Rivera *et al.*, 2014 and Kim *et al.*, 2013) .

The link between atmospheric rivers and flooding has also been shown to be true in the Atlantic Ocean. In Lavers *et al.* (2011) atmospheric rivers were detected by matching corridors of high specific humidity values in order to create a continuous axes of high specific humidity values using data taken from a combination of the Twentieth Century reanalysis project and ERA-interim. The study showed that out of 10 events which produced flooding in the United Kingdom each of the 10 events had an associated atmospheric river. It should be noted that the study conceded that each of these axes did not constitute the path of any one individual air parcel. In a similar study Lavers and Villarini (2013b) showed that in eight out of the top ten precipitation events over Europe the presence of an atmospheric river could be confirmed.

1.4.3.5 Atmospheric rivers and tropical moisture exports

In an attempt to objectively identify moisture transport by atmospheric rivers in a gridded dataset Zhu and Newell (1998) used the concept of splitting up the flow of moisture vapour into a component associated with the mean flow and a component which was associated with transient eddy perturbations. In particular the study noted that large transports of moisture may occur before the onset of cyclogenesis but that when cyclogenesis occurs moisture is "pushed to the eastern edge of the cyclone and may be intensified" thus demonstrating the important role played by mid latitude cyclones in the formation of atmospheric rivers but not necessarily linking these rivers solely with polewards transport of moisture by mid latitude cyclones. The importance of atmospheric rivers in the polewards transport of moisture was emphasised in Zhu and Newell (1998) when they showed that the majority of polewards moisture transport was achieved by atmospheric rivers which took up just 10% of the globe.

A study by Bao *et al.* (2005) looked at the formation of bands of integrated water vapour in satellite imagery off the west coast of America and asked whether or not the moisture that formed these structures was transported directly from the tropics or a result of the local convergence of air from moisture sources near to the cyclone's cold front. In order to study this problem they employed back trajectories released at 1km above the surface within the band of high integrated water vapour. The study concluded that in the majority of cases the band of integrated water vapour was formed by low level convergence of moisture. However, it was also speculated that transport of moisture from the tropics was possible, particularly in the neutral phase of the El

Nino – Southern Oscillation cycle. It is particuarly important to note that a height of 1 km was chosen for the trajectory release location as this is consistent with the height typically associated with the top of boundary layers off the west coast of America (von Engeln and Teixeira, 2013).

The idea that polewards transport of moisture was linked with moisture flows above the boundary layer was proposed by Knippertz and Martin (2007) in what they termed a moisture conveyor belt (MCB), a term that was chosen to distinguish these flows of moisture from the warm conveyor belt (WCB, Harrold, 1973 Carlson, 1980 and Browning, 1990). The MCB was defined as a flow of moisture from the tropics into the mid latitudes which occurred above the planetary boundary layer. In order to demonstrate the effect of this moisture flow on precipitation rates a case study was chosen which produced large amounts of precipitation in the regions of California, Nevada and Arizona. 866 back trajectories were calculated using the wind field supplied by an ECMWF analysis. These trajectories were then filtered in order to remove any that did not contribute to the poleward water vapour flux. Of the remaining trajectories the majority were found to originate at heights above the 850 hPa surface in the 24 hours preceding their release. The study also analysed the synoptic conditions associated with this event and found that a persistent upper level trough was present and that this was a crucial feature in determining the transport of moisture.

In two subsequent studies (Knippertz and Wernli, 2010 and Knippertz *et al.*, 2013) climatologies were produced of tropical moisture exports. These climatologies were composed of Lagrangian trajectories which traced the path of moisture flows through the 35°latitudinal band and above the planetary boundary layer. The first of these studies used the ERA-40 reanalysis data set whilst the second showed that the results were consistent between ERA-40 and ERA-interim. Only trajectories that constituted a moisture transport of greater than 100 g $kg^{-1}ms^{-1}$were retained and it was shown that trajectories related to discrete bands of moisture transport that were strongly linked with the occurrence of atmospheric rivers on the west coast of North America. The studies claimed without much evidence that the effect of surface evaporation was negligible outside of the sub tropical regions. The use of free tropospheric trajectories does not however take into account the phase changes of moisture which includes its loss by precipitation and its supplement by boundary layer ventilation.

The idea that atmospheric rivers are precursors to rather than a consequence of the transport

of moisture by the WCB has been proposed by Sodemann and Stohl (2013a). Their study investigated the month of December in 2006 using both observations and numerical weather prediction data (see Sodemann *et al.*, 2009 for details on the method of water vapour tagging). The study divided the Atlantic ocean up into latitudinal bands and used tracers in order to track moisture from its evaporative source region to the point at which it was precipitated out. The study showed that precipitation was mostly linked to locally derived evaporative sources but that in some instances moisture could be advected from lower latitudes (30°N- 40°N) to regions as far north as Iceland. The study does not take into account the role of the boundary layer in redistributing moisture. It is therefore likely that their water vapour tagging scheme overestimates the amount of time that individual molecules of moisture are present in the atmosphere and thus overestimates the meridional extent of their propagation. The study is also limited by the short period of time over which it was undertaken.

In an attempt to generalise the study of atmospheric rivers two studies have recently been produced, those of Newman *et al.* (2012) and Dacre *et al.* (2014). Newman *et al.* (2012) considered the fact that poleward moisture transports could be split up into events which were high in frequency and low in frequency ($<$10 days and $>$ 10 days). High frequency eddies were computed by removing the annual cycle and then filtered using a 121 point Lanczos filter that passes periods of more than 10 days. The residual eddies were then assigned to the low frequency category. 40 years worth of reanalysis data produced by NCEP-NCAR indicated that low frequency eddies contributed to a significant amount of moisture transported from the ocean to the land. It also indicated that these two transport terms were uncorrelated indicating that different dynamical forcing mechanisms were driving them. In contrast the study by Dacre *et al.* (2014) used a cyclone centric approach in order to show that large scale transports of moisture into each system were negligible and that local sources of water vapour were thus responsible for producing bands of total column water vapour seen in satellite images. This was achieved by using a moisture budget equation with terms representing the evaporation, precipitation, change in moisture content of the atmosphere, the advection of moisture and the convergence of water vapour weighted mass. This budget was applied to an individual cyclone in order to demonstrate the order of magnitude of each term and then applied to a database of 200 cyclones in order to show that the result obtained was representative of the group as a whole. In all cases it was seen that moisture flux convergence was a dominant term which transported moisture into the centre of the cyclone. However, by

only focusing on the transport by synoptic scale eddies the study failed to account for the low frequency eddies noted by the study of Newman *et al.* (2012). This approach was taken based upon a study by Hawcroft *et al.* (2012) who showed that the majority of precipitation in the northern mid latitudes was associated with mid latitude cyclones.

1.4.3.6 Outstanding issues in the current literature

The previous two sections have highlighted some of the problems faced by researchers in regards to poleward moisture transports. The majority of moisture that is transported polewards occurs in systems known as atmospheric rivers (Zhu and Newell, 1998). It has been shown that debates as to the origin of precipitation have long been present in the literature. On the one hand studies such as Boutle *et al.* (2010) and Dacre *et al.* (2014) have shown that the majority of precipitation in a mid latitude cyclone is sourced from areas local to the system, but on the other, studies such as Bao *et al.* (2005), Knippertz *et al.* (2013) and Sodemann and Stohl (2013a) suggest that tropical sources of moisture may have a role to play in the precipitation produced at higher latitudes. Also cases of large moisture fluxes poleward are rarer events than those sourced from local moisture sources (Bao *et al.*, 2005). Important questions that we might ask are

- Can we adapt the techniques of precipitation recycling in order to analyse the difference between tropical moisture exports and locally sourced precipitation?

and

- Can we extend the precipitation recycling methods to provide an estimate of the meridional extent to which moisture exported from the tropics penetrates into the mid latitudes?

It has also been discussed that much of the moisture that is exported from the tropics does so above the boundary layer in a flow which has been termed the moisture conveyor belt in order to distinguish it from the warm conveyor belt (Knippertz and Martin, 2007).

- Following this suggestion, can we use the boundary layer height as a suitable surface in order to separate out two distinct types of event, one of which is mainly forced by tropi-

cal moisture exports above the boundary layer and one of which is mainly forced by the boundary layer ventilation of moisture?

- Are the large tropical exports of moisture associated with specific synoptic patterns which cause precipitation in preferential locations in the mid latitudes?

The idea that atmospheric rivers are not solely a product of the flow of moisture within an extratropical cyclone has been suggested (Newman *et al.*, 2012 and Sodemann and Stohl, 2013a). Therefore

- Can we find any evidence that the large scale forcing (as opposed to the synoptic forcing) plays a role in determining whether or not events which have a high tropical moisture content occur?

An attempt will be made to answer all of these questions in chapter 4 of this thesis.

1.5 This thesis

1.5.1 The aims of this work

The aims of this work are to try to gain answers to following research questions:

1. Can global datasets with limited temporal resolution accurately represent the processes of boundary layer ventilation?
2. How does the turbulent boundary layer redistribute moisture within a mid latitude cyclone?
3. What is the role of moisture in events that transport high amounts of moist static energy polewards?

In chapter 2 ECMWF ERA-interim forecast model data will be used in conjunction with a Eulerian mass budget equation in order to analyse the ventilation rate of the boundary layer in a case study and to subsequently construct a climatology of boundary layer ventilation and entrainment.

This will allow us to assess whether or not a dataset with limited temporal resolution is capable of resolving the important features and mechanisms that we would expect to see.

In chapter 3 an Eulerian moisture budget equation will be applied to the same case study as presented in chapter 2 to identify the major areas of moisture ventilation within a mid latitude cyclone. This analysis will then be complemented by an analysis of the Lagrangian pathways between areas of high surface evaporation and their eventual locations within the cloud head passing through the turbulent boundary layer. A sensitivity study will be done in order to test the sensitivity of starting location and the action of convection and boundary layer turbulence, to each trajectory's final position.

In chapter 4 moist static energy is used in order to isolate the role that the boundary layer plays in supplying moisture to events within the top 10% of poleward energy transports. Events will be separated out into those which are predominantly supplied by moisture from the boundary layer and those which are supplied moisture predominantly from the tropics. The timing, mean synoptic conditions and poleward extent of moisture transport will all be analysed. Precipitation patterns will be compared and contrasted and some links to the literature on atmospheric rivers will be observed.

Chapter 2:
A Global Climatology of Boundary Layer Ventilation

2.1 Introduction

To date, no one has published a global climatology of boundary layer ventilation. The only study that attempts to quantify the amount of material that is vented by the atmospheric boundary layer by cloud type on the global scale is the study by Cotton *et al.* (1995). However this study only focuses on cloud systems and as such neglects the ventilation by coastal out flow and some of the orographic ventilation mechanisms described in chapter 1. The study also fails to provide us with a map describing the spatial distribution of boundary layer ventilation on the global scale. In this chapter, we apply the boundary layer mass budget equation of Sinclair *et al.* (2009) to a data set spanning the entire globe and derive some climatologies of the net mass flux through the top of the boundary layer. The divergence term of the boundary layer mass budget equation is also calculated in order that the full mass budget equation may be solved.

2.1.1 Aims of this work

The overall aims of this chapter are to produce global climatologies of boundary layer height and boundary layer ventilation for a 30 year period. Using these climatologies we will answer the following questions.

1. Where on the globe are the regions of strongest boundary layer ventilation?
2. Can we associate regions of ventilation with climatological features described in the literature?

The answer to question 1 will be used in order to test the hypothesis that, "the climatological ventilation of mass from the atmospheric boundary layer is dominated by processes occurring in the tropics". By answering question 2 we will then be able to ascertain which mechanisms of boundary layer ventilation are an important contributor to the overall circulation of air in the atmosphere on the timescale of a thirty year climatology. It is also hoped that by identifying these features, we will be able to show that the boundary layer mass budget equation is robust when used with a data set that uses a temporal resolution on the scale of a few hours.

2.1.2 The data set

In order to study this problem I have chosen to use the ECMWF ERA-Interim data set. ERA-Interim provides a high resolution data set which uses a boundary layer parameterisation scheme based around the same principles as the Reading Intermediate Global Circulation Model (IGCM) used by Sinclair *et al.* (2009). The use of the ERA-Interim data set as opposed to other re-analysis data sets was made in order to provide a data set with which to compare the idealised simulations of Sinclair *et al.* (2009). The data set is made up of two types of variables. A set of variables produced solely by the forecast model, and a set of variables that have been augmented by observations in order to form the re-analysis data set. In all of the work presented in chapters 2, 3 and 4 of this thesis (with the exception of the Lagrangian trajectory model which uses the Met Office Unified Model), we use the data derived directly from the forecast model. The model used in order to generate this data is the atmosphere / ocean integrated forecasting system (IFS), cycle CY31r2. I shall refer to this as simply the IFS for the remainder of this thesis, which should not be confused with the current operational IFS used by ECMWF. A brief description of the IFS is given in section 2.2.

2.2 The IFS

The IFS (see Dee *et al.* 2011) uses a time step of 30 minutes and has a horizontal spectral resolution of T255. This means that the mean horizontal grid spacing is approximately 80km. The model has 60 levels in the vertical, with the top level representing an atmospheric pressure of

0.1hPa. The distance between levels is approximately 30 metres near to the surface and up to 7km near the top of the atmosphere (see (Berrisford *et al.*, 2009)). The model uses a semi Lagrangian, semi-implicit time stepping scheme for calculating the prognostic variables. A hybrid sigma - pressure co-ordinate system is used in the vertical which means that the model follows the contours of orography in the lower portion of the atmosphere before gradually reverting to a constant pressure surface at the top of the atmosphere.

Due to the low horizontal resolution of the model, processes on the sub-grid scale are represented by various parameterization schemes. The most relevant parameterizations in relation to this study are described in the next few sections. For a complete description of the parameterization schemes, which includes information on the derivation and origins of the various equations, the reader should refer to ECMWF (2006b). Brief descriptions of the boundary layer, convection, precipitation and cloud schemes are laid out in sections 2.2.2, 2.2.3 and 2.2.4.

Each model run is initialised from the ECMWF ERA-interim Reanalysis (Dee *et al.*, 2011). This product combines elements of the forecast model with observations through a process called 4-D var in order to reproduce the best guess of the atmospheric state at any one time. The 4-D var system uses a combination of observations and model data which are taken from the preceding 9 hours and up to 3 hours (model data only) after the time that the analysis is being made. The IFS forecasts are therefore considered to be very close to the actual state of the atmosphere during the first six hours of the forecast with minimal deviations occurring from reality for the first 12 hours. Some deviations do occur within the fields of precipitation, the hydrological balance, surface energy balance and the radiation balance at the top of the atmosphere (Kallberg, 2009). However, this thesis has followed the recommendations of the report by Kallberg (2009) and used data in the range of 03h - 12h.

2.2.1 Terminology

In this chapter and subsequent chapters in this thesis we shall use the term “entrainment” to refer to areas where either mass or moisture is entering the boundary layer and “venting” to refer to areas where mass or moisture is leaving the boundary layer. These terms should not be confused with the entrainment and detrainment terms described in Section 2.2.2. The IFS has a 30 minute

time step but data is only archived once every three hours. For the rest of this thesis the phrase "time step" will be used to refer to this 3 hour period.

2.2.2 The boundary layer scheme

The role of a boundary layer parameterization scheme (described in (Köhler *et al.*, 2011) and the ECMWF documentation ((ECMWF, 2006b)) is to redistribute both heat and moisture throughout the model column due to the action of turbulent eddies which act on the sub grid scale. In order to do this the IFS defines two quantities that will be effectively mixed throughout the model column.

$$s_1 = gz + C_p T - L_{con} q_l - L_{dep} q_i \tag{2.1}$$

$$q_t = q_v + q_l + q_i \tag{2.2}$$

s_1 is the generalised liquid water static energy, g is the gravitational constant, C_p is the specific heat of dry air at constant pressure, T is the temperature of the air, L_{con} and L_{dep} are the latent heats of condensation and deposition of moisture and ice droplets respectively. q_t is the total water mass mixing ratio which is composed of the individual mixing ratios of gaseous (q_v), liquid (q_l) and solid (q_i) moisture. s_1 and q_t will be represented by the symbol $\mathcal{X}$ in the following description.

2.2.2.1 The boundary layer type

The type of mixing employed by the IFS is determined by the sign of the flux of virtual temperature at the surface. If this is positive or if cumulus cloud is present, then the eddy diffusivity mass flux (EDMF) is employed up to the boundary layer top or the base of the convective cloud. The EDMF scheme is also deployed in boundary layers which have additional mixing due to the presence of stratocumulus clouds at the top. If it is negative, then a scheme based upon K - diffusion profiles is used. Each of these two schemes is now described in turn.

2.2.2.2 The EDMF framework

The vertical flux $\overline{w'\mathcal{X}'}$ of a quantity $\mathcal{X}$ is given to be

$$\overline{w'\mathcal{X}'} = -K\frac{\partial\overline{\mathcal{X}}}{\partial z} + a(\overline{w}^u - \overline{w})(\overline{\mathcal{X}}^u - \overline{\mathcal{X}}) \tag{2.3}$$

where K is the diffusivity constant and z is the vertical height co-ordinate. a is the fraction of a grid square over which convective plumes act and $\overline{w}^u$ is the vertical velocity in one of these updraughts. $\overline{w}$ represents the velocity of the surrounding environment. The terms $\overline{\mathcal{X}}^u$ and $\overline{\mathcal{X}}$ represent the scalar quantity of variable $\mathcal{X}$ in the updraught and the environment respectively. The mass flux (M) of the plume can therefore be said to be equal to $a(\overline{w}^u - \overline{w})$.

2.2.2.3 The mass flux component

The second term on the right hand side of Equation 2.3 is calculated by following the properties of an individual air parcel as it moves up through the model column, and is calculated on a model level by level basis using the relationships

$$\frac{\partial\overline{\mathcal{X}}^u}{\partial z} = -\eta(\overline{\mathcal{X}}^u - \overline{\mathcal{X}}) \tag{2.4}$$

where η is the entrainment rate of environmental air into the convective plume and

$$\frac{\partial M}{\partial z} = (\eta - \delta)M \tag{2.5}$$

where δ is the rate of detrainment. Above the cloud base height (z_{cb}), δ =3.0x$10^{-4}m^{-1}$, and below (z_{cb}) δ= 0. η is given as a function of the timescale over which environmental air is entrained and mixed throughout the cloud, and the height at which entrainment is taking place. In order for these calculations to be performed the values of the updraught velocity $\overline{w}^u$ and the scalar quantity $\overline{\mathcal{X}}^u$ need to be set. For scalars this is done by assuming that value of $\overline{\mathcal{X}}^u$ at model level one directly scales with the surface fluxes. It is assumed that the vertical velocity of an updraught at model level one is a function of the area over which the updraught occurs and the standard deviation in vertical velocity.

2.2.2.4 K-diffusivity component in a daytime layer containing Stratocumulus

The K-diffusivity parameter is determined by using

$$K_h = K_h^s + K_h^t \tag{2.6}$$

where k_h^s is the K diffusivity due to the mixing caused by thermal eddies rising from the surface to the boundary layer top. K_h^t is the K-diffusivity due to the sinking of air which has been radiatively cooled at the top of stratocumulus clouds. At the boundary layer top, K_h^{entr} is due to the entrainment of air into the boundary layer from the free troposphere and may be substituted for K_h should it provide additional mixing.The value of K_h is determined for each model level using

$$K_h^s = k u_* \psi_h^{-1} \left(1 - \frac{z}{z_i}\right)^2 \tag{2.7}$$

where k is von Karmen's constant, u_* is the friction velocity, z is the height of the model level, z_i is the height of the capping inversion and ψ_h is a stability function which is a function of the Obukhov length L, the height at which buoyant production of turbulent kinetic energy dominates. The mixing due to the cooling of stratocumulus tops is described by

$$K_h^t = 0.85 k v_{cld} \frac{z}{z_i} \left(1 - \frac{z}{z_i}\right)^{\frac{1}{2}} \tag{2.8}$$

where v_{cld} is the cloud top entrainment velocity due to radiative cooling which is directly proportional to the radiative flux jump at the cloud top. At the top of the boundary layer, the entrainment of air from the free troposphere is described by

$$\overline{w'\theta_v'}^{entr} = -0.2\overline{w'\theta_v'}^{surf} - 0.2\frac{\delta R}{\rho C_p} = -K_h^{entr}\frac{\partial \theta_v}{\partial z} \approx -K_h^{entr}\frac{\delta \theta_v}{\delta z} \tag{2.9}$$

where δR refers to the jump in radiative flux at the top of the boundary layer and $\delta\theta_v$ and δz represent the jumps in θ_v and z across the boundary layer top. This is thought to be a good representation of the overturning convective thermals which penetrate through the overlying capping inversion due to an excess of momentum and drag down air of higher potential temperature Carson (1973). Similar calculations are carried out for momentum (see ECMWF 2006b for more details).

2.2.2.5 Stable layer diffusion

If a stable boundary layer is defined, then all of the mixing is caused by wind shear and as such is represented locally at each grid point as a function of the difference between the overlying and underlying winds. The IFS first makes a calculation of the Richardson number at each model level and then if the Richardson number is less than zero uses

$$K_H = \frac{l_H^2}{\psi_M \psi_H} \left| \frac{\partial U}{\partial z} \right| \tag{2.10}$$

where l is the mixing length and defined as

$$\frac{1}{l_\chi} = \frac{1}{kz} + \frac{1}{\lambda_\chi \beta} \tag{2.11}$$

where $\lambda_\chi = 150$ and $\beta = 1.0$ in the boundary layer. β is less than one above the boundary layer and scales with the formula given in ECMWF (2006b). The dimensionless gradient function is

$$\psi_H = (1 - 16\zeta)^{-1/2} \tag{2.12}$$

where ζ is a function of the height above ground and the Obukhov length.

$$K_h = l_h^2 \left| \frac{\partial U}{\partial z} \right| f_h(Ri) \tag{2.13}$$

where

$$f_h(Ri) = \frac{1}{1 + 10Ri(1+Ri)^{1/2}} \tag{2.14}$$

2.2.3 The convection scheme

2.2.3.1 Mass and moisture

The IFS convection scheme deals with the transport of: dry static energy, moisture, horizontal wind components and a passive chemical tracer. Since this thesis focuses on the transport of mass

and moisture out of the boundary layer, only the equations relevant to the transport of moisture are described here. (The large scale transport of mass is equal to that which would be parametrized by the convection scheme, its influence is not felt on the large scale mass transport within the model and as such does not need a separate parametrization (See Siebesma and Cuijpers 1995, Tiedtke 1989).

2.2.3.2 Equation for moisture

The change in moisture content of the atmosphere at any one single point due to the presence of cumulus cloud is described by:

$$\left(\frac{\partial \overline{q}}{\partial t}\right)_{cu} = g\frac{\partial}{\partial p}[M_{up}q_{up} + M_{down}q_{down} - (M_{up} + M_{down})\overline{q}] - c_{up} - e_{down} - e_{subcld} \tag{2.15}$$

where the large scale transport of mass is equal to $M_{up} + M_{down}$ which describes the net upward (up) and downward ($down$) fluxes of mass of the individual convective plumes within a grid square. The large scale specific humidity is represented by $\overline{q}$, whilst q_{up} and q_{down} are weighted averages which represent the transport of moisture by the convective plumes. c_{up} and e_{down} represent the condensation / sublimation of moisture in the updrafts and evaporation in the downdrafts. e_{subcld} represents the evaporation of precipitation in the unsaturated sub cloud layer.

Each of the terms in equation 2.15 are briefly described here, for a complete description please refer to ECMWF (2006b). The cloud updraughts are described by:

$$-g\frac{\partial M_{up}}{\partial p} = E_{up} - D_{up} \tag{2.16}$$

and

$$-g\frac{\partial M_{up}q_{up}}{\partial p} = E_{up}\overline{q} - D_{up}q_{up} - c_{up} \tag{2.17}$$

where E_{up} and D_{up} are the rate of entrainment and detrainment of mass respectively. The entrainment of mass into the convective plume is separated into two distinct processes: that which

occurs due to the turbulent exchange of mass through the cloud edges, and that which occurs due to organised inflow of mass near the cloud base. Similarly, detrainment is assumed to occur due to turbulent exchange at the cloud edges and through organised outflow at the cloud top. Cloud downdraughts are calculated from the level of free sinking which is defined to be the level where the amount of saturated air in the column becomes negatively bouyant with respect to the environmental air surrounding it. The downdraught mass flux is set to be proportional to the upward mass flux at the cloud base using

$$(M_{down})_{LFS} = -0.3(M_{up})_{base} \tag{2.18}$$

the change in mass flux with height is then calculated by

$$g\frac{\partial M_{down}}{\partial p} = E_{down} - D_{down} \tag{2.19}$$

and

$$g\frac{\partial M_{down} q_{down}}{\partial p} = E_{down}\overline{q} - D_{down} q_{down} - e_{down} \tag{2.20}$$

where E_{down} and D_{down} are the entrainment and detrainment rates within the downdraught and e_{down} is the evaporation of rain which is needed in order to maintain a saturated descent. In order to complete this set of equations we define the updraught at cloud base to be a function of convective cloud type which is described in Section 2.2.3.4.

2.2.3.3 The description of convective precipitation

The removal of moisture due to precipitation is described by

$$P_{rain}(p) = g\int_{P_{top}}^{P} (G^{rain} - e^{rain}_{down} - e^{rain}_{subcld} + M_{elt})dp \tag{2.21}$$

where the flux of rain P_{rain} at level p is defined by the variables G^{rain}, which is the conversion rate from cloud into liquid water and e^{rain}_{down} and e^{rain}_{subcld} are the evaporation rates of precipitation both

within the cloud and below the cloud's base respectively. M_{elt} denotes the contribution due to the melting of snow. A similar formulation is used for the rate of snowfall and can be found in the IFS documentation (ECMWF, 2006b).

2.2.3.4 Diagnosing presence of convection and the type

An algorithm is applied at each model time step in order to determine whether or not convection is taking place. Should the presence of convective cloud be determined the algorithm goes on to describe the cloud as shallow, mid level or deep by the use of a parcel ascent technique. The parcel ascent first diagnoses a lifting condensation level and then moves a parcel of air up through the model column level by level until the air of the parcel becomes negatively buoyant.

In all three types of convection the mass flux at the cloud base must be determined in order for the equations given in Section 2.2.3 to be applied. In the case of deep convection convective available potential energy or CAPE is used. In the case of shallow convection an initial determination of cloud base mass flux is made using the moist static energy budget as a first guess and then revising for the presence of any downdraughts. The mass flux at cloud base in mid level convection is simply assumed to be equal to the mass flux implied by the large scale flow. Details of the individual, schemes can be found in ECMWF (2006b).

2.2.4 The large scale cloud and precipitation scheme

The scheme used for the production of large scale (i.e. non convective) cloud and large scale precipitation is detailed by Tiedtke (1993). A brief description of this scheme is included here for reference. The IFS model uses prognostic equations for the change in cloud liquid water/ice content and the amount of area covered by cloud.

The prognostic equation for cloud liquid / ice (I) content depends upon the advection of moisture through the boundaries of each grid box, the rate at which moisture condenses, sublimates and evaporates. The rate that precipitation is generated within the cloud G_p is included along with source terms for boundary layer turbulence and convection. The flux of moisture through the boundary layer top into layers of Stratocumulus, should they exist is also included.

The prognostic equation for cloud fraction a depends upon the advection of a through the grid box boundaries and the formation of cloud due to convection, boundary layer turbulence and stratiform condensation processes. The rate at which cloud area diminishes due to the evaporation of water is also taken into account. The precipitation flux is described by the equation

$$P = \int (G_p - E_p)\rho dz \tag{2.22}$$

where ρ is the density of air, and E_p is the evaporation of precipitation as it falls through the atmosphere. The formation of precipitation G_p is a function of: the characteristic timescale of the conversion of cloud droplets into precipitation, the critical value for cloud liquid water content at which precipitation starts, and the specific cloud water content. E_p is determined using the scheme of Kessler (1969) (which is cited in (Tiedtke, 1993)) which gives the evaporation rate as

$$E_p = a_p 5.44 \times 10^{-4}(q_s - q)\left[\left(\frac{p}{p_0}\right)^{1/2}\frac{1}{5.9\times 10^{-3}}\frac{p}{a_p}\right]^{0.577} \tag{2.23}$$

where a_p is the fractional precipitation area and $a_p - a$ is the cloud-free area where precipitation occurs due to cloud in overlying layers. A threshold in terms of the grid box relative humidity is further defined whereby if it is exceeded evaporation of precipitation becomes zero. This threshold is described by

$$RH_{crit} = 0.7 + 0.3\frac{a_p}{1-a} \tag{2.24}$$

Here the assumption is made that in clear skies the relative humidity of the grid box that is increased due to the evaporation of precipitation is a function of the fractional area of precipitation within that grid box. The formation and evaporation of the individual cloud types are determined separately based upon the individual characteristics of each cloud. Full details of this are given in Tiedtke (1989) and the numerical implementation of the scheme is described in ECMWF (2006b).

2.2.5 Model data

As has been previously stated in Section 2.1.2 this project uses the IFS data set which is derived from a forecast model that has been initialised by data from the ERA-Interim reanalysis data set.

For clarity the time steps are presented as red squares in Figure 2.1. For the production of each of the climatologies in this chapter the first 21 model levels of the IFS have been used, which correspond to a height of roughly 4km within the mid latitudes, 1km greater than the maximum boundary layer heights for the globe as described by Stull (1989). The u and v components are only stored on the ECMWF MARS data archive in the form of vorticity and divergence and must be converted back to u and v components of wind using code running at ECMWF. It was necessary to do this in order to calculate the divergence of air within a sloping boundary layer as described in section 2.4.

2.3 Defining the boundary layer top

In order to quickly calculate the boundary layer top over numerous time steps a simple definition was needed. The definition chosen was that of Boutle (2009) who adapted the definition used by Sinclair *et al.* (2009) and Troen and Mahrt (1986) to include the additional variable of moisture. The boundary layer height is found by computing the bulk Richardson number for each successive model level within a column, finding the model level where the value of the critical Richardson number (0.25) is exceeded and then linearly interpolating between the model level below and this level to find a height that corresponds to the top of the boundary layer. The bulk Richardson number is defined by Stull (1989) to be

$$Ri(z) = \frac{(\frac{g}{\theta_s})(\theta_{vz} - \theta_s)z}{(u_z)^2 + (v_z)^2} \tag{2.25}$$

where θ_{vz} is the virtual potential temperature at model level z, u_z and v_z are the horizontal wind components at model level z and g is the acceleration due to gravity. θ_s is a temperature near the surface defined as

$$\theta_s = \theta_1 + b\frac{\overline{w'\theta'}_s}{(u_*/\phi_m)} \tag{2.26}$$

where θ_1 is the temperature at the lowest model level (approx 10m). 8.5 is given by Holtslag and Boville (1993) as a suitable value for b. u_* is the friction velocity and ϕ_m is the dimensionless vertical wind gradient given by

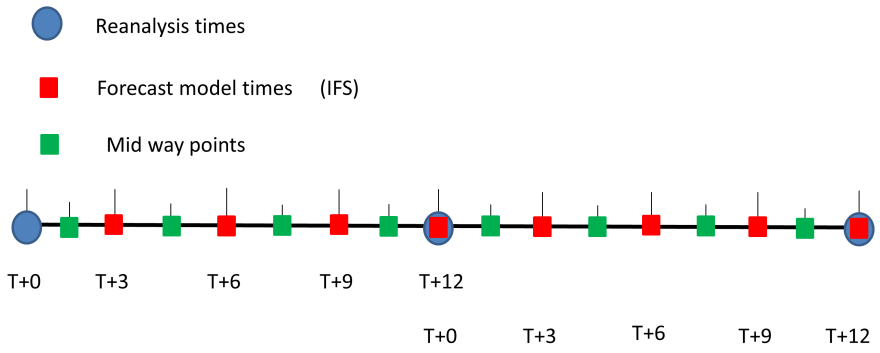

Figure 2.1: The IFS cycle (x2). Each time at which IFS data is available are shown as a red square. The ECMWF ERA-Interim time steps from which the forecast model is initialised are represented by blue circles. Mid way points are represented by green squares. The time that the model was run for is given by the time steps indicated underneath.

$$\phi_m = (1 - 15\frac{z}{L})^{-\frac{1}{4}} \tag{2.27}$$

The second term of equation 2.26 is only supplied when the Obukhov length L defined as

$$L = -\frac{u_*^3}{k(g/\theta_1)\overline{(w'\theta')}_s} \tag{2.28}$$

is negative (i.e. regions where the lowest level of the atmosphere is unstable to convective mixing), k is von Karman's constant (approx 0.4). $\overline{(w'\theta')}_s$ is the flux of sensible heat from the models surface. A value for u_* is not readily available from the ECMWF data server and so this data was reconstructed using the formulae provided in Holtslag and Boville (1992). Specifically

$$\overline{(w'u')}_s = -C_M|V_1|u_1 \tag{2.29}$$

$$\overline{(w'v')}_s = -C_M|V_1|v_1 \tag{2.30}$$

where $|V|$ is the absolute value of the horizontal wind velocity at model level 1 and

$$C_M = C_N f_M(Ri_0) \tag{2.31}$$

$$C_H = C_N f_H(Ri_0) \tag{2.32}$$

The neutral exchange coefficient is given by

$$C_N = \frac{k^2}{(ln((z_1 + z_{0M})/z_{0M}))^2} \tag{2.33}$$

where z_1 is the height of model level 1 and z_{0M} is the roughness length as defined for momentum. Here the surface bulk Richardson number is given by

$$Ri_0 = \frac{gz_1(\theta_{v1} - \theta_{v0})}{\theta_1 |V_1|^2} \tag{2.34}$$

Since the values of C_M and C_H are strongly dependent upon the stability of the atmosphere, the stability functions, which depend on the bulk Richardson number, are defined by Louis (1979) as:

$$f_{M/H} = 1 - \frac{MHRi_0}{1 + 75C_N([(z_1 + z_{0M})/z_{0M}]Ri_0)^{\frac{1}{2}}} \tag{2.35}$$

with MH representing a constant which is equal to 10 and 15 for momentum and heat respectively. u_* is given by

$$u_* = \sqrt[4]{\overline{u'w'}^2 + \overline{v'w'}^2} \tag{2.36}$$

The major disadvantage of using the bulk Richardson number is that it may underestimate the turbulence in the atmosphere at such time as the atmosphere is experiencing hysteresis (e.g. when the boundary layer is collapsing during the evening) (McTaggart-Cowan and Zadra, 2015) or when the bulk Richardson number smooths effects that would otherwise be picked up by use of a gradient Richardson number (Stull, 1989) (e.g. during the occurrence of the nocturnal jet, when increased mixing can occur due to turbulence caused by the local wind shear Barlow *et al.*, 2011). However, these errors are not expected to be significant, and the benefit of increased accuracy gained by using the gradient Richardson number does not outweigh the extra computational cost of the calculation. The choice of definition in boundary layer top is consistent with the choice of boundary layer top chosen by Zhang *et al.* (2013) and De Wekker *et al.* (2004) in their respective studies.

The main advantages in using the bulk Richardson number in defining the top of the boundary layer is that it can be applied to all types of boundary layer (e.g. convective, neutral etc) and as

such does not need any prior knowledge of the state of the atmosphere at individual grid points. The bulk Richardson number also allows us to compare our work directly with that of Sinclair *et al.* (2009) and Boutle (2009), making some comparisons between their idealised cyclones and our "real world" scenarios. The bulk Richardson number method is also a popular choice for other studies within the literature (e.g. De Wekker *et al.* 2004).

2.4 The boundary layer mass budget equation

The boundary layer mass budget equation was first described by Sinclair *et al.* (2009)

$$\frac{\partial \hat{\rho}}{\partial t} = \underbrace{\rho_h \left(\frac{\partial h}{\partial t} - \tilde{\mathbf{U}}.\mathbf{n} \right)_h}_{\text{entrainment term}} - \underbrace{\hat{\rho} \left(\frac{\partial \hat{u}}{\partial x} + \frac{\partial \hat{v}}{\partial y} \right)}_{\text{divergence term}} \tag{2.37}$$

where ρ is the density of air, h is the height of the boundary layer and t is time. $\tilde{\mathbf{U}}_h$ is the three dimensional wind vector at the top of the boundary layer and n is a vector normal to the boundary layer top defined to be

$$n = \frac{1}{[1 + (\partial h/\partial x)^2 + (\partial h/\partial y)^2]^{1/2}} \left(-\frac{\partial h}{\partial x} - \frac{\partial h}{\partial y} + 1 \right) \tag{2.38}$$

u is the component of the wind in the x direction and v is the component of the wind in the y direction. A " $\bigwedge$" symbol is used to indicate that the variable in question has been integrated between the surface and the boundary layer top. A subscript h indicates a variable that has been evaluated at the top of the boundary layer.

The "entrainment term" in Equation 2.37 is made up of two separate components. The first component represents the change in boundary layer height with time ($\frac{\partial h}{\partial t}$) which occurs due to the diurnal cycle Stull (1989) and during the passage of a synoptic system (Stull 1989 and Sinclair *et al.* 2009). The second component, $\tilde{\mathbf{U}}_h$, represents the advection of material through the top of the boundary layer surface. The second term in Equation 2.37, labelled as the "divergence term", describes the transport of boundary layer air horizontally from one location to another. The point of departure of this air is associated with divergence whilst the point of destination is described

by convergence. This gives us a purely Eulerian perspective on the flow of air but does not give us any information on the path taken by an individual air parcel (Stohl, 2001).

2.5 The numerical method

In the previous section we described the boundary layer mass budget equation. This equation describes the change in mass of the boundary layer in the real atmosphere where both spatial and temporal changes can occur on small scales. In contrast, the data set described in Section 2.2 is from a spectral model with a fixed spatial resolution and data which is only available at 3 hourly time periods. The data associated with each variable (e.g. temperature), is given for a fixed point in space and time ECMWF (2006a). In order to solve the mass budget equation a suitable numerical method was required, which would take into account these spatial and temporal variations and allow the calculation of the mass budget with the minimum amount of error. The method used for the results presented in section 2.6 and the subsequent chapters of this thesis proved to be the representation which produced the smallest errors in a balanced mass budget over for a single grid column and globally over a three month period. This method is described below.

2.5.1 Using a grid box interpretation of the data

In order to describe the ventilation of the boundary layer, a surface needs to be defined for mass to be transported through. This was achieved by visualising a box around each grid point with the grid point itself located at the centre (see Figure 2.2). In order to represent the flow through each side of the grid box, this single point measurement of velocity must be transformed into an average flow through the side of the grid box in question. (E.g. Imagine a situation where three grid boxes are stacked one above another. The lower box has a positive velocity in the x direction, the middle a negative velocity and the box on top a positive velocity. Each grid box is the same width and depth, but the height is different for each. If we were to try and calculate the flow through the right hand side of the middle grid box; using the point velocity alone we would overestimate the flow. However, by taking into account the flow above and below the middle grid

box we may approximate the flow at each half level, between grid points. Using these two new velocities we can estimate the average flow through the side of the grid box).

In order to correctly represent the location of each data point we must use a co-ordinate system which describes each point in space in terms of its Cartesian components. In order to do this the atmospheric pressure associated with each variable was computed using

$$P_k = \frac{1}{2}(P_{k-1/2} + P_{k+1/2}) \tag{2.39}$$

where

$$P_{k-1/2} = A_{k-1/2} + B_{k-1/2}P_s \tag{2.40}$$

where k is the model level and $k \pm 1/2$ are the corresponding half levels above and below level k. A and B are constants provided with the model data files. The value of pressure is then converted to a height using the assumption that

$$\delta h = \frac{\delta P}{-\rho g} \tag{2.41}$$

where ρ is the density of air within each grid box (see Section 2.5.2 for the calculation of ρ). g is set to be the gravitational acceleration, set to be equal to 9.80665. Both the pressures and then the heights are thus worked out up through the model column, starting from the bottom.

2.5.2 Calculating the divergence within the boundary layer

The divergence term is calculated first. In order to do this the flow of air through the side of an individual element is calculated. In order to do this we must first linearly interpolate each variable between levels in order to obtain the values at their respective half levels (Figure 2.3). Taking the average of these intermediate values will now give us a value for each variable which is representative of the horizontal transport of air. This is shown for u below

$$u_{i,j,k} = \frac{1}{2}(u_{i,j,k-1/2} + u_{i,j,k+1/2}) \tag{2.42}$$

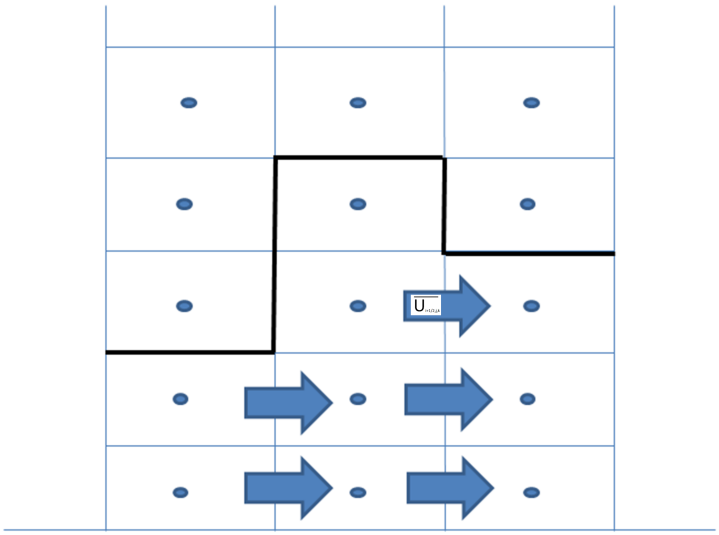

Figure 2.2: A representation of the grid box structure used. Each data point is represented by a point marked in blue. The flux through the sides of the box are represented by the blue arrows which represent the average flow of material between boxes. The boundary layer top is represented by the black line.

This technique was used for the horizontal components of velocity, pressure and temperature. The pressure (P) and temperature (T) were then used to calculate the density of air within the grid box using:

$$\rho = \frac{P}{RT} \tag{2.43}$$

where R is the universal gas constant given a value of 287.04 $JK^{-1}kg^{-1}$.

This value must now be adjusted by averaging the values of $u_{i,j,k}$ between two adjacent grid boxes. Therefore, in the x direction the flux through the side of a grid box becomes

$$u_{i+1/2,j,k} = \frac{1}{2}(u_{i,j,k} + u_{i+1,j,k}) \tag{2.44}$$

This flux is then integrated to the top of the boundary layer at point i. A similar calculation is performed for the flux of mass out of the other side of the grid box. This calculation is depicted in Figure 2.4. The calculation is then repeated in the y direction.

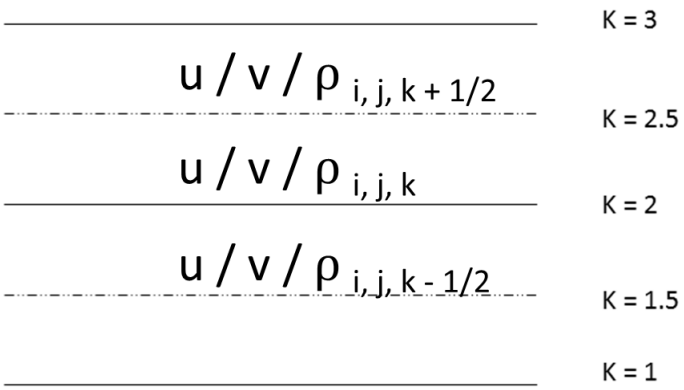

Figure 2.3: The model levels here are represented by a value k with i and j representing the indices of adjacent grid boxes. Using two model levels, e.g k=2 and k=3, we can do a linear interpolation in order to get the values of u, v and ρ at an intermediate level that we shall call $k+1/2$.

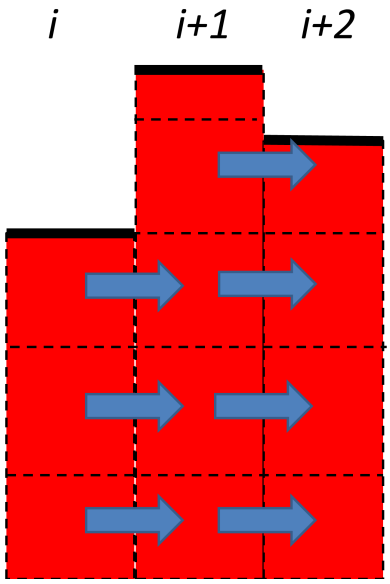

Figure 2.4: The divergence term of the boundary layer mass budget equation (Equation 2.37). Grid boxes are represented by dashed black lines and the boundary layer top is indicated by a solid black line. Mass transports through the sides of each grid box are represented by the blue arrows. The diagram is orientated along the x - axis. (Note that mass transports only take place up to the boundary layer top defined by the grid boxes located at i and $i+2$.)

2.5.3 Venting in the vertical

The term labelled "entrainment term" in Equation 2.37 has been split up into its vertical and horizontal components thus:

$$\underbrace{\rho_h \left(\frac{\partial h}{\partial t} - \tilde{\mathbf{U}}.\mathbf{n} \right)_h}_{\text{entrainment term}} = \underbrace{\rho_h \left(\frac{\partial h}{\partial t} - w \right)_h}_{\text{vert vent}} + \underbrace{H_h}_{\text{hor vent}} \tag{2.45}$$

The two terms on the right hand side of Equation 2.45 are calculated separately. In order to calculate the term labelled "hor vent" it was necessary to first recalculate the boundary layer divergence as described in the previous section, but instead of using the boundary layer height at grid points i and $i+2$ the central grid at point $i+1$ was used. This calculation is depicted in Figure 2.5. By subtracting this new calculation of divergence from the original calculation done in Section 2.5.2 we obtain a number for the flux of mass out of the top of the boundary layer in the horizontal direction (H_h).

In order to calculate "vert vent" the vertical velocities are taken on the model levels (k) above and below the boundary layer top, and linearly interpolated between them in order to estimate the vertical velocity at the top of the boundary layer (w). In order to compute the mass flux through the top of the boundary layer we must also take into account vertical motion of the boundary layer top. Combining this with the vertical velocity at the boundary layer top will give us an effective venting velocity in the vertical. This can then be combined with the density of air at the top of the boundary layer to give us the mass flux through the upper surface (see Equation 2.45). However, using these methods the boundary layer mass budget equation could not be balanced over land during non daylight hours when the boundary layer was at its lowest. By looking at many time frames it was determined that the vertical velocities provided by the ECMWF MARS archive were the reason that the budget could not be balanced.

In order to understand this problem it is instructive to consider the diagnostic equation used by ECMWF for ω. This is given to be

$$\omega = -\int_0^{\eta} \nabla \cdot \left(v_H \frac{\partial p}{\partial \eta} \right) d\eta + v_H \cdot \nabla p \tag{2.46}$$

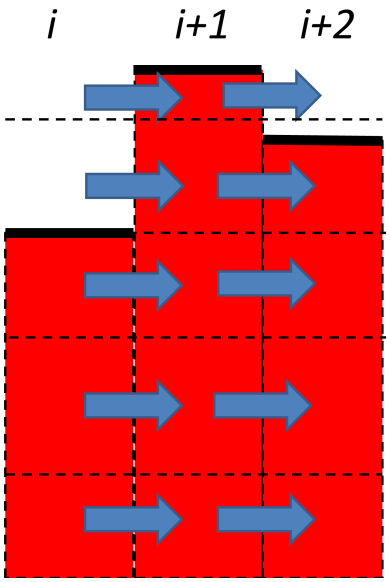

Figure 2.5: The divergence of air at point $i+1$. All symbols are the same as for Figure 2.4.

where ω is the pressure velocity given in Pas^{-1} and η is the vertical coordinate used. Here ∇ is the horizontal gradient operator in spherical coordinates, v_H is the horizontal wind and p is the pressure. The η coordinate system defines the top of the atmosphere as being equal to 0 and the surface as being equal to 1. The wind is thus calculated from the top of the atmosphere down. There are two possible sources of error that could lead to anomalously high vertical velocities near the model surface

1. Rounding errors in the calculation of ω.
2. The diagnostic described in equation 2.46 does not contain a bounding condition that would constrain the vertical velocities to zero at the Earth's surface.

It was therefore decided to recalculate all the vertical velocities for use within the climatologies presented in this thesis. These were calculated by

$$w = \int_0^Z \left(\frac{\partial u}{\partial x} + \frac{\partial v}{\partial y} \right) dZ \tag{2.47}$$

where u and v are the horizontal components of velocity in the x and y directions respectively, and Z is the height in the vertical z direction. w is the vertical velocity, given in Cartesian coordinates

and measured in ms^{-1}. (Note that this equation uses the Boussinesq approximation in order to neglect density variations which are assumed to be small. This is valid given our method for calculating the mean density at each grid box described in Section 2.5.2). The velocities were checked at the boundary layer top over the oceans and found to be in good agreement with those supplied by ECMWF.

The time frame over which $\frac{\partial h}{\partial t}$ needed to be calculated was tested using boundary layer heights that were six hours apart with the vertical velocity taken from the intermediate time step. However, this occasionally produced some unusually large values of boundary layer ventilation and entrainment, when tested over the mid latitudes. In order to smooth out these spikes in ventilation / entrainment, all of the data from each time step was averaged with the next time step in order to produce new averaged values at a mid point. The vertical velocities were then recalculated for this mid point value and the boundary layer heights were used at each adjacent IFS forecast model time step in order to calculate $\frac{\partial h}{\partial t}$. Although, this increased the amount of computational effort involved when the mass budget was calculated over a season any errors produced were significantly reduced. This means that the mass budget is produced every 3 hours at intermediate "mid points" between the IFS forecast times (see Figure 2.1).

2.6 Results

2.6.1 A case study 25th November 2009 00 UTC

In order to verify that both our definition of the boundary layer height and our mass budget calculation are performing correctly we have selected a suitable case study, which can be compared with a similar case from the existing literature on boundary layer ventilation. We have selected to highlight the ventilation and boundary layer structure associated with a mid latitude cyclone due to the large changes in boundary layer structure and complexity of the associated ventilation processes when compared with the other mechanisms of ventilation that have been highlighted in the introduction chapter. On the 25th November 2009 a mid latitude cyclone had developed over the UK and its centre of low pressure had dropped to around 960 hPa. A comparison between the operational analysis produced by the UK Met office at 00 UTC and the IFS data used for the

specified time revealed that the mean sea level pressure pattern was accurately represented both in terms of the location of the low centre and the extent to which the pressure has dropped. A full description of the development of this cyclone is provided in Chapter 3 along with a more detailed verification of the IFS forecast. For the purposes of this chapter a single time-step will be analysed at 00 UTC and compared with the idealised cyclone studied by Sinclair *et al.* (2009).

2.6.1.1 The boundary layer structure

Figure 2.6 a) (Hereafter referred to as CS1) shows the boundary layer top overlayed with the mean sea level pressure pattern. If compared with Figure 5 a) of Sinclair *et al.* (2009) (Hereafter referred to as S1) we can observe several similarities which make this a good case study and time step with which to make our comparison.

Both S1 and CS1 have a low pressure centre of around 960 hPa. To the south east and south west of the low pressure centre two high pressure centres are prominent in both cases, although, in the case of CS1 these are between 4 - 9 hPa higher than in S1. In both S1 and CS1 the boundary layer structure shows similar characteristics although the reader should be mindful of the differences in colour scales used, as in general the boundary layer is shallower in CS1 than in S1. In both studies the highest boundary layer tops appear to the west of the troughing in the isobars which is indicative of the presence of a cold frontal boundary (Sansom, 1951).

Lower boundary layer tops are present within the region of troughing in both S1 and CS1 which marks a line that runs from the centre of low pressure to the southern most tip of the cyclonic disturbance. To the east, the boundary layer top is depressed in CS1, which is probably due to the time of day which will be characterised by low (or negative) heat fluxes from the land. This, coupled with the low wind speeds due to the low horizontal gradients in MSLP create the conditions which are associated with the nocturnal boundary layer. In contrast the idealised study of S1 does not have any land included and as such the boundary layer tops begin to rise the further eastwards you go.

In both CS1 and S1 the black line drawn indicates the location of a cross section which is depicted for both studies in part b of each figure. To the west of CS1 b and S1 b both cross sections show good examples of a convective boundary layer rising to 1.8 km and 2.6 km respectively. In

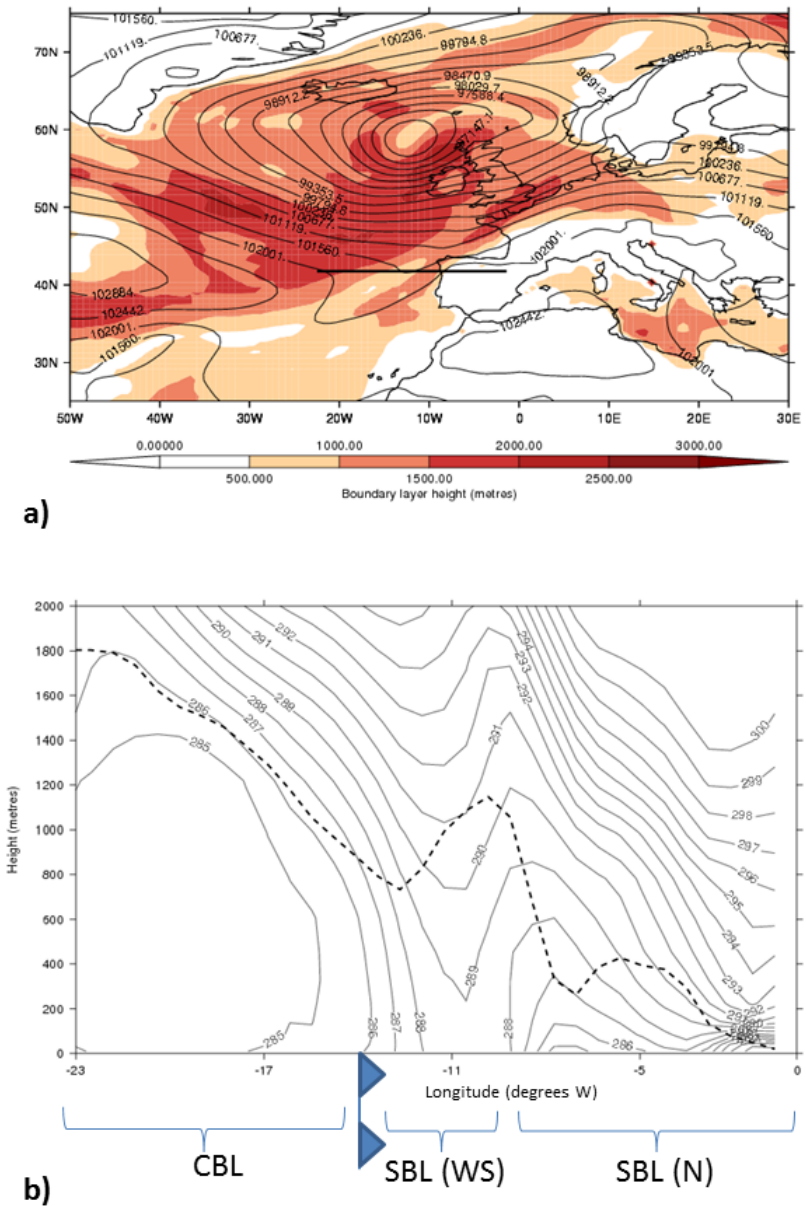

Figure 2.6: a) The boundary layer top during a mid latitude cyclone on the 25th November 2009 at 00 UTC. Overlayed is the mean sea level pressure and the black line represents the horizontal extent of the cross section presented in b). b) shows a horizontal cross section through the cold front of the mid latitude cyclone. The contours show potential temperature and the boundary layer top is indicated by the dashed line. The three regions indicated are a Convective boundary layer (CBL), a stable boundary layer in the warm sector (SBL (WS)) and a stable boundary layer induced by the cooling of the land overnight (SBL (N)). The position of the cold front is also shown.

both studies the cold front has been marked by a sharp horizontal gradient in the surface potential temperature (Sanders, 1999). To the east of the cold front the top of the boundary layer lowers to a height of 800 metres in CS1 and 500 metres in S1 this is followed by a brief rise in boundary layer top in both studies to a height of about 1.2km. Further east however, the similarity between the two cases ends. For the reasons discussed in the previous paragraph the boundary layer top drops rapidly due to presence of land in CS1 whilst gradually regaining its height of 2.6 km to become a convective boundary layer once again in S1. The similarities between the two cases, that have been outlined above, show that the case study (CS1) is an ideal choice with which to compare the results of the mass budget calculation. Conversely, the two case studies also confirm that the idealised modelling study of Sinclair *et al.* (2009) managed to accurately depict the detailed changes in the boundary layer structure that are caused by the passage of a mid latitude cyclone.

2.6.1.2 The Mass budget equation

In Figure 2.7 the results of the mass budget calculations are shown for the same time as presented in Figure 2.6. The Figures 2.7 a - c (Known here on in as CS 2 - 3 can be contrasted with Figures 9 b, 9 a and Figure 8 (known as S2 - 3) in Sinclair *et al.* (2009). (Note that in CS2 the colour scheme has been reversed from that shown in S2 in order to remain consistent with the climatologies presented later on in this thesis. S2 does not include the $\frac{\partial h}{\partial t}$ term, which is assumed to be negligible in the study by Sinclair *et al.* (2009) who only used a 15 minute time step for their data.)

CS2 shows the boundary layer ventilation rate (equivalent to -1.0 x "entrainment term" of Equation 2.37 overlaid with MSLP contours). The frontal locations have been subjectively analysed based upon the troughing of the isobars (Sansom, 1951) and large gradients in the contours of surface potential temperature (Sanders, 1999)(not shown). (Note that the system has been subjectively analysed based upon the scenario of frontal fracture taking place and thus follows the Shapiro Keyser model Shapiro and Keyser 1990.) Troughs have been analysed by picking out areas of high boundary layer ventilation that do not lie along large gradients of surface potential temperature. The analysis compares favourably with the one produced by the met office for this time and agrees upon the location of the three main fronts and the three major troughs. Directly to the east of the cold front in CS2 we see a large, elongated line of ventilation which corresponds

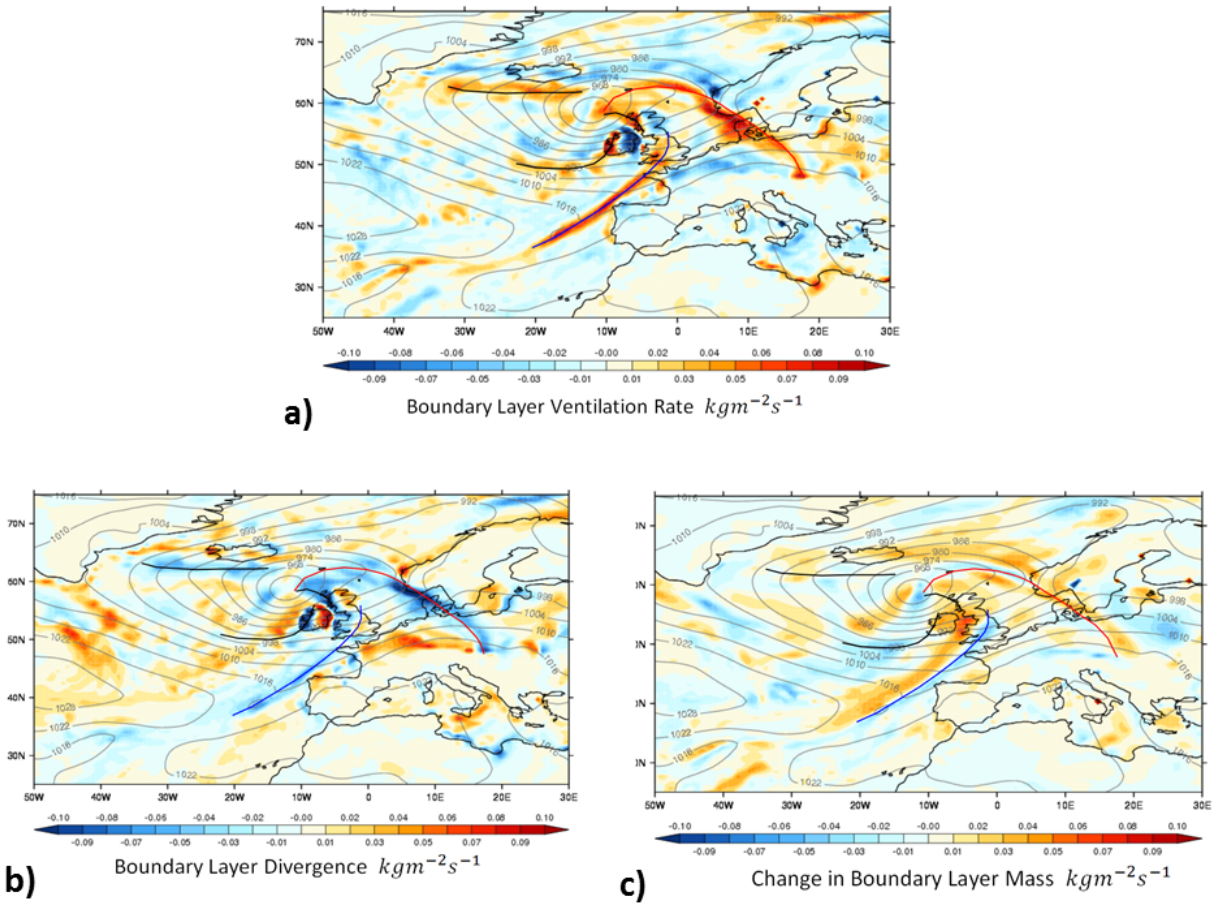

Figure 2.7: Three figures showing the mass budget of the boundary layer. a) depicts the venting of the boundary layer (-1.0 x "entrainment term") and the position of the cold front (blue) and warm front (red) which have been analysed with the help of surface potential temperature contours (not shown) and mean sea level pressure (gray). Troughs (black) are also included. b) depicts the divergence of air and c) shows the overall change in mass.

well with the ventilation seen in S2. However, the strong line of ventilation adjacent to the warm front and the occlusion does not appear in the plots depicted in S2 and in combination with the presence of troughs highlights the differences between the dry idealised systems of S2 with the more realistic simulation produced by the IFS.

An area of strong boundary layer entrainment exists over the eastern coast of Ireland which is consistent with the idea of a dry intrusion described in the conceptual model described in Chapter 1. This matches up well with the weak area of entrainment behind the cold front in S2, the strength of which is abnormally large when compared with its surroundings. The intensity of the ventilation produced along the trough line over the western coast of Ireland is similarly as strong. I would like to hypothesise that this area of entrainment is due to the dry intrusion which has been intensified by a mesoscale circulation.

If we apply the theory of conservation of mass to the boundary layer mass budget equation then; the removal of mass by a ventilation mechanism implies that mass will move from other areas of the system to replace that which is lost. In the case of Sinclair *et al.* (2009) it was suggested that this mass came from regions associated with the two large anticyclones either side of the cold front. In CS3 two areas of mass convergence can be identified; one to the east of the cold front and one which appears directly under the warm front. An area of divergence exists, located at 5° E and 48° N, which would account for these two areas of convergence. However, exactly where the air comes from is unknown and will be investigated in Chapter 3.

In Figure CS4 we see a similar picture to that described in S4 with a loss of mass associated with the warm conveyor belt and a gain of mass behind the cold front. Additionally, we find a slight gain in mass along the area depicted by the warm conveyor belt and a loss of mass along the line of the occlusion.

Once again, as with the comparison of boundary layer top, we find that the pattern of ventilation within the case study matches the general patterns of ventilation in the idealised system extremely well. This section has been used to verify that the numerical method used for solving the boundary layer mass budget equation, over a three hour time step, can accurately recreate the patterns of ventilation seen in an idealised study. We have confirmed that a major area of mass loss from the boundary layer is along the cold front. In addition we have found another area of

mass loss exists which is coincident with the point at which the warm front makes contact with the Earth's surface. Additional areas of ventilation have been noted in the presence of troughs, as analysed by the met offices operational analysis. These areas of ventilation are increased when air is raised up over the land surface. Ventilation over land due to the collapse of the boundary layer is minimal when compared to the ventilation associated with the cyclone. These factors combined give us confidence in our ability to create a climatology of boundary layer ventilation.

2.6.2 Climatologies of the boundary layer top

Before we look at the climatologies of boundary layer ventilation, it is first instructive to view some climatologies of the boundary layer top. Comparing these climatologies with others in the published literature will give us further confidence in our climatologies of ventilation that are presented in Section 2.6.3. The climatology of boundary layer top for the period 1979 - 2009 has been computed and is presented for the four seasons DJF (December, January and February), MAM (March, April and May), JJA (June, July and August) and SON (September, October and November) in figures 2.8 a-d.

In Figure 2.8 a we have plotted the boundary layer height climatology for DJF with the mean sea level pressure overlaid for the same period. We see low boundary layer heights of 400 m or less over much of continental Europe and North America, whilst over the oceans higher boundary layers of 1400 m or more can be seen to coincide with the higher sea surface temperatures of the Atlantic Gulf Stream and the Kushiro current in the western Pacific. The discrepancy between the heights of the boundary layer over land and over ocean is a consequence of the strong diurnal temperature cycle that typically acts over land in contrast to over the sea surface where temperatures remain fairly constant over the course of 24 hours. High boundary layers are also seen off the south coast of Greenland where colder arctic air masses have been advected south over warmer Atlantic waters by the well established centre of low pressure over the Greenland and Norwegian seas (See gradient in MSLP contours). Further to the south we see the subtropical high pressure regions, both to the north and the south of the equator with heights of typically 800 metres. In the tropics, boundary layer heights are typically slightly lower due to the lower wind speeds experienced in this region and cleanly divide the two regions of the subtropical highs in the northern and southern hemispheres. The extremely low tops that can be seen near the western coastlines in the

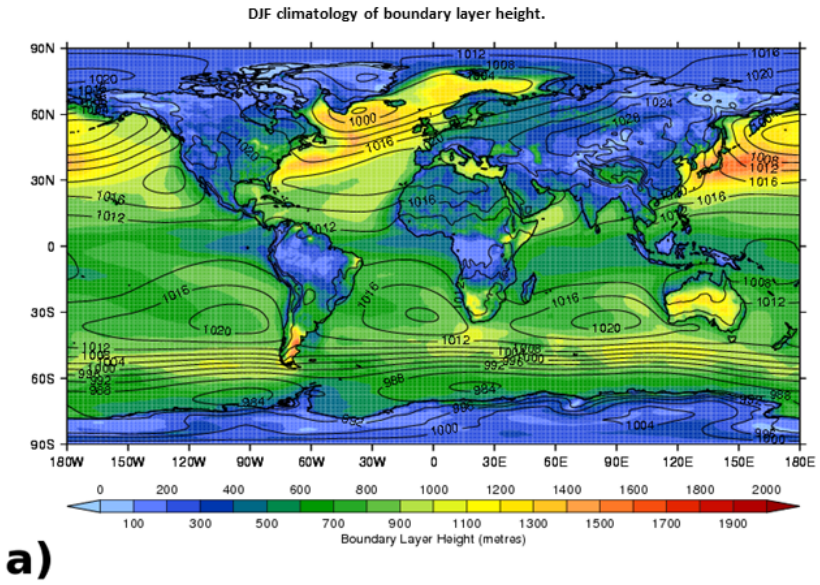

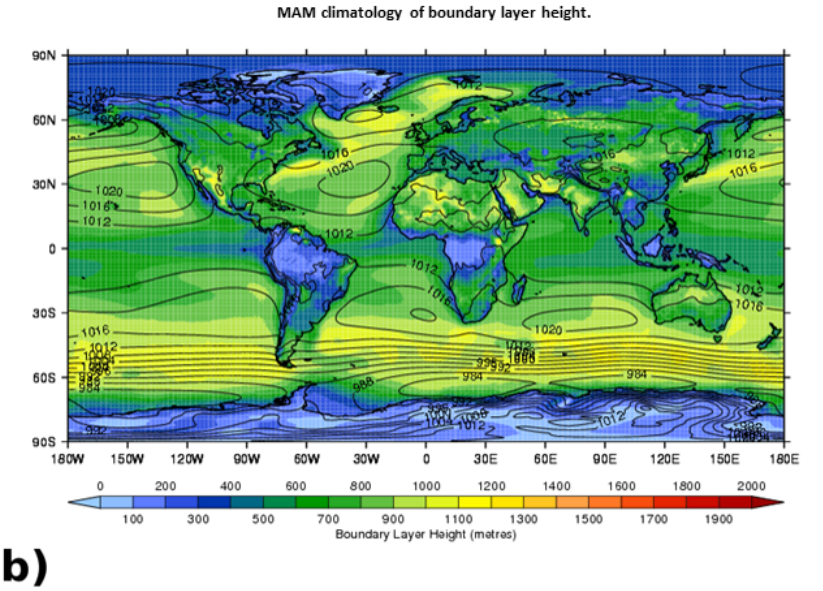

Figure 2.8: A mean climatology of height of the boundary layer for each of the four seasons (DJF, MAM, JJA, SON) for the years 1979 - 2009. Overlaid on top of each figure is the climatological average value of mean sea level pressure.

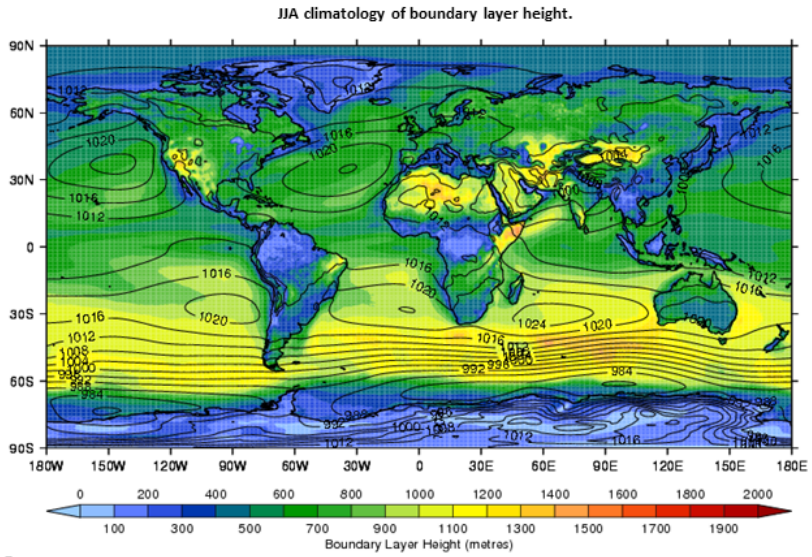
JJA climatology of boundary layer height.
90N
60N
30N
0
30S
60S
90S
180W 150W 120W 90W 60W 30W 0 30E 60E 90E 120E 150E 180E
0 200 400 600 800 1000 1200 1400 1600 1800 2000
100 300 500 700 900 1100 1300 1500 1700 1900
Boundary Layer Height (metres)

c)

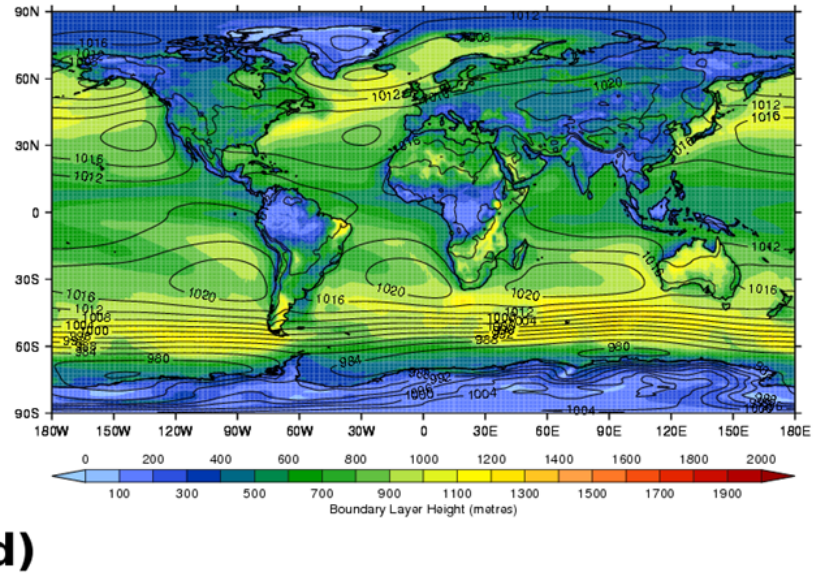
SON climatology of boundary layer height.
90N
60N
30N
0
30S
60S
90S
180W 150W 120W 90W 60W 30W 0 30E 60E 90E 120E 150E 180E
0 200 400 600 800 1000 1200 1400 1600 1800 2000
100 300 500 700 900 1100 1300 1500 1700 1900
Boundary Layer Height (metres)

d)

equatorial region are attributed to the lower than average sea surface temperatures which can be found in these regions (Reynolds and Smith, 1995). The southern hemispheric storm track is less pronounced than those in the north with an average height of 1000 metres. South Africa, Australia and the southern tip of South America (Argentina) have the highest boundary layer heights over the land, driven by the summertime convective thermals.

Figure 2.8 c shows the boundary layer height for JJA, again with the mean sea level pressure overlaid. In the northern hemisphere over land boundary layer heights are now typically up to 700 / 800 metres in height with notable exceptions over the Tibetan plateau, the Rocky mountains, the Sahara and the Arabian peninsula. The storm tracks are no longer identifiable in either the Atlantic or Pacific oceans, which are dominated by the subtropical highs that have now extended further north into the mid latitudes. Boundary layer heights have been suppressed over Australia, South Africa and Argentina. The storm track in the southern hemisphere is now much stronger with the highest boundary layer heights being to the south east of South Africa. In the northern hemisphere the storm tracks are weaker and this is the only season where the storm tracks are no longer distinguishable by raised boundary layer heights. The two climatologies for SON and MAM (Figures 2.8 b and d) show the transitions between DJF and JJA. Both of these plots show moderate increases in boundary layer height over both the Pacific and Atlantic oceans. Over land higher boundary layer heights are typically associated with the summer season and preceding spring season for each respective hemisphere.

It should be noted that several different climatologies of boundary layer height have been produced on the global scale. (e.g von Engeln and Teixeira 2013). In general the calculation that we have done produces similar results to that performed by von Engeln and Teixeira (2013). Where differences do occur it should be noted that the ventilation will be similarly altered at these points. The height climatology calculated by von Engeln and Teixeira (2013) in general exhibits higher values than have been presented here. This is most probably due to the fact that we have presented results based on a calculation of the bulk Richardson number and thus obtain a boundary layer height that is variable, not only over the course of a diurnal cycle due to changes in the surface heat flux but also due to the changes in the wind. e.g. If the winds are lower we obtain a lower boundary layer height as there is less mechanical turbulence generated at the surface. Whereas the calculation which bases the boundary layer top on a decrease in relative humidity,

such as in von Engeln and Teixeira (2013) does not take into account these effects.

This section has shown that the definition of boundary layer top used in this thesis is consistent with the methodologies used by other researchers. In particular, the strengths that are attributed to this method are the fact that it takes into account the changes in boundary layer structure due to the diurnal cycle over land and represents changes in height which are attributed to the variation in sea surface temperature.

2.6.3 Climatologies of ventilation

Four seasonal climatologies of boundary layer ventilation have been computed and are shown in Figure 2.9. The discussion of these Figures will be separated out into three sections. First, some aspects of the ventilation in Tropical regions will be discussed and put into context with the current literature concerning the Inter-tropical Convergence Zone. This is important, because, although the majority of this thesis deals with the northern hemisphere mid-latitudes, the tropics are undoubtedly a source of large amounts of moisture Trenberth and Stepaniak (2003), which we hypothesise will be transported out of the boundary layer along with the large amounts of mass that can be seen to exit the boundary layer along the ITCZ in Figure 2.9. Second, the ventilation of mass in the Northern hemisphere will be examined and compared to some studies of storm tracks in the literature. Finally, The ventilation pattern in the Southern hemisphere will be discussed and related to ventilation by mid latitude weather systems in the storm track. Comments will also be made about the ventilation over Southern Africa, Australia and South America and the continent of Antarctica.

2.6.4 The tropics

The most prominent feature, in terms of its length and consistency, in all four of the plots shown in Figure 2.9 is the strong line of ventilation located near to the equator (both to the north and south) encircling the entire globe. This line is continuous over the oceans and broken only by the intervening land masses of America, Africa and Asia. This line of ventilation matches the location of the ITCZ as described by both Waliser and Gautier (1993) and Berry and Reeder (2014), with

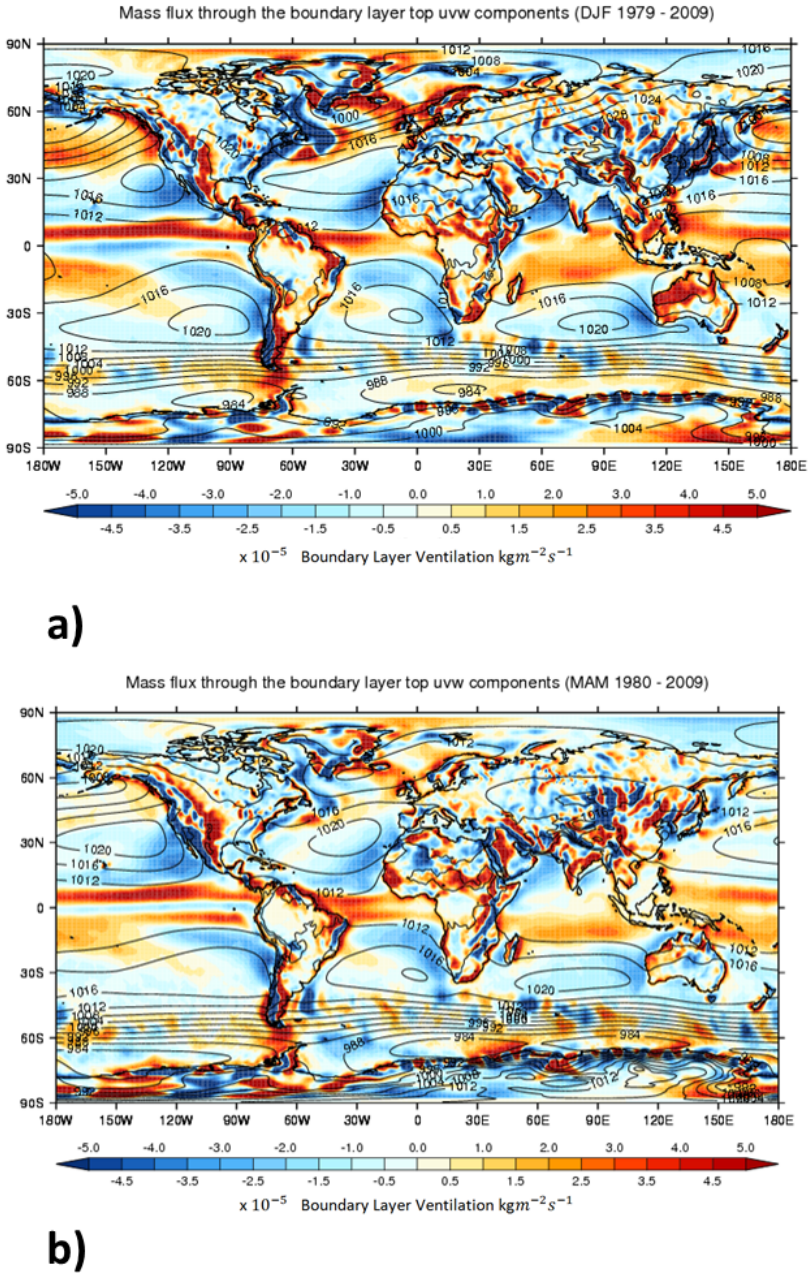

Figure 2.9: A mean climatology of the mass flux through the boundary layer top (-1.0 x "entrainment term") for each of the four seasons (DJF, MAM, JJA, SON). Includes components of ventilation in both the vertical and the horizontal direction. Overlayed on top of each figure is the climatological average value of mean sea level pressure.

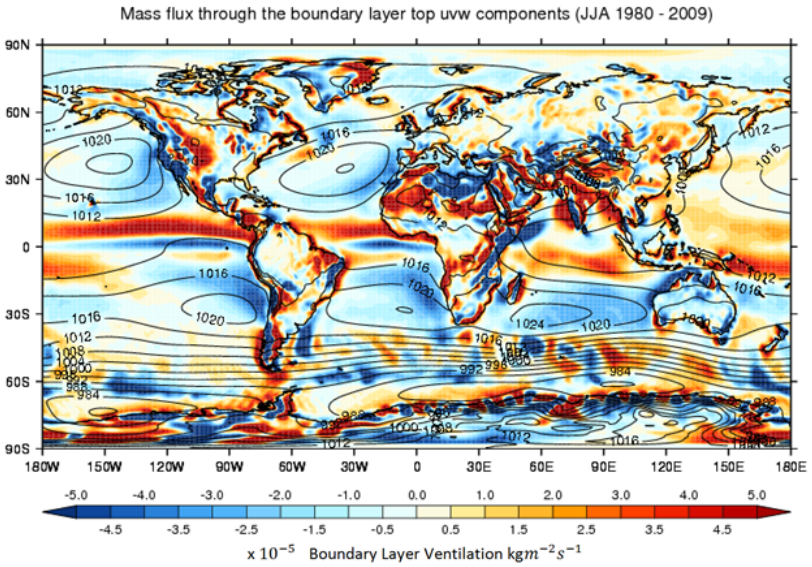
Mass flux through the boundary layer top uvw components (JJA 1980 - 2009)
90N
60N
30N
0
30S
60S
90S
180W 150W 120W 90W 60W 30W 0 30E 60E 90E 120E 150E 180E
-5.0 -4.0 -3.0 -2.0 -1.0 0.0 1.0 2.0 3.0 4.0 5.0
-4.5 -3.5 -2.5 -1.5 -0.5 0.5 1.5 2.5 3.5 4.5
x 10^{-5} Boundary Layer Ventilation kg$m^{-2}s^{-1}$

c)

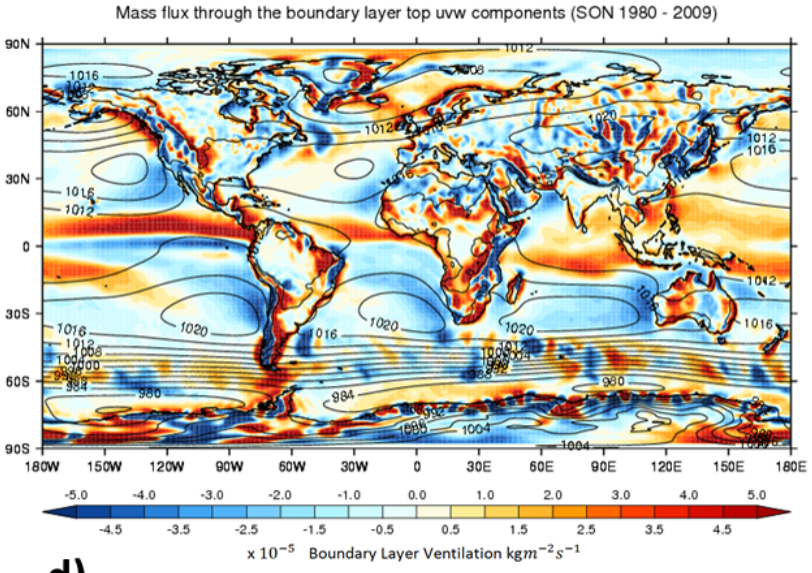
Mass flux through the boundary layer top uvw components (SON 1980 - 2009)
90N
60N
30N
0
30S
60S
90S
180W 150W 120W 90W 60W 30W 0 30E 60E 90E 120E 150E 180E
-5.0 -4.0 -3.0 -2.0 -1.0 0.0 1.0 2.0 3.0 4.0 5.0
-4.5 -3.5 -2.5 -1.5 -0.5 0.5 1.5 2.5 3.5 4.5
x 10^{-5} Boundary Layer Ventilation kg$m^{-2}s^{-1}$

d)

a few exceptions. In order to analyse this feature in more detail, we will make use of the fact that our ventilation climatology can be used as a proxy for divergence and thus compare our figures with those published by Berry and Reeder (2014).

2.6.4.1 The ITCZ over the oceans

Over the oceans the largest and strongest area of contiguous divergence in Figure 5 of Berry and Reeder (2014) is located in the eastern Pacific between $75°W$ and $150°W$. This region is characterised by a strong localised band of precipitation in the months of June, July and August (see Adler *et al.* 2003, Berry and Reeder 2014) which persists during the other seasons but at a weaker intensity. Figure 2.9 shows that this region is also a strong region of boundary layer ventilation although the seasonal variation is less obvious.

In the eastern Pacific ocean there exists another, much weaker, band of ventilation in Figure 2.9 which forms part of a double banded structure where ventilation is present to both the north and south of the equator. Whilst this feature has been observed by Zhang *et al.* (2013) in the season of MAM and briefly during the month of February it was not detected in any other months. The existence of the double ITCZ, due to the formation of shallow cumulus clouds was confirmed, during the season of DJF, in the study of Masunaga and L'Ecuyer (2010). Similarly the study of Berry and Reeder (2014) shows a weak double ITCZ detectable in the season of DJF and a stronger signal in MAM. Figure 2.9 shows that this feature can be detected all year round in the boundary layer ventilation climatologies although it is weaker in JJA and SON than in DJF and MAM, the season during which it is strongest and forms a continuous line of ventilation from the western Pacific to the east.

In the western Pacific strong ventilation persists to the north of the equator with another region of ventilation to the south which extends right across the Pacific basin in the season of MAM but is mostly confined to the west in other seasons. This region corresponds to a feature called the South Pacific Convergence Zone (SPCZ) (see Waliser and Gautier 1993). The SPCZ also shows up in the count plots of Berry and Reeder (2014) but is less well defined by their plot of divergence alone. One reason for this is that whilst our plots effectively show both negative and positive convergence, the method of Berry and Reeder (2014) neglect areas of positive divergence and

as such do not have this data in order to bound features. The two features of ventilation, which make up the double banded structure, are separated by a region of entrainment that matches the description given in Holton *et al.* (1971).

Over the Indian Ocean the count plots in Berry and Reeder (2014) show evidence of a double banded structure north and south of the equator in the seasons of DJF, MAM and SON. This double banded structure was also described by Zhang (2001) who showed that it occurred mainly in the months of November to February. Figure 2.9 shows evidence of the double banded structure in all seasons (although it is not as clearly defined as in the Pacific ocean) except JJA where a single banded structure persists over the oceans.

Over the Atlantic Ocean (see Figure 2.9) evidence of the double ITCZ is present in the plots for MAM and JJA whilst only a single band is present in the plots for SON and DJF. The existence of the double ITCZ was not noted in the study of Zhang *et al.* (2013) for the Atlantic ocean and only weakly for the months of JJA in Berry and Reeder (2014).

2.6.4.2 The ITCZ over land

The pattern of ventilation over land is less well defined than over the oceans. If the latitude of the band of ventilation over the Atlantic ocean with the region of strongest ventilation over central Africa are compared, it can be seen that the African ventilation band is displaced slightly to the north. This displacement of ventilation is best described in Figure 2.9 c with a corresponding area of entrainment aligned with the equator. This fits in well with the conceptual picture described by Nicholson (2009). In Figure 18 of their study they show that the main band of precipitation is located just north of the equator, but the surface convergence in the region of the ITCZ is some 10 degrees north of this precipitation band. This region of convergence matches up well with the region of maximum boundary layer ventilation described by Figure 2.9 c) and the work presented here complements the conceptual model developed by the study of Nicholson (2009).

Over India, the ventilation regime during the season DJF (see Figure 2.9 a) can be contrasted with that of the season of JJA (see Figure 2.9 c which is typical of that expected from the Indian monsoon as described by Yihui and Chan (2005)). In the Arabian sea, just off the west coast of India, a region of entrainment exists in the season DJF, whilst in the season JJA this is reversed.

Likewise in the Bay of Bengal and the Andaman sea a region of entrainment during DJF is replaced by a large area of ventilation in JJA. Over land in central and northern India a region of weak entrainment during DJF is replaced by a region of strong ventilation in JJA.

Similar patterns of ventilation and entrainment can be seen over the sea of Japan and over north western Australia which conform to the onset of the East Asian (Yihui and Chan, 2005) and Australian Monsoon (Hung and Yanai, 2004).

2.6.5 The northern hemisphere mid latitudes

In the mid latitudes of the northern hemisphere (30° N to 60° N) three features consistently show evidence of ventilation. The first two of these features are in regions that are typically associated with the north Atlantic and north Pacific storm tracks (Hoskins and Hodges 2002, Bengtsson *et al.* 2006). The third feature is present over the Rocky mountain chain which runs down the western side of North America. This can be compared with a map of orography generated from the IFS data set and given in Appendix A. Each of these features will now be discussed.

2.6.6 The Storm tracks

The regions of ventilation crossing both the Atlantic and Pacific Ocean are co-incident with areas that have long been associated with the the passage of low pressure systems (Klein, 1951, Klein, 1957 and Petterson, 1950). This signal is strongest in the months of DJF and weakest in the months of JJA, (see Figure 2.9). This, seasonality is best explained by the fact that the amount of boundary layer ventilation is directly related to the degree of baroclinicity in the atmosphere (Sinclair *et al.*, 2009), which in turn is controlled in part by the meridional temperature gradient (Lindzen and Farrell, 1980), and is in itself is a function of the season (White, 1982).

In Figure 1a of the study by Hodges *et al.* (2011) they show the track densities of extra-tropical cyclones. A comparison with our climatologies of boundary layer ventilation in Figure 2.9 show that the regions marked by positive boundary layer ventilation are coincident with the areas of high track densities. Each of the storm tracks will now be analysed in detail by splitting up the ventilation into its horizontal and vertical components as depicted in Figure 2.10.

2.6.6.1 The Atlantic Ocean

In the Atlantic Ocean, an area of strong boundary layer ventilation running from $30°N$,$70°W$ to $50°N$, $15°W$ can be seen in Figure 2.9 in all seasons. This is punctuated by a region of strong boundary layer entrainment at around $50°W$, $45°N$. In the season of DJF this region of ventilation is made up of a strong vertical component in the Southwest and a strong horizontal component in the Northeast (See Figure 2.10). The region of net ventilation in the Atlantic ocean just off the eastern seaboard of the United States of America, which can be seen in Figure 2.9 a is located to the south of the region of maximum track density as described by Hodges *et al.* (2011) and Hoskins and Hodges (2002). However, this region does match up well with the region associated with the highest values of mean growth rate of extra-tropical cyclones shown in Figure 5 - 6f of Hoskins and Hodges (2002). This maximum in cyclone growth rate implies a maximum in the meridional temperature gradient (Lindzen and Farrell, 1980) which in turn has been shown to produce the maximum ventilation of an idealised cyclone wave (Sinclair *et al.*, 2010).

The transition between a regime characterised by vertical ventilation to a regime characterised by horizontal ventilation is more complex. In order to understand this we can match the maximum in cyclone growth rate (Figure 6f of Hoskins and Hodges 2002) with the maximum in vertical ventilation (Figure 2.10 a), whilst to the north and east the area of high horizontal ventilation rates more closely matches areas of increased cyclogenesis and increased track densities (Figures 6 b and c Hoskins and Hodges 2002). This indicates that the horizontal ventilation rates are associated with well established systems which are already fully developed, but also have the capacity to sporn new systems along their pre-existing baroclinic lines. (Note that this area of increased cyclogenesis is only detected using the tracking method which utilises 850 hPa vorticity, (Figures 5 and 6c Hoskins and Hodges 2002), which is closer to the height at which we might expect the boundary layer top to be detected.) This is in agreement with the conclusion reached by Dacre and Gray (2009). Who showed that cyclones developing in the Eastern Atlantic are the result of secondary cyclogenesis occurring on the cold front of a pre-existing baroclinic wave. The combination of two baroclinic disturbances would constitute a much larger system than the ones seen in the west Atlantic. We therefore hypothesise that as a system grows its ventilation in the horizontal increases with respect to its ventilation in the vertical.

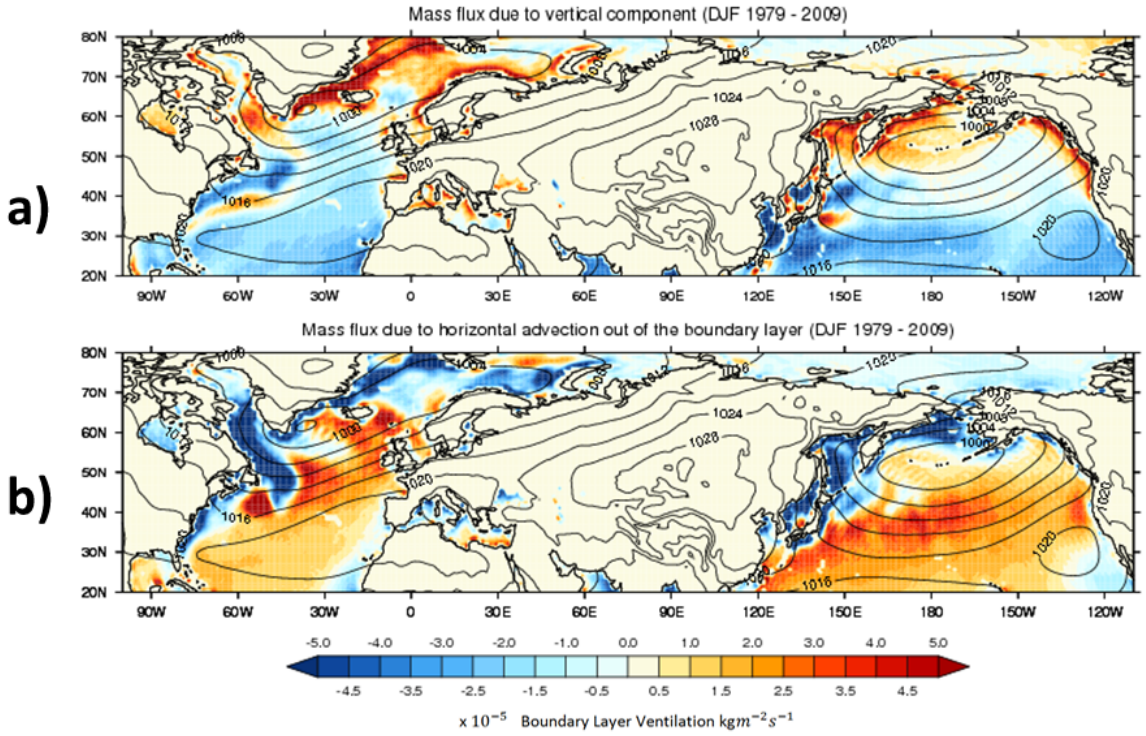

Figure 2.10: A mean climatology of the mass flux through the boundary layer top for the season DJF between the latitudes of 20° N and 80° N. The mass flux has been split into its horizontal component a) and its vertical component b). Overlaid are contours of the seasonal average mean sea level pressure. Only venting over the oceans is shown

2.6.6.2 The Pacific Ocean

In the Pacific Ocean the region of net ventilation of the boundary layer covers a much wider area than in the Atlantic ocean. In the western Pacific two distinct regions of ventilation can be seen: One off the eastern coast of Japan (from here on in referred to as the EJ) and the other to the east of the Kamchatka peninsula (from here on in referred to as the KP). In the eastern Pacific, these two filaments of ventilation merge into one contiguous area of ventilation between $35°N$ and $55°N$. The ventilation in this area weakens slightly further east before rapidly strengthening over the western coast of the United States of America.

EJ stretches from $35°N$, $160°W$ to $45°N$, $180°E$ and closely matches the location of the strongest track densities in the pacific as shown in Figure 1 in Hodges *et al.* (2011). A comparison between Figure 2.10a and Figures 5c and 6c of Hoskins and Hodges (2002) show that, as in the Atlantic Ocean, the vertical component of ventilation corresponds to the region of cyclogenesis picked out by the 850 hPa tracking routine used in Figure 6c of Hoskins and Hodges (2002). This also corresponds with regions of large growth rates (see Hoskins and Hodges 2002 Figure 6f) and can be explained by the action of growing baroclinc waves as described in the Atlantic Ocean. The large amount of horizontal ventilation throughout the storm track is more difficult to explain. But again we hypothesise that this increased ventilation in the horizontal when compared to the Atlantic ocean is a direct result of the increase in size of cyclones that are formed over the Pacific ocean when compared with the cyclones that form over the Atlantic Ocean (Rudeva and Gulev, 2007).

KP stetches from 55 N, $160°W$ to 55 N, $150W$, although it does not appear in the plot for JJA (see Figure 2.9 c) where entrainment seems to be slightly favoured. KP does not feature heavily in the analysis of Hoskins and Hodges (2002) although their does appear to be an increase in both feature density (see Figure 6 a Hoskins and Hodges 2002) and mean intensity (see Figure 6 e Hoskins and Hodges 2002) which suggests that this area is populated by relatively high intensity events which only have a short life span and as such would be consistant with ventilation due to Polar lows (Rasmussen and Turner, 2003) which is consistent with the lack of signal obtained in the months of JJA. The lack of any horizontal ventilation in the north of this area, above the Aleutian chain of islands (see Figure 2.10b) is also consistent with the idea that Polar lows are

formed due to instabilities that generate convection (Rasmussen, 1979). The comparrison between Polar lows and tropical cyclones has been made in the literature (Emanuel and Rotunno, 1989) and a comparrison between Figure 2.10 and a similar figure (not shown) over the tropical regions of the globe would confirm that vertical ventilation is the dominant form in both the tropics and to the north of the Aleutian chain of islands. Polar lows have been shown to be present over the north Pacific ocean in these locations (Chen *et al.*, 2012a) although their case studies do include the presence of a synoptic system which indicates that the ventilation seen in KP is due to a combination of both Polar lows and mid latitude weather systems This combination of the two types of weather system is also confirmed by the presence of horizontal ventilation in the region south of the Aleutian island chain, where the ventilation is also strongest.

Polar lows are not only located in the Pacific ocean but also occur off the north west coast of Norway and similar arguments, as to their impact on the vertical field of ventilation, can be applied to this region as have been applied to the region defined as KP. However, it should be noted that the IFS is only capable of reproducing 45% - 55% of the total number of Polar lows to occur (Laffineur *et al.* 2014, Zappa *et al.* 2014) and as such it is likely that the ventilation from these systems is under represented in the climatologies presented in Figures 2.9 and 2.10.

2.6.6.3 Other Storm tracks (northern hemisphere)

In Figure 1 of Hodges *et al.* (2011) an increase in track densities can be observed in the Mediterranean basin and off the east coast of Greenland. In Figure 2.9 a-d we can see that a large area of ventilation is present off the eastern coast of Greenland (albeit modulated by season). However, over the Mediterranean basin no discernible signal is present. The venting off the eastern coast of Greenland can be seen to be present in both the vertical and horizontal components of ventilation (see Figure 2.10). (Although, in the horizontal the signal is slightly displaced to the east). It should be noted that not all of the ventilation in this area can be attributed to mid latitude cyclones and that at least some of the ventilation might be due to the convergence of strong low level jets as described by Outten *et al.* (2009) which could be responsible for forcing air out of the boundary layer by purely mechanical means. The lack of any strong boundary layer entrainment signal in the local vicinity suggests that this would only be possible in conjunction with the diabatic addition of heat due to convection. It should also be noted that the large values of vertical

ventilation could be due to a larger proportion of smaller cyclones which are formed in this area (Bieltvedt Skeie *et al.* 2006, Kristjánsson and McInnes 1999).

In the Mediterranean region the vertical ventilation matches up well with the storm track depicted in Figure 1 of Hodges *et al.* (2011) which is mainly confined to the western coast of Italy and the southern most tip of Greece. However, no apparent signal is present in the field of horizontal ventilation. Since the storms that develop in the Mediterranean are typically small in size (Hoskins and Hodges 2002, Trigo *et al.* 1999) this is consistent with the conclusions reached in the previous section.

2.6.6.4 Coastal features

In Figure 2.10 a it is apparent that a large amount of ventilation takes place off the western coast lines of the continents in the regions associated with the storm tracks. One explanation for this large increase in vertical ventilation would be the release of potential instability that occurs due to a cyclone coming into contact with the coast due to the sudden increase in surface elevation (Kreitzberg and Perkey, 1976). Although this hypothesis is not directly tested it is supported by the pattern of ventilation seen over the coast of western Ireland which was associated with a trough line. (see section 2.6.1). The presence of ventilation due to coastal outflow is difficult to discern in Figure 2.9 and it is likely that coastal outflow is a relatively small process when compared with mid latitude cyclones on the large scales presented here, which due to a lack in horizontal resolution do not take into account, the smaller scale thermal circulations that are know to be important in enhancing ventilation by processes such as coastal outflow (Dacre *et al.* 2007,Monks *et al.* 2009).

2.6.6.5 The Southern hemisphere

The storm track in the Southern hemisphere is also depicted in Figure 1 of Hodges *et al.* (2011). The storm track stretches around the globe with its most dense region being just south of New Zealand. Our climatologies of boundary layer ventilation (see Figures 2.9 a-d) do exhibit a band of ventilation between around 40° S and 70° S although this is not continuous and is therefore

difficult to relate directly with the storm track apart from its physical location. More work would be needed in order to confirm this feature, although since this thesis concentrates on the northern hemisphere, this has not been attempted here.

2.6.7 Orography

Figure 2.9 clearly shows regions of ventilation that are coincident with the major mountain ranges included in the model (See the model orography depicted in Appendix A). In particular, the area of ventilation over the Rocky mountains is very prominent and appears as a constant feature in all four seasons.

In South America, the Andes mountain range provides another template for a region of increased ventilation. In Asia the Tibetan plateau generates a less consistent, but still well defined area of ventilation. Smaller mountain ranges such as the Alps are less well defined and in the case of 2.9 c in JJA the ventilation in these areas is no larger than in the surrounding non-mountainous terrain.

In the study of De Wekker *et al.* (2004) the ventilation of the boundary layer (calculated using a bulk Richardson number method) is described in terms of specific mechanisms for an individual case study. These mechanisms were described in Chapter 1. Figure 2.11 splits up the total venting into its vertical and horizontal components. These components are roughly equal in strength over the Rocky mountain range and suggest that the "advective" ventilation described by De Wekker *et al.* (2004), and shown in our plots of horizontal ventilation (Figure 2.11 b), is a major source of ventilation on the climatological scale along with the two vertical components of ventilation which De Wekker *et al.* (2004) described as mountain venting and cloud venting respectively.

We also hypothesise that the region of entrainment that appears on the slopes of Greenland are due to the entrainment of air into the boundary layer associated with a katabatic wind (Nyeki *et al.*, 2000). The flow pattern of winds over the Greenland ice sheet have been described by Bromwich *et al.* (1996) and it is known that the acceleration of the wind is more pronounced on the eastern side of the ice sheet. In the climatologies presented in Figure 2.9 an area of increased entrainment can be seen to be collocated with the eastern slope whilst at the edges of the ice sheet strong ventilation regimes are found which can be attributed to the convergence of mass in this

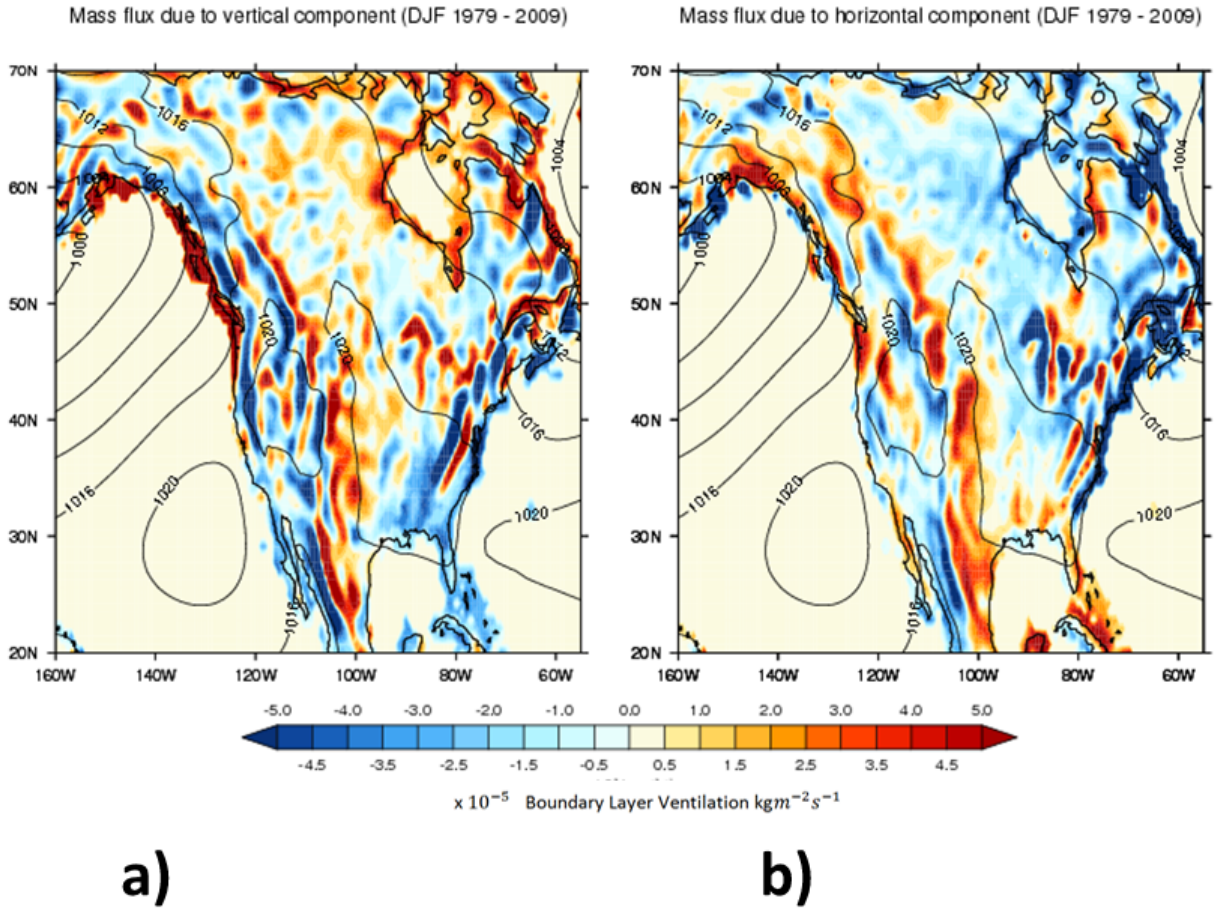

Figure 2.11: A climatology of the mean mass flux through the boundary layer top during DJF in north America. This region shows the ventilation associated with the Rocky mountains. The mass flux has been split up into its horizontal component a) and its vertical component b). Overlaid are contours of the seasonal average mean sea level pressure.

region as the katabatic winds quickly decelerate.

Apart from the features described above, it is difficult to define any additional features over land that can be definitively attributed to events described in the scientific literature. This is likely due to the diurnal cycle, which ventilates air during the night as the boundary layer collapses and entrains material during the day as the boundary layer grows which acts to mask any ventilation features other than those already mentioned. If Figure 2.9 is scrutinised carefully some smaller mountain ranges such as the Ural mountains (60° N and 60° E) and the Alps (46° N and 7° E) can be picked out as regions of net ventilation.

2.7 Discussion of errors

The mass budget of the boundary layer was balanced using the technique described in Section 2.5. It has been shown in the previous section that the results obtained from this calculation can be qualitatively explained by physical mechanisms recorded in the literature (e.g. the removal of air by the storm track). In order for a more robust and quantitative study to be performed, it is neccesary to balance the terms on the right hand side of Equation 2.37 with the left hand side. We can do this by assuming that $\frac{\partial \hat{\rho}}{\partial t} = 0$ over the 30 year data set.

Figure 2.12 is calculated by subtracting the divergence term from the ventilation term at each time step and subsequently calculating the mean of this field over the full 30 years worth of data. Figure 2.12 shows that our method balances the mass budget well over the seas and most of the continents with discrepancies occurring mainly over central Africa and parts of the middle east. Smaller discrepancies can also be seen to occur over Asia, Australia and the Rocky mountains in the season of JJA. At times these errors are of equal magnitude to the fluxes described in the previous section and care must be taken when interpreting the plots of boundary layer ventilation in these regions.

The mean value of this field during DJF has been calculated to be 2.79 x$10^{-5} kgm^{-2}s^{-1}$. If we take an average global boundary layer height of 600 metres and assume that the average density of air within that column is $1.0 kgm^{-3}$ then that would account for an emptying of the column of air within 250 days. This is clearly a large error on the climatological timescale. However, if

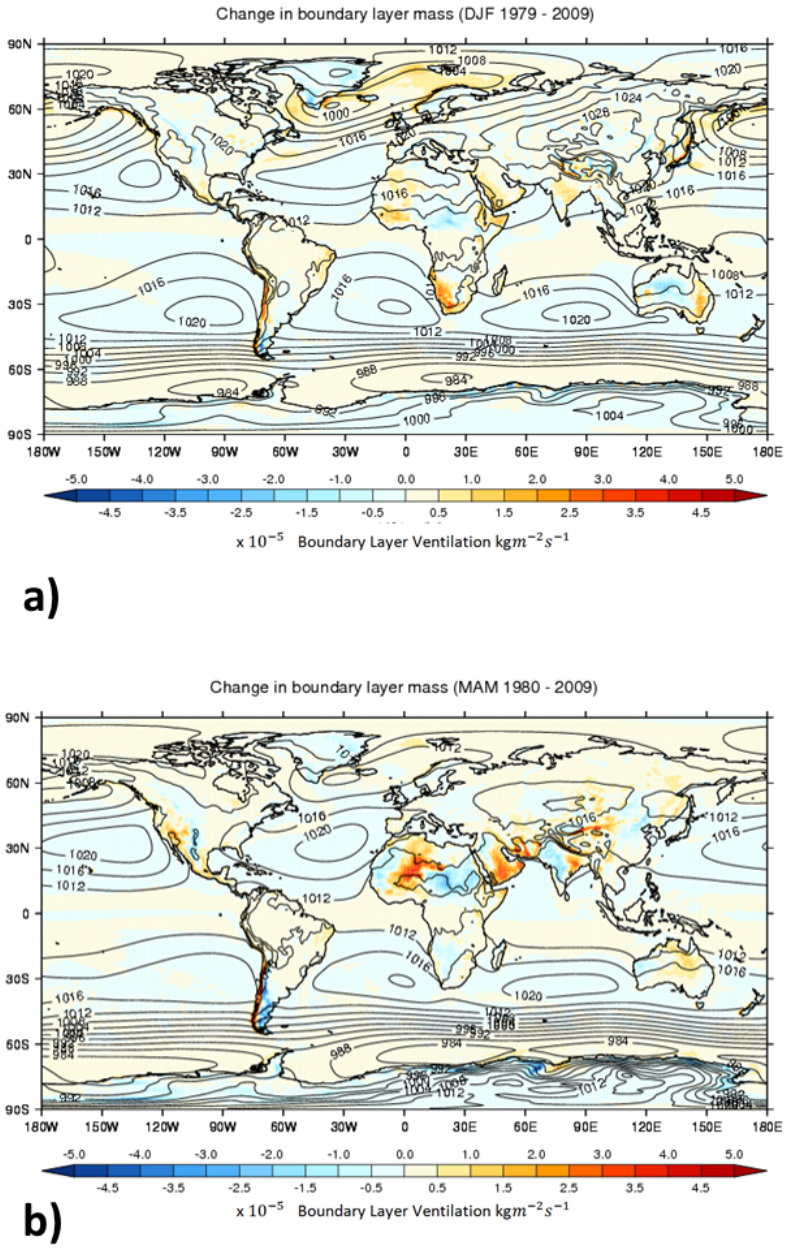

Figure 2.12: A mean climatology of the $\frac{\partial \hat{\rho}}{\partial t}$ term in the boundary layer mass budget for each of the four seasons (DJF, MAM, JJA, SON) over the entire 30 year period. Overlaid on each figure is the climatological average value of mean sea level pressure.

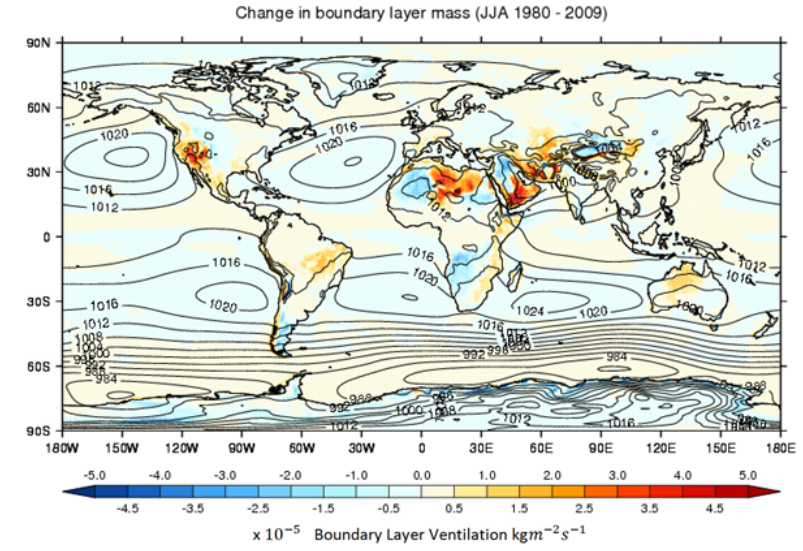
Change in boundary layer mass (JJA 1980 - 2009)
90N
60N
30N
0
30S
60S
90S
180W 150W 120W 90W 60W 30W 0 30E 60E 90E 120E 150E 180E
-5.0 -4.0 -3.0 -2.0 -1.0 0.0 1.0 2.0 3.0 4.0 5.0
-4.5 -3.5 -2.5 -1.5 -0.5 0.5 1.5 2.5 3.5 4.5
x 10^{-5} Boundary Layer Ventilation kg$m^{-2}s^{-1}$

c)

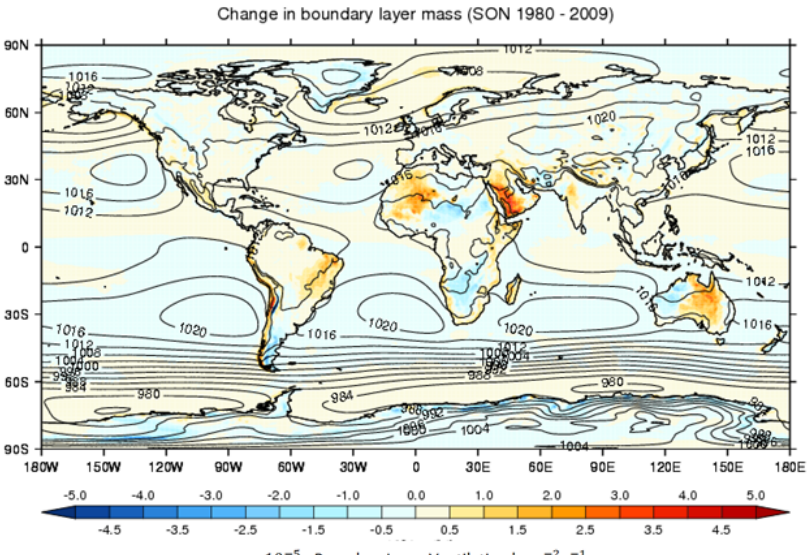
Change in boundary layer mass (SON 1980 - 2009)
90N
60N
30N
0
30S
60S
90S
180W 150W 120W 90W 60W 30W 0 30E 60E 90E 120E 150E 180E
-5.0 -4.0 -3.0 -2.0 -1.0 0.0 1.0 2.0 3.0 4.0 5.0
-4.5 -3.5 -2.5 -1.5 -0.5 0.5 1.5 2.5 3.5 4.5
x 10^{-5} Boundary Layer Ventilation kg$m^{-2}s^{-1}$

d)

we comapare the average ventilation rate ($0.002 kgm^{-2}s^{-1}$) with the change in mass at each point of ventilation (calculated to be 4.3 x$10^{-5} kgm^{-2}s^{-1}$) then we find the error associated with the calculation to be just 2% which is acceptable for the qualitative results that we have presented here.

A plot of $\frac{\partial h}{\partial t}$ has been produced for one year (not shown) and the areas that are shown to give the greatest error are coincident with the largest values of $\frac{\partial h}{\partial t}$. This suggests that the 3 - hourly data set used within this study is of insufficient temporal resolution to capture the boundary layer ventilation accurately in these regions. In the following chapters of this thesis, we will limit our study to the northern hemisphere between 30° N and 60° N in order to minimise the amount of error encountered in our calculations.

2.8 Conclusions

The work in this chapter has primarily shown that given a globally distributed atmospheric data set, such as that provided by the IFS model, individual features of boundary layer ventilation and entrainment can be clearly distinguished both on the time scale of a few hours and up to the time scale of a 30 year seasonal climatology. This work has shown the similarities in boundary layer structure and the mass budget which occur during the development of an idealised cyclone that was simulated in the work of Sinclair *et al.* (2009) and the simulation of a cyclone that occurred on the 25th November 2009. Our results show that to the west of the cold front the boundary layer gains mass. Whilst to the east, directly adjacent to the cold front, mass is lost. This pattern is mirrored in the idealised cyclone depicted in Sinclair *et al.* (2009) and gives us confidence in the results of the climatologies presented later in this chapter. By comparing the magnitude of this ventilation and the ventilation / entrainment of mass over the land for a similar time, it was shown that the ventilation occurring due to the mid latitude cyclone was of a higher magnitude.

Climatologies of boundary layer height over a 30 year period have been presented. These show a boundary layer which is elevated in the regions of the storm tracks whilst over land only moderate tops are attained. Low to moderate tops occur in the tropics and low boundary layers predominate nearer the poles. This is likely to be a consequence of the differing temperatures of the surface and the overlying air and the lack of any discernible pressure gradient causing

low winds over the tropics. The climatologies show similar characteristics to those produced by von Engeln and Teixeira (2013) except in the tropics. This difference is attributed to the method of determining the boundary layer top. The study of von Engeln and Teixeira (2013) used relative humidity as a determining factor whilst our method of using the bulk Richardson number relies heavily upon using the wind speed (see the denominator of Equation 2.25). Using a bulk Richardson number to define the boundary layer top allows us to represent the diurnal cycle in the height of the boundary layer top.

Climatologies have also been produced for a 30 year period which show the ventilation of the boundary layer and the mass budget of the boundary layer for each of the four seasons. These climatologies have demonstrated, the presence of a double ITCZ in data produced by a weather forecasting model (the IFS). This is then contrasted with the double ITCZ problem produced in climate models Zhang (2001). Our results suggest that the double ITCZ is a real feature, although the band to the south of the equator is much weaker than its northern hemispheric counterpart and, as such, does not appear in observationally based climatologies of precipitation Zhang (2001). Evidence has been provided for the existance of the extratropical strom tracks by contrasting the ventilation climatology with some of the existing literature on storm tracking (Hoskins and Hodges, 2002; Hodges *et al.*, 2011). The areas described by the storm tracking literature were show to agree well with areas of significant ventilation of the boundary layer. In addition, two further mechanisms of ventilation were identified; that due to orography and that due to Polar lows. Using evidence from the literature the areas associated with polar lows have been discounted from further study.

The boundary layer mass budget has been shown to balance to a satisfactory standard in most regions of the globe. However, major errors exist over continents where $\frac{\partial h}{\partial t}$ is particularly large and are attributed to the poor temporal resolution of the data provided by ECMWF for the IFS. Through research in the available literature it has been determined that the rest of this thesis should focus on the mid latitudes of the northern hemisphere. The reasons for this decision are:

1. The errors produced in the ventilation climatologies of the tropics are, in some areas, large and as such by limiting the area of interest to above 30 N we will eliminate much of this error in our future calculations.

2. Ventilation above 60 N, where systems such as Polar lows make up a large proportion of the overall ventilation, is not adequately represented due to the poor performance of the IFS in capturing such systems.

Mid latitude cyclones have been shown to contribute the greatest amount to the global ventilation budget (Cotton *et al.*, 1995). The next chapter will therefore take a detailed look at the turbulent redistribution of moisture within a mid latitude cyclone.

Chapter 3:

The origins of moisture ventilation in a Baroclinic wave: A Lagrangian and Eulerian analysis of a case study

3.1 Introduction

In the previous chapter, we have shown that the mass budget of a baroclinic wave can be adequately represented by the IFS data set (the ERA-interim forecast model). In this chapter, we now focus on an individual case study of a mid latitude cyclone and graphically map all of the different components of the boundary layer moisture budget equation first described by Boutle *et al.* (2010).

In Chapter 2 it was shown that the areas of mass ventilation within the idealised cyclone wave of Sinclair *et al.* (2008) are similar to that produced by the mass budget equation being applied to the IFS. This analysis will be repeated for the moisture budget and inferences drawn as to the applicability of the idealised model framework employed by Boutle *et al.* (2010) to the "real world" case study analysed using the IFS. Suitable sources of moisture will then be identified from the surface evaporation rate and linked to positions of boundary layer ventilation via use of the Met Office Numerical Atmospheric Dispersion Modelling Environment (NAME). This will allow us, not only to connect the point of evaporation with the point at which moisture is vented out of the boundary layer, but to also assess the mechanism by which particles can escape from the boundary layer.

3.1.1 Aims of this work

This chapter aims to answer the following two research questions:

1. Where is the source region for the large amounts of moisture which are ventilated by the warm and cold fronts of a mid latitude cyclone?
2. What roles do boundary layer turbulence and convection play in determining how and when particles exit the boundary layer?

3.2 Methodology and models used

3.2.1 Choice of models

This chapter is split into 2 parts. The first part uses the IFS data set, described in chapter 2, combined with the boundary layer moisture budget equation described in Boutle *et al.* (2010) (which is presented in section 3.2.2) in order to describe the moisture cycle within the boundary layer for a case study which was introduced within chapter 2. The second part of this chapter describes an investigation into the Lagrangian pathways taken by moisture particles, from release points within the system. In order to do this we ran the Met Office Unified Model (UM) and combined the model output with the Met Office offline particle dispersion model.

A brief summary of the major differences between the UM boundary layer scheme and the IFS boundary layer scheme follows in section 3.2.3 along with a more comprehensive description of the NAME dispersion scheme which is provided in Section 3.2.4. Using an independent model in order to provide the meteorological inputs into NAME has the advantages that

1. The UM only applies one data assimilation routine which ensures dynamical consistency throughout the 4 day period.
2. The UM is run at a horizontal resolution of roughly 40 km x 40 km in the mid latitudes which is roughly half the resolution of the IFS data set used. This will allow us to better pick out frontal boundaries and better represent the action of parameterized convection.

3. By comparing the results of the NAME simulation with the boundary layer moisture budget and showing that individual features can be seen in both we will be able to generalise our results and not confine our conclusions to any one particular model.

3.2.2 The moisture budget equation

The boundary layer moisture budget Equation was first described by Boutle (2009) to be

$$\frac{\partial \widehat{\rho q}}{\partial t}_{bl} = \underbrace{(\rho q)_h \left(\frac{\partial h}{\partial t} - \vec{U}.n \right)_h}_{\text{Entrainment}} \underbrace{- \widehat{\rho q} \left(\frac{\partial \hat{u}}{\partial x} + \frac{\partial \hat{v}}{\partial y} \right)}_{\text{Divergence}} - \underbrace{(\rho \overline{w'q'})_h}_{\text{Unresolved ventilation}} + \underbrace{(\rho \overline{w'q'})_0}_{\text{Evaporation}} + \underbrace{\hat{S}}_{\text{Precipitation}} \tag{3.1}$$

where ρ represents the density of air, h the boundary layer height, u and v the horizontal wind components and $\vec{U}$ is the full, three dimensional, wind vector. n is a vector normal to the boundary layer top. $\overline{w'q'}$ represents the turbulent flux of moisture either at the boundary layer top (h) or at the surface (0). The $\hat{S}$ term accounts for the addition of moisture as rain evaporates on its way between the boundary layer top and the surface or the removal of moisture through precipitation formed by clouds which reside within the boundary layer. Quantities which appear under a ˆ are evaluated as the integral sum between the surface and the boundary layer top. Quantities which appear with a subscript h are evaluated at the boundary layer top. q, which represents the total moisture content of the atmosphere, is given to be

$$q = q_v + q_l + q_i \tag{3.2}$$

where q_v is the amount of moisture present as vapour in the atmosphere (i.e. the specific humidity), q_l is the amount of liquid water and q_i is the amount of water contained within the atmosphere in the form of solid ice.

In addition to the entrainment and divergence terms, which are analogous to the entrainment and divergence terms presented in Chapter 2 in the mass budget equation, three additional terms

are present in Equation 3.1. The first of these we have labelled unresolved ventilation and comprises two components, firstly the moisture transport due to the process of entrainment at the top of the boundary layer and secondly the transport due to non-resolved fluctuation of moisture within areas of convective activity (see ECMWF 2006b). (Note that the unresolved ventilation term will also include any numerical errors generated by the numerical method used to calculate each of the other terms in the boundary layer moisture budget equation.) The second and third additional terms are the evaporation of moisture from the surface (obtained directly from the ECMWF data set) and the precipitation term, which can be calculated by subtracting the amount of moisture falling at the surface from the amount of moisture which is falling through the boundary layer top. The amount of moisture falling through the boundary layer top is calculated by linearly interpreting the total precipitation profile (available from ECMWF) between the model level above and below below the diagnosed boundary layer top.

The IFS data set can be used to re-create each of these terms individually except for the unresolved ventilation term. In order to calculate a value for the unresolved ventilation we first have to calculate $\frac{\partial \widehat{\rho q}}{\partial t}_{bl}$ on the lhs of Equation 3.1 directly and then re-arrange Equation 3.1 to find the unresolved ventilation term as a residual. Before doing this however, it was important to test that the change in moisture content of the atmosphere could accurately be determined by calculating $\frac{\partial \rho q}{\partial t}$ for the atmosphere as a whole using a three hour time step.

The calculation of $\frac{\partial \rho q}{\partial t}$, for the atmosphere as a whole using the IFS data over the course of a season, agreed with the calculated change in total column water vapour published for the ERA-interim data set by Berrisford *et al.* (2011) to an accuracy of 1 decimal place. This proved that Forecast drift was not a major factor in defining the total amount of moisture in the atmosphere and that large errors were not being encountered in our calculation of $\frac{\partial \rho q}{\partial t}$ by using a three hourly time step. The data presented in this chapter uses the time steps T+9 and T+12, where T is the start of the IFS forecasting cycle, and as such issues pertaining to the spin up of precipitation (Kallberg, 2009) do not arrise.

3.2.3 The Met Office Unified Model

The Unified Model (UM) version 7.3 was run in its global configuration with a horizontal grid spacing of 0.4°X 0.4°and seventy model levels. The data for the start dump of the model run was provided by the National Centre of Atmospheric Science and based upon ERA-interim reanalysis data.. The timestep used was 12 minutes and output was produced for every 3 hour period between 00 UTC on the 22nd November to 00 UTC on the 26th November 2009. Small scale processes are represented by the various parameterisation schemes. The UM was chosen in order to provide a consistent data set over a period of 4 days which does not suffer from abrupt changes due to the use of data assimilation which appear every 12 hours in the IFS data set.

3.2.3.1 Parameterising small scale processes

It is necessary to parameterise processes that occur on scales smaller than the 0.4°X 0.4°resolution of the model grid spacing in order to represent their effects on the system as a whole.

The cloud scheme is based upon the work of Smith (1990) which has since been updated by Wilson and Ballard (1999). The scheme uses a statistical approach in order to determine the fraction of cloud and the mean grid box cloud water content within a grid box. The fluctuations in cloud liquid water and temperature throughout the grid box are represented by a triangular probability density function G. This distribution is then used in order to calculate a cloud fraction and a new cloud liquid water content from the input variables of mean water vapour (q_v), original liquid water content (q_l) and mean liquid temperature (T_L) (the temperature of an air parcel if all of the latent heat stored in liquid water for was released). The scheme then determines a variable $Q_c$which is defined to be

$$Q_c = a_l\{q_{v+cl} - q_{sat}(T_L, P)\} \tag{3.3}$$

where $q_{v+l} = q_v + q_l$, $q_{sat}(T_L, P)$ is the saturation specific humidity which is a function of $T_L$and the pressure P, and $a_l = 1/(1 + L\alpha/C_p)$ where $\alpha = \frac{\partial q_{sat}}{\partial T_{L:}}$. Deviations around $Q_c$are defined to be

$$s = a_l\{q'_{v+cl} - \alpha T'_L - \beta P'\} \tag{3.4}$$

where the quantities with a $'$ are defined to be deviations around their mean values as defined by the PDF described above and $\beta = \frac{\partial q_{sat}}{\partial P}$. This allows us to say that at any particular point within the grid box

$$q_{cl} = Q_c + s \tag{3.5}$$

and that the cloud volume fraction is now

$$C = \int_{s=-Q_c}^{\infty} G(s)ds \tag{3.6}$$

and the mean condensate ($\bar{q_{cl}}$) is

$$\bar{q_{cl}} = \int_{s=-Q_c}^{\infty} (Q_c + s)G(s)ds \tag{3.7}$$

A further description of the treatment of cloud ice is given in Wilson and Ballard (1999). The surface precipitation rate is calculated by the parameterisation scheme of Wilson and Ballard (1999) which, starting at the highest model level, can also determine the thermodynamic changes that occur in the atmosphere as water vapour changes into its different states (i.e. atmospheric water vapour to ice to liquid water).

Convection is represented within the model by the scheme described by Gregory and Rowntree (1990). This uses a mass-flux approach in order to represent convective activity. In order for the convective parameterization scheme to come into effect, the model column is tested from the bottom up one grid level at a time for buoyant parcel ascent. The parcel entrains dry air and detrains cloudy air as it ascends. Ascent is stopped when the air parcel is either no longer buoyant or when the convective mass flux falls below a minimum level. The amount of mass flux that occurs within the plume is separated out in terms of whether the convection can be considered shallow (i.e. less than 2.5 km in depth or below the freezing level) or deep. For shallow convection the mass flux is related to the turbulent kinetic energy (Grant, 2001) whereas for deep convection the removal of buoyant energy is related to the convective available potential energy (CAPE) described by Fritsch and Chappell (1980).

The model uses parameterisations of upwards and downwards vertical fluxes in both the short wave and the long wave radiation as prescribed by Edwards and Slingo (1996). This includes the interactions that both ice crystals and liquid water will have on the fluxes as well as the flux from the gaseous component of the atmosphere.

3.2.3.2 The UM boundary layer scheme

The UM boundary layer scheme is described by Lock *et al.* (2000) and updated in the technical documentation provided by the Met Office (Lock, 2007). Just like the boundary layer scheme described for the IFS (see Section 2.2.2) the UM boundary layer scheme describes mixing due to a combination of wind shear, surface driven convective overturning or the top down mixing caused by the cooling of stratocumulus tops, which subsequently allows parcels of air at the top of the cloud to become negatively buoyant.

In order to represent each of the processes described in the previous paragraph the boundary layer is initially prescribed a boundary layer type based upon the stability of the model column and the occurrence of any cloud which appears at the top of the boundary layer. In an unstable model column (determined by a positive buoyancy flux at the surface) the boundary layer top is determined by a parcel ascent up the model column until a level of neutral buoyancy is reached. A determination as to whether or not cumulus cloud is present is based upon the gradient in mean total atmospheric water content between the lifting condensation level and the boundary layer top being greater than a threshold value. The threshold value is given to be 1.1 times the magnitude of the mean gradient below the lifting condensation level. If cumulus clouds are diagnosed then the boundary layer top is set at the lifting condensation level and mixing above this level is prescribed by the convection scheme already described. In stable layers (i.e. where the surface buoyancy flux is negative) the boundary layer top is set by choosing the model level where the gradient Richardson number is greater than one.

Whilst the determination of mixing is similar between the IFS scheme and the UM scheme for stable boundary layers at night and the top down mixing provided by stratocumulus clouds, the treatment of the daytime convective boundary layer is different. Whilst the IFS scheme uses the EDMF framework in order to represent the mixing by convective thermals alongside any

mixing due to locally driven mechanical mixing, the UM scheme only represents the mixing due to the dry convective overturning, which controls the majority of boundary layer mixing. This difference in approach is important conceptually. However, in Section 3.3.2 we will show that the forecast evolution of a case study using the IFS data matches well with the evolution provided by the Unified Model.

3.2.4 Numerical Atmospheric Dispersion Modelling Environment NAME III Vn 5.0

3.2.4.1 A particle advection model

The numerical atmospheric dispersion modelling environment (NAME) tracks individual particles along the Lagrangian trajectories provided by the wind fields from a numerical weather prediction model. In addition to this each particle is given a random perturbation to its trajectory in order to simulate the effect of atmospheric turbulence. The version of the model used in this research was NAMEIII Vn 5.0. No single official document outlines the internal workings of the model. The information given below has been obtained by using past versions of the model documentation (Maryon *et al.*, 1999; Webster *et al.*, 2003), looking at the model code and conversations with staff currently working at the Met Office. Some information was also gleaned from the study of Ryall and Maryon (1998) who documented the NAME model at version 2.0. The basics of its operation are described here.

In order to represent the turbulent dispersion of particles the NAME advection scheme independently calculates the new position ($x_{t+\Delta t}$) of each particle at each subsequent time step using

$$x_{t+\Delta t} = x_t + [\mathbf{u}(x_t) + \mathbf{u}'(x_t) + \mathbf{u}'_{\mathbf{l}}(x_t)]\Delta t \tag{3.8}$$

where $\mathbf{u}$ (linearly interpolated to the particle's location in space from the data supplied by an NWP model) is the mean velocity vector provided by the UM and $\mathbf{u}'$ is the turbulent component of velocity that is independently calculated by NAME based on prescribed profiles of velocity variance and a corresponding Lagrangian time scale. The $\mathbf{u}'_{\mathbf{l}}$ term is called the meander, a component of velocity added to the mean wind ($\mathbf{u}$) and turbulent ($\mathbf{u}'$) components of the flow in order to account for the likely advection of a particle between the times that model data are provided to

the NAME offline model. Δt is the model timestep being used. During the first thirty minutes of the simulation Δt is typically in the range of 0-100 seconds and is calculated using the change in vertical velocity variance with height whilst being limited by the Lagrangian timescale which is described below in Section 3.2.4.6. After thirty minutes, the value of Δt is fixed at 15 minutes. Both the $\mathbf{u}'$and $\mathbf{u}'_\mathbf{l}$ components are described in the following sections along with a description of how the boundary layer depth is determined by the NAME model and two additional schemes (convection and skewed turbulence) which can be switched on and off when the NAME model is run.

3.2.4.2 The representation of boundary layer depth

In order for Equation 3.8 to be solved, it is first necessary to define the region of space in which the turbulence generated within the boundary layer can act upon individual particles and thus alter their trajectories. The boundary layer is therefore defined and treated separately from the rest of the atmosphere. NAME uses two different schemes in order to define the boundary layer depth. The boundary layer depth is then calculated using each of these schemes and the maximum value obtained is used.

The first method uses a calculation of the gradient Richardson Number R_{grad} for each model level. This is computed using

$$R_{grad} = \frac{g\Delta\theta/\Delta z}{\overline{T}(\Delta u/\Delta z)^2} \tag{3.9}$$

where $\Delta\theta/\Delta z$ and $\Delta u/\Delta z$ represent the vertical gradient in potential temperature (θ) and wind speed (u) which are both calculated from the numerical model which is driving NAME. (In this case the UM). g is the acceleration due to gravity and $\overline{T}$ is the mean temperature over the distance Δz. The value for R_{grad} is then calculated up through the model column and when it exceeds 1.3 the top of the boundary layer is defined as being the top of the model level below.

The second method utilizes a parcel ascent in order to calculate the boundary layer top. In order to do this the 1.5 metre temperature is increased by 1.2 °C (except in stable situations when the increase is lowered to 0.5 °C) and a dry adiabatic lapse rate is followed up to a point

where it intersects the environmental lapse rate as defined by the model. This height at which this intersection occurs is then used as the boundary layer top.

3.2.4.3 The meander term ($\mathbf{u_l'}$)

The velocity component describing the meander of the particle is assumed to be constant with height within the boundary layer and zero in the free troposphere. It is given by

$$u'_{l,t+\Delta t} = u'_{l,t} - \frac{u'_{l,t}\Delta t}{\tau_{u,l}} + \left(\frac{2\sigma^2_{u,l}\Delta t}{\tau_{u,l}}\right)^{1/2} r \tag{3.10}$$

The Lagrangian timescales ($\tau_{u,l}$) are based on mean periods of wind oscillations as described by Maryon (1998) whilst the velocity variance ($\sigma_{u,l}$) is given by

$$\sigma^2_{u,l} = 2c_l u_{10}\Delta T_F \tag{3.11}$$

where ΔT_F is the time resolution of the wind fields supplied by the Unified Model (in our simulation $\Delta T_F = 3$hours) and c_l is a constant dependent upon the value of ΔT_F (in our simulation $c_l = 0.0260\, ms^{-1}$). u_{10} is the ten metre wind speed. Δt is the model timestep described in Section 3.2.4.6 below.

3.2.4.4 The turbulence term ($\mathbf{u'}$)

In order to calculate the $\mathbf{u}'$ perturbation the advection of particles is split up into a component that represents the horizontal motion and a component that represents the vertical motion. The values of $\mathbf{u}'$ are calculated differently dependent upon the time of travel. For the first 30 minutes of our simulations the horizontal component of the turbulent flow u' is calculated by

$$u'_{t+\Delta t} = \underbrace{u'_t}_{original\ perturbation} + \underbrace{\left(1 - \frac{\Delta t}{\tau_u}\right)}_{damping\ term} + \underbrace{\left(\frac{2\sigma^2_u\Delta t}{\tau_u}\right)^{1/2} r}_{new\ perturbation} \tag{3.12}$$

and the vertical component of the turbulent flow is given by

$$w'_{t+\Delta t} = \underbrace{w'_t}_{original\ perturbation} + \underbrace{\left(1 - \frac{\Delta t}{\tau_w}\right)}_{damping\ term} + \underbrace{\left(\frac{2\sigma^2_w\Delta t}{\tau_w}\right)^{1/2} r}_{new\ perturbation} + \underbrace{\frac{\Delta t}{\sigma_w}\frac{\partial\sigma_w}{\partial z}(\sigma^2_w + w'^2_t)}_{adjustment\ term} \tag{3.13}$$

where r is a random Gaussian deviate which has a mean of zero and a variance of one. The values associated with r are taken from a set of pseudo random numbers. Therefore if we run the model multiple times we will always use the same values of r that were used in the initial run. σ is a velocity variance profile and τ is the Lagrangian timescale. σ and τ are described in Sections 3.2.4.5 and 3.2.4.6.

Equations 3.12 and 3.13 both contain a number of terms which relate to the original particles perturbation which is superimposed upon the large scale flow by Equation 3.8, the damping of this motion with time and a new perturbation which is developed by use of the random deviate (r). Equation 3.13 contains an additional term which only become important in regions where $\sigma_w$is small. This term is included in order to stop the artificial build up of particles in these regions (Maryon *et al.*, 1999).

After 30 minutes have elapsed a much less computationally expensive process is adopted in order to advect the particles. The horizontal velocity variance is now defined as

$$u' = \sqrt{2\sigma_{u(eff)}}r \tag{3.14}$$

with a similar formulation applied in the vertical. The effective velocity variance ($\sigma_{u(eff)}$) is defined by

$$\sigma_{u(eff)} = \sigma_u^2 \frac{\tau_u}{\Delta t_d} \tag{3.15}$$

where Δt_d is a timestep of 15 minutes.

3.2.4.5 Profiles of velocity variance

The profiles used in determining the velocity variance are different based upon whether the short or long range advection scheme is being used. In the long range scheme the turbulence profiles are described as being homogeneous (i.e. they do not change with height in the boundary layer). The short range profiles are however dependent on height and as such are termed inhomogeneous. The profiles of each scheme which are described below have all been verified by comparison with observational data sets and shown by Webster *et al.* (2003) to be valid for each respective case (e.g

stable or unstable situations). In each case it is assumed that lateral dispersion is more important than dispersion in the along wind direction, thus $\sigma_{u,v}$ is matched to observed values of σ_v. For the inhomogeneous scheme σ is given to be a function of the friction velocity (u_*) and the convective scaling velocity (w_*) where

$$\frac{U}{u_*} = \frac{1}{k} ln \frac{z}{z_0} \tag{3.16}$$

and

$$w_* = u_* \left(\frac{kz}{L} \right)^{1/3} \tag{3.17}$$

The friction velocity for each height z is calculated using the roughness lengths (z_0) and mean wind speeds (U) supplied by the UM. The convective scaling velocity is taken to be a function of the friction velocity and the Obukhov length (L) which is again supplied by the UM. Von Karman's constant (k) is set to be equal to 0.4. The stability of the atmosphere is determined from the value of L with $L < 0$ indicating an unstable boundary layer and $L > 0$ indicating a stable case. In the boundary layer and in stable conditions the velocity variances are

$$\sigma_u = 2u_* \left(1 - \frac{z}{z_h} \right)^{3/4} \tag{3.18}$$

$$\sigma_w = 1.3u_* \left(1 - \frac{z}{z_h} \right)^{3/4} \tag{3.19}$$

whilst for unstable conditions they are given by

$$\sigma_u^2 = \underbrace{0.4w_*^2}_{1} + \underbrace{4.0u_*^2 \left(1 - \frac{z}{z_h} \right)^{3/2}}_{2} \tag{3.20}$$

$$\sigma_w^2 = \underbrace{1.2w_*^2 \left(\frac{z}{z_h} \right)^{2/3} \left(1 - \frac{z}{z_h} \right)}_{1} + \underbrace{1.69u_*^2 \left(1 - \frac{z}{z_h} \right)^{3/2}}_{2} \tag{3.21}$$

where z_h is the height of the boundary layer. Equations 3.20 and 3.21 have both been optimised to give a smooth transition between stable and unstable conditions. Terms 1 on the rhs of Equations 3.20 and 3.21 are representative of convective mixing whilst terms 2 are representative of the shear driven mixing.

In order to calculate the homogeneous profiles for long range transport the profiles given in Equations 3.18 - 3.21 are simply integrated over the boundary layer height and then divided by the height of the boundary layer. This gives us for stable conditions

$$\sigma_u^2 = 1.6u_*^2 \tag{3.22}$$

$$\sigma_w^2 = 0.676u_*^2 \tag{3.23}$$

and for unstable conditions

$$\sigma_u^2 = 0.4w_*^2 + 1.6u_*^2 \tag{3.24}$$

$$\sigma_w^2 = 0.27w_*^2 + 0.676u_*^2 \tag{3.25}$$

Above the boundary layer the profiles are fixed to be $\sigma_u = 0.25$ ms^{-1}and $\sigma_w = 0.1$ ms^{-1}. These values are also used to limit the minimum amount of turbulence experienced within the boundary layer.

3.2.4.6 Lagrangian timescales

The advection of particles is dependent upon the amount of time that coherent turbulent motion will act upon a particle before the turbulence is dissipated by viscous forces. Therefore in order to describe advection of a particle, a profile of Lagrangian time scales must also be prescribed alongside the velocity variance profile. The Lagrangian timescales for inhomogeneous turbulence in unstable conditions are given by

$$\tau_{u/w} = \frac{2\sigma^2}{C_0\varepsilon} \tag{3.26}$$

where C_0 is a value between 1 and 5 dependent upon stability and being calculated as a function of the Obukhov length. ε is the rate of dissipation of turbulent kinetic energy and is given by the formula

$$\varepsilon = \left[1.5 - 1.2\left(\frac{z}{z_h}\right)^{1/3}\right]\frac{w_*^3}{z_h} + \frac{u_*^3}{kz}\left(1 - 0.8\frac{z}{z_h}\right) \tag{3.27}$$

Equation 3.27 has been shown to fit with profiles observed by Grant (1992). In stable conditions the Lagrangian timescales are given by

$$\tau_{u/w} = A\frac{\sigma^2}{C_0\varepsilon} \tag{3.28}$$

with A = 8.0 in the horizontal direction and A=3.38 in the vertical direction. In the case that the boundary layer is neutral

$$\tau_{u/w} = Akz_0\frac{\sqrt{1-\frac{z_h}{L}}}{C_0 u_*} \tag{3.29}$$

with C_0 = 5. The Lagrangian timescales in homogeneous turbulence for stable conditions are given by

$$\tau_{u,w} = Bk\frac{f\left(\frac{z_h}{L}\right)}{120u_*} \tag{3.30}$$

where $B = 4.0$ in the horizontal direction and $B = 1.69$ in the vertical direction. The numerator in Equation 3.30 is a function which is determined by an initial calculation of $\frac{z_h}{L}$ (as given in the NAMEIII vn5.0 code). For a more complete description the reader is advised to refer to Webster *et al.* (2003). In unstable conditions the value of the Lagrangian timescale in the horizontal is given to be

$$\tau_u = Min(\frac{z_h}{C_0 w_*}(3.125log(5.0) - 3.5), 32k\frac{z_h}{15C_0 u_*}) \tag{3.31}$$

whilst in the vertical the Lagrangian timescale is provided by

$$\tau_w = Min(\left(\frac{z_h}{C_0 w_*}\right)\left(\frac{335919}{14336}\right) - \left(\frac{114375}{8192}\right)log(5.0), 13.52k\frac{z_h}{(15.0C_0 u_*)}) \tag{3.32}$$

Each of the formulae given have been formulated by calculating the mean value of Equation 3.30 over the boundary layer and represent inferred values from both the velocity variances given in Equations 3.18 - 3.25 along with profiles of Equation 3.27. All of the Lagrangian timescales used are combined with the appropriate velocity variance in order to give a K diffusion co-efficient. The boundary layer terms are then further limited by the lower bound in K diffusion set in the troposphere. This is done in order that the boundary layer is always more turbulent than the free atmosphere.

3.2.4.7 Advection across the boundary layer top

In order to stop particles from advecting across the temperature inversion a scheme is employed which takes into account the change in turbulence profiles in the free troposphere compared with those found in the boundary layer. However, this scheme is effectively an artificial construct and does not affect the physics of what is happening to particles crossing the inversion level (personal communication Dave Thomson, Met Office, 2011). As such it is not described in detail here. (see Ryall and Maryon (1998) for more details).

All of the model formulations that have been described so far are used as standard by the NAME model. A number of options exist which can be turned on or off by the user as desired. The options used in this project are detailed below.

3.2.4.8 The NAME convection scheme

The NAME convection scheme in this version of the model is a very simple redistribution of particles, randomly between the surface and cloud top with a probability of 1 /25th the cloud fraction. Cloud top and cloud fraction are both input parameters supplied by the meteorological model in order to provide input into NAME (in this case the UM.) Only clouds that have a depth of greater than 500 metres are used by this scheme (personal communication D Thomson: The Met Office, 2011). This option was switched on as standard in the simulations described in this thesis and turned off where necessary for the sensitivity analysis described in Section 3.4.3.5.

3.2.4.9 Skewed turbulence

NAME provides an option to allow skewed turbulence in the boundary layer for the first 30 minutes of the simulation. This represents the effect on particles that are caught in an updraught in a convective regime

$$w'_{t+\Delta t} = \underbrace{w'_t}_{1} + \underbrace{C\Delta t}_{2} + \underbrace{(C_0\varepsilon\Delta t)^{1/2} r}_{3} \tag{3.33}$$

where terms 1 and 2 in Equation 3.33 are analogous to terms 1 and 2 in Equation 3.12, C being a probability density function consisting of two functions describing the probability of a particle

being in either an updraught or a downdraught (Thomson, 1987). Term 3, which describes an additional component of turbulent advection, is based on Kolmogorov inertial subrange theory, where ε is the rate of dissipation of turbulent kinetic energy and C_0 is a universal constant. In the NAME scheme C_0 is given by

$$C_0 = 2.1log3|L| - 1.5 \tag{3.34}$$

with the limits that $C_0 = 1$ in unstable conditions and $C_0 = 5$ in stable conditions (Webster *et al.*, 2003). This option is turned off except for the sensitivity analysis described in Section 3.4.3.5.

3.2.4.10 The wet deposition scheme

The process of wet deposition tries to mimic the action of material being removed from the atmosphere by being swept out by falling rain and by the loss of material to rain drops as they form around cloud condensation nuclei (assumed to be a proportion of the mass of a particle). Both of these processes are represented in the NAME model by the use of a scavenging co-efficient which is included in an equation which models the depletion of mass by assuming that

$$\Delta m = m(1 - exp(-C_1\Delta t)) \tag{3.35}$$

where m is the mass of a particle, $C_1$is a scavenging co-efficient. The scavenging co-efficient is a function of rain rate and two empirically derived constants based on the table given in Maryon *et al.* (1999). In order to calculate the rainfall rate the amount of dynamic precipitation is taken directly from the numerical weather prediction model whilst the convective precipitation rate is scaled up. This is done in order to account for the parameterization of convection in numerical models which produces rain rates that are based upon grid box averages.

The wet deposition scheme therefore provides us with an ideal tool with which to investigate the residence times of moisture in the atmosphere. This option was turned off for all of the experiments except for those described in Section 3.2.4.10.

3.2.4.11 NAME vs UM and IFS boundary layer schemes

The fundamental difference between the boundary layer schemes described in this chapter and the NAME model is the different perspectives with which they represent the turbulent motion encountered in the boundary layer. The NAME model advects particles around in the atmosphere and records the state of the atmosphere as felt by the individual particle. This approach uses a Lagrangian method (Nakayama and Boucher, 1998) for tracking and calculating the changes to each individual particle.

Numerical weather prediction models and in particular the boundary layer schemes used within these models avoid the large computational costs which are incurred by using the Lagrangian method by focusing on the bulk properties of the atmosphere. An approach that uses the Eulerian perspective (Nakayama and Boucher, 1998) can then be used in order to calculate the change in these bulk properties at the point in space labelled x, y, z with respect to time. The differences between the Lagrangian and Eulerian perspectives in a change in $\mathcal{X}$ can be best described by the material derivative given to be

$$\frac{D\mathcal{X}}{Dt} = \frac{\partial \mathcal{X}}{\partial t} + \mathbf{U} \cdot \nabla \mathcal{X} \tag{3.36}$$

where $\mathbf{U}$ is the three dimensional wind vector and t is the time. The two terms on the right hand side of Equation 3.36 describe the flow at a particular point in space and time, whilst the left hand side of Equation 3.36 represents the change in the properties of $\mathcal{X}$ as experienced by a particle moving through point x, y and z at time t.

The action of turbulent mixing within the boundary layer upon a quantity $\mathcal{X}$ can be described by splitting up the motion of a particle into a component due to the action of the mean flow and a component due to the action of turbulent eddies. Breaking down the motion of a particle in this way is known as Reynolds decomposition and can be described mathematically as

$$\frac{D\mathcal{X}}{Dt} = \underbrace{\frac{\partial \mathcal{X}}{\partial t}}_{1} + \underbrace{\overline{U} \cdot \nabla \overline{\mathcal{X}}}_{2} + \underbrace{U' \cdot \nabla \mathcal{X}'}_{3} + \underbrace{\overline{U} \cdot \nabla \mathcal{X}'}_{4} + \underbrace{U' \cdot \nabla \overline{\mathcal{X}'}}_{5} \tag{3.37}$$

where a line placed directly over each symbol represents the mean of a parameter over a grid-box and a parameter marked by a $'$ represents the deviation from this mean flow. A numerical model

will be able to evaluate terms 1 and 2 in Equation 3.37 directly. It is the job of the boundary layer scheme to try and represent terms 3, 4 and 5. This is achieved by first taking the spatial average of each of the terms over the size of the grid box being represented which has the effect of setting terms 4 and 5 to zero. Term 3 is then split up into its vertical and horizontal components to give

$$\overline{U' \cdot \nabla \mathcal{X}'} = \underbrace{\frac{\partial \overline{u'\mathcal{X}'}}{\partial x}}_{1} + \underbrace{\frac{\partial \overline{v'\mathcal{X}'}}{\partial y}}_{2} + \underbrace{\frac{\partial \overline{w'\mathcal{X}'}}{\partial z}}_{3} \tag{3.38}$$

where the lower case letters u', v' and w' represent velocity fluctuations in the x, y and z directions independently. Numerical models such as the IFS and the UM used in this thesis ignore terms 1 and 2 because the horizontal grid spacing used (i.e. ∂x and ∂y) is so large as to make these terms insignificant. Thus the boundary layer schemes only need to calculate term 3 for inclusion in these models.

NAME has been designed to represent the effects of the three dimensional action of turbulence on each of its particles. Since NAME is a Lagrangian particle model the properties of $\mathcal{X}$ are linearly interpolated onto the particle from the driving numerical model. Thus fluctuations are only represented in the position of individual particles within the velocity field but do not represent any changes in the quantity $\mathcal{X}$ itself.

The main advantage that is gained by using the NAME model is the fact that we will be able to directly test the link between the source regions of moisture at the Earth's surface with the large regions of boundary layer ventilation found in weather fronts. Not only does the NAME model track air flows, but also allows for the representation of turbulence to be included in the calculation, which is known to be important in redistributing moisture within the atmospheric boundary layer (Boutle *et al.*, 2010). This Lagrangian viewpoint will form a unique contribution to the literature on the ventilation of boundary layer moisture.

3.2.5 Calculating the equivalent potential temperature.

In order to calculate the equivalent potential temperature θ_e associated with each particle in Section 3.4.3.3 the formula used was

$$\theta_e = \theta exp\left(\frac{Lr_s}{C_pT}\right) \tag{3.39}$$

(from Holton, 1972) where θ is the potential temperature of the particle, L is the latent heat of condensation, T is the temperature of the air in degrees Kelvin, C_p is the specific heat capacity of dry air and r_s is the saturated mixing ratio. The NAME model provides us with the values of potential temperature, temperature and pressure of each particle directly. The saturated mixing ratio was derived from the formula

$$r_s = \frac{0.622e_s}{P(hPa)} \tag{3.40}$$

given in Andrews (2010) where e_s is the saturated vapour pressure of water and $P(hPa)$ is atmospheric pressure at the location of the particle. In order to calculate the saturated vapour pressure, Tetten's formula was used in the form

$$e_s = 6.112exp\left(\frac{17.67T_c}{T_c + 243.5}\right) \tag{3.41}$$

which is given in Ambaum (2010). T_c is the temperature in degrees Celsius. It should be noted that this formulation makes several approximations, most notably the use of Tetten's formula for the calculation of the saturation vapour pressure and that a more desirable choice would have been to use the method described in Bolton (1980) which has been shown to be more accurate below temperatures of 0 degrees Celsius. However, several fields would have had to be interpolated from the UM output data in order to achieve this. It was therefore decided to use the method given above in order to minimise any error incurred from the interpolation process. (note that this formulation for equivalent potential temperature only produces accurate results in saturated conditions, since we are investigating flows within the warm conveyor belt where levels of moisture are very high this formulation was considered sufficient.)

3.2.6 Calculating the number of particles

The mass of each particle has been assigned a mass of 1 gram. This mass is not considered by the NAME setup as previously described when redistributing the particles throughout the atmosphere

(assuming that the wet deposition scheme is turned off). Turning the wet deposition scheme on has the effect of depleting the mass of each individual particle by applying Equation 3.35. It was thus necessary to chose a value that would be representative of the size of an individual raindrop which is 0.065 grams (given an average size of approximately 2.5mm Joss and Gori 1978). The larger value of 1 grams was thought to be a sensible choice given the spread in possible sizes.

In Section 3.4.5 the model was set to output concentration of particles which was subsequently projected onto a grid equal to the horizontal resolution of the UM and with a vertical grid spacing of 50 metres using 200 levels. Thus, by decreasing the the mass of the rain drops by the wet deposition process (which should approximate the process of collision and coalescence) we should be able to assign an outer limit to the amount of time that moisture is present in the presence of a precipitating system such as a mid latitude cyclone by assesing when the mass of particles in the system drops to zero.

3.3 The case study

3.3.1 Synoptic situation

The development of the storm can be seen in Figure 3.1. At 0000 UTC on the 22nd November 2009, two cyclonic systems were present over the northern Atlantic ocean. To the west, a depression was forming just off the north eastern coastline of Newfoundland. The Met Office analysis for this time shows a double warm front, cold front and an already developed occlusion. The low surface pressure associated with this system has dropped to 991hPa whilst to the south east a strong anticyclone dominates over the Azores with a high pressure of in excess of 1033 hPa. It is this low system that will be the focus of our case study, whilst to the east a deep depression has developed just off the western coast of Ireland exhibits the frontal structure associated with the Norwegian model (Bjerknes and Solberg, 1922). Over the next 72 hours the low pressure centre to the north east of Newfoundland, moves across the Atlantic Ocean to the north western coast of Ireland. The centre of low pressure drops to 960 hPa and the frontal structure simplifies to the classical cold, warm and occluded frontal structures. By this time several trough lines have developed within the flow behind the cold front. To the south east of the low pressure centre a

broad expanse of high pressure dominates over central Europe, whilst to the rear of the cold front a strong anticyclone has developed to give a pressure of 1033 hPa.

The positioning of the anticyclones relative to the position of the low pressure centre between 0000 UTC 24th November and 0000 UTC 25th November (see Figures 3.1 c and d), closely resembles the spatial layout of the low pressure centre and the two anti-cyclones of the idealised studies of Boutle *et al.* (2010) and Sinclair *et al.* (2009). This makes the case study an ideal storm with which to compare the boundary layer ventilation rates given in Boutle (2009).

3.3.2 Model verification

It can be seen from Figure 3.2a that the drop in mean sea level pressure is consistent between the two modelled data sets, the re-analysis product and the analysis produced by the Met Office. The largest deviations occur at around 2100 UTC on the 22nd November when the UM data set drops the minimum mean sea level pressure in the storm by approximately 4hPa below that shown by the IFS and ERA-interim data set and towards the end of the simulation where the UM is approximately 4 hPa above the IFS and ERA-interim data sets.

Figure 3.2b shows a comparison between the spatial positioning of the low pressures centres 72 hours into the UM run. Good agreement is displayed between all three data sets. Differences exist in the troughing of the isobars on the cold front and in the spatial location of the low pressure centre. However, these differences are small and are not likely to adversely affect the characteristics of the NAME trajectories in any way.

3.3.2.1 Particle release locations

Figure 3.3 shows the release locations of particles within the vicinity of the cyclone's warm sector. Release locations have been labelled A-I. Location A was chosen because it represents a location within the anticyclone to the east of the cold front where the surface evaporation is at its maximum. This location has been chosen primarily to test the hypothesis proposed by Boutle *et al.* (2010), who suggested that moisture evaporated from within the anticyclone, associated with a mid latitude cyclone, is transported within the boundary layer into the centre of the cyclone wave

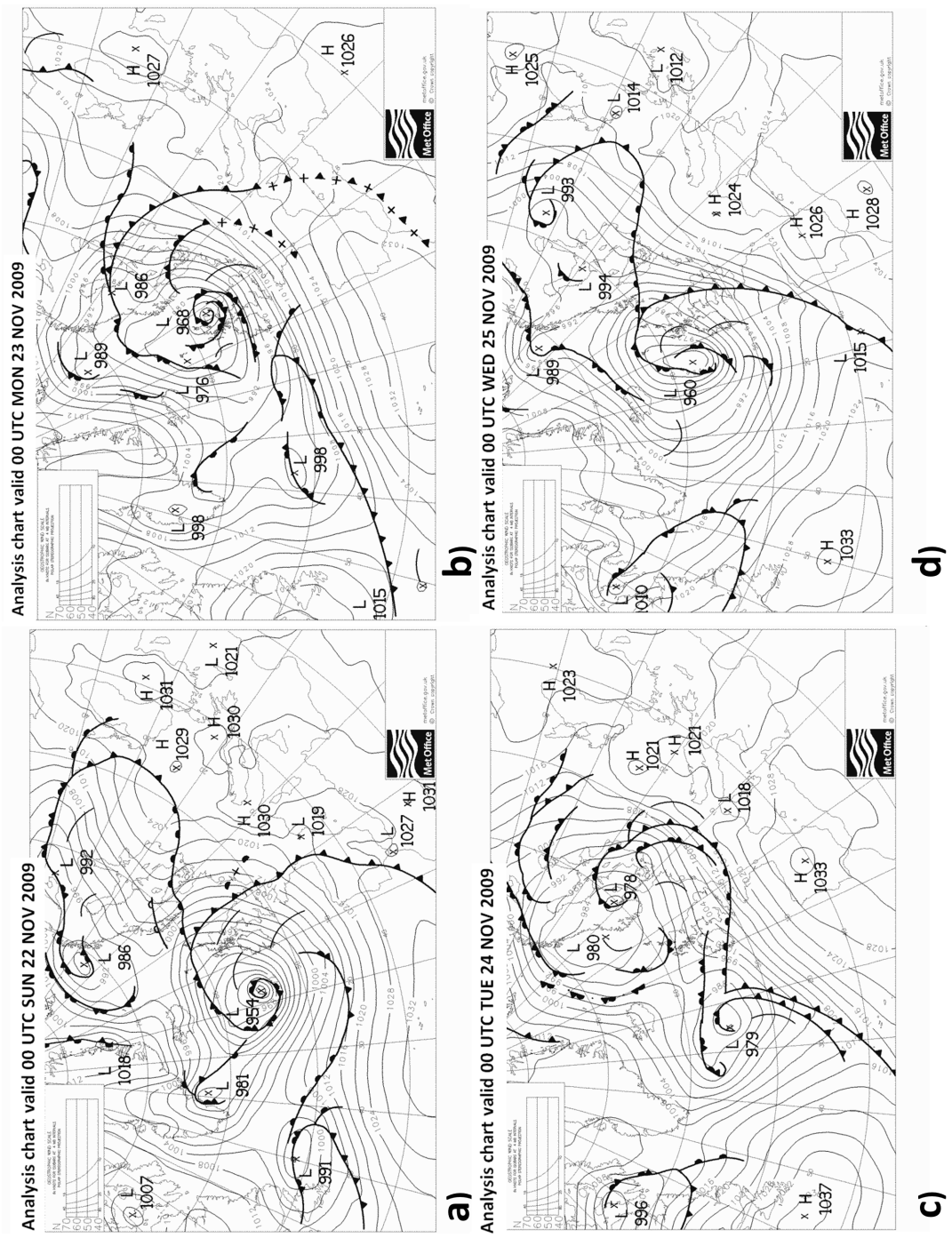

Figure 3.1: The synoptic situation between the 22nd November 2009 to 25th November 2009 at 0000 UTC as analysed by the UK Met Office.

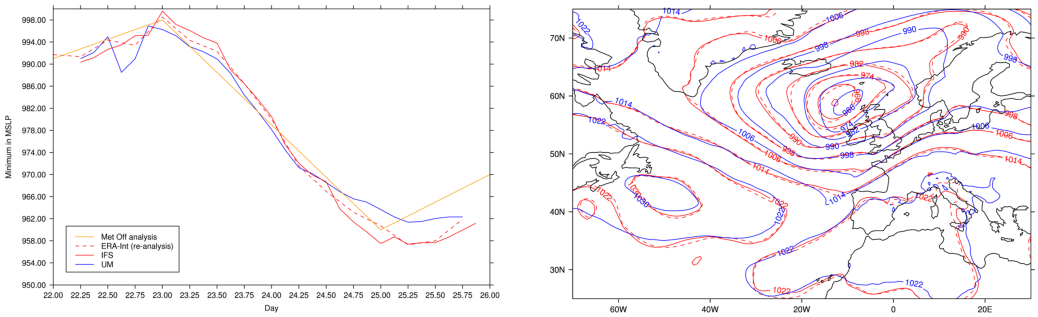

a) **b)**

Figure 3.2: Panel a The minimum mean sea level pressure for the case study taken from ERA-interim reanalysis (dashed red), the IFS (red), the Unified model (blue), Met Office analysis charts (orange). Panel b depicts the mean sea level pressure (analysed at every 8 hPa) on the 25th November 2009 at 0000 UTC for ERA-interim reanalysis (dashed red), IFS (red) and the Unified model (blue).

before being ventilated by the warm conveyor belt. Locations E and F are located just behind the warm front in the warm sector and have been positioned in order to represent the moisture already within the warm conveyor belt whilst locations B, C and D have been positioned at regular intervals (approx every 5°latitude) between locations E / F and location A. In particular locations B and C correspond to the secondary source of high evaporation described in the previous section and could be described as analogous to the second source of low level moisture as described by Figure 3 in Harrold (1973).

The locations G, H and I represent the inflow of moisture from tropical sources. These three locations were included in order to test the hypothesis that not all of the moisture within the warm conveyor belt is derived from sources within the latitudinal band of 30- 60 N.

3.4 Results

3.4.1 Eulerian moisture budget

The full boundary layer moisture budget of our case study is shown in Figure 3.4. Panel a shows that a large loss of moisture is occurring along the cold front whilst a gain in moisture is occuring

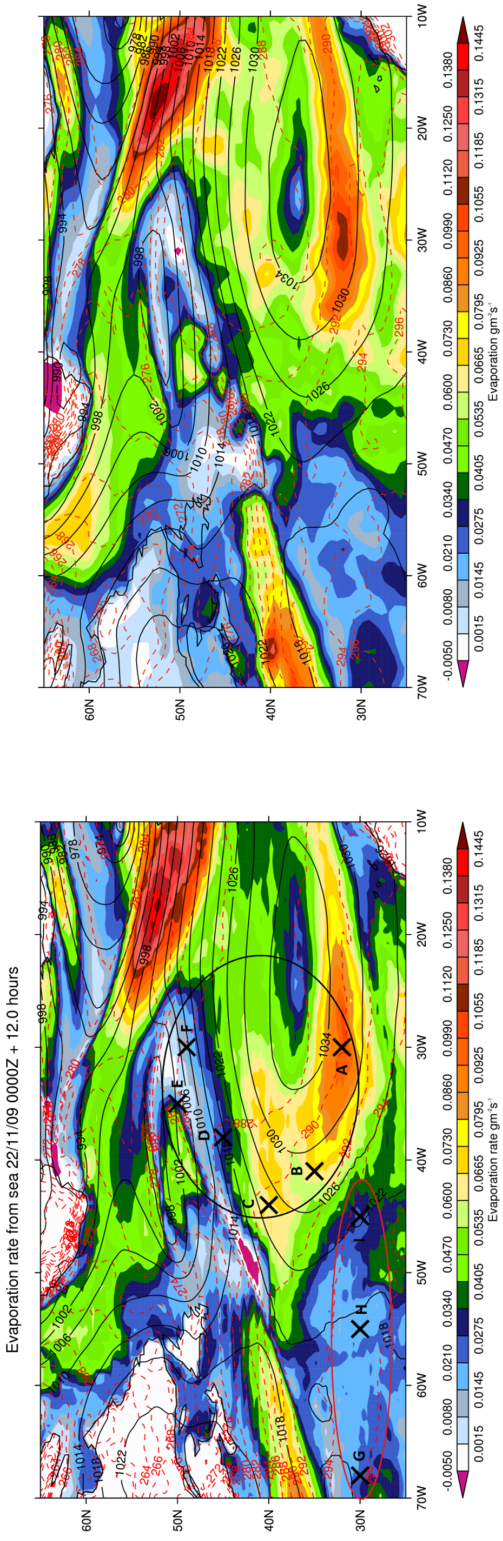

Figure 3.3: a) The evaporation rate overlayed with the mean sea level pressure (4 hPa contours) and frontal positions for 1200 UTC 22nd November 2009 (T+00 hours). Each of the positions marked with an X corresponds to a location chosen for release of particles. The warm and cold fronts can be distinguished by the troughing of the isobars (Sansom, 1951) and the potential temperature contours at 10 m. (Sanders, 1999). b) The evaporation rate based on the IFS data set run for the same time as panel a. MSLP contours are contoured every 4 hPa and potential temperature contours are given for the first model level at 20 m above the surface.

behind the warm front in the warm sector of the storm. This panel should be contrasted with panels b, c and d which show that both of these areas are ventilating moisture at this time (although very weakly in the case of the unresolved ventilation on the eastern end of the warm front).

The pattern of changing boundary layer moisture content described in panel a, can be directly compared with Figure 4.5 a in Boutle (2009) (also described in Boutle *et al.* (2010) although not all of the figures for comparison are in this publication). At first glance the data sets do not seem to compare very well with the majority of moisture lost in the simulations of Boutle (2009) appearing in the central region of their cyclone's warm sector. The loss of moisture in panel a is spatially correlated with large amounts of boundary layer ventilation shown in panels b, c and d. A closer inspection of Figures 4.5 a and b show us that the loss of moisture is closely correlated with the change in boundary layer height in the area aligned with the surface troughing in the isobars which has been shown to be a good indicator of the position of the cold front (Sansom, 1951). If we reanalyse the position of the cold front in the work done by Boutle (2009), bearing this in mind then the location of the change in boundary layer moisture content in Figure 4.5 a of Boutle (2009) agrees well with panel a of Figure 3.4. The method used by Boutle (2009) was originally developed by Hewson (1998) and relies on the analysis of gradients in theta-w at 850 hPa in order to place the location of the front. However, it is acknowledged that for an accurate depiction of any individual front that the positioning given by the objective method should be adjusted by a qualified weather forecaster (Hewson, 1998).

The source regions for the large amounts of moisture being ventilated from the boundary layer were postulated by Boutle *et al.* (2010) to be from within the anticyclone. Figure 3.4, panels e and g show that large areas of evaporation are present in areas that also have a large divergence in the boundary layer moisture field. It is natural to assume that these regions are therefore supplying moisture into the regions of strong ventilation seen in panel d. This link between the sources of moisture and ventilation within the cyclonic wave will be tested in Section 3.4.2.

By comparing panels b, c and d in Figure 3.4 it can be seen that a large contribution to the loss of moisture from the boundary layer is provided by the unresolved ventilation term in Equation 3.1. It can also be seen in panel d of Figure 3.4 that the ventilation described by this term is not confined to the cold front (indicated by the resolved ventilation in panel b) but covers a wide area approximately 400 km in width. This is a very large region compared with the observed frontal

width of 600 metres reported in the study of this storm conducted by Martínez-Alvarado *et al.* (2014) (as part of their model verification). The width of the resolved ventilation is approximately 200 km. This disparity between what has been observed by a field campaign and our findings here is almost certainly due to the resolution of the model that we are using. This point will be addressed later in Section 3.5.

The width of the warm conveyor belt has previously been described in case studies by (Harrold 1973, Wernli and Davies 1996) and is approximately equal to the width of the resolved ventilation being diagnosed. The warm conveyor belt has also been investigated previously by studies which have used trajectories as a method for studying the ascent within the warm conveyor belt (Joos and Wernli 2012, Martínez-Alvarado *et al.* 2014). However, the unresolved ventilation of the boundary layer offers another source of moisture into the mid troposphere which could also go on to modify the potential vorticity due to latent heating and thus change the evolution of the storm (Rossa *et al.*, 2000).

Figure 3.4 f shows the precipitation term of the boundary layer moisture budget. This term is a factor of 10 smaller than any of the other terms studied in this section and therefore only forms a very small component of the moisture budget. None the less, two of the features displayed in panel f are of particular interest to this study. Firstly, it can be seen that a loss of moisture is occurring in the boundary layer within the warm sector. This loss of moisture can be explained by the boundary layer top cutting through layers of cloud which are precipitating and as such some of the unresolved ventilation rate is likely to be due to updraughts occurring in stratocumulus layers. The second feature of note is the large gain of moisture in the boundary layer to the north of the warm front. This gain in moisture due to the evaporation of precipitation falling through the boundary layer from cloud above on the sloping warm front was mentioned by Schultz and Vaughan (2011) and has been determined to be a key component in modifying the distribution of potential vorticity in the cold conveyor belt (Schemm and Wernli, 2014). The analysis here is believed to be the first time that this process has been demonstrated in a numerical model.

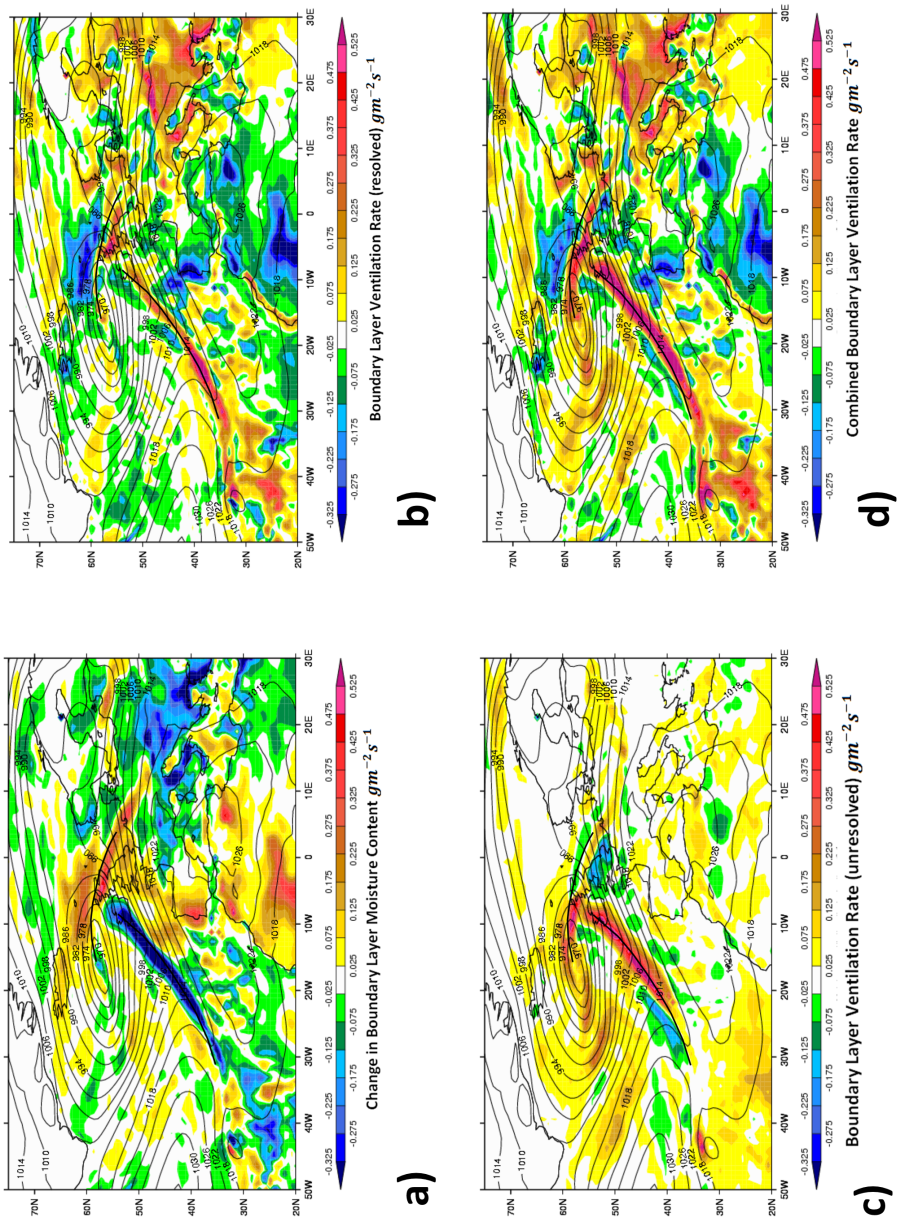

Figure 3.4: Moisture budget of the boundary layer for the 24th November 2009, 12:00 UTC. a) Total change in boundary layer moisture content ($gm^{-2}s^{-1}$) b) Boundary layer ventilation (resolved) ($gm^{-2}s^{-1}$) c) Boundary layer ventilation (unresolved) ($gm^{-2}s^{-1}$) d) Combined Resolved + Unresolved ventilation processes ($gm^{-2}s^{-1}$) e) Boundary layer divergence ($gm^{-2}s^{-1}$) f) Change in moisture content (other processes) (x $10gm^{-2}s^{-1}$) g) Evaporation. Overlayed are the mean sea level contours (gray) every 4hPa, the frontal positions, warm and cold (marked in black), have been marked on by using a combination of the surface potential temperature contours (Sanders, 1999 not shown) and the troughing in the isobars (Sansom, 1951).

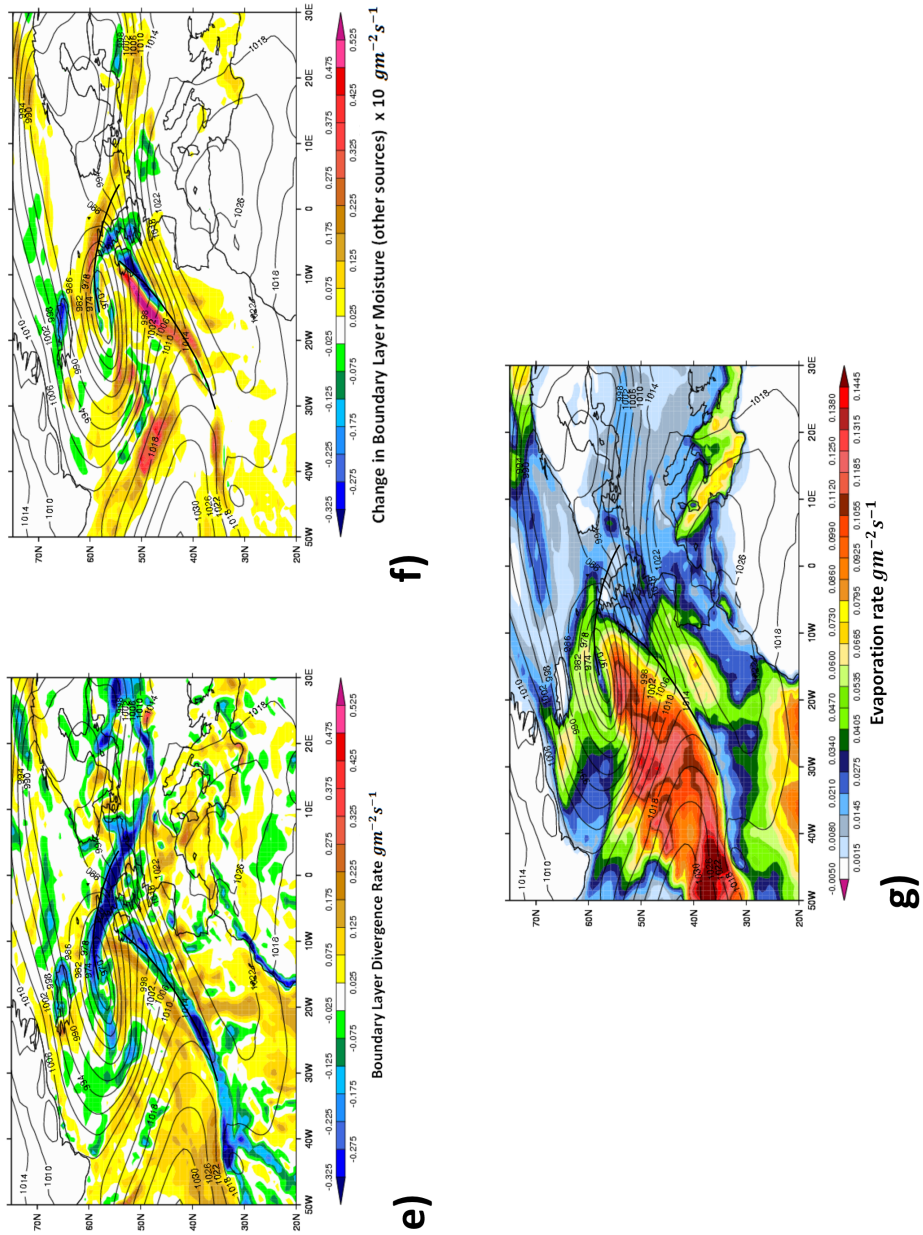
Boundary Layer Divergence Rate $gm^{-2}s^{-1}$
e)
Change in Boundary Layer Moisture (other sources) x 10 $gm^{-2}s^{-1}$
f)
Evaporation rate $gm^{-2}s^{-1}$
g)

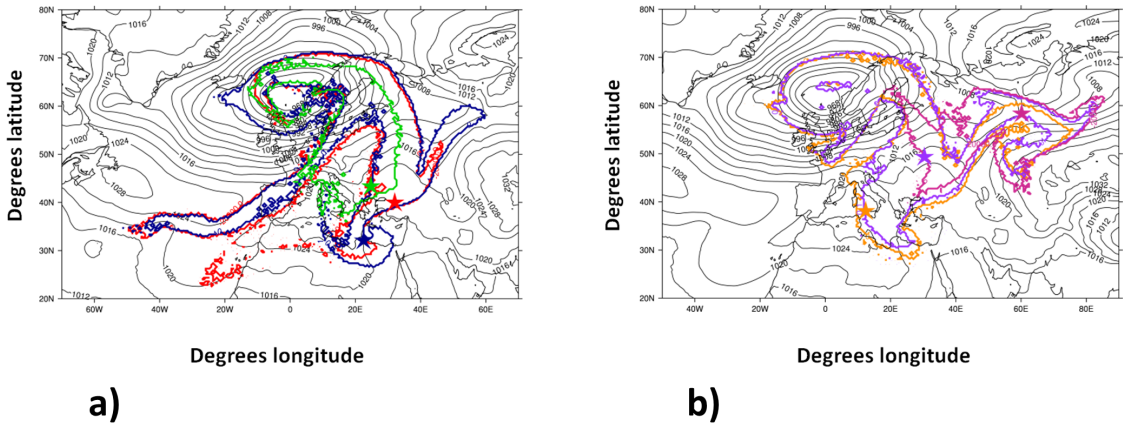

Figure 3.5: Panels a and b show a contour that represents the horizontal extent of particle dispersion (i.e. model grid squares inside the contour are occupied by particles whilst model grid squares that fall outside the contour do not have any particles present). Panel a shows extent of the dispersion after 81 hours for release points A (red), B (blue) and C (green) located as described in Figure 3.3. Panel b shows the dispersion after 81 hours for release points D (orange), E (purple) and F (pink). The coloured stars represent the point of maximum concentration within each plume. Underlayed is the mean sea level pressure as simulated by the UM run. The contour interval applied to the mean sea level pressure is 4hPa.

3.4.2 Lagrangian particle transports and ventilation

3.4.2.1 Dispersion from multiple points within the cyclone wave.

Figure 3.5, panels a and b, show the dispersion of particles for the release locations labelled A - C and D - F which are highlighted by the black circle shown in Figure 3.3. It can be seen in panel a that the release points that were initialised to the south (A-C) produce a spread in particles that encompasses a large proportion of the area that is commonly attributed to the warm conveyor belt (see Harrold 1973; Carlson 1980; Browning and Roberts 1994).

The release points that were initialised further north (E-F) are shown in panel b. The spread of these particles occupies an area that is attributed to the cloud head (Carlson, 1980; Browning and Roberts, 1994). Additionally, to the east, the anticyclonic flow out of the warm conveyor belt separates out into a further two branches. One of these continues in its path in an anticyclonic pattern to the south of the domain (particuarly the orange flow pattern) and another turns cyclonically into another area of low pressure associated with the developing system to the east (shown

in pink). This second split in the airflow is also demonstrated in the spread of particles released from points A and B shown in red and blue in panel a.

In the next section the flow of particles released from point B is examined in more detail. This release point was chosen because it not only resides in an area of enhanced evaporation in the anticyclone (see Figure 3.3) but also because particles from this point produce the most widespread dispersion at 81 hours into the NAME simulation (see Figure 3.5).

3.4.3 Dispersion from a single point

It is clear from Figure 3.5 that particles are widely spread by the action of both turbulence and convective dispersion (see Section 3.2.4. In order to investigate this spread of particles, a single release point will now be looked at in more detail. In particular, a more detailed look at the location and mechanisms by which particles escape from the boundary layer are investigated. This will be achieved by splitting the flow up into different regions at the end of the simulation. Two methods will then be used in order to investigate how particles are dispersed into each region. The first involves tracking the properties of individual particles in an attempt to show how and when each group of particles exit the boundary layer. The second will try to see how changes in turbulence, and methods of dispersion, affect the final distribution of particles. A comparison will also be made by using non turbulent trajectories.

3.4.3.1 The boundary layer structure

The tephigram associated with release point B (see Figure 3.3) is shown in Figure 3.6. Several different layers of air are marked out on the tephigram, which are defined by the temperature structure of the atmosphere. The temperature of the atmosphere is represented by the red line. In the lowest layer this line is parallel to the lines of constant potential temperature. This region of the atmosphere has its upper bound at a small inversion in potential temperature and is marked by the horizontal green line, which represents the boundary layer top as diagnosed by the NAME model. The fact that the potential temperature does not change with height indicates that this is a well mixed layer, with turbulent eddies mixing the air from the bottom of the layer to the top.

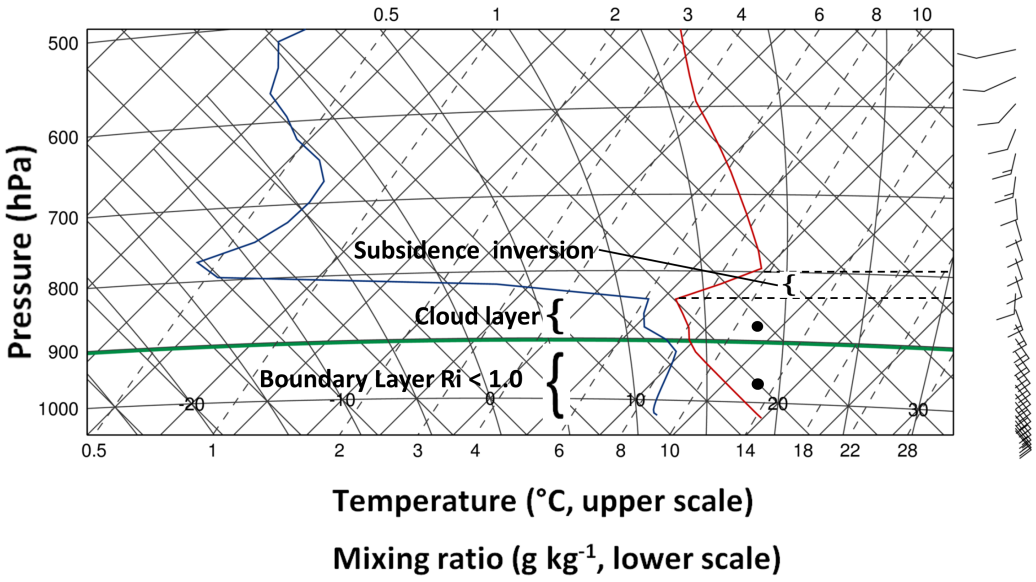

Figure 3.6: The lower portion of the troposphere at 41°W, 35°N. The temperature is represented by the red line and the dew point by the blue line. Wind arrows represent the speed (ms^{-1})and direction (in degrees from north) of the wind at different levels in the atmosphere. The different layers of the atmosphere are explained in the text. Height is indicated by the atmospheric pressure, listed on the y-axis in hPa. On the x-axis two scales give the atmospheric temperature and the mixing ratio. The two black dots indicate the release level of two additional groups of particles.

The layer of air above the diagnosed boundary layer has been labelled as the cloud layer. Using a Normand's point construction (not shown, see Office, 1996) and following the path of a saturated adiabatic lapse rate up to the height of the subsidence inversion, it can be seen that this layer is capable of producing cumulus cloud. This is confirmed by the UM, which diagnoses shallow convective cloud of 81hPa in thickness at this point. The base of this cloud is diagnosed as being at 910 hPa. The cloud base is thus placed just below the boundary layer top. Above this layer is a layer of air which is characterised by the strong subsidence inversion which has formed due to the heating of air which has descended from the free troposphere aloft (Stull, 1989).

3.4.3.2 The ventilation of the boundary layer

In Figure 3.7 it can be seen that the ventilation of the boundary layer can be split up into three stages. Stage 1 last for the first 21 hours of the NAME simulation. The number of particles

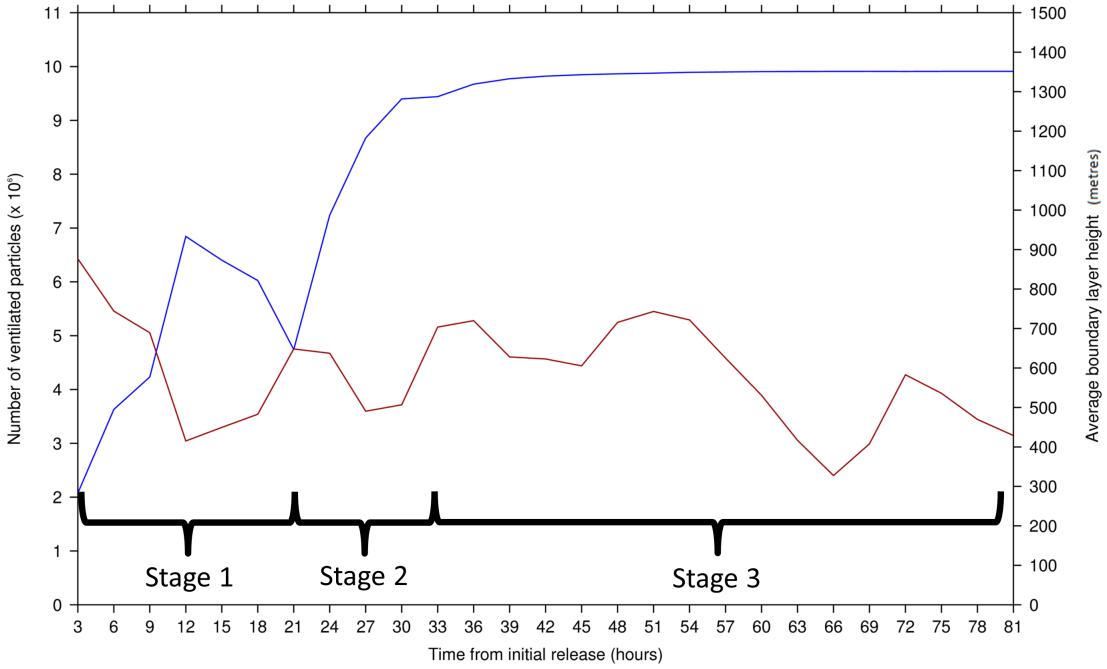

Figure 3.7: The blue line represents the number of particles that have been ventilated by the boundary layer (y-axis, left hand side) as a function of time in hours from initial release (x-axis). The red line represents the particle weighted mean boundary layer height (y-axis, right hand side) measured in metres as a function of time.

above the boundary layer (represented by the blue line) rises and falls. If compared with the red line which depicts the change in boundary layer height, it can be seen that these two are anti-correlated. This behaviour is explained in Ryall and Maryon (1998) and consists of particles being ventilated and re-entrained back into the boundary layer either due to being advected into regions of differing boundary layer heights (horizontal ventilation) or due to the movement of the top of the boundary layer.

In stage 2, which occurs between 21 and 33 hours into the simulation, the majority of particles that have been left in the boundary layer are ventilated rapidly and particles do not appear to be re-entrained into the boundary layer after this point. In stage 3 of the simulation, the last few remaining particles are ventilated from the boundary layer until all the particles are removed at a time of approximately 54 hours. In the later part of stage 2 and during stage 3, the ventilation of the boundary layer appears to be independent of changes in boundary layer height.

3.4.3.3 Grouping trajectories by final position

The red shading in Figure 3.8 shows the horizontal dispersion of particles at 81 hours after their initial release. Plotted on top of the red shading is the final location of the first 10000 particles released, which were used in order to help with defining individual sectors. Overlayed are the horizontal boundaries of four separate masks that were used in order to split up the particles into four separate groups. The masks are each identified as belonging to a sector in the dispersion plume. The sectors are labelled west, central, north east and south east respectively.

The western sector accounts for particles that had been advected in a cyclonic motion around the low centre of the cyclone. The western sector corresponds to the WC2 outflow of the warm conveyor belt described in the conceptual model presented in Chapter 1. The south eastern sector accounts for particles which had been advected in an anticyclonic path after being raised up on the warm conveyor belt and this constitutes part of the outflow associated with the WC1 flow of the warm conveyor belt, also described by the conceptual model. The north eastern sector also corresponds to the flow of the WC1 outflow of a warm conveyor belt but after its initial anticyclonic path the flow turns cyclonically. Particles in this flow are propagated the furthest east. The central sector accounts for particles which have not made it into either the cyclonic or anticyclonic flows of the warm conveyor belt. Using these characteristics the boundaries were defined subjectively.

In order to determine how the particles have been transported into each of these locations we first need to differentiate between the trajectories. One way of doing this is to use potential and equivalent potential temperature. Both of these variables are approximately conserved following the process of isentropic uplift on the warm conveyor belt.

A previous study of this system by Martínez-Alvarado *et al.* (2014) showed that the warm conveyor belt can be split up into two separate branches by the use of a potential temperature threshold. The study showed that trajectories, after 42 hours of ascent, which ended up with a potential temperature of less than 307.5 K belonged to the cyclonic branch of the storm, wrapping around the low pressure centre whilst trajectories that followed the anticyclonic branch attained a potential temperature of more than 307.5 K. These two flows were identified as belonging to the WC1 and WC2 conveyor belt flows described by Browning and Roberts (1994). The study

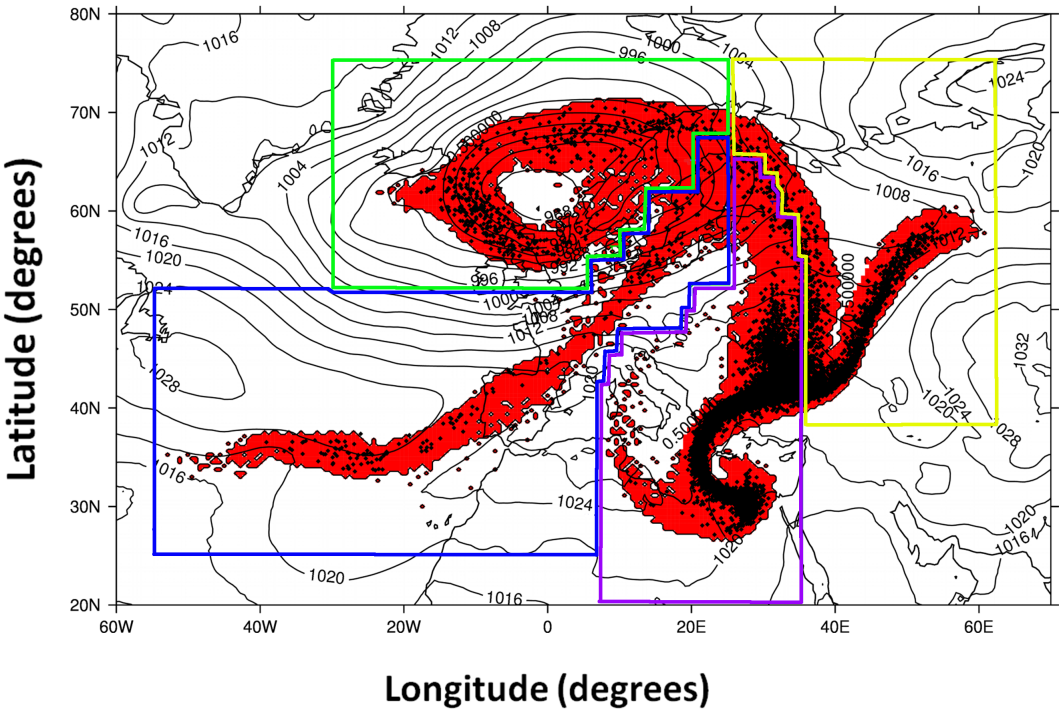

Figure 3.8: All of the model grid squares in which particles are present are shown in red at T+81 hours. The individual positions of the first 10000 trajectories are indicated by black dots. Four masks have been subjectively defined in order to group the trajectories based upon their final locations within the plume. Each mask is indicated by a colour and is referred to in the text as follows: west (green), central (blue), north east (yellow) and south east (purple).

by Martínez-Alvarado *et al.* (2014) went on to show that differences in the convective parameterization scheme used made a significant contribution to the amount of heating experienced by particles ascending each of these branches and thus influenced the amount of particles in each branch of the warm conveyor belt.

The spread in potential temperature for each of the sectors is given in Figure 3.9, panels a and b. The particles have been split up using the masks highlighted in Figure 3.8 at a time of 81 hours into the simulation. Panel a represents the spread in potential temperature at 42 hours into the simulation whilst panel b represents the spread in potential temperature at 81 hours into the simulation.

In both panels a and b of Figure 3.9 it can be clearly seen that the majority of particles (as determined by their interquartile ranges) in western and south eastern sector lie below and above

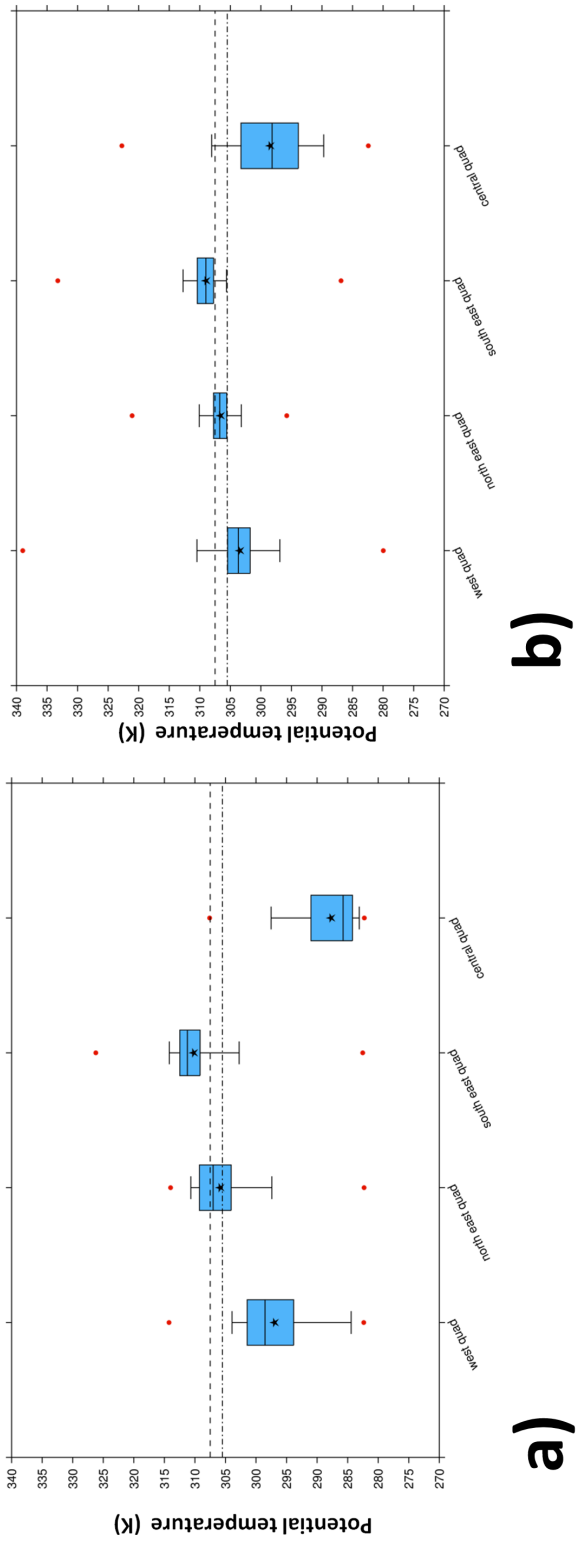

Figure 3.9: The spread in potential temperature for each group of particles at times T+42 (a) and T+81 (b). The grouping of the particles is based upon their final position, the masks for which are shown in Figure 3.8. The boxes represent the 25th and 75th percentile of each distribution. The whiskers represent the 5th and 95th percentile of each distribution. The limit of the distribution is indicated by a red dot. Two thresholds which represent temperatures of 305.5 K and 307.5 K are merked on the plots by a dash - dot line and a dashed line respectively.

the 307.5 K threshold respectively. The particles that lie in the north eastern sector however, straddle either side of the 307.5 K threshold. If a threshold of 305.5 K is chosen, however, at 81 hours into the simulation it can be seen that the anticyclonic and cyclonic branches of the warm conveyor belt are separated such that 75 % of the particles in the western sector fall below the threshold of 305.5 K whilst over 75 % of the particles in north eastern and south eastern sectors fall above this threshold.

In order to examine the role that boundary layer ventilation plays in determining the final thermodynamic properties of the particles in each sector the average temporal evolution of the first 100 000 particles was plotted for the parameters of potential temperature, equivalent potential temperature and height. In order to calculate each of these variables the simulation was limited to 100 000 particles in order to limit the size of the model output file which stores the individual location of each particle at each timestep. A comparison between a model run using 100 000 particles and a model run using 1 000 000 particles is given in Table 3.1 in order to demonstrate that 100 000 particles are sufficient in number to represent the dispersion of 1 000 000 particles. The proportion of particles above the boundary layer has also been plotted with time, normalised by each sectors maximum value, in order that the times at which boundary layer ventilation occurs can be compared. These evolutions of the average particle properties and the normalised values of boundary layer ventilation are displayed in Figure 3.10 a - d. In particular, it is of interest to look at the changes in θ and θ_e which are conserved variables of air parcels in dry and moist conditions respectively during the process of uplift on the warm conveyor belt. Any changes in these variables will indicate the influence of diabatic processes or the mixing of air parcels.

As shown in Figure 3.7 the panels in Figure 3.10 can be split up into three different stages although the lengths of each stage are not necessarily the same for each sector. As for Figure 3.7, we can split up the stages based upon the rate at which particles are ventilated from the boundary layer. It can be seen from Figure 3.10 d, that stage one lasts for the first 21 hours of the simulation for all four sectors. During this time particles leave and re-enter the boundary layer as they are advected along a plane of constant potential temperature, shown in Figure 3.10 b. The particles remain at a constant average geometric height, which is initially limited by the capping inversion above the cloud layer (see Figure 3.6) and at other times by the boundary layer top (which is equal to the height of the capping inversion or in a stable atmosphere to a point where the mechanical

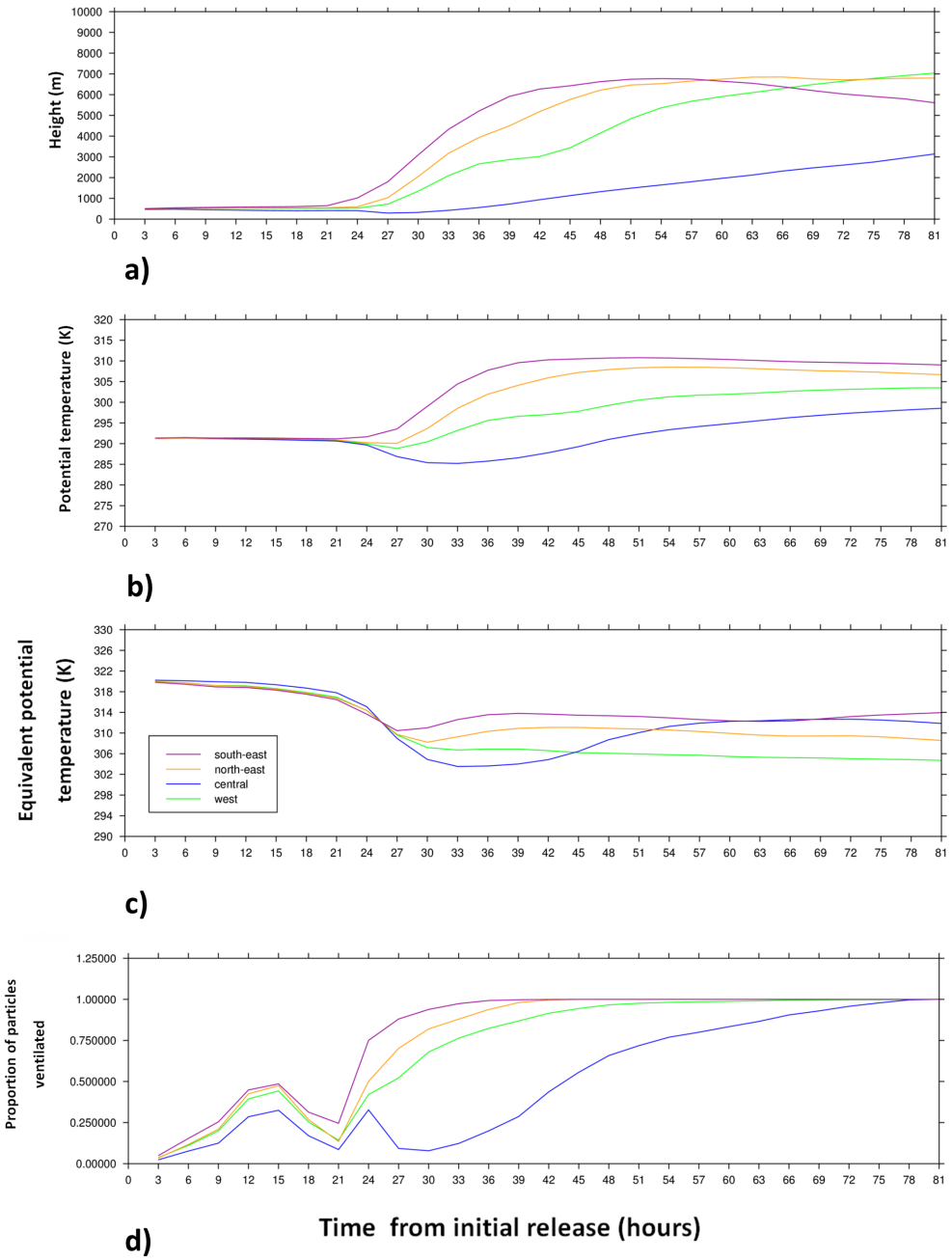

Figure 3.10: The time evolution of a) height above the model surface, b) potential temperature, c) equivalent potential temperature for the western (green), central (blue), north eastern (yellow) and south eastern (purple) sectors. A normalised plot of boundary layer ventilation is shown in panel b with colours that are associated with the same sectors as for panels a, b and c.

mixing generated by the surface dissipates).

Particles that end up in the central sector of the cyclonic wave can not be grouped in the same way as the other particles due to their small number and wide distribution in space mean that their average properties will have little meaning and as such will not be considered in the following analysis of stage two and three.

Stage two is where the different sets of particles separate out into distinct groups based on their average thermodynamic properties. Particles that end up in the south eastern sector are the first to begin their ascent into the free troposphere (see Figure 3.10 a) followed by particles which end up in the north eastern sector and finally by particles that end up in the western sector of the cyclonic wave. Similarly the largest number of particles is found in the south east sector (see Table 3.1), the second largest number of particles is found in the north east and the smallest number of particles are found in the west. A comparison between Table 3.1 and Figure 3.10 reveals that the rate of ventilation of particles is quickest for the south east sector, followed by the north east sector and the west sector has the slowest ventilation rate.

The ascent of the particles out of the boundary layer can be examined with reference to the average change in equivalent potential temperature. In each of the sectors ascent is accompanied by a sharp drop in equivalent potential temperature, followed in the north and south eastern sectors by a rise. Particles that flow into the western sector do not experience this subsequent rise in equivalent potential temperature. We will now consider what these changes in equivalent potential temperature mean.

Equivalent potential temperature is an approximately conserved variable for a parcel of air

	West	North east	South east	Central
1 000 000 particles	45986 (4.6 %)	182153 (18.22 %)	753029 (75.3 %)	18832 (1.88 %)
100 000 particles	4571 (4.6 %)	19371 (19.4 %)	74211 (74.2 %)	1847 (1.85 %)

Table 3.1: The distribution of particles in each of the Sectors at time T+81 for the release point B. Small differences are obtained between the run containing 100 000 particles and the run containing 1 000 000 particles. Computations containing more than 1 000 000 particles proved to be to commputationaly expensive.

(see Holton 1972) changing only by the diabatic addition of heat and their radiative heating and cooling which we shall assume to be small in this case and thus neglect in our analysis. However, it is here that we must make the distinction between a particle in space and an air parcel. The particle is free to move between air parcels and thus change its equivalent potential temperature accordingly. Therefore, this change in equivalent potential temperature implies a mixing of air parcels. Two such mechanisms are employed by the NAME model in order to represent particles moving between air parcels. The first of these mechanisms is the use of the convection scheme in NAME which is described in Section 3.2.4.8. The second mechanism involves the particles hopping from one streamline to another due to the turbulent motion. This process of hopping streamlines is described in Aref (1990) where it is called chaotic advection and is represented in the NAME model by using a random number in the random walk method (see Section 3.2.4).

In order to test whether convection or turbulence is responsible for removing the particles from the boundary layer we re-ran NAME with the convection scheme turned off. The resulting grouping of the particle paths was almost identical to those shown in Figure 3.10. This result suggests that turbulence and not convection is responsible for the redistribution of particles in stage 2 which is contrary to the general findings of Martínez-Alvarado *et al.* (2014). However, the study by Martínez-Alvarado *et al.* (2014) distributed particles throughout the system and did not focus on looking at transports of moisture from significant source regions. Our result shows that turbulent trajectories can be found that directly link an area of high evaporation rates and the ventilation of moisture from the boundary layer and as such convection is not an important process altering these trajectories.

To further investigate the lack of convective influence we have plotted the average location of each group of particles at time T+21, T+24, T+27 and T+30 (times that correspond with the ventilation of particles out of the boundary layer) in Figure 3.11, panels a - d respectively. By comparing Figure 3.11 panel a and b with Figure 3.10 d it can be seen that when all of the particles that are grouped in the south eastern sector have been ventilated from the boundary layer the majority have yet to come into contact with any convective activity. The same is true for the majority of particles that have been ventilated in both the north eastern sector and the western sectors of the domain. This result is to be contrasted with the large flux of unresolved ventilation observed in Figures 3.4 b and c to the East of the resolved ventilation on the cold front. This

demonstrates that small scale turbulent processes are responsible for ventilating the boundary layer within the warm conveyor belt. An important point to note is the close proximity of the three groups of particles, indicating that the end point of each particle's trajectory is likely to be highly sensitive to the exact point that they exited the boundary layer.

In the second half of stage two ventilation it has already been observed that the rate of increase in equivalent potential temperature is indicative of the separation of particles between the four sectors. This rise in equivalent potential temperature is likely to do with the increase in heat supplied by diabatic processes (Ahmadi-Givi *et al.*, 2004) due to the large scale formation of cloud. The amount of diabatic heating which can take place in a cyclone is a current topic of much interest (Rossa *et al.*, 2000; Joos and Wernli, 2012).

The small scale processes which are responsible for changing the equivalent potential temperatures of particles could be better resolved by using large eddy simulations. However, working on this scale is beyond the scope of this thesis.

This section has examined in detail the transport of particles out of the boundary layer, and into the three sectors of the warm conveyor belt. It has been shown that the average location of the particles on the cold front when they are ventilated, along with the mechanism of turbulence, is responsible for determining their final location. In the next section we will examine the roles of convection, turbulence and the effect of releasing particles at different heights into the boundary layer have on their final location.

3.4.3.4 A comparison with trajectories following the resolved flow

The individual positions of the first 10000 individual trajectories are plotted in Figure 3.12 at a time of 3 hours from the initial release. It can be seen that by this time the particles are well mixed throughout the boundary layer and that some particles have been ventilated through the boundary layer top with particles obtaining an altitude of up to 1400 metres. Whilst the majority of particles have moved in a westerly direction a few remain near the original release point at 319° E (41°W).

In order to test the effect that the turbulent mixing has in redistributing particles throughout the boundary layer and just above it, three additional releases were performed. In each of these

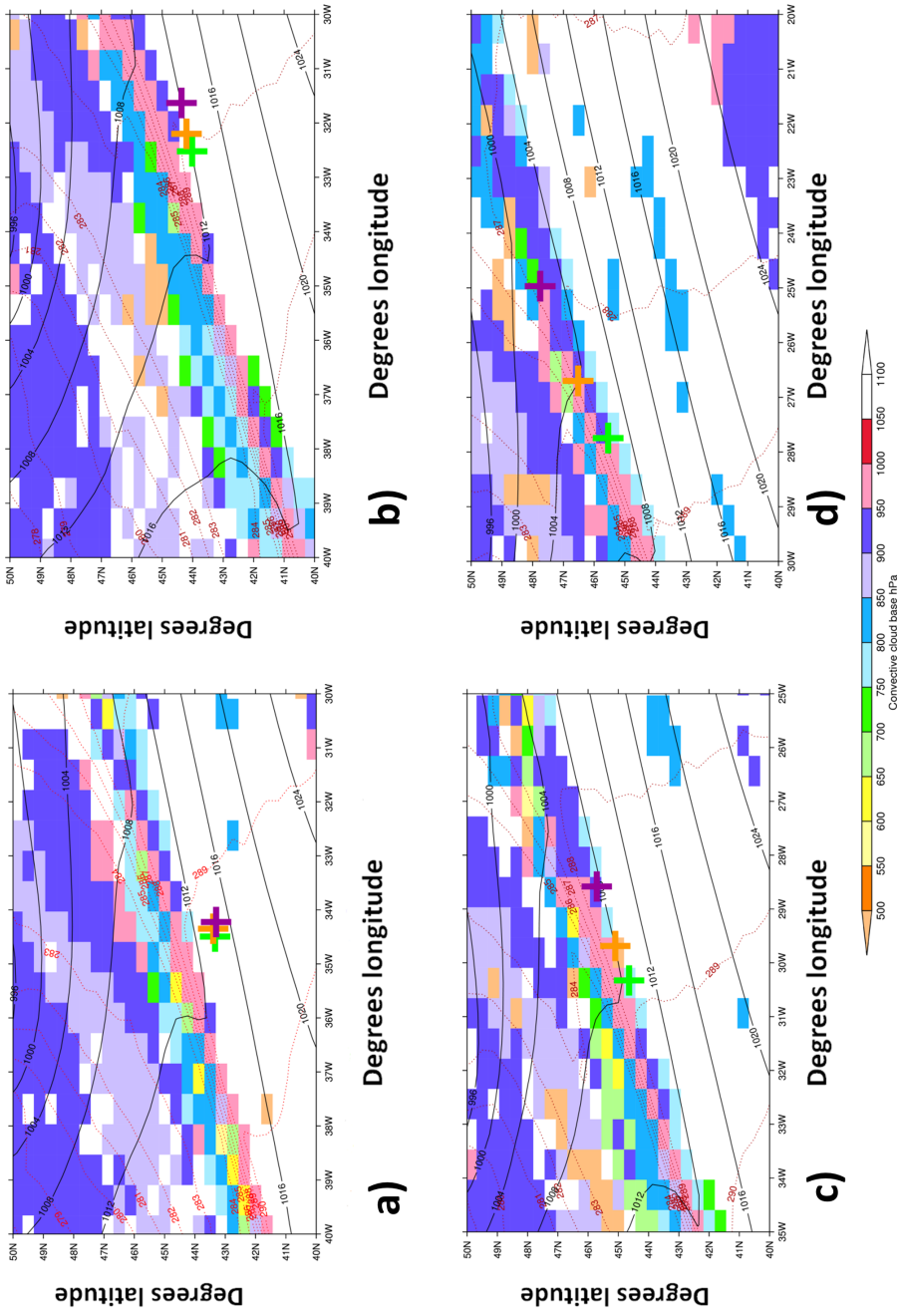

Figure 3.11: The mean sea level pressure (contoured in black at 4 hPa intervals) is overlayed onto a plot of the base height of convective clouds marked by the coloured squares. The red contours show the surface potential temperature (contoured at 1 K intervals). The locations of groups of particles associated with the west (green), north east (yellow) and the south east (purple) sectors are marked by crosses at times a) T+21 b) T+24 c) T+27 and d) T+30 hours into the NAME simulation.

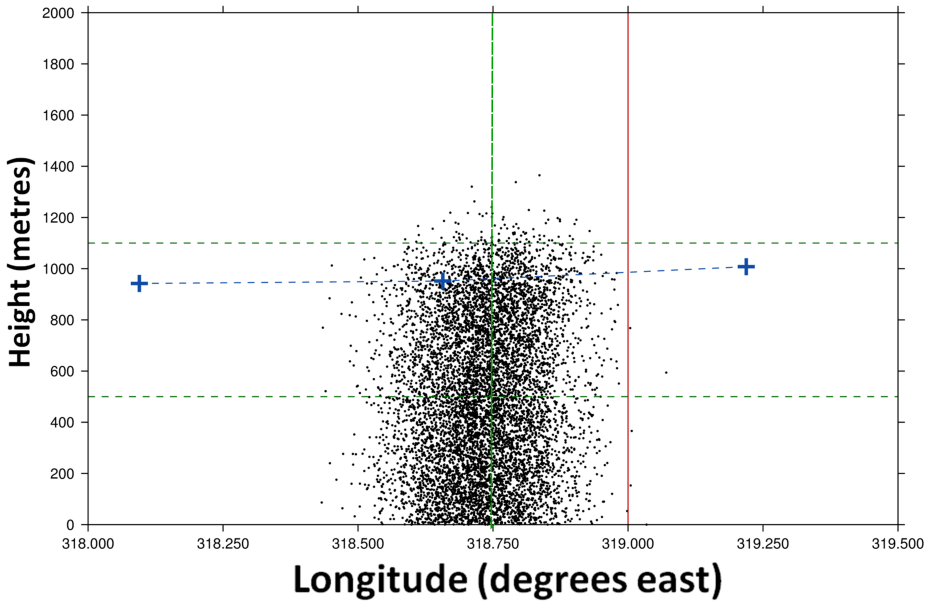

Figure 3.12: The position of the first 10000 particles as a function of longitude (x-axis) and height (y-axis) at time T+3 hours. The latitudes represented are between 35.8 and 36.0 degrees. The release point at 1200 UTC on the 22nd November 2009 is indicated by the red line. Particles were released at 1 m above the surface. The boundary layer height is indicated by the blue dashed line. Each individual particle is indicated by a black dot. The heights of two additional elevated release points are indicated by the crossing of the dashed green lines.

experiments all of the turbulence and convective motion was turned off to produce a single deterministic trajectory. The release points were chosen such that they were initialised within the distribution of particles represented by Figure 3.12.

The first release point was at 1 m above the surface and at a longitude of 318.75° E and 35.9°W. The particles did not move far from the original release point (<0.25°) which shows that at this point turbulence is necessary in order to facilitate particle advection and that the resolved flow is not large enough in order to remove particles from the surface layer.

The second release point was set to be at 500 m above the surface and is indicated by the lower green cross in Figure 3.12. This will be called trajectory B1 in the following discussion. This release location was chosen because it resides near to the centre of the plume at a time of T+3 hours from release within the boundary layer. The third release point that was chosen is indicated by the upper green cross in Figure 3.12 and resides within the plume of particles just above the

top of the boundary layer. This will be called trajectory B2 in the following discussion.

Figure 3.13 shows the positions of the two deterministic trajectories and allows a comparison with the distribution of particles both from a release at point B and at a release point situated at 500 m above the surface. Initially the particles start out in close proximity to each other but by T+27 hours (see panel c of Figure 3.13 or Figure 3.14) it is evident that the trajectory B2 (approximately 100 metres above the boundary layer top) is situated to the east of the plume, whilst the trajectory B1 occupies a position that is to the west of the dispersion plume.

Panels d, e and f demonstrate that the trajectory B2 does not progress as quickly (despite initially being above the boundary layer and so experiencing winds that are not subjected to the frictional retardation force of the surface) into the south east quadrant of the plume as the trajectory B1. This suggests that trajectory B2 is lifted up into a region of high winds within the warm conveyor belt at a later stage than trajectory B1 and that the removal of particles from the boundary layer in the early stages of the simulation delays the particles in joining the flow of the warm conveyor belt.

It is worth noting that by the end of the simulation at T+81 hours both of the deterministic trajectories end up in the south east sector of the dispersion plume. It is therefore difficult to draw any definitive conclusions at this stage as to the origins of particles in the other sectors due to the stochastic nature of dispersion. However, it can be concluded that turbulence is responsible for altering trajectories in such a mannor that advection into these other sectors is possible.

3.4.3.5 Processes controlling the dispersion of particles

The red shading in Figure 3.13 shows the distribution of particles released at 500 m above the surface at 318.75°E and 35.9°N. This can be contrasted with the positions of particles released from point B in Figure 3.3 and indicated by the orange contour in Figure 3.13. Both release points provide an almost identical horizontal distribution although the numbers of particles which end up in each sector (west, central, north east and south east) at T+81 are slightly different. This demonstrates the validity of using the same sectors in order to conduct our sensitivity analysis.

Table 3.2 shows the results of a sensitivity analysis conducted using the release point situated

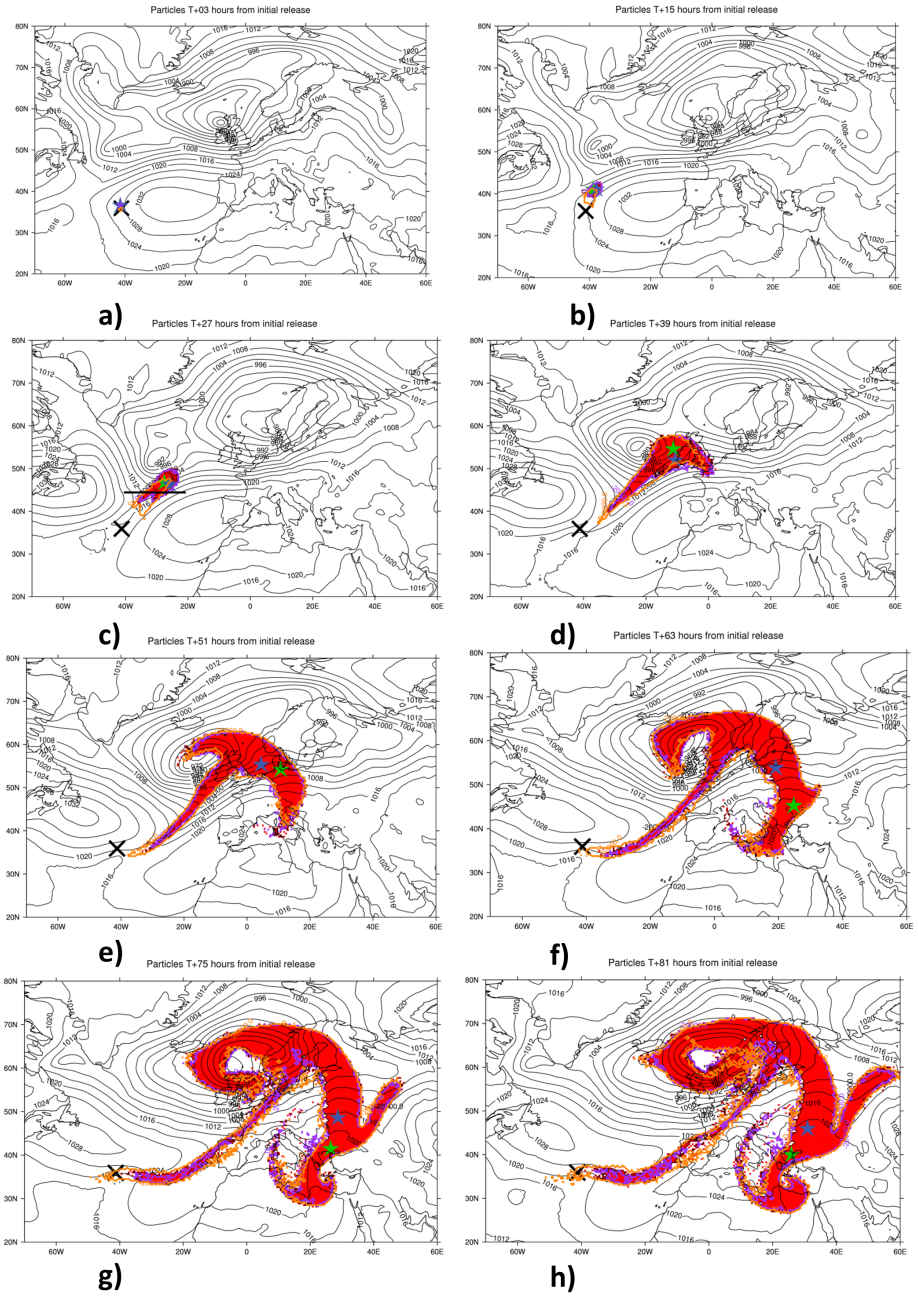

Figure 3.13: The distribution of particles from release points close to 319°E and 45° N given at time periods 3 - 81 hours after their initial release is shown by the orange contour. The red shading indicates the distribution of particles that were released at 500 m above the surface at a position of 318.75°E and 35.9°N. The purple contour represents particles which were released at 1100 m above the surface. Two deterministic trajectories are also represented by stars. The green star represents the deterministic trajectory of a particle released at 500 m above the surface. The blue star represents the deterministic trajectory of a particle that was released at 1100 m above the surface.

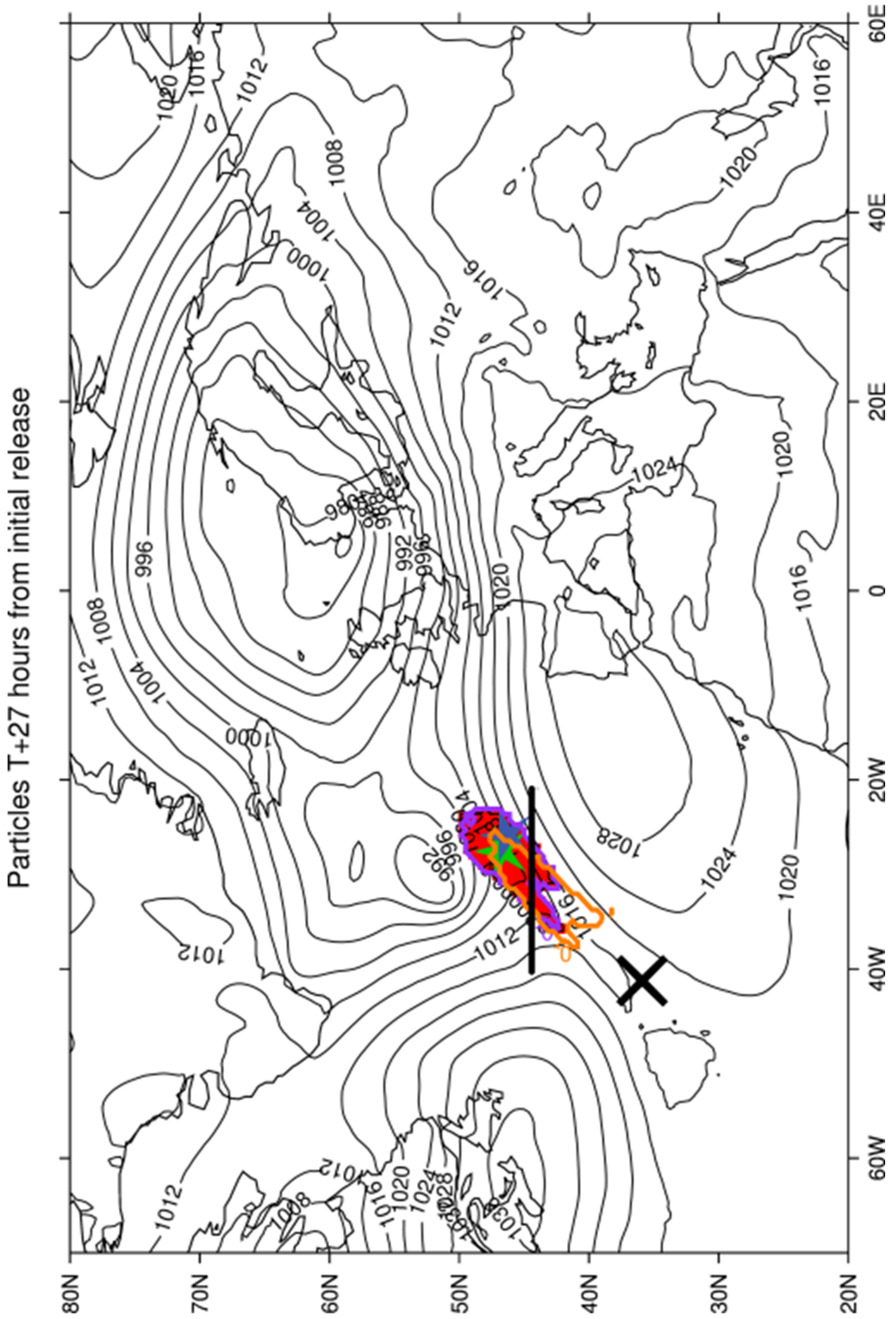

Figure 3.14: Expanded version of panel c of Figure 3.13

	West	North east	South east	Central
Control (500 m)	78838 (7.88 %)	196117 (19.61 %)	718411 (71.84 %)	6634 (0.66 %)
Only convection (500 m)	455 (0.046 %)	2398 (0.24 %)	997057 (99.71 %)	90 (0.01%)
Only turbulence (500 m)	77968 (7.80 %)	199845 (19.98 %)	715641 (71.56 %)	6546 (0.65 %)
Skewed turbulence (500 m)	78288 (7.83 %)	197462 (19.75 %)	717625 (71.76 %)	6625 (0.66 %)
Surface (1 m)	73190 (7.31 %)	200967 (20.10%)	718937 (71.89 %)	6906 (0.69 %)
Above bl (1100 m)	130361 (13.04 %)	117050 (11.71 %)	747032 (74.70 %)	5557 (0.56 %)

Table 3.2: The results of six experiments designed to test the sensitivity of different methods of dispersion to the final distribution of points in the sectors described in Figure 3.8. Each of the experiments is listed in the left hand column. Each experiment is described in the main body of text.

at 318.75°E and 35.9°W. The table gives the number of particles out of one million that ended up in each sector. The number in brackets represents the percentage of particles in each sector. In these experiments we used the release at 500 m above the surface as the control experiment with both the dispersion by convection and by turbulence switched on.

Three experiments were subsequently performed. The first experiment only switched on the dispersion by convection (see Section 3.2.4.8) and turned off the turbulent dispersion options in NAME. The second experiment turned off the dispersion by convection and kept the dispersion by turbulence turned on. In the third experiment the skewed turbulence option (see Section 3.2.4.9) was turned on for the first 30 minutes of the run along with the dispersion by convection. This experiment was used in order to test whether or not the initial distribution of particles within the NAME column made a significant difference to the final distribution of particles.

An additional two experiments were also performed by altering the height at which particles were released within the atmospheric column. The first released particles within the surface layer at a height of 1 m. The second released particles at a height of 1100 m, approximately 100 m above the boundary layer top. The second of these two experiments was designed to test the hypothesis that by releasing particles above the top of the boundary layer, a delay in their uplift on the warm conveyor belt is caused which subsequently allows an increased number of particles to be diverted into the western sector (i.e. into the cyclonically turning path of the warm conveyor belt around the low pressure centre).

In the control run the majority of particles (71.84 %) end up in the south east sector. This is in

agreement with the final position of the deterministic trajectory displayed in Figure 3.13. For the result of the second experiment 99.71 % of particles are delivered to this location when only the dispersion by convection is turned on. It is therefore clear that turbulence is responsible for the majority of particles that end up on potential temperature surfaces associated with the west, north east and center sectors of the domain. This is confirmed by the experiment which only made use of the turbulence and delivered 71.56 % of the particles into the south east sector.

The final three experiments looked at how the distribution of particles within the atmospheric column affected the final locations of particles in the dispersion plume. The results for applying skewed turbulence during the first 30 minutes of the NAME simulation (see Section 3.2.4.9) show a small change in the number of particles separated out by each mask. However, the use of a pseudo random number generator in the NAME code ensures that the same random perturbations are always applied and as such even small changes in the numbers reported in Table 3.2 can be viewed as significant. The experiment shows that whilst the number of particles found in the western sector and south eastern sector decrease slightly this is compensated for by the number of particles advected into the north eastern sector increasing slightly. It would be extremely interesting to adapt the NAME code in order to investigate this result more fully by extending the amount of time that skewed turbulence is applied to the boundary layer. Unfortunately this would significantly increase the time it takes in order to complete a run of the NAME model and as such has not been attempted here.

The significance of initial particle location within the atmospheric column is also highlighted by the results of the two further experiments performed with release points near the surface and above the boundary layer. When particles are released above the boundary layer the number of particles that finally, end up in the western sector is increased by 78 %. Conversly, when particles are released near the surface this increases the number of particles that end up in the north east sector of the outflow of the warm conveyor belt. The link between the number of particles released above the boundary layer and their final position in the western sector is further explored in Section 3.4.3.6 . By comparing the results presented in Table 3.2 from a release at the surface with the results presented in Table 3.1 it can be seen that by altering the release position of the particles by just a small fraction can have a large impact on the final destinations of particles. In the case presented the adjustment in lattitude and longitude increases the final

number of particles that end up in the western sector by 62% . This suggests that the results presented are specific to the release points chosen.

These results are important when considered in the context of current research which has linked the growth in forecast error with potential vorticity anomalies which are propagated in the warm conveyor belt (Martinez-Alvarado *et al.*, 2015). In particular, it is important to note that the traditional use of boundary layer schemes which determine the bulk properties of an atmospheric column within the boundary layer (see Section 3.2.4.11) may not be sufficient to represent the exact distribution of moisture within an atmospheric column, particuarly in the region above the boundary layer where the rate of moisture ventilation will be important in deciding this amount. In our case the distribution of particles throughout the atmospheric column which we have determined to use as a proxy for moisture molecules will be dependant on the terms described in Section 3.2.4 of this thesis, which include both a random element and empirically defined formulae for the velocity variance and Lagragian timescales, neither of which have not been independantly confirmed to represent the true nature of turbulent dispersion within the warm conveyor belt. Similarly, the Eulerian moisture budget, presented in Section 3.4.1, shows us that a large proportion of the moisture advected out of the boundary layer within the vicinity of the warm conveyor belt is removed by the unresolved component of the flow, this suggests that models of a higher resolution may represent this venting in a different manner and thus change the location of the ventilation on the front which would ultimately change the distribution of moisture in the cloud head.

3.4.3.6 A cross section through the dispersion plume

A cross section through the dispersion plume at T+27 hours is depicted in Figure 3.15. The blue dashed contour represents the extent to which particles have been dispersed, whilst the blue and green shading represents the number concentration of particles at any given point. It can be seen from panel b that at time T+ 27 hours the dispersion plume is split into three maxima of particle numbers, labelled A, B and C.

In order to determine the cause of each of these maxima in number concentration we refer back to the results of Sections 3.4.3.3 and 3.4.3.5. These results showed that on average the

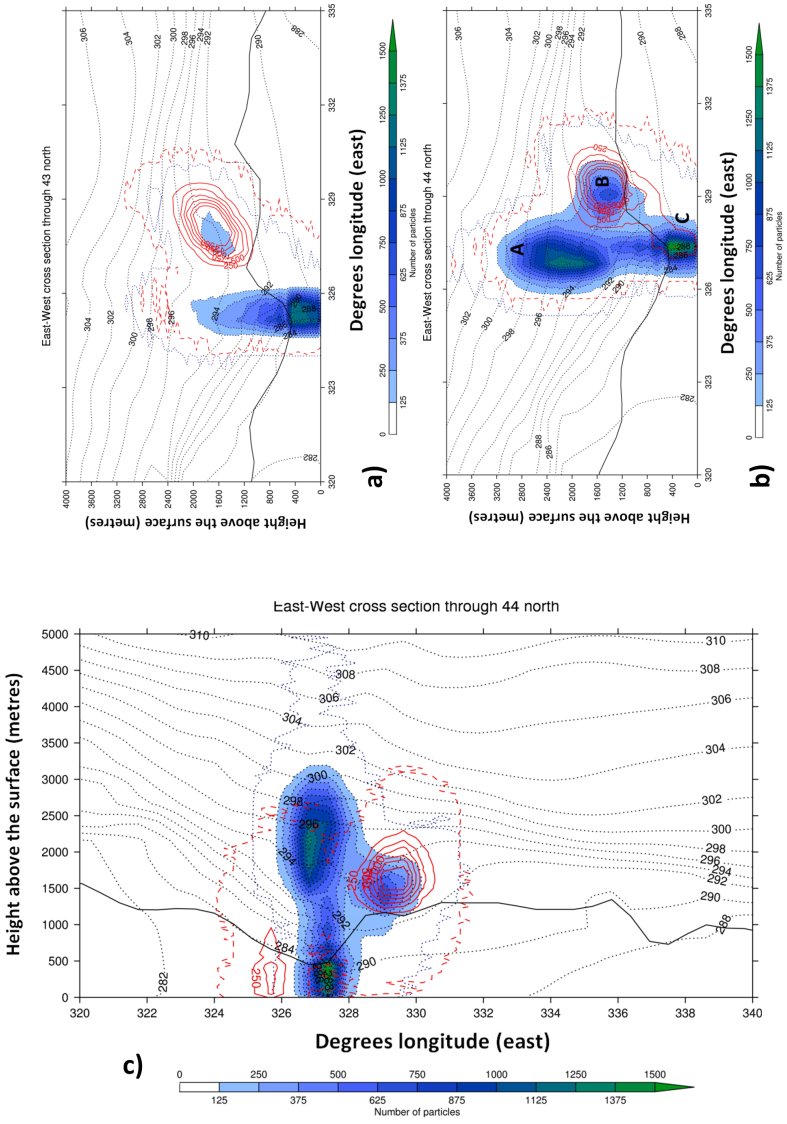

Figure 3.15: Cross sections through the dispersion plume at 43°N and 44°N at T+27 hours into the NAME simulation. The location of the cross section at 44°N is described by Figure 3.13c. The number concentration of particles is represented by the blue and green shading. The extent to which the particles have been dispersed is indicated by a dashed blue line. The exact number of particles is given by the colour bar beneath each plot. The cross section shows the distribution of particles as a function of height above the model surface and the horizontal distance, measured in degrees longitude. The potential temperature contours are shown as black dotted lines and the boundary layer top is indicated by a solid black line. The cross sections also shows the positions of particles for the release at 1100 m above the surface. Panel c uses data from a release point started at position B1 to overlay the red contours as described by the upper green cross in Figure 3.12. In panels a, b and c the extent of the particles dispersion is indicated by a dashed red line whilst solid red contours indicates the particles concentration.

particles that ended up in the western sector of the dispersion plume at T+81 hours were located slightly to the east of the other two groupings of trajectories during the time period T+21 - T+27 hours. It was also shown in Section 3.4.3.4 that the deterministic trajectory of particles that had been lofted above the boundary layer top during the first 3 hours of release were advected to the east of the dispersion plume. We therefore overlayed a cross section of the dispersion plume from the release point 1100 metres above the surface which had all the dispersion and convection options switched on. The results of this experiment have been overlayed with the results of the original dispersion plume and plotted as red contours in at time T+ 24 hours Figures 3.15.

In Figures 3.15 a and b a clear spatial correlation can be seen between the particles that are released above the boundary layer and the particles that make up the area B. Whilst evidence has been provided in diagram 3.7 that a certain proportion of the particles are present above the boundary layer from T+3 onwards. Figure 3.15c shows that if particles are released within the dispersion plume at T+3 at trajectory location B2 (see Section 3.4.3.4) that once again the majority of particles, indicated by the red contour lines, end up in a location that is co-incident with positioin B in the dispersion plume. (It should be noted that the particles that end up in position C are displaced to the west due to the mismatch in times being displayed here.) This combined with the evidence supplied in Sections 3.4.3.3 and 3.4.3.5 shows that on average it is the particles in the number concentration maxima labelled B that are delayed in joining the warm conveyor belt, lifted on the warm conveyor belt at a later time and thus responsible for contributing to the number of particles that end up in the western sector. It has also been shown that particles that end up in the south eastern sector of the warm conveyor belt are those which are vented from the boundary layer relatively early and these are responsible for the increased number concentration in particles labelled A. The particles which have remained in the boundary layer and are ventilated relatively late are those which have been labelled C in Figure 3.15.

The results presented in this section are important when considering moisture flows into a warm conveyor belt. Changes in the distribution of moisture are likely to effect the overall development of the cyclone through the application of latent heating (Chang *et al.* 1982, Stoelinga, 1996 and Ahmadi-Givi *et al.* 2004) which can change the cyclones overall distribution of potential vorticity (Stoelinga, 1996 and Rossa *et al.*, 2000) and can then cause a rapid intensification of the cyclone (Kuo *et al.*, 1991).

3.4.4 The warm conveyor belt (tropical sources)

In order to test the hypothesis that most of the moisture being ventilated by the boundary layer within a mid latitude cyclone is sourced from sources of moisture within the system of anticyclones adjacent to the low pressure centre (Boutle, 2009) trajectories were initiated to the south of the domain in order to represent moisture flowing into the system from the tropics.

Particles which represent the possible flux of moisture in from the tropics were released from positions G, H and I in Figure 3.3. Their final horizontal distributions are shown in Figure 3.16 panel a. It can be immediately seen from this distribution that release points G and H do not allow for material to propagate into the warm conveyor belt flow and do not add any additional material to any of the three defined sectors which make up the anticyclonic and cyclonic paths in the outflow of the warm conveyor belt. Some material which has been released from release point I, which is influenced by the flow associated with the south western flank of the anticyclone (see Figure 3.3) , does get entrained into the northward propagating flow of the warm conveyor belt. However, the black contours in Figure 3.16, panel b show that only a small number of particles are present in the northward propagating branch of the plume.

The results of this experiment along with supporting evidence from the literature (e.g. Knippertz and Martin, 2007, Sodemann and Stohl, 2013a and Dacre *et al.*, 2014) suggests that any moisture entrainment into the system from tropical sources is likely to be from a position above the boundary layer. The difference between events that are dominated by tropospheric moisture flows compared with events which are dominated by boundary layer moisture sources will be investigated in the next chapter.

3.4.5 The residence times of trajectories due to wet deposition

The timescale for the atmospheric residence of moisture is reported to be between 3 - 20 days Van der Ent and Savenije (2011) and the topic of moisture recycling has been widely studied for individual regions of the earth (e.g. Trenberth 1999, Eltahir and Bras 1994 and Savenije 1995) but very little amount of attention has been paid to the amount of time it takes for the recycling of precipitation in an individual synoptic system. In order to assess the amount of time that it takes

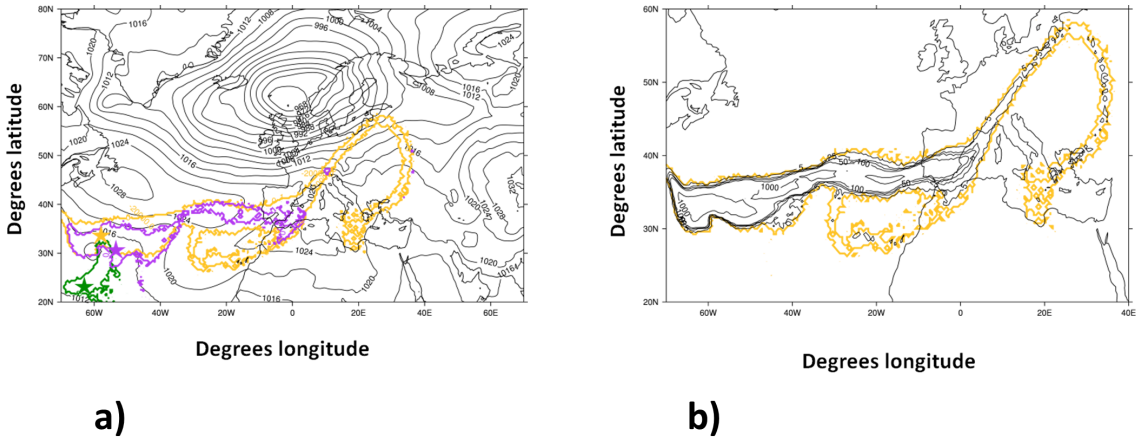

Figure 3.16: The distribution of particles at 81 hours into the NAME simulation released from points G (green), H (purple) and I (yellow) and shown in panel a. Mean sea level pressure contours are plotted at 4 hPa intervals. Panel b shows a close up of the distribution of particles for point I with additional contours applied for 5, 25, 50, 100,1000 and 10000 particles.

for moisture to cycle from the point of evaporation to the point of deposition on the surface by precipitation the wet deposition scheme was turned on in the NAME model. The results of each of these calculations is presented in Figure 3.17 for each of the release points described by Figure 3.3a in Section 3.3.2.1. Each line represents the change in mass of the particles as defined by Equation 3.35.

It can be seen by comparing the dark blue line (release point B) in Figure 3.17 with the blue line in Figure 3.7 that immediately after ventilation from the boundary layer at T+21 hours the mass of the particles rapidly decreases as they come into contact with precipitation. By T+39 all of the mass associated with the particles from release point B is removed from the system. A similar pattern of removal is repeated for the particles that have been released from point A. The mass associated with these particles is all removed from the domain by T+45 hours into the NAME simulation and is similarly removed rapidly after they have been ventilated from the boundary layer (Figure not shown).

Particles that were released at locations D and F are rapidly removed initially but then more slowly from T+21 hours into the NAME simulation. However, by T+45 hours all of the mass has been removed. This is in contrast to the mass loss experienced by the particles which were released at points C and E which is much more gradual. The mass loss from point C is incomplete

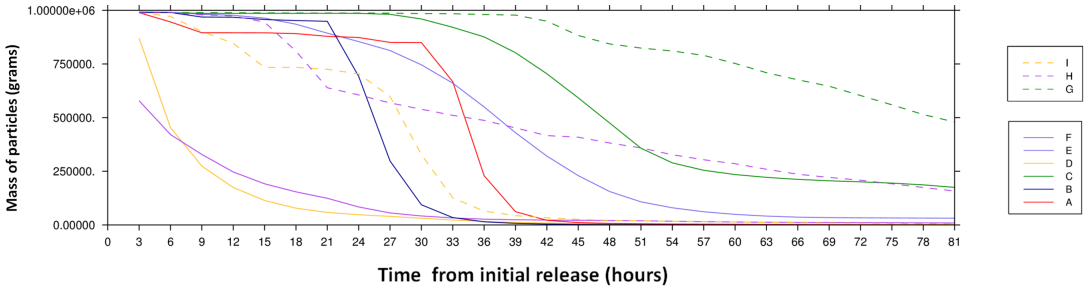

Figure 3.17: The depletion of mass for particles released from each of the locations in Figure 3.3 due to the NAME wet deposition scheme being activated. The initial mass of all of the particles was arbitrarily set as 1.0 x 10^6 grams. The dashed lines represent particles that have been released on the tropical moisture source border whilst the solid lines represent extra-tropical sources.

with approximately 20 % of the mass associated with the particles remaining at the end of the simulation. Such particles do not encounter much heavy precipitation during transit. However, these two release points do highlight the sensitivity of mass loss via precipitation to the exact location of the initial release point within the warm conveyor belt and have been included in order to illustrate this.

Particles that were released at locations G and H only lose mass slowly. However it is clear from the results in Section 3.4.4 that the particles associated with these release points do not join the warm conveyor belt. The mass associated with particles that were released from point I decrease in a fashion that is very similar to the sources from release points A and B. However, only a small percentage of these particles are actually drawn into the trunk of the warm conveyor belt and as such most of the mass must be removed by precipitation processes produced on the trailing cold front front of the system.

The large range in the time that it takes to remove all of the particles between the different release points shows that large transports of moisture through the boundary layer are not all associated with areas of heavy precipitation. However, in locations where the evaporation rate is large wet deposition occurs relatively quickly after the process of boundary layer ventilation is complete. Only a small amount of advection of particles is possible in the 6 - 9 hours that particles are above the boundary layer in these cases (assuming an above boundary layer airspeed of 15 ms^{-1}).

This cycling of moisture from evaporation, through the boundary layer and back to earth in precipitation will be of interest to model developers who need to better represent this process in NWP models as the resolution of such models increases.

3.5 Conclusions

The purpose of this chapter was to investigate the origin of the moisture that is ventilated by the boundary layer in large quantities on the warm, cold and occluded fronts of a baroclinic wave. In section 3.4.1 we investigated a real world case study and showed that moisture ventilation within the frontal regions is jointly determined by the sub grid scale processes of convection and turbulent boundary layer detrainment. It was also shown that a possible source region for the moisture being ventilated on the cold and warm fronts was from the region to the east of the warm conveyor belt in the vicinity of the nearby anticyclone. This agreed with the results of Boutle *et al.* (2010), who initially theorised using the idea of conservation of mass that, in the case of an idealised baroclinc cyclone, the source regions of moisture were to be found in the large areas of divergence generated within the anticyclonic regions to the west and east of the cold front. In order to test the hypothesis that the anticyclonic regions were responsible for the majority of moisture being ventilated by the baroclinic wave, a Lagrangian particle tracking model, which used stochastic methods in order to represent the turbulent nature of the boundary layer, was used here in order to establish the feasibility of such pathways.

In section 3.4.2 it was shown that from a single source of moisture, turbulent processes would result in the transport of particles to positions occupying the anticyclonic branch, cyclonic branch and the entire longitudinal extent of the warm conveyor belt. An investigation into the thermodynamical characteristics of each of these pathways revealed them to be of a similar nature to the air parcel trajectories studied using a purely deterministic approach by Martínez-Alvarado *et al.* (2014). The main factor responsible for the spread of particles into the different pathways was determined to be turbulent motion in the atmosphere as opposed to atmospheric convection.

The structure of the warm conveyor belt was first conceptualised in the work of Carlson (1980), who described the splitting of the warm conveyor belt into an cyclonic branch, wrapping around the low pressure centre and an anticyclonic branch which flows into the ridge preceding

the passage of the low pressure centre. This concept of the dichotomous structure of the warm conveyor belt has been used ever since and the differences in the two branches have recently been studied by Martínez-Alvarado *et al.* (2014). However, in Section 3.4.3.3 we showed that the warm conveyor belt (excluding the small number of particles that exist in the trunk) in this cyclone can be split up into three different sections: the cyclonic flow around the low pressure centre, the anticyclonic flow into the ridge structure which then further splits into a cyclonic flow and an anticyclonic flow which returns back towards the equator. In each of these three "sectors" it was found that both 42 and 81 hours after the particles were released they could be distinctly identified by both their final spatial location, their mean value of potential temperature and their spread in the inter quartile range of potential temperature.

The position where the majority of particles were ventilated the quickest was shown to be in the area to the east of the warm conveyor belt. This matches up well with the region of enhanced moisture ventilation associated with the unresolved ventilation shown in the Eulerian moisture budget of the case study shown in Section 3.4.1. The removal of both the majority of moisture by the unresolved ventilation term of Equation 3.1, and the ventilation of particles in this region, is indicative of small scale processes being responsible for the majority of boundary layer ventilation that occurs within the warm conveyor belt. It has been shown that turbulence is the dominant mechanism for removing particles from the boundary layer. This region of ventilation was not influenced by the parameterized process of convection.

The three sectors of the warm conveyor belt were shown to arise from differing processes through which particles are ventilated from the boundary layer. All of these processes occur due to the action of turbulence in the boundary layer, whilst small changes in the initial release location can greatly influence the final position of particles in the warm conveyor belt (e.g. increasing the number of particles in the western sector by 62 % by shifting the release location by less than a degree latitude and longitude). The distribution of particles in the cloud head is also highly sensitive to the venting of the boundary layer, which is in itself a function of the boundary layer structure, which affects the distribution of particles on route into the warm conveyor belt. The boundary layer structure is in turn a function of the large scale synoptic forcing (Sinclair *et al.*, 2009) associated with the passage of a mid latitude cyclone. This circular link between the large scale forcing of the boundary layers structure and the mechanisms of ventilation, which

may in turn lead to changes in the cyclone structure (Rossa *et al.*, 2000; Joos and Wernli, 2012) demonstrate the importance of representing the boundary layer correctly in numerical weather prediction models. It was also demonstrated that very few of the particles that were intialised near the surface on the border between what might be deemed the sub tropics and the middle latitudes were entrained into the warm conveyor belt. This last point is an important one when considered from the point of view of an atmospheric river (Sodemann and Stohl, 2013b), however, it should be recongnised that this result is only applicable to this one particular case study. Further investigation into tropical moisture sources will be looked at in the next chapter.

In the final section of this chapter we showed that the amount of time that particles are within the system before being removed by wet deposition is heavily dependent upon the exact location of the particle release point. However, in the case of release point A, which has the highest evaporation rates, the time it takes from evaporation to removal by precipitation is approximately two days.

The work presented in this chapter will be of interest, not only to researchers working on the development of new boundary layer parameterization schemes which try to represent the properties of the mixed boundary layer and the transport of material out of the boundary layer due to the influence of turbulence, but also to researchers that work on the development and decay of large scale synoptic structures in the atmosphere such as Rossby waves. It is also hoped that the results presented in Section 3.4.5 will be of interest to researchers in the hydrological community working on the concepts such as the transport of moisture by atmospheric rivers.

In the next chapter we will look at the advection of moisture into cyclonic waves on a much larger scale focusing on the amount of precipitation produced by moisture that is advected in from the tropics compared with moisture that is ventilated from the boundary layer.

Chapter 4:
The moisture component in moist static energy transports

4.1 Introduction

In chapter 2 we have shown that the mass budget of the boundary layer can be solved using the 3 hourly data set provided in the form of the IFS by ECMWF. It was then shown in chapter 3 that the moisture budget for the northern hemisphere mid latitudes could be balanced and that the areas of ventilation produced for the case study of a mid latitude cyclone matched those produced in the idealised model simulations produced by Boutle *et al.* (2010). The presence of a large area of unresolved ventilation to the east of the resolved ventilation diagnosed on the cold front was verified by the using the NAME particle dispersion model in conjunction with a simulation done using the unified model.

The aim of this chapter is to investigate the occurrence of large tropical moisture exports, above the boundary layer (Knippertz and Martin, 2007), which have been shown to correlate to increased precipitation within the mid latitudes (Knippertz and Wernli, 2010). In order to separate out a suitable set of events on the scale of a hemisphere the concept of moist static energy as described by Messori and Czaja (2013) will be used. Using the concept of moist static energy (as opposed to moisture) will allow us to calculate a set of events which are only partially dependant on high levels of moisture and are thus unbiased with respect to large fluxes of moisture from tropics. The events will then be separated out into a group that have their source of precipitation dominated by poleward fluxes of moisture from within the tropics and a group that have their source of precipitation dominated by locally sourced boundary layer ventilation. Once each set of events has been identified the timing of differing events, precipitation patterns and large scale forcing will all be analysed. An analysis will then be made of how far tropical moisture can

advance in the poleward direction before being precipitated out.

4.2 Purpose of this work

The motivation for this chapters work revolves around the research question

- What is the role of moisture in events that transport high amounts of moist static energy polewards?

In order to answer this question it has been broken down into several sub questions that must be answered. These are

1. What percentage of moisture is transported in the events which transport the largest amounts of moist static energy polewards?
2. Can we adapt the techniques of precipitation recycling in order to analyse the difference between tropical moisture exports and locally sourced precipitation?
3. Can we extend the precipitation recycling methods to provide an estimate of the meridional extent to which moisture exported from the tropics penetrates into the mid latitudes?
4. Are the large tropical exports of moisture associated with specific synoptic patterns which cause precipitation in preferential locations in the mid latitudes?
5. Can we find any evidence that the large scale forcing (as opposed to the synoptic forcing) plays a role in determining whether or not events which have a high tropical moisture content occur?

4.3 Data

As with previous chapters we use the IFS dataset in order to produce all of the results presented within this chapter. This dataset has been limited to the seasons of DJF 1994 - JJA 2005. This

was done in order to limit the number of different sources of data being used in the process of data assimilation (see Dee *et al.* 2011) whilst maintaining a suitable length of time with which to complete our analysis. Eleven years was judged to be a sufficient amount of time with which to work with.

4.4 Methods

4.4.1 Moist static energy

The redistribution of heat and moisture within the Earth's climatic system can be described by a single variable, that of Moist Static Energy (H) which is defined as follows:

$$H = C_p T + gz + Lq_v \tag{4.1}$$

where T is the temperature in Kelvin, q_v is the specific humidity of the air, g is the gravitational acceleration, z is the height in metres, C_p is the heat capacity of air with a given moisture content derived as

$$C_p = 1004.67(0.84q_v + 1) \tag{4.2}$$

and L is the specific latent heat of water at a given temperature (T_c in degrees Centigrade), defined as

$$L = 1.0 \times 10^6[2.501 - (0.00237T_c)] \tag{4.3}$$

for these definitions, see Stull (1989).

Both moist static energy and the meridional velocity can be split into two terms. e.g. for the velocity

$$v = \underbrace{\bar{v}}_{\text{term1}} + \underbrace{v'}_{\text{term2}} \tag{4.4}$$

Term 1 on the right hand side of Equation 4.4 describes the flow component associated with the mean flow of the atmosphere and stationary waves which are described in Section 1.3.2 whilst term 2 describes the transient perturbations from this mean flow as described in Sections 1.3.2. In practice term 1 can be calculated by computing a linearly detrended seasonal mean for both the variables giving $\overline{v}$ and $\overline{H}$. By subtracting these from the intitial values we can compute the transient perturbations described by term 2 in Equation 4.4. v' is then multiplied by H' in order to calculate an eddy flux representing the eddy transport at a particular location. This has been done for each individual point between 30°north and 60° north in the northern hemisphere. The results of this calculation can then be used in order to define a set of events which transport a large amount of moist static energy poleward similar to the calculation done in the work of Messori and Czaja (2013).

4.4.2 The box model

Once the events have been distinguished, a box model will be used in order to separate out events which rely on high tropical moisture exports for there precipitation from events which rely on high boundary layer moisture fluxes. The box model used in this investigation is depicted in Figure 4.1. Although we describe the set up as a box model approach, it should be kept in mind that the boundary layer top is capable of moving up and down due to diurnal variations in surface temperature (Carson, 1973) and forced by synoptic systems (Sinclair *et al.*, 2009). Thus the boundary layer top, separating the boundary layer box from the free atmosphere box, is dynamic and ever changing. However, mean fluxes through this surface can be determined (as shown in the previous chapter) and these are used in our "box model". The boxes are constructed in order to contain the whole of the northern hemisphere mid latitudes. Thus, one side runs along the 30° N line of latitude and the other along the 60° N line of latitude. Each side circumvents the globe.

Each of the terms which appear in Figure 4.1 are now described. The amount of moisture flowing through the latitudinal wall at 30° north above the boundary layer ($F_{in\,fa}$) is given by

$$F_{in\_fa} = r \cdot \int_0^{2\pi} \int_{bl\_top}^{top} \overline{v\rho q}_{\phi_1} \cdot cos\phi_1 \cdot dz \cdot d\lambda \tag{4.5}$$

and below the boundary layer ($F_{in\,bl}$) is given by

$$F_{in\_bl} = r \cdot \int_0^{2\pi} \int_0^{bl\_top} \overline{v\rho q}_{\phi_1} \cdot cos\phi_1 \cdot dz \cdot d\lambda \tag{4.6}$$

where quantities presented with an overbar represent grid box averages of fluxes as described in chapter 2 of this thesis multiplied by the total humidity given in the left hand side of Equation 3.2. r represents the radius of the earth and ϕ represents the latitude described in radians. The subscript 1 represents the fact that ϕ is taken to be 30 degrees north in radians. Similar Equations can be used in order to calculate the horizontal flow of moisture out of the poleward side of the boxes ($F_{out\,fa}$ and $F_{out\,bl}$) substituting the fluxes at 30 degrees with the fluxes at 60 degrees which is represented with ϕ_2. The limits bl_top and top represent the height of the boundary layer top and the top of the atmosphere.

The flux of moisture through the boundary layer top (BL) is represented by the combination of the resolved and the unresolved flows such that

$$BL = r^2 \cdot \int_0^{2\pi} \int_{\phi_1}^{\phi_2} \left[\rho_h(\overline{w'q'})_h - (\rho q)_h \left(\frac{\partial h}{\partial t} - \tilde{\mathbf{U}}.\mathbf{n} \right) \right] \cdot cos^2\phi \cdot d\phi \cdot d\lambda \tag{4.7}$$

whilst the flux of moisture due to precipitation at the surface (P_s) or through the boundary layer top (P_h) can be given by

$$P_h/P_s = r^2 \cdot \int_0^{2\pi} \int_{\phi_1}^{\phi_2} p_{h/s} \cdot cos^2\phi \cdot d\phi \cdot d\lambda \tag{4.8}$$

where p is the precipitation rate at the surface (p_s) and through the boundary layer top (p_h). Similarly the net evaporation of moisture from the surface is given by

$$EV = r^2 \cdot \int_0^{2\pi} \int_{\phi_1}^{\phi_2} E \cdot cos^2\phi \cdot d\phi \cdot d\lambda \tag{4.9}$$

where E represents the rate of evaporation at the surface. In Figure 4.1 dq represents the change in moisture content of either the boundary layer (subscripted bl) over a three hour period or of the free atmosphere (subscripted fa) which is calculated as the residual leftover when the terms calculated by Equations 4.5 - 4.9 are summed up.

In order to estimate the ratio between the amount of precipitation formed from the moisture that has been advected into the mid latitudes in comparison with the amount of precipitation produced from local venting of the boundary layer we adapt the method described in Trenberth (1999). The derivation of this ratio is presented here with a generalisation in order to take into account the change in atmospheric moisture content with time.

If we consider the area bounded by 30° and 60° north, then the flux out at 60° will be given by

$$F_{out\_fa} = F_{in\_fa} + (BL - P_h) - dq_{fa} \tag{4.10}$$

The average horizontal flux (F) through the box will thus be given as

$$F = 0.5(F_{in\_fa} + F_{out\_fa}) = 0.5(F_{in\_fa} + F_{in\_fa} + (BL - P_h) - dq_{fa}) \tag{4.11}$$

which can be simplified to

$$F = F_{in\_fa} + 0.5(BL - P_h) - 0.5dq_{fa} \tag{4.12}$$

We can then split the precipitation up into two parts, that produced by the advection of moisture and that produced by the moisture vented from the top of the boundary layer, such that

$$P_h = P_a + P_{bl} \tag{4.13}$$

where subscripts *a* and *bl* denote quantities associated with the advection of moisture into the box and the local ventilation of the boundary layer respectively. The average horizontal flux of moisture (F_a) that has been advected into a region is thus

$$F_a = F_{in\_fa} - 0.5P_a - 0.5\alpha dq_{fa} \tag{4.14}$$

where α is the fraction of moisture that has been used to change the atmospheric moisture content (dq_{fa}) due to the average advective flux of moisture. The average horizontal flux of moisture due to the ventilation of the boundary layer F_{bl} is given by

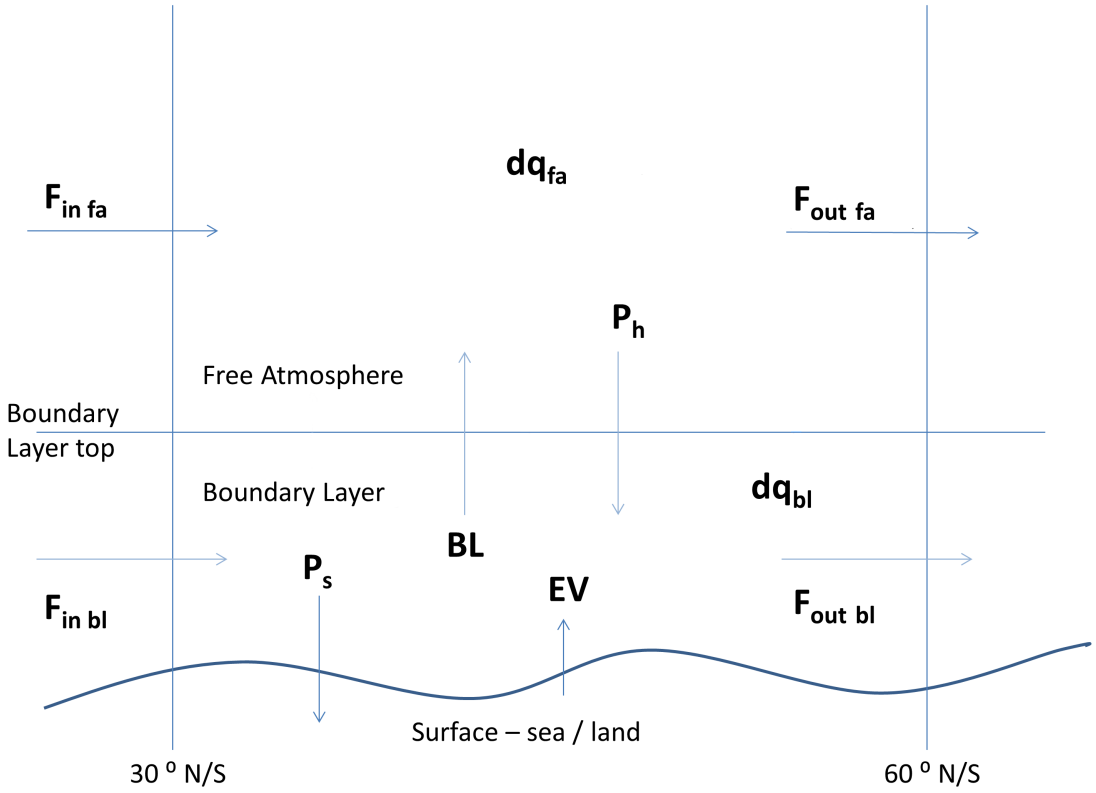

Figure 4.1: The inputs and exports of moisture described by the box model and applied to both the boundary layer and the free troposphere.

$$F_{bl} = 0.5(BL - P_{bl}) - 0.5\beta dq_{fa} \tag{4.15}$$

where β is the equivalent of $1-\alpha$ or the fraction of moisture that has been used to change the atmospheric moisture content (dq_{fa}) due to the venting of moisture from the boundary layer. (note that Equation 4.15 + Equation 4.14 = Equation 4.12.) This means that

$$\frac{F_a}{F_{bl}} = \frac{P_a}{P_{bl}} = \frac{F_{in\_fa} - 0.5P_a - 0.5\alpha dq}{0.5(BL - P_{bl}) - 0.5\beta dq} \tag{4.16}$$

which simplifies to

$$\frac{P_a}{P_{bl}} = \frac{2F_{in\_fa} - \alpha dq_{fa}}{BL - \beta dq_{fa}} \tag{4.17}$$

Several important assumptions are made in this derivation that will now be stated.

1. The assumption that $\frac{F_a}{F_{bl}} = \frac{P_a}{P_{bl}}$ due to the atmosphere being well mixed, this should be particularly relevant for the large length scales (i.e an entire latitudinal ring) that we will be using.

2. Exchange of moisture between the box representing the free troposphere and the box representing the boundary layer is only achieved through the process of precipitation. (i.e. moisture is not advected downward).

3. The use of universal values for α and β.

Assumption number 1 is fairly generic and made by most researchers in the precipitation recycling community (e.g Trenberth, 1999). Assumption 2 can be justified by considering a typical synoptic situation where this assumption might not apply. One such situation is within an anticyclone where descending air is entrained through the top of the boundary layer. The subsiding air during situations like this is generally very dry. It is assumed that in other situations the moisture that is advected through the boundary top has been derived from local sources of boundary layer ventilation and not advected along a warm conveyor bet (Harrold, 1973, Carlson, 1980). Since by the definition of a warm conveyor belt describes air as moving upwards and out of the boundary layer along an isentropic surface (Carlson, 1980).

Assumption 3 is taken care of by assuming that $\alpha = P_a/P_h$ and $\beta = P_{bl}/P_h$, (ie the proportion of dq_{fa} that is due to moisture advected in from the south is the same as the proportion of precipitation that this moisture produces). This is a reasonable assumption given the use of assumption 1. (i.e. that $P_a \propto F_a$ and assuming that F_a is the source of moisture for αdq.) It must be kept in mind however, that other values are possible for α and β. Given assumption 3 the Equation 4.17 now simplifies to

$$\frac{P_a}{P_{bl}} = \frac{2F_{in\_fa}}{BL} \tag{4.18}$$

Combining Equation 4.18 with Equation 4.13 it can be shown that the ratio of precipitation sourced from moisture advected in from the free troposphere to the total amount of precipitation

can be given to be

$$\frac{P_a}{P_h} = \frac{2F_{in\_fa}}{2F_{in\_fa} + BL} \tag{4.19}$$

However, a simple calculation over the whole box as pictured in Figure 4.1 will not give us any details about where the precipitation due to P_a is falling. In order to gain insight into the location of P_a the calculation will have to be repeated multiple times over smaller boxes (e.g. 5° in length). This will allow the proportion of the flux to be calculated on the poleward side of the box that is directly sourced from the moisture advected in from the tropics on the equatorward side of the box. This is given by

$$F_{out\_fa}(adv)_1 = F_{in} - \frac{2F_{in\_fa}P_h}{2F_{in\_fa} + BL} \tag{4.20}$$

where $F_{out\_fa}(adv)_1$ is the amount of precipitation that leaves the poleward side of the box that has been supplied by the flow of moisture into the box on the equatorward side. After calculating this for the first latitudinal band (subscript 1) the transport of moisture by subsequent latitudinal bands is calculated by the formula

$$F_{out\_fa}(adv)_k = F_{out\_fa}(adv)_{k-1} - \frac{2F_{out\_fa}(adv)_{k-1}P_h}{2F_{out\_fa}(adv)_{k-1} + BL} \tag{4.21}$$

where $F_{out\_fa}(adv)_k$ is the new poleward flux of moisture directly associated with the original advective flux of moisture in from the tropics ($F_{in\_fa} = F_{out\_fa}(adv)_{k-1}$). However, the use of Equations 4.20 and 4.21 implicitly assumes that the atmosphere does not mix the air flowing out of a box that is directly associated with a moisture flow in from the tropics with the moisture flowing out of the box that is supplied from the boundary layer. A second calculation can therefore be performed in which this mixing of the air is assumed.

In order to include the action of mixing on air parcels we define a mixing ratio such that

$$\gamma_k = \frac{F_{out\_fa}(adv)_k}{F_{in\_fa(k)}} \tag{4.22}$$

where

$$F_{in\_fa(k)} = F_{out\_fa}(adv)_k + F_{out\_fa}(bl)_k \tag{4.23}$$

where $F_{out\_fa}(bl)_k$ is the amount of moisture coming out of the box which is directly derived from ventilation of the boundary layer within the defined box. Once this ratio has been defined we can define a new advective flux out of the boundary layer to be

$$F''_{out\_fa}(adv)_{k+1} = \gamma_k \left(F_{in\_fa(k)} - \frac{2F_{in\_fa(k)}P_h}{2F_{in\_fa(k)} + BL} \right) \tag{4.24}$$

instead of Equation 4.21. The quantity $F''_{out\,fa}(adv)_{k+1}$ can then be used in order to define the fraction of moisture that has been transported to any given location that is derived directly from the tropical moisture source such that

$$\frac{\iota}{100.0} = \frac{F''_{out\_fa}(adv)_{k+1}}{F_{in\_fa(0)}} \tag{4.25}$$

where $F_{in\_fa(0)}$ is the flow of moisture in from the tropics across 30°N and ι is the percentage of moisture that has been advected poleward.

This new formulation makes the assumption that all flow in from the tropics is either removed from the box by the process of precipitation or by advection out of the poleward side of the box and that none of the moisture is lost by entrainment into the boundary layer. This assumption was based on the findings of Zhu and Newell (1998) who showed that over 90 % of poleward moisture transport was by the warm conveyor belt combined with the findings of Sinclair *et al.* (2008) who showed that the warm conveyor belt could be defined by only positive values of vertical velocity which had been interpolated onto the boundary layer top.

The well mixed atmosphere assumption is used in many versions of precipitation recycling models, details of which can be found in Burde (2006). However, the question as to whether or not the well mixed assumption holds has been questioned by Burde (2006) and in some instances been shown to be false by Sodemann and Stohl (2013a). As such in Section 4.5.7 results using both of these methods will be presented.

4.4.3 The spin up of precipitation

The report by Kallberg (2009) explicitly recomends that the time steps T+0 - T+12 be used for the extraction of precipitation data in the ERA-interim archive. This recommendation is based upon the fact that whilst precipitation is known to be less than that detected by the global precipitation climatology project (GPCP, Adler *et al.*, 2003), the data in the range of T+12-T+24 is known to be more than that detected by GPCP and less synoptically accurate. In addition two recent studies by de Leeuw *et al.* (2015) and Betts *et al.* (2009) it was demonstrated that using the T+0 - T+12 accumulated precipitation variable produced precipitation totals that were less than 5 % of the values obtained by using the T+12 - T+24 precipitation data. Thus by using the precipitation data in the range of T+0 - T+12 we obtain estimates that are synoptically more accurate and only slightly under playing the actual amount of precipitation that fell.

In order to satisfy the boundary layer moisture budget equation it was necessary to obtain the amount of moisture passing through the boundary layer top as precipitation (i.e. P_h). In order to determine this quantity the model level total precipitation accumulation variable (P_{acc}) was used which is available from the ECMWF MARS data servor. This variable is only available between time steps T+3 and T+12 hours (Berrisford *et al.*, 2009). In order to compute the boundary layer moisture budget it was neccesary to determine which time steps to use. A balance had to be struck between accurately depicting the ventilation of moisture through the boundary layer top (ideally using all of the available data points) and accurately measuring the amount of precipitation falling through the boundary layer top and reaching the surface (which involves removing some of the time steps from the calculation). In order to satisfy the moisture budget equation P_{acc} has been converted into a precipitation rate representing the three hour period by taking the cumulative total in precipitation at the end of each three hour period (between T+3 and T+12) in question and subtracting the total of the cumulative precipitation at the beginning of the three hour period in question. This gave the accumulation of precipitation for each three hour period. This total was then divided by 10800 seconds to give us an average precipitation rate for the three hours in question. Each individual data value was scaled up by the area that it represents and summed up between 30°N and 60°N in order to represent the total precipitation rate within the mid latitudes. The results of this calculation for the first 8 days of December 1994 are given in Figure 4.2.

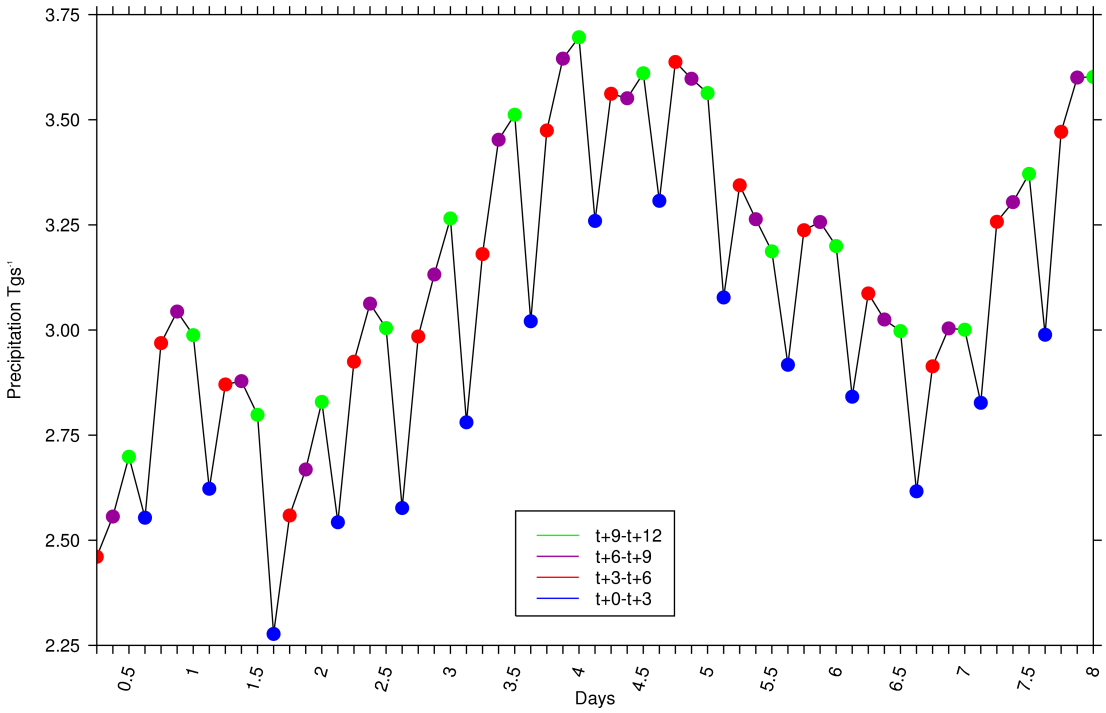

Figure 4.2: The total precipitation rate between 30° N and 60°N during the first 8 days of December in 1994. Data is taken from different model lead times which are indicated by the coloured dots.

It is clear from Figure 4.2 that when using data between T+0 and T+3 hours (the blue dots) that systematically less precipitation is produced by the IFS model than for the case when time steps T+3 - T+12 are used. In order to evaluate the moisture budget of the boundary layer it was thus determined that time steps T+0 - T+3 would not be used. Differences between T+3-T+6, T+6-T+9 and T+9-T+12 are more subtle. Between 1.5 and 2 days the rate of precipitation is lower using the T+3-T+6 dataset than the rate of precipitation at T+9-T+12 hours. At 5 to 5.5 days the situation is reversed.

In order to determine whether or not to use the T+3-T+6 data in our moisture budget the seasonal average rate of precipitation was determined for each of these times. These averages are displayed in Table 4.1 along with a percentage comparison against the T+9-T+12 data which best fits observations (Kallberg, 2009).

Table 4.1 shows us that for the region between 30°N and 60°N the difference in the average precipitation rate between T+3 and T+6 hours is 1.69% less than that at T+9-T+12 hours. This level of error was considered to be negligible given the large errors found in the GPCP dataset

	T+0-T+3	T+3-T+6	T+6-T+9	T+9-T+12
Average precipitation	2.78763×10^9	3.09844×10^9	3.15483×10^9	3.15165×10^9
percentage change from T+9-T+12	-11.55%	-1.69%	+0.1%	0%

Table 4.1: The seasonal average (DJF) precipitation rate for 1994-1995 between 30°N and 60°N for each set of times is given in Tgs^{-1} in the first row. The percentage difference from the T+9-T+12 rate is given in the second row.

itself, especially over regions such as the storm tracks (Adler *et al.*, 2003) which were used by Kallberg (2009) in order to validate the ECMWF dataset.

4.4.4 Events

In order to compare the ventilation of boundary layer moisture with the flow of moisture in from the tropics each of the variables described in Section 4.4.2 will be calculated for a set of events which will be based upon the top ten percent of net polewards moist static energy transports over the whole latitudinal band of 30° N-60° N during each year. Thus, at each time step the mean poleward transport is calculated at 850 hPa for all of the model grid squares taking into account their differing sizes with latitude. Each year all of these energy transports will be summed up for each season and the top ten percent of energy transports will be separated out and used as event times. Each of the events will include all of the time steps for two days preceding the event time and two days after the event time. This totals 8 time steps (2 days using T+3-T+6 data and T+9-T+12 data) before the event takes place and eight time steps after the event has taken place. Each of the variables described in Section 4.4.2 will be computed as a mean value over the 4 day time period of each event. These events will then be used as the basis for the analysis performed in Section 4.5.3.

In order to decide upon the length of an event all of the meridional wind velocities were considered over the latitudinal band of 30°- 60°N at 850 hPa. Since the distance between 30°N and 60°N is approximately 3.5 x 10^6m which would take an air parcel travelling at 10 ms^{-1}approximately 4 days to traverse the mid latitudes. It was then determined that 10 ms^{-1} was lower than 50 % of the meridional velocities produced by the IFS for DJF and lower than 30 % of

the velocities produced by the IFS for JJA. It was therefore considered to be a suitable time frame for our purposes.

4.5 Results

4.5.1 Individual moist static energy transports

In order to investigate the partition between moisture and heat in the polewards transport by transient eddies we calculated $v'H'$ at each grid point at a height of 850 hPa over the 30°N - 60°N band of latitudes. As with the work of Messori and Czaja (2013) we expect a small fraction of these transient eddies to transport a large proportion of the total amount of energy. The fluctuations were first calculated using the ERA-interim dataset for the DJF season of 1994 and compared with the results of Messori and Czaja (2013) in order to check that the calculation methods were consistent, which they were (personal communication, Messori 2013). It was then necessary to recalculate all of the transient eddy values using the IFS dataset for the 11 year period 1994 - 2005 for both the DJF and JJA seasons. The total flux of energy poleward was then calculated by first multiplying each value by the area of its gridbox and then summing up the whole dataset. A second calculation was also done which only considered the poleward component (i.e. when v' is positive). These two values were then compared with a summation of the top two, five and ten percent of events (In this case an event corresponds to a single transport by an individual grid square. This should not be confused with the events calculated in Section 4.4.4 which represent a climatological mean transport of energy over an entire latitudinal band for 4 days). The results of this comparison are presented in Tables 4.2 and 4.3 as a percentage of the overall poleward transport of moist static energy by each set of events when compared to the total transport.

In order to seperate out the individual transports of moisture and heat from the transport of moist static energy each component was calculated seperately and the results are also presented in Tables 4.2 and 4.3. In each case large proportions of both heat and moisture are transported polewards by only a small fraction of the total events. The results for the transport of MSE agree with those already published by Messori and Czaja (2013) and it can be seen that a similar property occurs in both the components of heat and moisture that make up the poleward transport

DJF	N-hem (Sorted by MSE)	N-hem (Sorted by heat transport)	N-hem (Sorted by moisture transport)
MSE transport	T+3-6 - T+9-12		
2%	29.1 (23.2)	26.5 (21.1)	27.1 (21.6)
5%	51.0 (40.6)	46.9 (37.4)	46.9 (37.4)
10%	73.7 (58.8)	68.6 (54.7)	67.4 (53.8)
Temperature component			
2%	25.5 (19.9)	28.0 (22.0)	19.9 (15.5)
5%	46.7 (36.4)	50.7 (39.8)	35.5 (27.7)
10%	70.0 (54.6)	75.3 (59.1)	53.3 (41.6)
Moisture component			
2%	34.0 (27.9)	25.0 (20.4)	36.6 (30.3)
5%	57.3 (46.8)	43.0 (35.2)	62.1 (51.3)
10%	79.6 (65.1)	61.5 (50.3)	86.5 (71.5)

Table 4.2: The contributions to the poleward transport of moist static energy, its moisture component and its temperature component are shown for the time steps T+3 - T+6 and T+9 - T+12. Row 1 shows the transport of the top 2, 5 and 10 % transports of moist static energy. Row 2 shows the transport of the top 2, 5 and 10 % transports of heat. Row 3 shows the transport of the top 2, 5 and 10 % transports of moisture. Numbers in brackets represent the percentage of poleward transport (v'¿ 0) only whilst numbers outside brackets represent the percentage of total transport.

JJA	N-hem (Sorted by MSE)	N-hem (Sorted by heat transport)	N-hem (Sorted by moisture transport)
MSE transport	T+3-6 - T+9-12		
2%	33.1 (22.0)	25.9 (17.0)	31.0 (20.4)
5%	59.9 (39.8)	48.1 (31.6)	56.0 (36.8)
10%	88.5 (58.7)	72.6 (47.7)	82.8 (54.4)
Temperature component			
2%	28.4 (19.6)	36.7 (25.3)	18.3 (12.7)
5%	53.1 (36.7)	66.8 (46.0)	34.8 (24.1)
10%	80.6 (55.7)	99.3 (68.4)	53.7 (37.1)
Moisture component			
2%	37.0 (23.3)	19.0 (11.9)	40.0 (25.1)
5%	66.0 (41.5)	36.2 (22.8)	71.4 (44.9)
10%	96.0 (60.5)	55.6 (35.0)	103.9 (65.4)

Table 4.3: As for Table 4.2 but for the season JJA.

of moist static energy (see the results in column 1 in Tables 4.2 and 4.3). It can also be seen that the transports of temperature and moisture are fairly evenly split with similar percentages of the overall transports assigned to each proportion of events.

If the events are sorted purely by the temperature transports it can be seen that whilst the net transport of temperature north is increased by a small amount the net transport of moisture is decreased when compared to the same transports sorted by transport of moist static eneregy. Similarly, if the events are sorted by the moisture transport component then the net transport of temperature polewards from each subset of events is decreased to around two thirds of its value than when sorted by transport of moist static energy. This discrepancy seen in the transports of moisture and heat suggests that the largest transports of moisture do not occur at the same time as the largest transports of heat.

Since the transports of heat and moisture described in Tables 4.2 and 4.3 have been shown to be consistent with height (Messori and Czaja, 2013) and are associated with eddies which are superimposed onto the mean flow of the atmosphere (Oort, 1971, Zhu and Newell, 1998) we can associate the largest of them as the poleward component of the flow within atmospheric rivers (Zhu and Newell, 1998). These results suggest that some systems are large poleward transporters of moisture whilst a separate set of events are associated with the large poleward transport of heat. The idea that events can be split up into those which are associated with large poleward fluxes in moisture and those which transport less moisture forms the motivation for the rest of this chapter.

4.5.2 Mean box model

The precipitation associated with each of the events described in Section 4.5.1 is produced by the flow of moisture from the tropics (Knippertz and Wernli, 2009), the convergence, and subsequent ventilation, of moisture from the boundary layer (Boutle *et al.*, 2010) or a combination of the two (Bao *et al.*, 2005). In order to investigate these two sources of moisture it was first necessary to balance the moisture budgets of both the boundary layer and the free atmosphere above in order to establish a baseline with which to make our comparisons. The results are presented in Figure 4.3 for the entire latitudinal band between 30°- 60° N for the DJF season between December 1994 and February 2005 (panel a) and the JJA season between June 1995 and August 2005 (panel b).

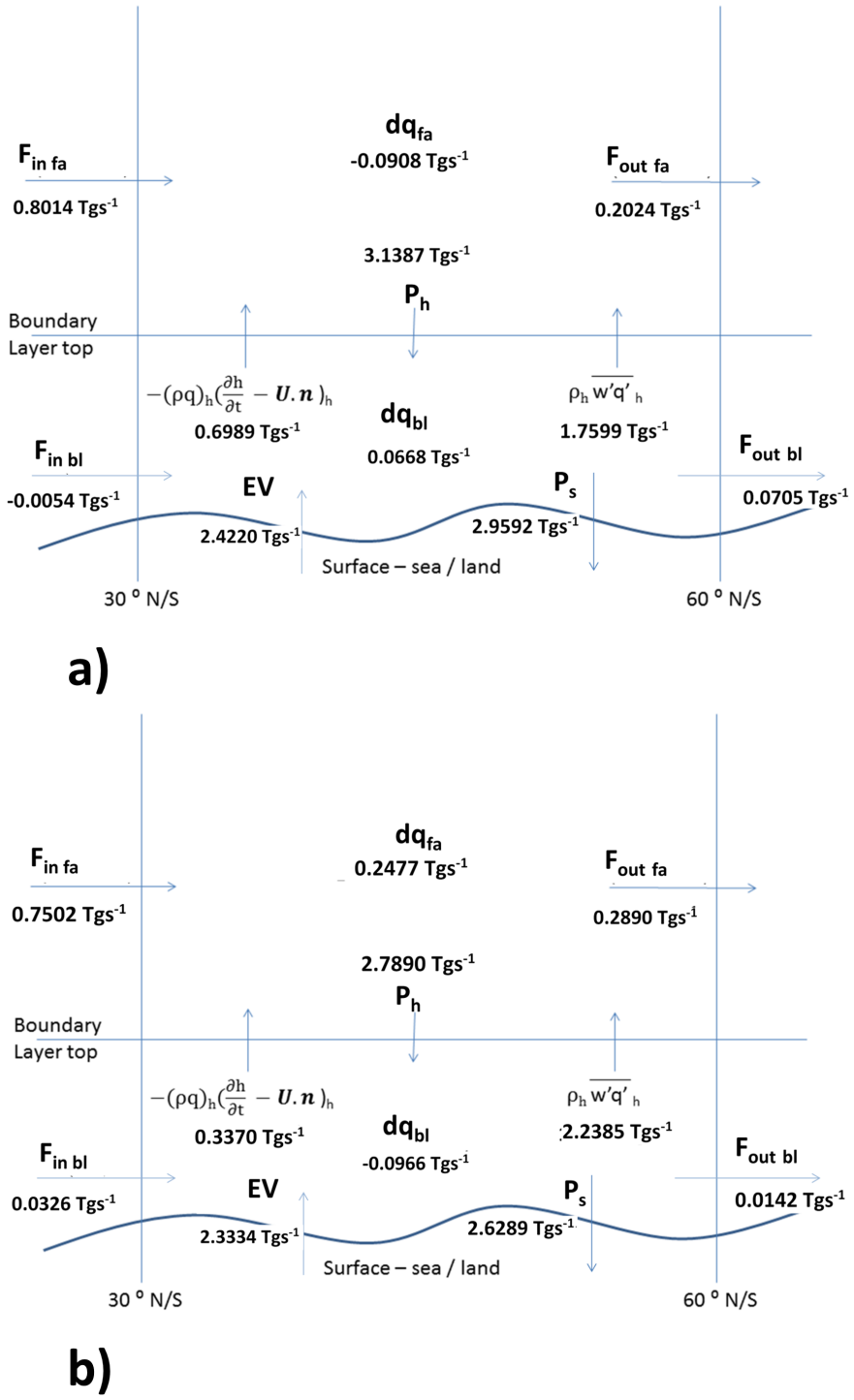

Figure 4.3: The full, balanced, moisture budget for the free atmosphere and the boundary layer. The two panels represent DJF (a) and JJA (b).

The largest flux of moisture, described by Figure 4.3a, is due to the falling of precipitation through the boundary layer top. This loss of moisture from the free troposphere is compensated for by the influx of moisture in from the tropics combined with the resolved and unresolved fluxes of moisture from the boundary layer (see Equation 3.1). The largest of these fluxes is the unresolved flow which is roughly 2.5 times the resolved flow and 2.1 times the transport of moisture coming in from the tropics.

When viewing Figure 4.3 it must be remembered that the disparity in size between the unresolved and resolved flows of moisture out of the boundary layer is a function of the horizontal resolution of the model used. In the IFS, the net flux of moisture due to convection is partly represented by the resolved flow and partly represented by the unresolved flow. The unresolved flow also includes a component which is due to the convective overturning of the boundary layer air near the top of the boundary layer (Carson, 1973) which acts to entrain material from aloft (Medeiros *et al.* 2005, Soares *et al.*, 2004). Higher model resolutions would increase the resolved flow of moisture and decrease the unresoloved flow of moisture into the free troposphere.

Combining the resolved and unresolved flows in Figure 4.3 of moisture out of the boundary layer top reveals the flux out of the boundary layer to be approximately 2.4588 Tgs^{-1}. When compared with the amount of precipitation falling this reveals that at least 20 % of the precipitation through the boundary layer top is derived from other (tropical) sources. However, if we assume that the bulk of moisture transport being represented by the unresolved flow is due to convective processes (not entirely true) which precipitate in the immediate vicinity of the upward flux of moisture from the boundary layer and that the amount of moisture transport represented by the resolved flow that is due to convection is small then we can subtract this resolved flux from the amount of precipitation falling through the boundary layer top. We are then left with an estimate of 1.3788 $Tgs^{-1}$of precipitation falling through the boundary layer top which is due to non convective processes. The flux of moisture in from the tropics is then responsible for 58 % of this precipitation and thus contributes to a large proportion of the dynamic precipitation. (In reality, neither of these two assumptions are strictly true (see Chapter 3 and the previous paragraph). This simple calculation highlights the need for more investigation into the multiple sources of moisture for precipitating systems.

By comparing the combined amount of the unresolved and resolved flows with the amount of

evaporation that is taking place at the model's surface we find that the flow through the boundary layer top is only slightly greater (roughly 1.5 % larger) than the amount of evaporation within the box. The remainder of the moisture flow is being supplied by the difference in moisture being deposited by precipitation at the surface and the flow of moisture through the boundary layer top due to precipitation. Both of the horizontal transports of moisture from within the boundary layer, at 30°N and 60 ° N, transport moisture out of the lower box during this season.

The changes in moisture content of both the boundary layer and the free atmosphere appear large at first inspection. However, when divided by the total number of grid columns within the box the change in moisture content of each model column becomes insignificant and as such we do not comment further on this value except to say that it is unlikely to yield any useful information regarding the Earth's climate (Sherwood *et al.*, 2010).

Since it is known that mid latitude cyclones transport a large proportion of moisture poleward (Zhu and Newell, 1998) and that the baroclinicity of the mid latitudes is reduced during the summer season due to the decreased meridional temperature gradient (White, 1982). It follows that the flow of moisture through 30° N would be expected to be less in JJA (although in our analysis it is only fractionally so). The increased flow at 60°N is dominated by the transient eddy fluctuations which have moved poleward (Oort, 1971) in space with the change in season.

Figure 4.3b also shows us a reduction in the resolved flux of moisture out of the boundary layer and an increase in the unresolved flux. This is unsurprising since the ventilation by mid latitude cyclones is expected to decrease in a less baroclinic environment (Sinclair *et al.*, 2008) whilst the amount of convection in the area increases, which agrees with the increase in our unresolved ventilation rate during this season.

It is likely that the increase in relative humidity during the summer months (Peixoto and Oort, 1996) has the effect of decreasing the amount of evaporation that can take place from rain (See Equation 2.23) passing through the boundary layer and thus the difference in rain falling at the surface and through the boundary layer top is not as much as for the DJF season. Since more moisture is transported through the boundary layer top than provided by evaporation, the extra moisture must be supplied by transport into the boundary layer from the tropics.

4.5.3 Events box model

Figure 4.4 depicts the ratio of precipitation formed by the advection of moisture into the free troposphere from the tropics (above the boundary layer) to the amount of precipitation formed by the moisture ventilated by the boundary layer, as a function of the latitudinal extent of the box over which this ratio is calculated. The ratio was calculated using Equation 4.18. The mean climatological values for the 11 year period are shown by the solid red line. The dashed red line indicates the outlying years within this 11 year period. The ratio has been calculated by increasing the size of the box by 5 degree intervals except for the first box chosen to be 10 degrees in length.

The 396 individual events (defined in Section 4.4.4) associated with the strongest moist static energy transports that were calculated during the eleven year period are represented by the grey lines. The mean ratio of all of these events is indicated by the blue line and the dashed blue lines represent 1 standard deviation from the mean. Panel a depicts the DJF season whist panel b depicts the JJA season.

It can be seen from the red and grey lines in Figure 4.4 that the change in ratio with distance is almost linear in both the climatological mean and in each of the events. The only notable change in gradient occurs between 30 ° and 45° N. This suggests that in the region of 30°- 45° N the flow of moisture through the 30° latitudinal band, above the boundary layer, is more influential on the amount of precipitation falling within the 30°-45° region than it has influence on the precipitation falling within the region of 45°-60° N.

In order to determine a length scale over which the dominant source of moisture is from the tropics we must look for the position where each line crosses the 1.0 mark on the y-axis. By noting this position on the x-axis and assuming that the change in ratio is linear with distance we can then say that positions points falling to the left of this point are dominated by mosture which is sourced from the tropics whilst the positions to the right of this point have the majority of precipitation sourced directly from the boundary layer. This point occurs just short of the 30°-45° N box for the climatological values of P_a/P_{bl} which suggests that the transition between dominant moisture sources occurs at around 1400km.

A large number of events appear with a ratio of more than one for the 30°-40°N box which

demonstrates that advection of moisture in from the free troposphere is extremely important for the production of precipitation over distances of up to about 1000 km. This agrees qualitatively with the results of Trenberth (1999) who showed that 80 % of the precipitation within a 1000 km box was associated with precipitation that had been advected in. Using equation 4.19 we can calculate the percentage of precipitation associated with the advective flux of moisture in from the tropics over the 30°-40°N range to be 52 % for the mean climatology. This value is much less than that calculated by Trenberth (1999), however, the Trenberth (1999) calculation takes into account grid squares where no evaporation is taking place in order to produce an average evaporation over the area of interest, whilst our calculation is done over the entire latitudinal band and uses net boundary layer ventilation which may account for the difference in results.

The range of events in the season of JJA (see Figure 4.4) span a much greater range of $\frac{P_a}{P_{bl}}$ than the events which were depicted for DJF. Due to the increase in convection during the summer months it is not surprising that more of the events are dominated by ventilation of moisture from the boundary layer. It is more surprising that large ratios of tropospheric moisture advection to boundary layer ventilation are observed with the highest ratios showing that more than three times as much precipitation is produced by the tropospheric moisture fluxes when compared with the amount of moisture coming from boundary layer ventilation in the region between 30° N and 40°N. It is also notable that a greater proportion of the events are dominated by tropospheric moisture fluxes over the region 30°N to 60°N than seen in the season DJF. At least two events have ratios as large as 1.5 over the distance 30° N to 60°N.

In both the DJF and JJA season it is possible to split up the events into ones that are dominated by boundary layer moisture ventilation and events which are dominated by fluxes of moisture from the tropical troposphere. This was done by grouping all of the events which had higher ratios of $\frac{P_a}{P_{bl}}$ than one standard deviation from the mean value of $\frac{P_a}{P_{bl}}$. This group represented events which were dominated by tropical moisture flows and shall be denoted EVTROP in the following discussion. Another group of events was similarly formed by taking all of the events which had a ratio of $\frac{P_a}{P_{bl}}$ that was more than one standard deviation lower than the mean value of $\frac{P_a}{P_{bl}}$. This group represented events which were strongly dominated by boundary layer moisture fluxes and will be denoted EVBL in the following discussion.

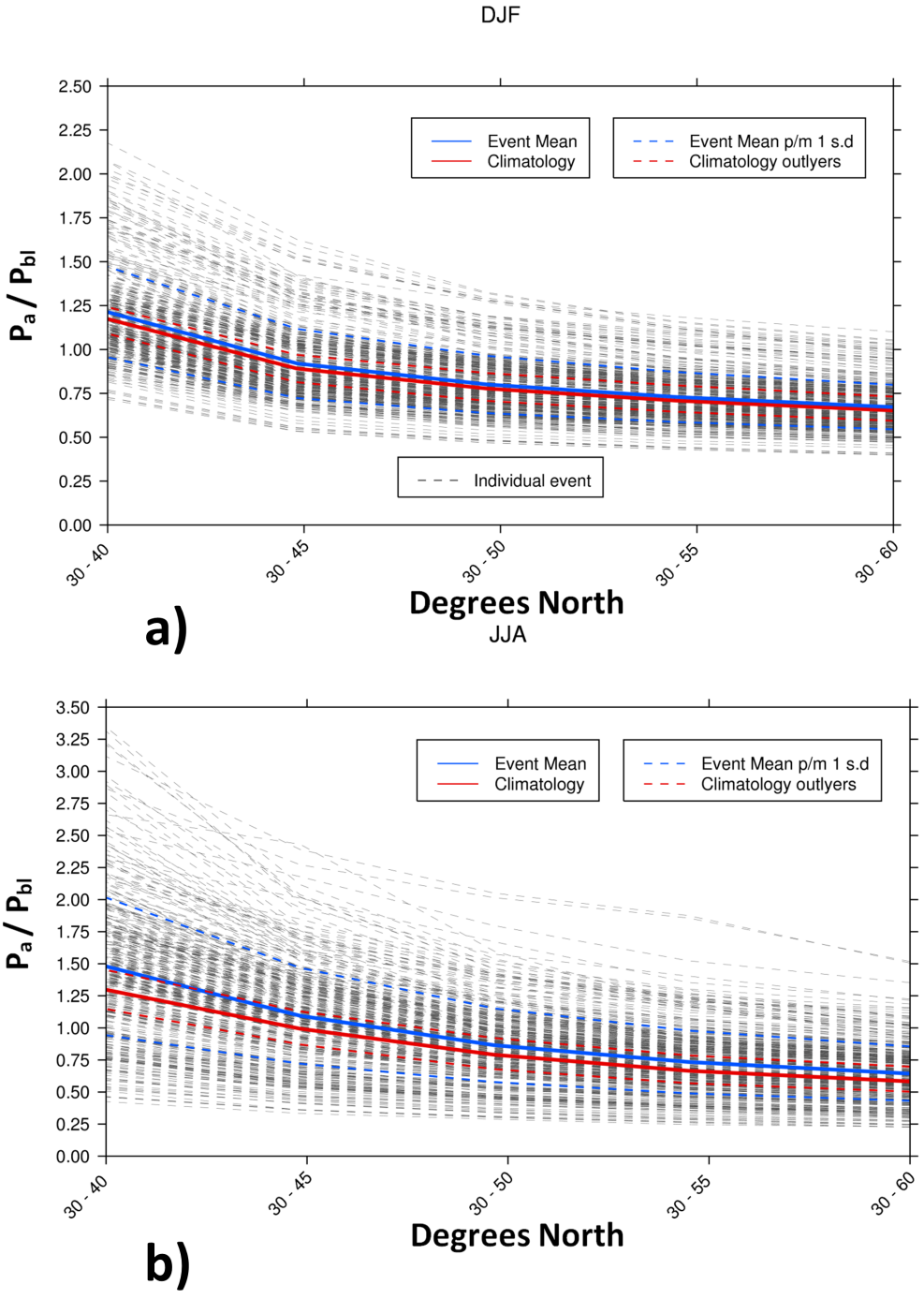

Figure 4.4: The ratios of precipitation produced by tropical moisture exports compared with the precipitation produced by boundary layer ventilation. Each value is given for boxes of different lengths described on the x-axis of the plots. Panel a represents the situation during the season DJF whilst panel b represents the situation during the season JJA.

4.5.4 DJF event frequency

The frequency with which large transport events occur was shown to be extremely sporadic by the study of Messori and Czaja (2013) and this is confirmed in Figure 4.5 which shows the timing of events along with the timing of events that were strongly dominated in terms of their precipitation by tropical moisture fluxes (blue) and events that were strongly dominated in terms of their precipitation by boundary layer ventilation (red). It can be seen from Figure 4.5 that events tend to group into clusters throughout the eleven year period. This result expands on the work of Messori and Czaja (2013) by taking into account the net transport of moist static energy over the mid latitudinal band between 30°N and 60 °N as opposed to concentrating on the transport of moist static at a single point on a latitudinal circle as was originally described by Messori and Czaja (2013).

It can be seen in Figure 4.5 that seasons exist where none of the extreme events were influenced by strong tropospheric moisture fluxes (e.g. 02 - 03) and that seasons exist where none of the extreme events were influenced by strong boundary layer moisture fluxes (e.g. 95 - 96). This result justifies our use of a 11 year dataset in order to try and study these two types of events.

4.5.5 Event precipitation distributions and synoptic settings

In order to investigate the extent of the poleward moisture transport, climatologies of the precipitation and mean sea level pressure were produced for each type of event and compared against the seasonal climatologies of each variable. The results of this analysis are presented in Figures 4.6 and 4.7.

The most prominent difference between events EVTROP and EVBL in the DJF season is the presence of two centres of high pressure in the eastern Atlantic and in the eastern Pacific oceans which appear to determine the overall pattern of precipitation for the events designated EVTROP. In the Atlantic ocean the presence of this large high pressure system appears to break up the Atlantic storm track into two bands of increased precipitation (see Figure 4.6b) extending from 30°N to approximately 50°N in the western and central Atlantic respectively. In the Pacific ocean the anticyclone is weaker than its counterpart in the Atlantic and acts to allow an increase in the

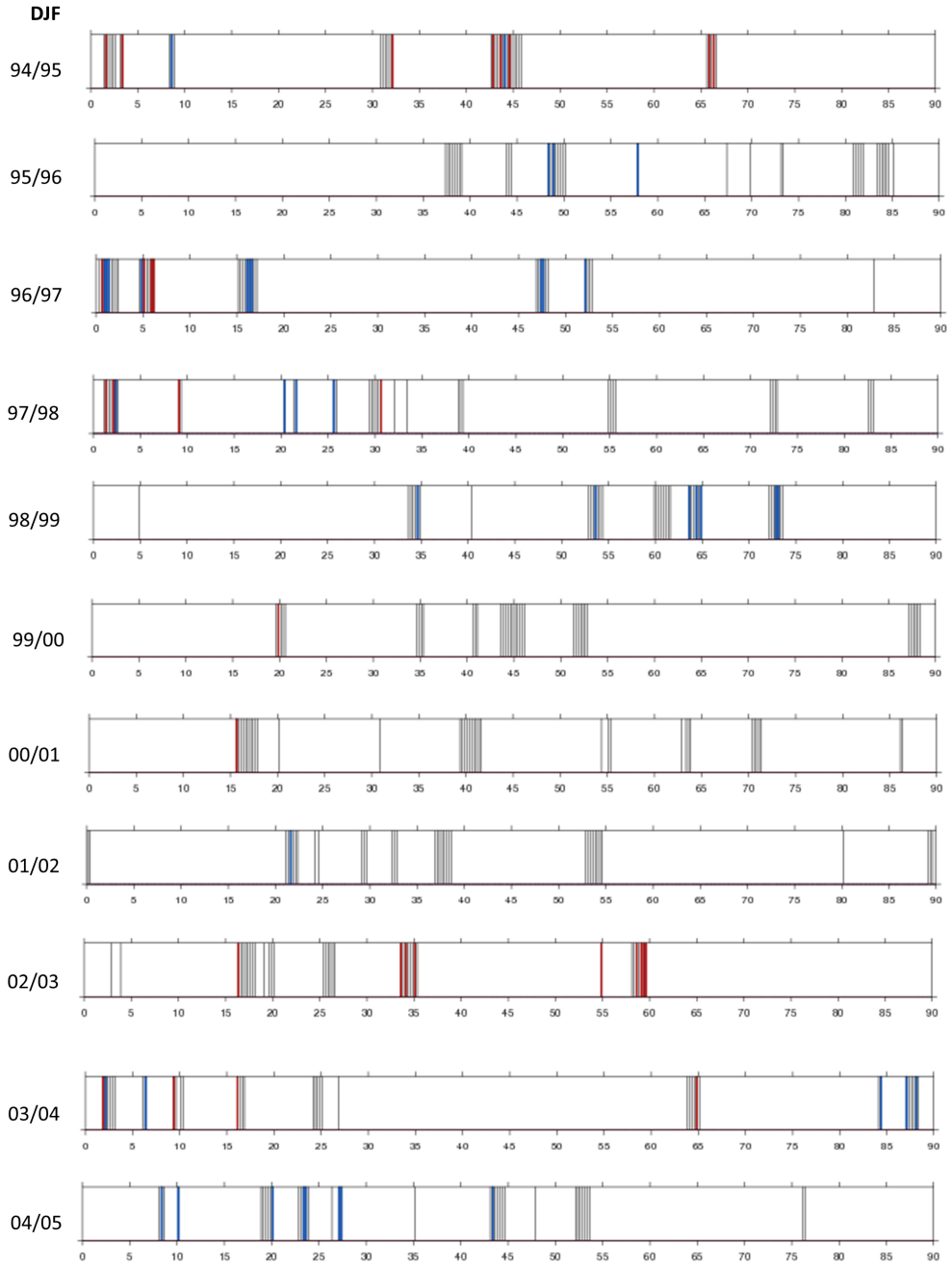

Figure 4.5: The occurance of events during the season DJF is marked by the thin black lines whilst, blue lines represent events which have their precipitation sourced from the advection of moisture in the free troposphere and events that are marked in red source their moisture mainly from the local boundary layer. Each year contains 36 events,

amount of precipitation along the western coast of North America by directing the flow of air anticyclonically around its upper extent and into a trough which forms on its eastern side. In the western Pacific the precipitation pattern is similar to what we might expect from the Pacific storm track (see Adler *et al.*, 2003, Hoskins and Hodges, 2002 and Hawcroft *et al.*, 2012). The change in mean sea level pressure pattern from the climatological pressure pattern (see Figure 4.6b) exhibits a series of alternating highs and lows which is indicative of the presence of a stationary wave in the upper atmosphere (Nigam and DeWeaver, 2003). This pattern will be investigated further in Section 4.5.6.

In contrast to the events designated EVTROP, events which are designated EVBL do not have anticyclones present in either the Pacific or the Atlantic oceans. In the case of the Atlantic ocean this has the effect of allowing a much better defined storm track to appear in the western Atlantic (see Figure 4.6c) and a large area of increased precipitation is associated with the troughing in the isobars that appears in the eastern Atlantic and over northern Spain and Portugal. In the western Pacific ocean, the storm track is once again visible but not as well defined as for the case of EVTROP. The pressure pattern in the eastern Pacific is dominated by a low pressure system, centered at 52°N. This pressure pattern appears to be influential in focusing the precipitation just off the coast and to the north west of the American continent. Over the areas of California, Oregon and Nevada precipitation is less than the climatological mean value (see Figure 4.6c). The change in mean sea level pressure pattern similarly produces regions that are alternatively lower and higher than the climatological mean. These regions are roughly the opposite polarity to those described by the EVTROP events, although some similarities remain (e.g. over western Europe). No increase in the precipitation over the North Sea and southern Scandinavia is apparent which is a consequence of the development of a ridge over the region occupied by the UK.

It has been well established that atmospheric rivers are a contributing factor to the amount of precipitation occurring over California (Smith *et al.*, 2010, Dettinger *et al.*, 2011, Dettinger, 2013 and Kim *et al.*, 2013) and they have been linked to inland precipitation events in Nevada (Smith *et al.*, 2010). Additionally it has been highlighted that only a few storm systems contribute a large amount to the annual precipitation in California (Dettinger *et al.*, 2011) due to the desert like conditions. However, this is believed to be the first time that events have been shown to produce increased precipitation in this region based upon large exports of moisture from tropical regions

when compared to events which are dominated by large boundary layer exports of moisture, both of which are in association with large poleward moisture transports that are a feature of atmospheric rivers (Zhu and Newell, 1998).

The precipitation patterns that occur further north on the western coast of the North American continent have also been shown to occur in conjunction with atmospheric rivers (Neiman *et al.* 2008a, Neiman *et al.* 2008c and Matrosov 2013) . However, in events which are designated EVBL the climatological values of precipitation are greater than those associated with EVTROP. This suggests that locally derived boundary layer moisture sources are more important at this latitude.

In the Atlantic ocean, however, it is clear that events designated as EVTROP cause large precipitation anomalies over southern Scandinavia, a region that has also been linked to atmospheric rivers (Sodemann and Stohl, 2013a). In section 4.5.7 we will further assess the of moisture travelling polewards.

The analysis presented above has been repeated for the season JJA and the results are presented in Figure 4.7. Regions of high pressure now dominate over both the Atlantic and Pacific oceans in both cases involving EVTROP and EVBL. In both cases the storm tracks have been weakened, which is consistent with the findings of Adler *et al.* (2003). However, unlike in the DJF season clear bands of increased levels in precipitation span the whole latitudinal range from 30°N - 60°N in the Atlantic for EVTROP and in the Pacific for EVBL. The largest area of precipitation change is centered to the south of Japan at around 120 E in the region of Meiyu-Baiu precipitation band (Ninomiya, 2009) during events which are designated EVTROP. For events that are designated EVBL the area of heaviest precipitation is centered over central Japan which corresponds with the location of the Baiu branch (see Figure 1 of Ninomiya, 2009) of the Meiyu-Baiu band of precipitation. These maxima in precipitation suggest a link between the Madden Julian Oscillation (MJO) (Zhang, 2005) and the determination of whether or not an event falls into the EVTROP or the EVBL category. Although an investigation into the MJO is beyond the scope of this thesis it should be noted that the phase of the MJO has been linked to the large scale circulation pattern (Baxter and Nigam, 2013) and as such would make an interesting extension to this work.

Over the central North American continent it is clear that an increase in precipitation is asso-

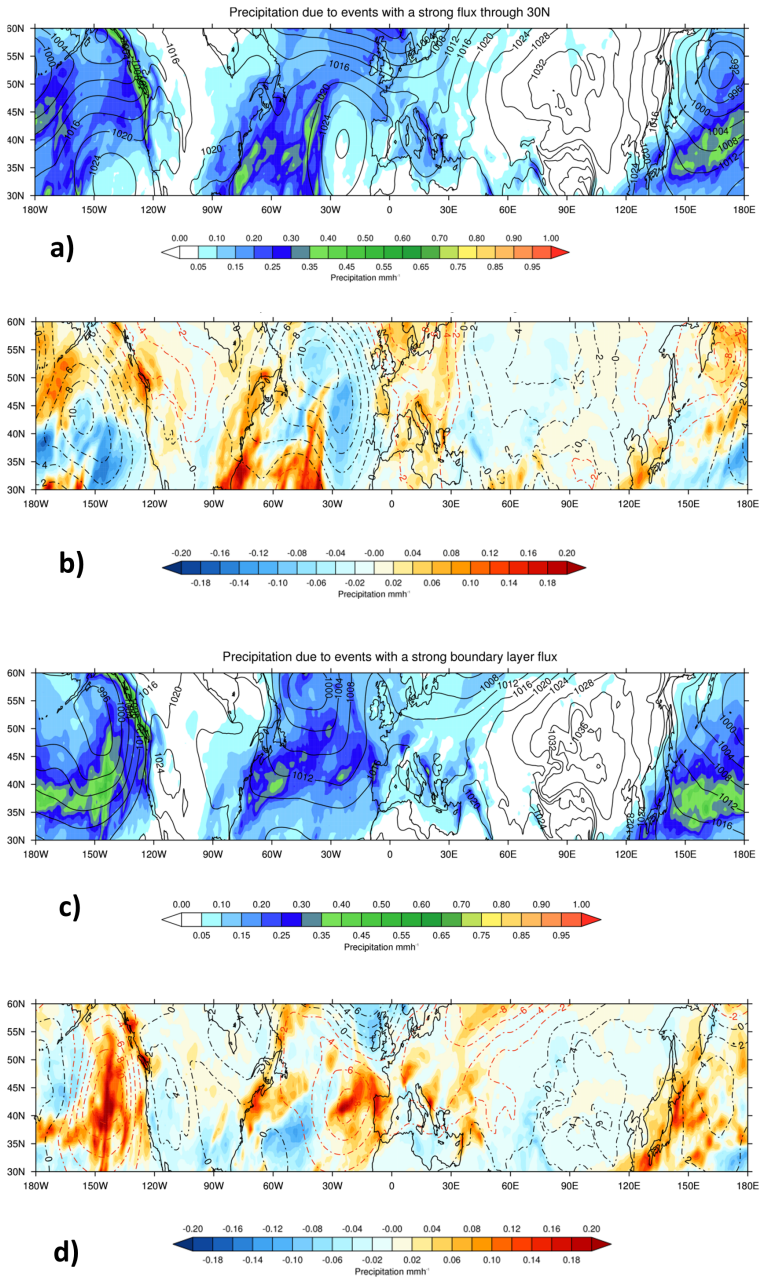

Figure 4.6: The spatial pattern of precipitation (for the season DJF) associated with events designated EVTROP (a) and EVBL (c) is overlaid with the MSLP pattern contoured every 4 hPa. Panels b and d show the difference between the precipitation produced by each of these sets of events compared with the mean climatological precipitation pattern. The contoured lines in each of these panels shows the difference in MSLP when compared with the climatological mean MSLP pattern. Red contours signify areas where the MSLP is less than the climatological mean whilst black contours signify regions where the MSLP pattern is higher than the climatological mean.

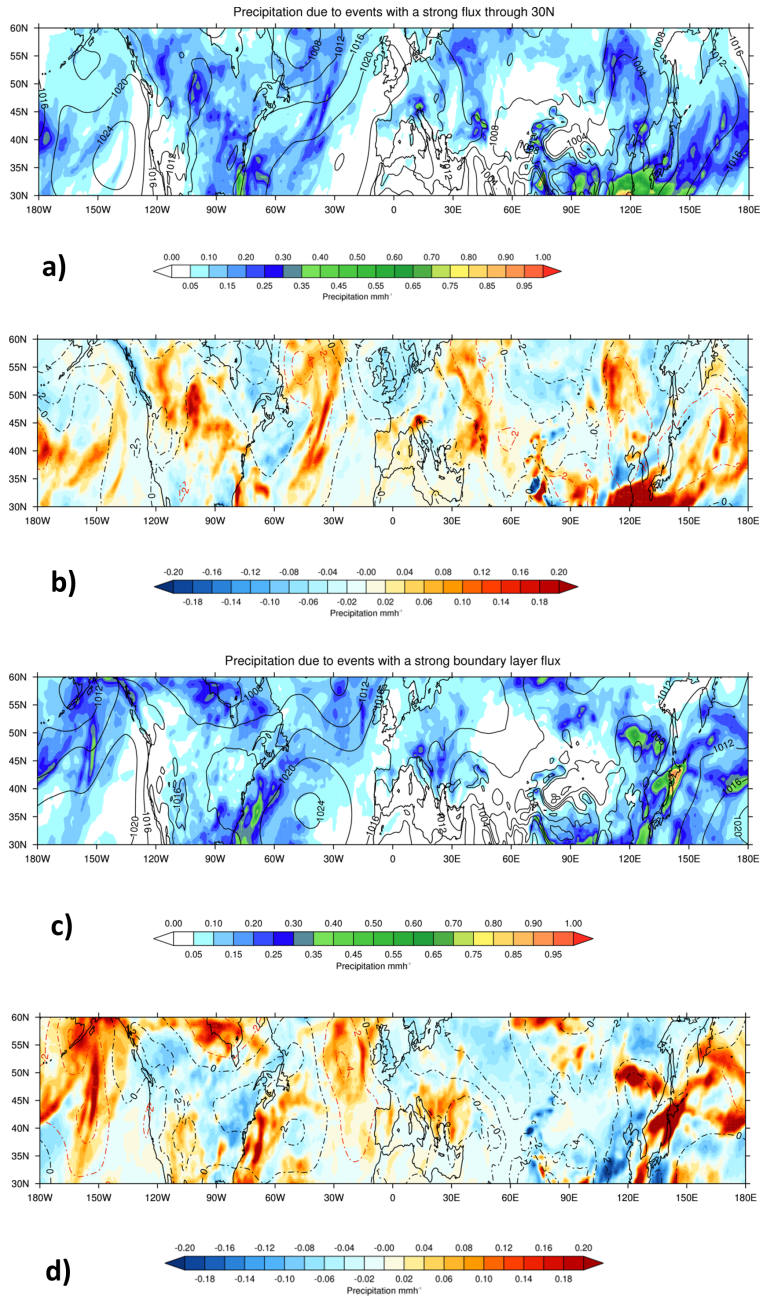

Figure 4.7: As for Figure 4.6 but for the season JJA.

ciated with the events designated EVTROP, whilst events that have been designated EVBL do not show any such increases (see Figures 4.7b and d). The synoptic pattern is similar in the EVTROP situation to that of the studies by Nakamura *et al.* (2013) and Lavers and Villarini (2013a) who showed that a ridge of high pressure just off the east coast of America was an important ingredient in directing moisture from the tropics up over the American continent. Over the regions of Nevada and Arizona, increases in precipitation occur during events which are designated as EVBL whilst no such increases are apparent in events designated EVTROP. This is in contrast to the season DJF where the opposite situation occurred.

4.5.6 Connection with the large scale flow pattern

The geopotential height of the 500 hPa surface is shown for the two types of events during the winter and summer seasons in Figure 4.8. Figure 4.8 shows that for events designated EVTROP the Atlantic ocean has a upper level ridge over eastern side, whilst to the west a trough is present, which extends over the eastern sea board of America. This pattern in the flow is consistent with the pattern of standing waves that would be expected over this area due to the influence of orography on the large scale flow (see Figure 7 of Grose and Hoskins, 1979). Similarly a very weak ridge appears over the west coast of the America, but no ridging appears over the western Pacific near the start of the Pacific storm track as implied by the work of Grose and Hoskins (1979). Since the transport of atmospheric moisture is a function of both standing waves and the smaller scale eddy fluctuations (Oort, 1971) this implies that the events diagnosed as EVTROP in the winter are likely to be driven by changes in the region of the Atlantic storm track. This argument is partly supported by the work of Messori and Czaja (2013) who showed that the strongest fluctuations in transient eddies appeared in the Atlantic Ocean.

The events diagnosed as EVBL show a very different spatial pattern in the 500hPa geopotential height field (see Figure 4.8b). Relative to the events diagnosed EVTROP the ridge in the eastern Atlantic has shifted polewards and to the east, whilst a prominent ridge has developed just to the east of the western coast of America. This explains why the large precipitation totals are confined to the edge of the north American continent, with there moisture being sourced from the strong convergence of boundary layer moisture (Boutle *et al.*, 2010) into the system by the high rates of boundary layer ventilation which are typicallyt found near to the coast at this point (See

Figure 2.9). The flow over the Atlantic ocean however, is zonal in nature indicating that boundary layer convergence of moisture alone is responsible for the increased precipitation over western Spain or that at the very least no fixed synotic patterns play a significant role. It is known that the amplification of Rossby wave patterns is important for the production of extreme weather events (Petoukhov *et al.*, 2013) and this chapter has shown that both large tropospheric moisture fluxes and large boundary layer moisture fluxes are in some way regulated by this mechanism.

In the season JJA the poleward gradient in geopotential heights is much reduced (see Figure 4.8c and d). This reduction in the geopotential heights is associated with a weakening of the transient eddies. The lack of difference between the two plots also suggests that standing waves are not a contributing factor. Two possible explanations can explain this behaviour. Firstly, the only term left to describe the difference in poleward moisture transport, as described by Oort (1971), is the mean atmospheric circulation which at 30°north is a function of the strength of the Hadley cell, however, the Hadley cell was shown to be of little significance to the poleward transport of energy and latent heat in the study of Oort (1971). Another explanation would be however, that only looking at the mean heat transport over the 30°N to 60°N latitudinal band which implicitly implies that the zonal integrated extremes are more important than the local extremes is not the case during the summer. This is an interesting area of current research (Messori and Czaja, 2015).

4.5.7 Extent of poleward moisture transport

In order to determine the influence of tropospheric moisture flows on the downstream precipitation it is important to determine how much of the moisture that was advected from the tropics is still available as a moisture source in the more northerly latitudes. In order to do this $F_{out\_fa}(adv)$ and $F''_{out\_fa}(adv)$ were calculated using Equations 4.20, 4.21 and 4.24. The results of this calculation are presented for the mean climatological value of $\frac{P_a}{P_{bl}}$ in Table 4.4.

If we first look at the values of $F_{out\_fa}(adv)$ we can see that all of the moisture gets used up in the production of precipitation between 35° - 40° N. This matches well with the results presented in Section 4.5.3 which demonstrated that local boundary layer ventilation becomes the most prominent source of moisture at approximately 43° N (i.e. approximately 1 box further

north than the final box where all of the moisture sourced from the tropics is used up).

In order to assess the effect of mixing in the atmosphere the calculation was redone in order to calculate $F''_{out}(adv)$ as defined by Equation 4.24 and the results are displayed in column 8 of table 4.4. These results for the of advective moisture transport have been expressed as a percentage of the initial moisture flow in from the tropics which are presented in column 9 of Table 4.4. The results show that if mixing of moisture parcels is taken into account a small fraction of the original moisture that flows from the tropics is transported to 60° N.

This result is repeated for the event which had the highest ratio of $\frac{P_a}{P_{bl}}$ in the DJF season between 30°N and 60°N. The results for this calculation are displayed in Table 4.5. As can be seen from column 2 of Table 4.5, the flux of moisture into the box from the tropics is roughly 40 % larger than the initial flux of moisture provided in the mean climatology (depicted in Table 4.4). This large flux of moisture produces over double the amount of moisture advected into the box between 40°N and 45°N, when mixing of air parcels is accounted for (compare column 8 of Table 4.4 with column 8 of Table 4.5). However, less than half of the original flux of moisture is transported into the box between 50°N and 55°N.

The results from calculating both $F_{out}(adv)$ and $F''_{out}(adv)$ for each of the events during the seasons of DJF and JJA are presented in Figure 4.9. In Figures 4.9 a and b, it can be seen that all the moisture that has flowed in from the tropics has been removed by precipitation by 45°N in the DJF season and by 50°N in the JJA season using Equations 4.20, 4.21 and 4.24. If we apply the mixing assumption, moisture advected in from the tropics is allowed to be advected over the entire latitudinal band. However, it can be seen from Figures 4.9c and d that the amount of moisture being advected polewards is less than 5% of the original value by 45°N - 50 °N of the mean. However, events that supply large amounts of moisture in from the tropics have the ability to transport 5% of this moisture as far north as 55 °N in the JJA season and 50 °N in the DJF season. Referring to the values from Table 4.3 for the total transports this translates to less than 1 % of the total moisture flux at these latitudes.

It is therefore, not unreasonable to conclude that the large amounts of precipitation seen at higher latitudes in Figures 4.6 and 4.7 are sourced mainly from the local convergence of moisture within the boundary layer which is subsequently ventilated (Boutle *et al.*, 2010) and precipitated

	F_{in_fa}	BL	P_h	F_{out_fa}	$F_{out}(adv)$	γ	$F''_{out}(adv)$	$\frac{F''_{out}(adv)_{(k)}}{F_{in(0)}}$ x 100.0(%)
30-35	8.014 x 10^8	7.213x10^8	6.702x10^8	8.380x10^8	3.392x10^8	-	3.392x10^8	42.326
35-40	8.380 x 10^8	7.361x10^8	8.195x10^8	7.826x10^8	-5.384x10^7	0.4048	1.087x10^8	13.564
40-45	7.826x10^8	5.17x10^8	6.910x10^8	6.457x10^8	N/A	0.1390	3.658x10^7	4.565
45-50	6.457x10^8	3.114x10^8	5.365x10^8	4.661x10^8	N/A	0.0567	1.210x10^7	1.510
50-55	4.661x10^8	2.335x10^8	4.227x10^8	3.221x10^8	N/A	0.0260	3.330x10^6	0.416
55-60	3.221x10^8	2.220x10^8	3.780x10^8	2.024x10^8	N/A	0.0103	4.221x10^5	5.2x10^{-2}

Table 4.4: The climatological values for the poleward transport of moisture for the season DJF. The first column represents the size of the box over which the climatological values were calculated, the flux of moisture in over the top of the boundary layer (F_{in_fa}), the boundary layer ventilation of moisture (BL), the precipitation of moisture through the top of the boundary layer (P_h), and the overall flux of moisture polewards through the poleward side of the box (F_{out_fa}). The poleward transport of moisture originating from the flow at 30°N and is given by the units kgs^{-1}, calculated by Equation 4.20 ($F_{out}(adv)$) and by Equation 4.21 ($F''_{out}(adv)$). The ratio γ is given by Equation 4.22. Whilst the percentage of the transport polewards due to mixing is given by the last column.

	F_{in_fa}	BL	P_h	F_{out_fa}	$F_{out}(adv)$	γ	$F''_{out}(adv)$	$\frac{F''_{out}(adv)_{(k)}}{F_{in(0)}}$ x 100.0
30-35	1.140x10^9	5.469x10^8	5.785x10^8	1.027x10^9	6.735x10^8	-	6.735x10^8	59.079
35-40	1.027x10^9	5.629x10^8	6.565x10^8	8.460x10^8	2.105x10^8	0.656	3.357x10^8	29.446
40-45	8.460x10^8	4.292x10^8	6.743x10^8	6.057x10^8	-1.234x10^8	0.397	1.223x10^8	10.731
45-50	6.057x10^8	3.612x10^8	6.285x10^8	4.080x10^8	N/A	0.107	1.301x10^7	1.142
50-55	4.080x10^8	2.918x10^8	4.468x10^8	3.000x10^8	N/A	0.0319	2.517x10^6	0.221
55-60	3.000x10^8	2.264x10^8	3.297x10^8	2.434x10^8	N/A	2.21x10^{-3}	1.340x10^5	0.012

Table 4.5: As for Table 4.4 but for the event which exhibited the highest ratio of $\frac{P_a}{P_{bl}}$ for the DJF season.

out over the north west coastline of America and over northwestern Europe. This supports the conclusions of the study by Dacre *et al.* (2014) who suggested that atmospheric rivers were just remnants of systems undergoing such a process. It is however, possible to envisage a more indirect link between the precipitation produced over the North Sea and southern Scandinavia in the season of DJF and the large tropical moisture fluxes which are associated with this precipitation. The broadscale pattern shown in Figure 4.8 represents a consistent pattern of Rossby wave breaking over the north Atlantic which has been linked with large poleward transports of moisture (Liu and Barnes, 2015). The jet exit region associated with the poleward ridge of the breaking Rossby wave (Palmén *et al.*, 1990) is a region of cyclogenesis and thus produces increased precipitation in the local region (Browning, 1990). These events have the potential to produce other disturbances at lower latitudes in the form of secondary cyclogenesis (Rivals *et al.*, 1998) which may be influenced by moisture supplied from the tropics. This hypothesis is consistent with the work of Dacre *et al.* (2014) in their explanation of atmospheric rivers whilst it also explains the concurrent dominance of precipitation due to large flows of moisture from tropical sources into the mid-latitudes.

It is interesting to note that for the events designated EVTROP over California, Oregon and Nevada only 10-20% of the original tropical flux of moisture into this region produces precipitation. However, this extra moisture may be crucial in a region that suffers from frequent droughts (Dettinger *et al.*, 2011; Dettinger, 2013).

In order to simplify the problem and in order that our results may be compared with those of the study of Messori and Czaja (2013) our study only used the poleward wind vectors in order to identify suitable events and as such it would be interesting to extend this work by using the horizontal wind vectors as described by Zhu and Newell (1998). However, we do not expect any dramatic changes in the results presented here in this chapter.

4.6 Conclusion

This chapter has shown that large transports in moist static energy are accompanied by large transports in moisture. During an eleven year period in the season of DJF the top 10% of events in poleward moist static energy were shown to contribute to 73.7% of the net poleward transport of

moist static energy and 58.8% of the of the gross poleward transport of moist static energy. In the season of JJA these percentages were 88.5% and 58.7% respectively. It was then shown that in DJF the same events transported 79.6% of the gross polewards moisture transport and 65.1% of the net polewards moisture transport. In the season of JJA these figures were 96% and 60.5% respectively. Events which transport large amounts of moist static energy are therefore comprised a large proportion of the poleward moisture transport. The Figures obtained for the poleward transport of moist static energy are in agreement with those produced by previous studies (Swanson and Pierrehumbert, 1997 and Messori and Czaja, 2013).

It was demonstrated in Section 4.5.2 that on the scale of a hemisphere, large net transports of moisture occur above the boundary layer from the tropics. Section 4.5.3 demonstrated that over the course of each year the top 10% of events could be split up into a set of events which mainly sourced their precipitation from boundary layer moisture exports (EVBL) and a set of events which mainly sourced their precipitation from tropical moisture exports above the boundary layer (EVTROP). The occurrence of these individual events was not correlated over the course of the eleven year period. In Section 4.5.4 we showed that in individual years one type of event tended to be more dominant than the other than the other type (e.g. Figure 4.5 shows that in the season of 02/03, out of the two types of events, only events which produce precipitation due to high boundary layer moisture ventilation appear). This confirms the more limited result provided by Bao *et al.* (2005) who suggested that the occurrence of large tropical moisture exports were rare.

In Section 4.5.5 it was demonstrated that significant differences can be seen between the precipitation patterns occurring due to events associated with EVTROP and events associated with EVBL. It was then demonstrated through comparisons with the literature (e.g. Dettinger, 2013) that some similarities existed between the precipitation which is produced by atmospheric rivers and the precipitation pattern produced by events designated to be EVTROP. The average synoptic conditions controlling each set of events was also shown to differ by computing the average mean sea level pressure pattern for each set of events. This pattern in mean sea level pressure was also compared with the climatological mean sea level pattern for the two seasons of DJF. This comparrison revealed a wave like structure which we noted was similar to the effect of standing waves in the upper atmosphere.

Patterns for the 500 hPa geopotential height fields were produced for events designated to be

EVTROP and EVBL in order to investigate the hypothesis that it was standing waves which were responsible for the events that were designated EVTROP. Evidence to support this hypothesis was found in the pattern seen over the Atlantic ocean during the season of DJF. The absense of any strong signals in the other season suggest that the moisture transports within the two oceanic basins do not occur simultaneously in JJA. A more robust conclusion for JJA might be obtained by studying each basin separately. Whilst the signal observed in DJF suggests that either simultaneous poleward transports of moisture occur simultaneously in both ocean basins or that the majority of moisture transports occur within the Atlantic ocean basin. Further study on the scale of an individual ocean basin would be necessary in order to investigate these two possibilities.

The extent to which moisture can be transported poleward during each individual event was investigated in Section 4.5.7. It was found that in DJF less than 10% of the original moisture that was advected in from the tropics made it past the 45th parallel. This suggests that any patterns in precipitation found north of this line are produced by episodes of high boundary layer ventilation within the mid latitudes. This supports the conclusions of Boutle *et al.* (2011) who showed a direct relationship between precipitation and boundary layer ventilation in an idealised mid latitude cyclone. This is also consistent with the conclusions found in Dacre *et al.* (2014) who showed that in the majority of cases local sources of moisture were responsible for the high concentration of total column water vapour ahead of a cyclones warm front. A larger proportion of the original moisture was found to be transported past the 45th parrallel during the season of JJA. This result suggests that in the summer a greater number of cyclones may derive their moisture content from tropical sources (For evidence of cyclones being fed by tropical moisture sources see Knippertz and Martin, 2007, Knippertz and Wernli, 2010 and Sodemann and Stohl (2013a)).

As atmospheric warming continues (Stocker *et al.*, 2013) it is expected that an increase in poleward moisture transports is going to occur (Held and Soden, 2006) it is therefore important to assess the impact of these changes in precipitation on the regional scale. It is suggested that the framework provided by this chapter will be useful for evaluating this problem in climate models and that the methods presented here should be adopted by future climate modellers in order to assess the possible consequences of living in a warmer world.

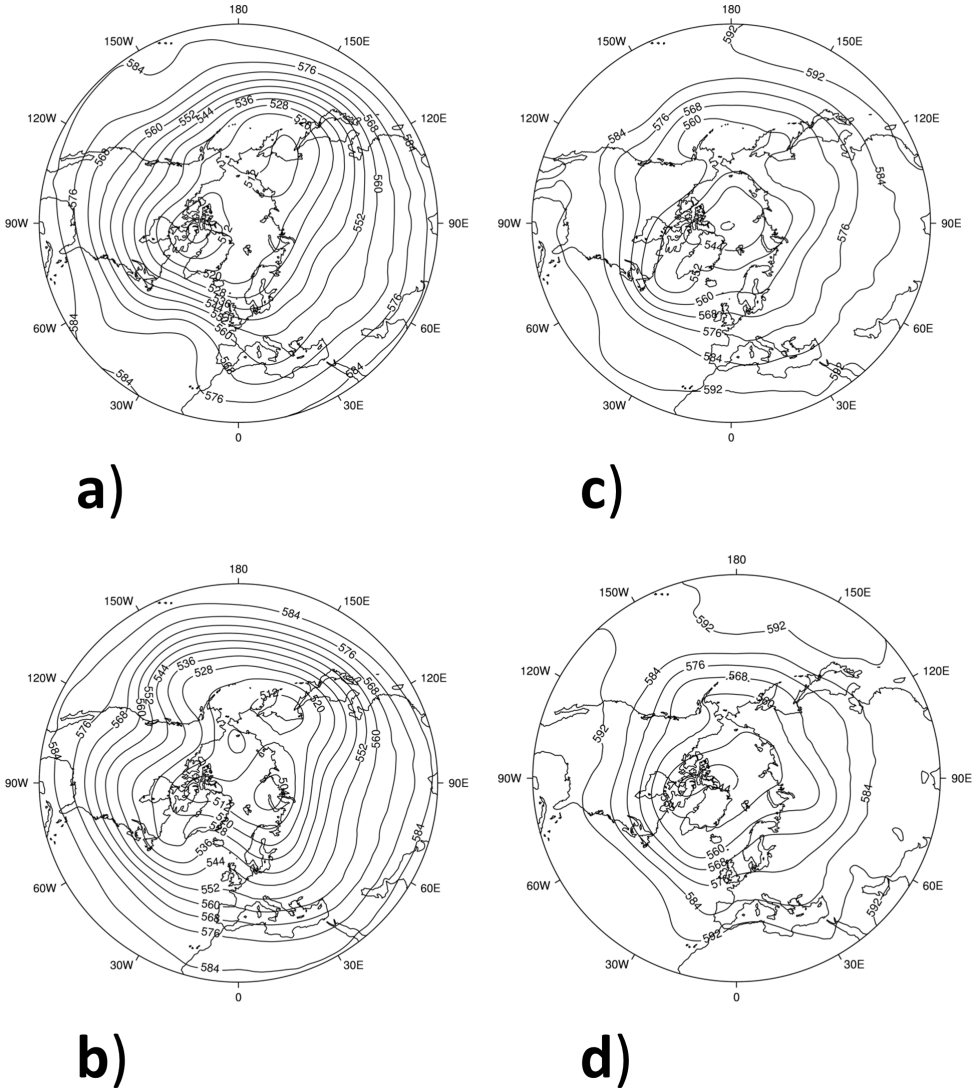

Figure 4.8: The geopotential heights of the 500 hPa surface for EVTROP (a) and EVBL (b) in the season DJF and for EVTROP (c) and EVBL (d) in the season JJA.

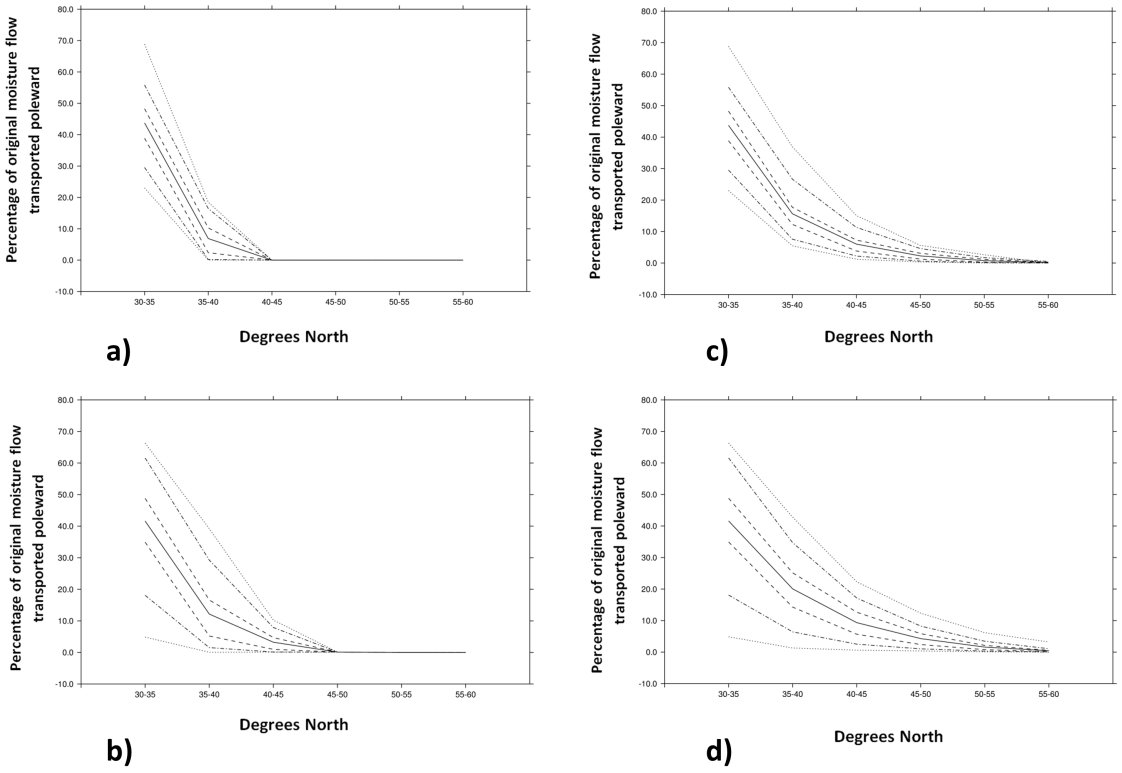

Figure 4.9: Panels a and b show the mean percentage of poleward moisture advected from the tropics (solid line) as described by Equations 4.20 and 4.21 for the seasons DJF and JJA. Panels c and d show the mean poleward advection of moisture as described by Equations 4.20 and 4.24 for the seasons DJF and JJA. The lines made up of dashes and dots describe the distribution of the data in terms of the 5, 25, 75, 95 percentiles along with the outer limits. All events are included in each case. The number of contributing events decreases in panels a and b as the residual amount of moisture that is being advected decreases to zero.

Chapter 5:
Conclusions

5.1 Introduction

The aim of this thesis was to investigate the ventilation of the atmospheric boundary layer. In particular the thesis aimed to answer the following questions:

1. Can global datasets with limited temporal resolution accurately represent the processes of boundary layer ventilation?
2. How does the turbulent boundary layer redistribute moisture within a mid latitude cyclone?
3. What is the role of moisture in events that transport high amounts of moist static energy polewards?

These questions have been addressed using the ECMWF forecast model in conjunction with Eulerian mass budget equation described by Sinclair *et al.* (2009) and the Eulerian moisture budget equation described by Boutle *et al.* (2010). In addition the Lagrangian perspective on boundary layer ventilation was investigated in a case study by using the NAME particle dispersion model in conjunction with the Met Office's Unified Model version 7.4. Using these tools we were able to create the first global climatology of boundary layer ventilation. It was shown that the turbulent boundary layer was responsible for the majority of moisture ventilation that occurred within the warm conveyor belt of a mid latitude cyclone and that the redistribution of moisture within a mid latitude cyclone was highly dependent upon the exact source location of the moisture. By contrasting the precipitation patterns associated with episodes of strong boundary layer ventilation with the precipitation patterns associated with high tropical moisture exports it was shown that the synoptic patterns associated with each regime were distinct and that a lot of the variability in mean sea level pressure occured in the Atlantic ocean.

5.2 Discussion of results

The boundary layer mass budget equation has been calculated using the ECMWF forecast model data in an attempt to validate its use with a dataset of limited temporal resolution. In order to do this it was first necessary to calculate the height of the boundary layer top. To do this a bulk Richardson number was used in order that the results could be compared with the idealised simulations of Sinclair *et al.* (2009). This height was then used as a surface with which to calculate the boundary layer ventilation rate. A suitable mid latitude cyclone was then chosen and the results of the calculations were compared with the idealised study of Sinclair *et al.* (2009). The results of this comparison showed that both the boundary layer structure and ventilation rates agreed well with the results of Sinclair *et al.* (2009) who used a much shorter time step in order to calculate the ventilation rate of the boundary layer in their idealised simulations. The comparison did however, reveal much stronger ventilation rates along the warm front which were not apparent in the results of Sinclair *et al.* (2009). This extra line of ventilation is hypothesised to be due to the release of latent heat as air rises up the warm front and out of the boundary layer. Similar effects were observed when trough lines passed over areas of land. Boundary layer ventilation due to the release of latent heat were not seen in Sinclair *et al.* (2009) who used a dry simulation in order to recreate the boundary layer mass budget.

Climatologies of the boundary layer height were produced for a 30 year period between December of 1979 and November 2009 for each of the four seasons (e.g. December, January and February). The results of these climatologies compared well with similar climatologies produced by other researchers (e.g. von Engeln and Teixeira 2013) who used changes in the relative humidity in order to define the boundary layer top. Key features of the climatologies were areas of raised boundary layer height within the storm tracks and low boundary layer heights over the equator. Climatologies were also constructed for the mass ventilation rate of the boundary layer and the solutions to the mass budget equation were presented. In some areas the boundary layer mass budget was not in balance and hence results in these regions need to be treated with care. These areas were shown to mostly occur within the tropical latitudes and over land. The climatologies of boundary layer ventilation did show the structure of the ITCZ and mid latitude storm tracks extremely well. In addition areas of ventilation occurred over the major mountain ranges of the globe. The ECMWF forecast model which has data archived every 3 hours was thus shown

to be capable of reproducing the main patterns of ventilation but great care must be taken when interpreting the results over land in the tropical regions.

In Chapter 3 we extended the calculation to moisture and compared the results for the same case study that was used in chapter 2 with the results of the moisture budget used by Boutle (2009). The results of the moisture budget compared very well with the idealised simulation results of Boutle (2009) although the unresolved ventilation of moisture in the region of the warm conveyor belt was shown to be much stronger than exhibited in the simulations by Boutle (2009). It was shown by the use of Lagrangian trajectories that a direct route linked the areas of increased evaporation and the areas of increased moisture ventilation within the warm conveyor belt. Further investigation demonstrated that the area of unresolved ventilation in the ECMWF forecast model simulations was a major exporter of Lagrangian particles. This leads us to conclude that ventilation of the warm conveyor belt is controlled by turbulent processes. It was further shown that boundary layer turbulence was responsible for redistributing particles throughout the warm conveyor belt and that these particles could be grouped according to their final location. The grouping of particles was shown to be consistent with work done by Martínez-Alvarado *et al.* (2014). However, the final proportion of the number of particles which ended up in each group was shown to be dependent upon the initial release location within the boundary layer. In terms of moisture distribution within the cyclonic structure this result is significant in that it highlights the need for accurate representations of boundary layers mixing and ventilation in order to accurately describe the distribution of moisture within the system which has shown to be instrumental in determining cyclone development (Smith, 2000).

The role of moisture has been investigated in terms of its role in the polewards transport of moist static energy. The majority of polewards moist static energy transport occurs in a small number of events (Messori and Czaja, 2013). It is found that such events also dominate the total polewards moisture transport (65.1% and 60.5% for the top 10% of events during the seasons of DJF and JJA). These events are considered on the scale of a hemisphere and are used to identify a subset of events which are associated with large tropical moisture exports (EVTROP) and a subset of events which are associated with large exports of moisture from the boundary layer (EVBL). These two sub-sets of events are isolated and the precipitation patterns for each are compared against the climatological rate of precipitation for the seasons of DJF and JJA. It is shown that

some similarities exist between the precipitation pattern associated with large tropical moisture exports and that expected from atmospheric rivers. The polewards transport of moisture from 30° N is shown to be mainly limited to latitudes between 30° N and 45° N. Any large amounts of precipitation produced north of the 45° latitude line must therefore be produced by large amounts of moisture exported from the mid latitude boundary layer. It was however noted that in the months of JJA a small number of events could potentially draw moisture from the tropics in order to enhance precipitation in the northern mid latitudes. Unique climatological patterns of mean sea level pressure were associated for each sub set of events and the climatological pattern of 500 hPa geopotential heights are shown to represent the difference between EVTROP and EVBL in the season of DJF.

The role of the boundary layer has been shown to be important for both the distribution of moisture within individual mid latitude cyclones. A useful diagnostic tool has been presented for identifying events which allow large amounts of moisture to flow into the middle latitudes from tropical sources in flows which share similar characteristics to that of the moisture conveyor belt (Knippertz and Martin, 2007). It is hoped that the work presented within this thesis will convince future researchers to consider the boundary layer and boundary layer ventilation, not just as a local phenomena, but as one that can be used to investigate meteorological systems on a global scale.

5.3 Future Work

The results presented in the mass budget Chapter are encouraging in that it should be possible to use the mean ventilation rates calculated as a basis for assessing whether or not the episodes of boundary layer ventilation presented in case studies (e.g. De Wekker *et al.* 2004, Henne *et al.* 2004b) are exceptional events or not. In order to validate the climatology it would be useful to compare climatologies of individual areas with results generated by high resolution numerical weather prediction models in order to asses the effect of sub grid scale process such as thermal circulations which have been shown to enhance ventilation in areas such as the coast and over mountain topography. The mass budget of the boundary layer that is presented in Chapter 2 is an approximation, it would therefore be an interesting challenge in order to develop a scheme

that was capable of calculating the boundary layer height as a prognostic variable by taking into account suitable parameterisations of the entrainment and ventilation of mass through the boundary layer top. Such an endeavour would remove the necessity of using methods such as the bulk Richardson number for determining boundary layer height. A scheme which is capable of standardising the boundary layer height would remove any uncertainty as to the mechanism by which pollutant layers are formed above areas of mountainous terrain in a region currently referred to as the aerosol layer (De Wekker *et al.*, 2004).

In Chapter 3 it was shown that the dispersive properties of the boundary layer were capable of producing a redistribution of pollutants throughout the entire structure of the warm conveyor belt. It would be especially interesting if we could track the potential vorticity associated with each individual Lagrangian particle. Using the methods of Chapter 3 we could then isolate the particles to the north east of the cyclone wave and determine how much the transport of boundary layer material could be capable of altering the shape and structure of the overriding Rossby wave. This type of experiment could be repeated for different strengths of boundary layer mixing in order to determine the influence that the boundary layer has in determining possible forecast outcomes. In order to do this the code which controls the turbulent motion of particles within the NAME model would have to be adjusted.

It would be interesting to confirm the link made between the ventilation which occurs to the east of the cold front in the NAME calculations performed for the work in Chapter 3 and the additional ventilation of moisture due to the unresolved flux in the moisture budget analysis of Chapter 3, which has the effect of increasing the area which can be associated with the warm conveyor belt. We could use the cyclone compositing techniques of Dacre *et al.* (2012) in order to test whether or not this feature is present as a general feature of extra-tropical cyclones. Most current studies suggest that either advection or convection is the dominant mechanism for removing material from the boundary layer (e.g. Donnell *et al.* 2001, Purvis *et al.* 2003) but our results suggest that turbulent transports also have an important role to play.

In order to continue the work presented in Chapter 4 it would be valuable to further adapt the methods of precipitation recycling in order to repeat the calculations that were applied to the northern hemisphere and repeat them for individual oceanic basins. The results presented in this chapter suggest that much of the variability is controlled by patterns in the upper level flow

patterns over the Atlantic ocean. It would be interesting to contrast the results from the Atlantic basin with the Pacific basin in order to determine whether the results obtained are controlled by the Atlantic basin, the Pacific basin or a combination of the two. By repeating the calculation of moisture transport at the basin level we could further confirm the result that that tropical moisture exports do not have much direct influence on the precipitation patterns seen at latitudes north of 45°. It would also be interesting to further investigate the importance of ENSO in determining the large scale weather patterns which control the occurrence of events which exhibit a large export of tropical moisture into the mid latitudes. This would test the hypothesis of Bao *et al.* (2005) who suggested that neutral ENSO conditions would be the most favorable for enhanced tropical moisture exports. In addition the results presented in Chapter 4 suggest that the MJO is instrumental in regulating the transport of moisture but in order to confirm this result a more comprehensive investigation into this link is neccesary.

Appendices

Appendix A:
The IFS Orography

A.1 Orography

The orographic height is calculated using

$$Z = \frac{\phi}{9.80665} \tag{A.1}$$

where ϕ is the geopotential at the surface and Z is the corresponding geopotential height. Near the surface this approximates to geometric height since the constant 9.80665 is the acceleration due to gravity near the surface. Z is measured in m whilst ϕ is measured in $m^2 s^{-2}$. The height of orography in the IFS model is depicted in Figure A.1.

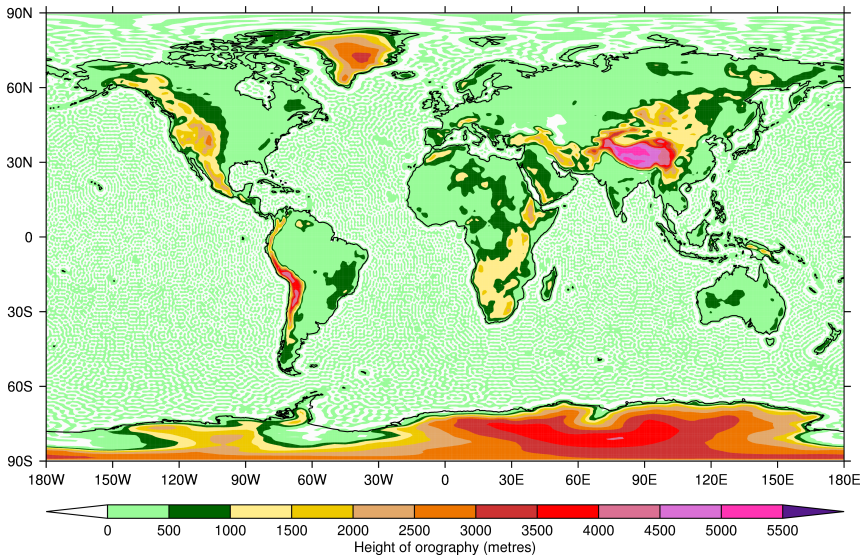

Figure A.1: The height of the orography in the IFS model.

Appendix B:
Balancing the Moisture Budget

B.1 Balancing the moisture budget

In order to check that the fluxes of moisture out of the boundary layer were consistent with the overall change in moisture described by the IFS two calculations were performed. The first calculation performed was

$$\frac{\partial q_{fa}}{\partial t}_{direct} = \frac{\int_{bl\,top}^{toa}\int_S(\rho q)_2 - (\rho q)_1 dAdz}{\Delta t} \tag{B.1}$$

where Δt is a time difference of 3 hours (measured in seconds), (ρq) is the density of air multiplied by the total amount of moisture in the air ($q = q_v + q_l + q_i$) at each timestep $()_2$ minus the equivalent amount at the previous timestep $()_1$. q_{fa} is the total amount of moisture in the free atmophere. The latitude is designated by ϕ whilst the geometric height is designated by z. The first integral is between the boundary layer top ($bl\,top$) and the top of the atmosphere (toa) whilst the second integral is taken over the surface of the boundary layer top (S) between 30° N and 60° N, with dA being representative of a unit of area on surface S.

The second calculation uses the fluxes in and out of the region in order to do the complimentary calculation

$$\frac{\partial q_{fa}}{\partial t}_{fluxes} = F_{in\,fa} - F_{out\,fa} + BL - P_h \tag{B.2}$$

where each of the terms on the right hand side are defined in Chapter 4. The results of these two calculations are presented in Figure B.1a which shows that the calculations are consistent. Figure B.1b demonstrates the differences seen in Figure B.1a mainly occur at 12 hour intervals. In order to investigate this Figure B.2 was produced which separates out the calculations of $\frac{\partial q_{fa}}{\partial t}$ based

upon the model time steps used.

It is clear, by comparing Figures B.2a - d, that when calculating $\frac{\partial q_{fa}}{\partial t}$ the use of data at T+0 / T+12 and T+3 hours causes the systematic differences observed in Figure B.1b. Two possible explanations exist for these systematic differences.

1. The data assimilation cycle makes changes to the T+12 data in order to produce the re-analysis dataset which is used to initialise the model. We are using T+12 data in order to do this comparison.

2. In order to calculate the amount of precipitation that is falling through the boundary layer top (P_h) an accumulation of the total precipitation between T+0 and T+3 hours was taken and divided by the 3 hour time period in order to give an average flux of moisture through the boundary layer top.

Any differences due to point 1 above are likely to be small as this difference is included in both calculations of $\frac{\partial q_{fa}}{\partial t}$. In chapter 4 the effect of the spin up of precipitation was clearly demonstrated and as such we attribute most of the differences found in the calculation of to $\frac{\partial q_{fa}}{\partial t}$ to the spin up problem (point 2 above).

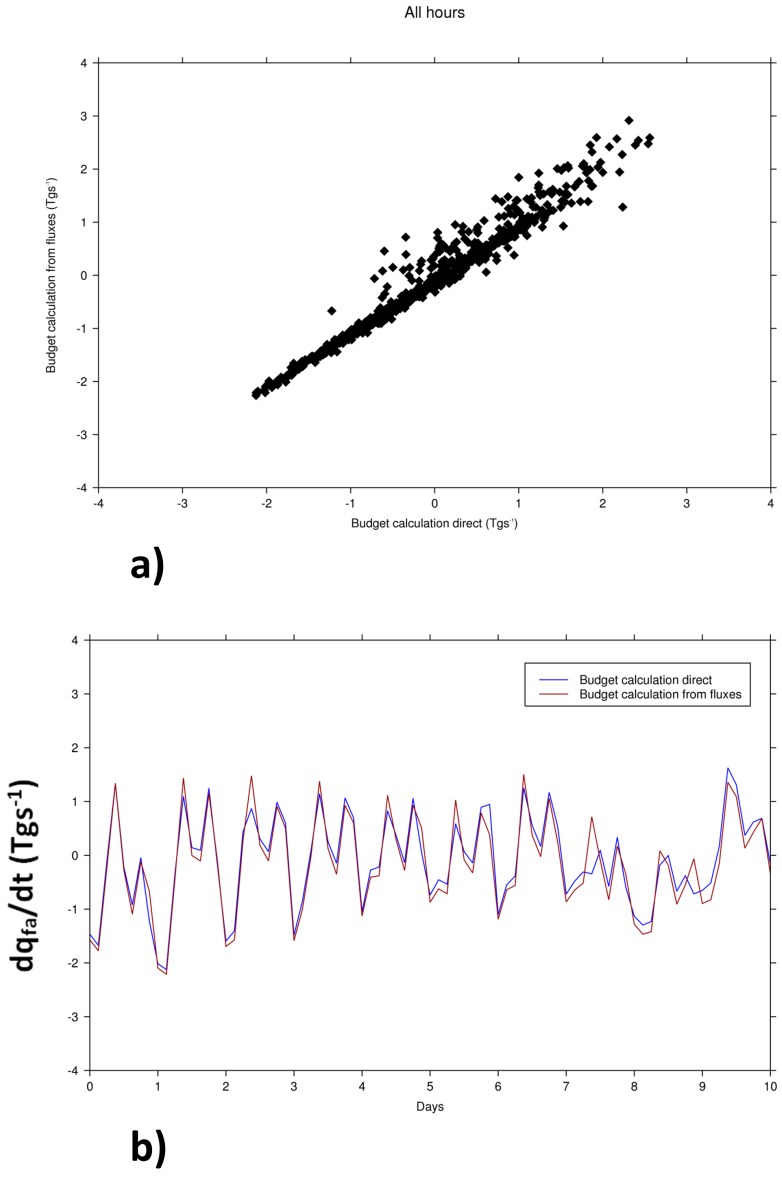

Figure B.1: Panel a shows the change in atmospheric moisture at every available time interval for the season DJF in the years 1994 to 1995. The x-axis shows the calculation using the values of volume integrated moisture which were directly extracted from the ECMWF data set. The y-axis shows the calculation done using the flux budget. Panel b shows the change $\frac{\partial q_{fa}}{\partial t}$ for both calculations as a function of time.

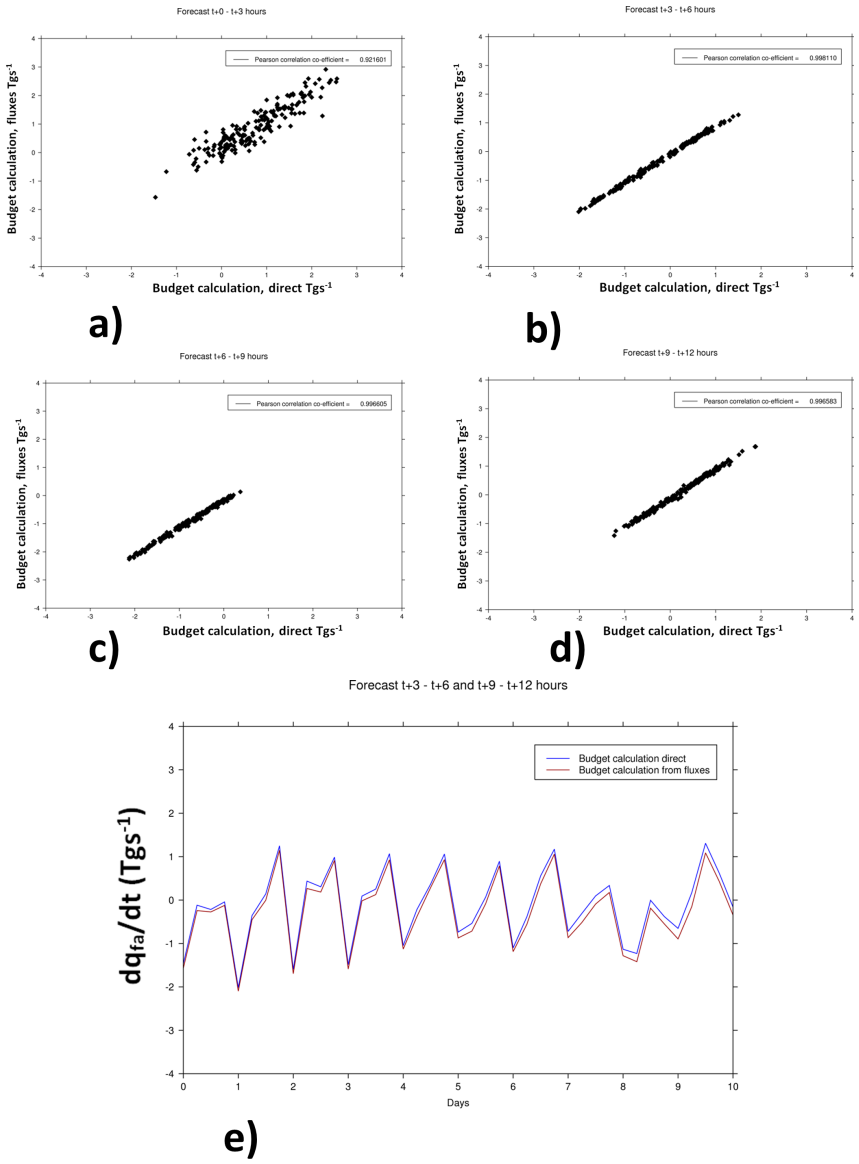

Figure B.2: Panels a-d show the results for the calculation of $\frac{\partial q_{fa}}{\partial t}$ by Equations B.1 and B.2 across each of the time periods T+12-T+3 (a), T+3-T+6 (b), T+6-T+9 (c) and T+9-T+12 (d). Panel e shows the results of the T+3-T+6 data and the T+9-T+12 data as a function of time.

Appendix C:
The Eady Model

C.1 The Eady model

C.1.1 Basic definitions

The Eady model is a good example of a baroclinically unstable situation. The following description is based on Vallis (2006). Before describing the model it is first neccesary to define some variables. The buoyancy (b) of an air parcel can be written

$$b = -g\frac{\delta\rho}{\rho_0} \; or \; b = g\frac{\delta\theta}{\overline{\theta}} \tag{C.1}$$

where g is the acceleration due to gravity, $\rho$is the density and ρ_0 is a reference density, θ is the potential temperature of an air parcel and $\overline{\theta}$ is the mean potential temperature of the air within the column. The stream function (ψ) can be used to define the flow in terms of the horizontal velocities (u, v) or the bouyancy (assuming hydrostatic balance)

$$\psi = -uy \; or \; \psi = vx \; or \; \psi = \frac{1}{f_0}bz \tag{C.2}$$

where $f_0 = 2\Omega sin\phi$, Ω being the rate of rotation of the Earth and ϕ being the latitude.

C.1.2 The basic state

The basic state of the model is set up with a zonal wind flow (U) increasing from $U = 0$ at the surface to $U = \frac{\partial U}{\partial z}H$ at the point H which is a rigid surface at the top of the model. The rigid surface at the top represents the tropopause. z is the vertical co-ordinate. The vertical wind speed

(ω) is set to be zero at both the surface and at height H. In its basic state the fluid is uniformly stratified which means that there is a constant value of

$$N^2 = \frac{g}{\overline{\theta}}\left(\frac{\partial\overline{\theta}}{\partial z}\right) \tag{C.3}$$

The model uses an f-plane with the β-parameter being set to zero (i.e. $f = f_0$). There is a horizontal temperature gradient in the y direction as implied by the zonal wind flow. All calculations are constrained by the fact that in the interior of the system, quasi geostrophic potential vorticity perturbations (q') are not allowed. The definition of q' is

$$q' = \left[\frac{\partial^2}{\partial x^2} + \frac{\partial^2}{\partial y^2} + \frac{f^2}{N^2}\frac{\partial^2}{\partial z^2}\right]\psi \tag{C.4}$$

In this model the Rossby deformation radius (L_D) can be set to be

$$L_D = \frac{NH}{f} \tag{C.5}$$

thus:

$$q' = \left[\frac{\partial^2}{\partial x^2} + \frac{\partial^2}{\partial y^2} + \frac{H^2}{L_D^2}\frac{\partial^2}{\partial z^2}\right]\psi = 0 \tag{C.6}$$

C.1.3 Edge waves

Within the stably stratified atmophere of our model air parcels can freely move around on isentropic surfaces without causing any perturbations in the basic state. However, at the top of the model and at the surface ω is set to be zero and so any momentum that an air parcel has will be transferred into the horizontal directions. This allows for perturbations to take place in the y plane. In order to describe this each variable is split up into its mean state (indicated with an overbar) and a perturbation (indicated by a dash) thus

$$u = \overline{u} + u' \tag{C.7}$$

$$v = \overline{v} + v' \tag{C.8}$$

$$b = \overline{b} + b' \tag{C.9}$$

Given the conditions that $\frac{Db}{Dt} = 0$ and that we assume $\frac{\partial \overline{b}}{\partial y}$ is constant the linearised form of the thermodynamic equation is

$$\frac{\partial b'}{\partial t} + v' \frac{\partial \overline{b}}{\partial y} = 0 \tag{C.10}$$

at the surface and

$$\frac{\partial b'}{\partial t} + \overline{u} \frac{\partial b'}{\partial x} + v' \frac{\partial \overline{b}}{\partial y} = 0 \tag{C.11}$$

at the height H. Using the definitions of the stream-function given in Section C.1.1 and introducing that $\Lambda = \frac{\partial u}{\partial z}$ we can re-write Equations C.10 and C.11. As an example Equation C.11 will give us

$$\left(\frac{\partial}{\partial t} + \Lambda z \frac{\partial}{\partial x} \right) \frac{\partial \psi'}{\partial z} - \Lambda \frac{\partial \psi'}{\partial x} = 0 \tag{C.12}$$

In order to solve Equation C.12 the general solution $\psi' = Re\Phi(z) sin(ly) e^{ik(x-ct)}$ is used where Φ represents the geo-potential height, l is the wave number in the y-direction and k is the wave number in the x-direction. c is the phase velocity of the wave and t represents time. *Re* indicates that we are only taking the real part of a complex number. (Note that using this solution assumes a fixed width for y being equal to L and as such imposing the constraint that $\psi = 0$ at $y = +L/2$ *and* $y = -L/2$. Therefore $l = 2\pi/L$).

The solution to Equation C.12 is given by

$$(c - \Lambda z) \frac{d\Phi}{dz} + \Lambda \Phi = 0 \tag{C.13}$$

where at the tropopause $z = H$. (note that at the surface $\Lambda z = 0$ and as such this solution will also satisfy Equation C.10.)

C.1.4 Solving for a growing wave

All solutions satisfy Equations C.13 and C.6. Using the definition that $\frac{Dq}{Dt} = 0$ the linearised potential vorticity equation can be written as

$$\frac{\partial q'}{\partial t} + U\frac{\partial q'}{dx} = 0 \tag{C.14}$$

which by substituting in Equation C.6 can be re-written as

$$\left(\frac{\partial}{\partial t} + \Lambda z\frac{\partial}{\partial x}\right)\left(\nabla^2\psi' + \frac{H^2}{L_D^2}\frac{\partial^2\psi'}{\partial z^2}\right) = 0 \tag{C.15}$$

substituting the solution $\psi' = Re\overline{\psi}(y,z)e^{ik(x-ct)}$ into Equation C.15 gives

$$(\Lambda z - c)\left[\frac{H^2}{L_D^2}\frac{\partial^2\Phi}{\partial z^2} - (k^2+l^2)\Phi\right] = 0 \tag{C.16}$$

solutions for waves can be found for this equation when the phase velocity does not equal the speed at which the system is moving and we can write Equation C.16 as

$$H^2\frac{d^2\Phi}{dz^2} - \mu^2\Phi = 0 \tag{C.17}$$

where $\mu^2 = L_d^2(k^2+l^2)$. In order for a wave to grow solutions must exist that satisfy both Equation C.17 and the two forms of Equation C.13 (at $z = 0$ and $z = H$). Solutions exist in the form of

$$A\underbrace{[\Lambda H]}_{x_1} + B\underbrace{[\mu c]}_{x_2} = 0 \tag{C.18}$$

$$A\underbrace{[(c-\Lambda H)\mu sinh\mu + \Lambda H cosh\mu]}_{y_1} + B\underbrace{[(c-\Lambda H)\mu cosh\mu + \Lambda H sinh\mu]}_{y_2} = 0 \tag{C.19}$$

Equations C.18 and C.19 are of the form $Ax + By = 0$. Non trivial solutions will be found if $x_1y_2 - x_2y_1 = 0$ i.e

$$[\Lambda H][(c-\Lambda H)\mu cosh\mu + \Lambda H sinh\mu] - [\mu c][(c-\Lambda H)\mu sinh\mu + \Lambda H cosh\mu] = 0 \tag{C.20}$$

which can be re-written as

$$c^2 - Uc + U^2(\mu^{-1}coth\mu - \mu^{-2}) = 0 \tag{C.21}$$

which is a quadratic equation and as such has solutions

$$c = \frac{U}{2} \pm \frac{U}{\mu}\left[\left(\frac{\mu}{2} - coth\frac{\mu}{2}\right)\left(\frac{\mu}{2} - tanh\frac{\mu}{2}\right)\right]^{1/2} \tag{C.22}$$

Since we assumed that the original solution was of the form $\psi' = Re\overline{\psi}(y,z)e^{ik(x-ct)}$ the wave will only grow if Equation C.22 has an imaginary solution. This happens when μ exceeds a value of 2.4.

BIBLIOGRAPHY

Adler RF, Huffman GJ, Chang A, Ferraro R, Xie PP, Janowiak J, Rudolf B, Schneider U, Curtis S, Bolvin D, *et al.* 2003. The version-2 global precipitation climatology project (GPCP) monthly precipitation analysis (1979-present). *Journal of Hydrometeorology* **4**(6): 1147–1167.

Agustí-Panareda A, Gray SL, Belcher SE. 2009. On the dependence of boundary layer ventilation on frontal type. *Journal of Geophysical Research: Atmospheres* **114**(D05305), doi:10.1029/2008JD010694.

Agustí-Panareda A, Gray SL, Methven J. 2005. Numerical modeling study of boundary-layer ventilation by a cold front over Europe. *Journal of Geophysical Research* **110**(D18304), doi:10.1029/2004JD005555.

Ahmadi-Givi F, Craig G, Plant R. 2004. The dynamics of a midlatitude cyclone with very strong latent-heat release. *Quarterly Journal of the Royal Meteorological Society* **130**(596): 295–324.

Akimoto H. 2003. Global air quality and pollution. *Science* **302**(5651): 1716–1719.

Alizadeh Choobari O, Zawar-Reza P, Sturman A. 2012. Atmospheric forcing of the three-dimensional distribution of dust particles over Australia: A case study. *Journal of Geophysical Research* **117**(D11206), doi:10.1029/2012JD017748.

Allan RP, Liu C, Zahn M, Lavers DA, Koukouvagias E, Bodas-Salcedo A. 2014. Physically consistent responses of the global atmospheric hydrological cycle in models and observations. In: *The Earth's Hydrological Cycle*, Springer, pp. 533–552.

Ambaum MH. 2010. *Thermal physics of the atmosphere*, vol. 1. John Wiley & Sons.

Andrews DG. 2010. *An introduction to atmospheric physics*. Cambridge University Press.

Aref H. 1990. Chaotic advection of fluid particles. *Philosophical Transactions of the Royal Society of London A: Mathematical, Physical and Engineering Sciences* **333**(1631): 273–288.

Bao J, Michelson S, Neiman P, Ralph F, Wilczak J. 2005. Interpretation of enhanced integrated water vapour bands associated with extratropical cyclones: Their formation and connection to tropical moisture. *Monthly Weather Review* **134**: 1063–1080.

Barlow JF, Dunbar T, Nemitz E, Wood CR, Gallagher M, Davies F, O'Connor E, Harrison R. 2011. Boundary layer dynamics over london, uk, as observed using doppler lidar during REPARTEE-II. *Atmospheric Chemistry and Physics* **11**(5): 2111–2125.

Barnston AG, Schickedanz PT. 1984. The effect of irrigation on warm season precipitation in the southern Great Plains. *Journal of Climate and Applied Meteorology* **23**(6): 865–888.

Barthe C, Mari C, Chaboureau J, Tulet P, Roux F, Pinty J. 2011. Numerical study of tracers transport by a mesoscale convective system over West Africa. *Annales Geophysicae-Atmospheres Hydrospheresand Space Sciences* **29**(5): 731–747.

Baxter S, Nigam S. 2013. A subseasonal teleconnection analysis: PNA development and its relationship to the NAO. *Journal of Climate* **26**(18): 6733–6741.

Bengtsson L. 2010. The global atmospheric water cycle. *Environmental Research Letters* **5**(2), doi:10.1088/1748-9326/5/2/025002.

Bengtsson L, Hodges KI, Roeckner E. 2006. Storm tracks and climate change. *Journal of Climate* **19**(15): 3518–3543.

Benton G, Blackburn R. 1950. A comparison of precipitation from maritime and continental air. *Bulletin, American Meteorological Society* **31**(7): 254–256.

Benton GS, Blackburn RT, Snead VO. 1950. The role of the atmosphere in the hydrologic cycle. *Eos, Transactions American Geophysical Union* **31**(1): 61–73.

Benton GS, Estoque MA. 1954. Water-vapor transfer over the North American continent. *Journal of Meteorology* **11**(6): 462–477.

Bergeron T. 1930. Richtlinien einer dynamischen klimatologie. *Met. Zeit* **47**(7): 246–262.

Bernard M. 1938. Hydrometeorology a coordination of meteorology and hydrology. *Eos, Transactions American Geophysical Union* **19**(2): 598–604.

Berrisford P, Dee D, Fielding K, Fuentes M, Kallberg P, Kobayashi S, Uppala S. 2009. The ERA-Interim archive. *ERA Report Series; http://old.ecmwf.int/publications/library/do/references/list/782009* .

Berrisford P, Kallberg P, Kobayashi S, Dee D, Uppala S, Simmons A, Poli P, Sato H. 2011. Atmospheric conservation properties in ERA-Interim. *ERA Report Series; http://old.ecmwf.int/publications/library/do/references/list/782009* .

Berry G, Reeder MJ. 2014. Objective Identification of the Intertropical Convergence Zone: Climatology and Trends from the ERA-Interim. *Journal of Climate* **27**(5): 1894–1909, doi: 10.1175/JCLI-D-13-00339.1.

Bertram TH, Perring AE, Wooldridge PJ, Crounse JD, Kwan AJ, Wennberg PO, Scheuer E, Dibb J, Avery M, Sachse G, *et al.* 2007. Direct measurements of the convective recycling of the upper troposphere. *Science* **315**(5813): 816–820.

Betts AK, Köhler M, Zhang Y. 2009. Comparison of river basin hydrometeorology in ERA-Interim and ERA-40 reanalyses with observations. *Journal of Geophysical Research* **114**(D2), doi:10.1029/2008JD010761.

Bieltvedt Skeie R, Egill Kristjánsson J, Ólafsson H, Røsting B. 2006. Dynamical processes related to cyclone development near greenland. *Meteorologische Zeitschrift* **15**(2): 147–156.

Bjerknes J. 1919. On the structure of moving cyclones. *Monthly Weather Review* **47**(2): 95–99.

Bjerknes J, Solberg H. 1922. *Life cycle of cyclones and the polar front theory of atmospheric circulation*. Grondahl.

Bolton D. 1980. The computation of equivalent potential temperature. *Monthly weather review* **108**(7): 1046–1053.

Bosilovich MG, Chern JD. 2006. Simulation of water sources and precipitation recycling for the mackenzie, mississippi, and amazon river basins. *Journal of Hydrometeorology* **7**(3): 312–329.

Boutle I. 2009. Boundary-layer processes in mid-latitude cyclones. PhD thesis, Department of Meteorology, University of Reading.

Boutle I, Beare R, Belcher S, Brown A, Plant R. 2010. The moist boundary layer under a mid-latitude weather system. *Boundary Layer Meteorology* **134**: 367–386.

Boutle I, Belcher S, Plant R. 2011. Moisture transport in midlatitude cyclones. *Quarterly Journal of the Royal Meteorological Society* **137**(655): 360–373.

Bromwich DH, Du Y, Hines KM. 1996. Wintertime surface winds over the Greenland ice sheet. *Monthly weather review* **124**(9): 1941–1947.

Brown-Steiner B, Hess P. 2011. Asian influence on surface ozone in the United States: A comparison of chemistry, seasonality, and transport mechanisms. *Journal of Geophysical Research: Atmospheres* **116**(D17), doi:10.1029/2011JD015846.

Browning K. 1990. Organisation of clouds and precipitation in extratropical cyclones. *Palmen Memorial Volume, American Meteorological Society* : 129–153.

Browning K. 1997. The dry intrusion perspective of extra-tropical cyclone development. *Meteorological Applications* **4**(4): 317–324.

Browning K, Roberts N. 1994. Structure of a frontal cyclone. *Quarterly Journal of the Royal Meteorological Society* **120**(520): 1535–1557.

Burde GI. 2006. Bulk recycling models with incomplete vertical mixing. Part I: Conceptual framework and models. *Journal of Climate* **19**(8): 1461–1472.

Cape J, Methven J, Hudson L. 2000. The use of trajectory cluster analysis to interpret trace gas measurements at Mace Head, Ireland. *Atmospheric Environment* **34**(22): 3651–3663.

Carlson TN. 1980. Airflow through midlatitude cyclones and the comma cloud pattern. *Monthly Weather Review* **108**(10): 1498–1509.

Carson D. 1973. The development of a dry inversion-capped convectively unstable boundary layer. *Quarterly Journal of the Royal Meteorological Society* **99**(421): 450–467.

Chagnon J, Gray S, Methven J. 2013. Diabatic processes modifying potential vorticity in a North Atlantic cyclone. *Quarterly Journal of the Royal Meteorological Society* **139**(674): 1270–1282.

Chang C, Perkey D, Kreitzberg C. 1982. A numerical case study of the effects of latent heating on a developing wave cyclone. *Journal of the Atmospheric Sciences* **39**(7): 1555–1570.

Chang EK, Lee S, Swanson KL. 2002. Storm track dynamics. *Journal of Climate* **15**(16): 2163–2183.

Charney JG. 1947. The dynamics of long waves in a baroclinic westerly current. *Journal of Meteorology* **4**(5): 136–162.

Chen F, Geyer B, Zahn M, von Storch H. 2012a. Toward a multi-decadal climatology of North Pacific Polar Lows employing dynamical. *Terrestrial, Atmospheric and Oceanic Sciences* (3): 291–301.

Chen G, Xue H, Feingold G, Zhou X. 2012b. Vertical transport of pollutants by shallow cumuli from large eddy simulations. *Atmospheric Chemistry and Physics* **12**(23): 11 319–11 327.

Chen Y, Zhao C, Zhang Q, Deng Z, Huang M, Ma X. 2009. Aircraft study of mountain chimney effect of Beijing, china. *Journal of Geophysical Research: Atmospheres* **114**(D08306), doi: 10.1029/2008JD010610.

Cooper O, Moody J, Davenport J, Oltmans S, Johnson B, Chen X, Shepson P, Merrill J. 1998. Influence of springtime weather systems on vertical ozone distributions over three North American sites. *Journal of Geophysical Research: Atmospheres* **103**(D17): 22 001–22 013, doi: 10.1029/98JD01801.

Cooper O, Moody J, Parrish D, Trainer M, Ryerson T, Holloway J, Hübler G, Fehsenfeld F, Evans M. 2002. Trace gas composition of midlatitude cyclones over the western North Atlantic ocean: A conceptual model. *Journal of Geophysical Research: Atmospheres* **107**(D7): ACH–1–13, doi:10.1029/2001JD000901.

Cotton W, Alexander G, Hertenstein R, Walko R, McAnelly R, Nicholls M. 1995. Cloud venting - a review and some new global estimates. *Earth Science Reviews* **39**: 169–206.

Croci-Maspoli M, Schwierz C, Davies HC. 2007. Atmospheric blocking: space-time links to the NAO and PNA. *Climate dynamics* **29**(7-8): 713–725.

Dacre H, Clark P, Martinez-Alvarado O, Stringer M, Lavers D. 2014. How do atmospheric rivers form? *Bulletin of the American Meteorological Society* (96): 1243–1255.

Dacre H, Hawcroft M, Stringer M, Hodges K. 2012. An extratropical cyclone atlas: A tool for illustrating cyclone structure and evolution characteristics. *Bulletin of the American Meteorological Society* **93**(10): 1497–1502.

Dacre HF, Gray SL. 2009. The spatial distribution and evolution characteristics of North Atlantic cyclones. *Monthly Weather Review* **137**(1): 99–115.

Dacre HF, Gray SL. 2013. Quantifying the climatological relationship between extratropical cyclone intensity and atmospheric precursors. *Geophysical Research Letters* **40**(10): 2322–2327.

Dacre HF, Gray SL, Belcher SE. 2007. A case study of boundary layer ventilation by convection and coastal processes. *Journal of Geophysical Research* **112**(D17106), doi:10.1029/2006JD007984.

Davis CA, Emanuel KA. 1991. Potential vorticity diagnostics of cyclogenesis. *Monthly Weather Review* **119**(8): 1929–1953.

Davis CA, Stoelinga MT, Kuo YH. 1993. The integrated effect of condensation in numerical simulations of extratropical cyclogenesis. *Monthly Weather Review* **121**(8): 2309–2330.

Davis S, Talbot R, Mao H. 2012. Transport and outflow to the North Atlantic in the lower marine troposphere during ICARTT 2004. *Atmospheric Chemistry and Physics Discussions* **12**(1): 2395–2434.

de Leeuw J, Methven J, Blackburn M. 2015. Evaluation of ERA-Interim reanalysis precipitation products using England and Wales observations. *Quarterly Journal of the Royal Meteorological Society* **141**(688): 798–806.

De Wekker S, Steyn D, Nyeki S. 2004. A comparison of aerosol layer and convective boundary layer structure over a mountain range during STAAARTE'97. *Boundary Layer Meteorology* **113**: 249–271.

Dee D, Uppala S, Simmons A, Berrisford P, Poli P, Kobayashi S, Andrae U, Balmaseda M, Balsamo G, Bauer P, *et al.* 2011. The ERA-Interim reanalysis: Configuration and performance of the data assimilation system. *Quarterly Journal of the Royal Meteorological Society* **137**(656): 553–597.

Dettinger MD. 2013. Atmospheric rivers as drought busters on the US West Coast. *Journal of Hydrometeorology* **14**(6): 1721–1732.

Dettinger MD, Ralph FM, Das T, Neiman PJ, Cayan DR. 2011. Atmospheric rivers, floods and the water resources of California. *Water* **3**(2): 445–478.

Deveson A, Browning K, Hewson T. 2002. A classification of FASTEX cyclones using a height-attributable quasi-geostrophic vertical-motion diagnostic. *Quarterly Journal of the Royal Meteorological Society* **128**(579): 93–118.

Dickerson R, Huffman G, Luke W, Nunnermacker L, Pickering K, Leslie A, Lindsey C, Slinn W, Kelly T, Daum P, *et al.* 1987. Thunderstorms: An important mechanism in the transport of air pollutants. *Science* **235**(4787): 460–464.

Domeisen DI, Plumb RA. 2012. Traveling planetary-scale Rossby waves in the winter stratosphere: The role of tropospheric baroclinic instability. *Geophysical Research Letters* **39**(L20817), doi:10.1029/2012GL053684.

Donat M, Pardowitz T, Leckebusch G, Ulbrich U, Burghoff O. 2011. High-resolution refinement of a storm loss model and estimation of return periods of loss-intensive storms over Germany. *Natural Hazards and Earth System Science* **11**(10): 2821–2833.

Donnell EA, Fish DJ, Dicks EM, Thorpe AJ. 2001. Mechanisms for pollutant transport between the boundary layer and the free troposphere. *Journal of Geophysical Research* **106**(D8): 7847–7856.

Eady E. 1949. Long waves and cyclone waves. *Tellus* **1**(3): 33–52.

Eckhardt S, Stohl A, Wernli H, James P, Forster C, Spichtinger N. 2004. A 15-year climatology of warm conveyor belts. *Journal of Climate.* **17**: 218–237.

ECMWF. 2006a. IFS documentation CY31r1: Dynamics and numerical procedures. *https://software.ecmwf.int/wiki/display/IFS/CY31R1* : 1–31.

ECMWF. 2006b. IFS documentation CY31r1: Physical processes. *https://software.ecmwf.int/wiki/display/IFS/CY31R1* : 1–162.

Eddy J, Stidd C, Fowler W, Helvey J. 1975. Irrigation increases rainfall? *Science (New York, NY)* **188**(4185): 279.

Edwards J, Slingo A. 1996. Studies with a flexible new radiation code. I: Choosing a configuration for a large-scale model. *Quarterly Journal of the Royal Meteorological Society* **122**: 689–719.

Eltahir EA, Bras RL. 1994. Precipitation recycling in the Amazon basin. *Quarterly Journal of the Royal Meteorological Society* **120**(518): 861–880.

Eltahir EA, Bras RL. 1996. Precipitation recycling. *Reviews of Geophysics* **34**(3): 367–378.

Emanuel KA. 1988. Observational evidence of slantwise convective adjustment. *Monthly weather review* **116**(9): 1805–1816.

Emanuel KA, Rotunno R. 1989. Polar lows as arctic hurricanes. *Tellus A* **41**(1): 1–17.

Fink AH, Brücher T, Ermert V, Krüger A, Pinto JG. 2009. The european storm Kyrill in january 2007: synoptic evolution, meteorological impacts and some considerations with respect to climate change. *Natural Hazards and Earth System Science* **9**(2): 405–423.

Flossmann AI. 1998. Interaction of aerosol particles and clouds. *Journal of the Atmospheric Sciences* **55**(5): 879–887.

Flossmann AI, Wobrock W. 1996. Venting of gases by convective clouds. *Journal of Geophysical Research: Atmospheres* **101**(D13): 18 639–18 649.

Freitag S, Clarke A, Howell S, Kapustin V, Campos T, Brekhovskikh V, Zhou J. 2014. Combining airborne gas and aerosol measurements with HYSPLIT: a visualization tool for simultaneous evaluation of air mass history and back trajectory consistency. *Atmospheric Measurement Techniques* **7**(1): 107.

Fritsch J, Chappell C. 1980. Numerical prediction of convectively driven mesoscale pressure systems. part i:convective parameterisation. *Journal of the Atmospheric Sciences* **37**: 1722–1733.

Garratt JR. 1994. *The atmospheric boundary layer*. Cambridge university press.

Gill AE. 1982. *Atmosphere-ocean dynamics*, vol. 30. Academic press.

Grant A. 1992. The structure of turbulence in the near-neutral atmospheric boundary layer. *Journal of the Atmospheric Sciences* **49**(3): 226–239.

Grant ALM. 2001. Cloud-base fluxes in the cumulus-capped boundary layer. *Quarterly Journal of the Royal Meteorological Society* **127**: 407–421.

Grant WB, Browell EV, Butler CF, Fenn MA, Clayton MB, Hannan JR, Fuelberg HE, Blake DR, Blake NJ, Gregory GL, *et al.* 2000. A case study of transport of tropical marine boundary layer and lower tropospheric air masses to the northern midlatitude upper troposphere. *Journal of Geophysical Research* **105**: 3757–3769.

Gray SL, Dacre HF. 2006. Classifying dynamical forcing mechanisms using a climatology of extratropical cyclones. *Quarterly Journal of the Royal Meteorological Society* **132**(617): 1119–1137.

Grazzini F, Vitart F. 2015. Atmospheric predictability and Rossby wave packets. *Quarterly Journal of the Royal Meteorological Society* **141**: 2793–2802.

Gregory D, Rowntree P. 1990. A mass flux convection scheme with representation of cloud ensemble characteristics and stability dependant closure. *Monthly Weather Review* **118**: 1483–1506.

Griffiths M, Thorpe AJ, Browning KA. 2000. Convective destabilization by a tropopause fold diagnosed using potential-vorticity inversion. *Quarterly Journal of the Royal Meteorological Society* **126**(562): 125–144.

Grose WL, Hoskins BJ. 1979. On the influence of orography on large-scale atmospheric flow. *Journal of the Atmospheric Sciences* **36**(2): 223–234.

Hannan JR, Fuelberg HE, Crawford JH, Sachse GW, Blake DR. 2003. Role of wave cyclones in transporting boundary layer air to the free troposphere during the spring 2001 NASA/TRACE-P experiment. *Journal of Geophysical Research: Atmospheres* **108**(D20), doi: 10.1029/2002JD003105.

Harding KJ, Snyder PK. 2012. Modeling the atmospheric response to irrigation in the Great Plains. Part II: The precipitation of irrigated water and changes in precipitation recycling. *Journal of Hydrometeorology* **13**(6): 1687–1703.

Harrold T. 1973. Mechanisms influencing the distribution of precipitation within baroclinic disturbances. *Quarterly Journal of the Royal Meteorological Society* **99**(420): 232–251.

Hawcroft M, Shaffrey L, Hodges K, Dacre H. 2012. How much Northern Hemisphere precipitation is associated with extratropical cyclones? *Geophysical Research Letters* **39**(24): L4809, doi:10.1029/2012GL053866.

Held IM, Soden BJ. 2006. Robust responses of the hydrological cycle to global warming. *Journal of Climate* **19**(21): 5686–5699.

Henne S, Furger M, Nyeki S, Steinbacher M, Neininger B, de Wekker S, Dommen J, Spichtinger N, Stohl A, Prevot A. 2004a. Quantification of topographic venting of boundary layer air to the free troposphere. *Atmospheric Chemistry and Physics* **4**: 497–509.

Henne S, Furger M, Nyeki S, Steinbacher M, Neininger B, De Wekker S, Dommen J, Spichtinger N, Stohl A, Prévôt A. 2004b. Quantification of topographic venting of boundary layer air to the free troposphere. *Atmospheric Chemistry and Physics* **4**(2): 497–509.

Heo KY, Seo YW, Ha KJ, Park KS, Kim J, Choi JW, Jun K, Jeong JY. 2015. Development mechanisms of an explosive cyclone over East Sea on 3–4 april 2012. *Dynamics of Atmospheres and Oceans* **70**: 30–46.

Hess P. 2005. A comparison of two paradigms: The relative global roles of moist convective versus nonconvective transport. *Journal of Geophysical Research: Atmospheres (1984–2012)* **110**(D20302), doi:10.1029/2004JD005456.

Hess P, Vukicevic T. 2003. Intercontinental transport, chemical transformations, and baroclinic systems. *Journal of Geophysical Research: Atmospheres* **108**(D12): 4354, doi:10.1029/2002JD002798.

Hewson TD. 1998. Objective fronts. *Meteorological Applications* **5**(01): 37–65.

Hodges K, Lee R, Bengtsson L. 2011. A comparison of extratropical cyclones in recent reanalyses ERA-Interim, NASA MERRA, NCEP CFSR, and JRA-25. *Journal of Climate* **24**(18): 4888–4906.

Hodges K, *et al.* 1994. A general-method for tracking analysis and its application to meteorological data. *Monthly Weather Review* **122**(11): 2573–2586.

Holton J. 1972. An Introduction to Dynamic Meteorology, 3rd edn.

Holton JR, Wallace JM, Young J. 1971. On boundary layer dynamics and the ITCZ. *Journal of the Atmospheric Sciences* **28**(2): 275–280.

Holtslag A, Boville B. 1992. Local Versus Nonlocal Boundary-Layer Diffusion in a Global Climate Model. *Journal of Climate* **6**: 1825–1842.

Holzman B, *et al.* 1937. *Sources of moisture for precipitation in the united states*. US Department of Agriculture.

Horton RE. 1943. Hydrologic interrelations between lands and oceans. *Eos, Transactions American Geophysical Union* **24**(2): 753–764.

Hoskins B. 1990. Theory of extratropical cyclones. *Extratropical Cyclones: The Erik Palmén Memorial Volume* : 64–80.

Hoskins BJ, Hodges KI. 2002. New perspectives on the northern hemisphere winter storm tracks. *Journal of the Atmospheric Sciences* **59**(6): 1041–1061.

Hoskins BJ, Karoly DJ. 1981. The steady linear response of a spherical atmosphere to thermal and orographic forcing. *Journal of the Atmospheric Sciences* **38**(6): 1179–1196.

Hov Ø, Flatøy F. 1997. Convective redistribution of ozone and oxides of nitrogen in the troposphere over europe in summer and fall. *Journal of atmospheric chemistry* **28**(1-3): 319–337.

Huber DB, Mechem DB, Brunsell NA. 2014. The effects of Great Plains irrigation on the surface energy balance, regional circulation, and precipitation. *Climate* **2**(2): 103–128.

Hung CW, Yanai M. 2004. Factors contributing to the onset of the australian summer monsoon. *Quarterly Journal of the Royal Meteorological Society* **130**(597): 739–758.

Huntrieser H, Feigl C, Schlager H, Schröder F, Gerbig C, Van Velthoven P, Flatøy F, Théry C, Petzold A, Höller H, *et al.* 2002. Airborne measurements of NOx, tracer species, and small particles during the European Lightning Nitrogen Oxides Experiment. *Journal of Geophysical Research: Atmospheres* **107**(D11): ACH–5, doi:10.1029/2000JD000209.

Huntrieser H, Schlager H, Lichtenstern M, Stock P, Hamburger T, Höller H, Schmidt K, Betz HD, Ulanovsky A, Ravegnani F. 2011. Mesoscale convective systems observed during AMMA and

their impact on the NOx and O3 budget over west africa. *Atmospheric Chemistry and Physics* **11**(6): 2503–2536.

Jensen JC. 1936. Evaporation and rainfall studies in the northwest Minnesota Lake region. *Proceedings of the American Philosophical Society* **76**(6): 747–759.

Jensen JC. 1938. Evaporation and rainfall studies in the northwest Minnesota Lake region. *Proceedings of the American Philosophical Society* **78**(4): 651–670.

Joos H, Wernli H. 2012. Influence of microphysical processes on the potential vorticity development in a warm conveyor belt: A case-study with the limited-area model COSMO. *Quarterly Journal of the Royal Meteorological Society* **138**(663): 407–418.

Joss J, Gori EG. 1978. Shapes of raindrop size distributions. *Journal of Applied Meteorology* **17**(7): 1054–1061.

Kallberg P. 2009. Forecast drift in ERA-Interim. *ERA Report Series; http://old.ecmwf.int/publications/library/do/references/list/782009* .

Kalnay E, Kanamitsu M, Kistler R, Collins W, Deaven D, Gandin L, Iredell M, Saha S, White G, Woollen J, *et al.* 1996. The NCEP/NCAR 40-year reanalysis project. *Bulletin of the American meteorological Society* **77**(3): 437–471.

Kessler E. 1969. On the distribution and continuity of water substance in atmospheric circulation. *Meteorological Monographs* **32**(10): 84 pp.

Kim J, Waliser DE, Neiman PJ, Guan B, Ryoo JM, Wick GA. 2013. Effects of atmospheric river landfalls on the cold season precipitation in California. *Climate dynamics* **40**(1-2): 465–474.

Kirshbaum DJ, Wang CC. 2014. Boundary layer updrafts driven by airflow over heated terrain. *Journal of the Atmospheric Sciences* **71**(4): 1425–1442.

Klein WH. 1951. A hemispheric study of daily pressure variability at sea level and aloft. *Journal of Meteorology* **8**: 332–346.

Klein WH. 1957. *Principal tracks and mean frequencies of cyclones and anticyclones in the northern hemisphere*. US Department of Commerce, Weather Bureau.

Knippertz P, Martin JE. 2007. A Pacific moisture conveyor belt and its relationship to a significant precipitation event in the semiarid southwestern United States. *Weather and forecasting* **22**(1): 125–144.

Knippertz P, Wernli H. 2009. A lagrangian climatology of tropical moisture exports to the northern hemispheric extratropics. *Journal of Climate.* **23**: 987–1003.

Knippertz P, Wernli H. 2010. A lagrangian climatology of tropical moisture exports to the northern hemispheric extratropics. *Journal of Climate* **23**(4): 987–1003.

Knippertz P, Wernli H, Gläser G. 2013. A global climatology of tropical moisture exports. *Journal of Climate* **26**(10): 3031–3045.

Köhler M, Ahlgrimm M, Beljaars A. 2011. Unified treatment of dry convective and stratocumulus-topped boundary layers in the ECMWF model. *Quarterly Journal of the Royal Meteorological Society* **137**(654): 43–57.

Kossmann M, Lugauer M, Steyn D, Weingartner E, Wirths M, Baltenspergerl U. 2000. Convective boundary layer evolution to 4 km asl over'high-alpine terrain: Airborne lidar observations in the alps. *Geophysical Research Letters* **27**(5): 689–692.

Kowol-Santen J, Beekmann M, Schmitgen S, Dewey K. 2001. Tracer analysis of transport from the boundary layer to the free troposphere. *Geophysical Research Letters* **28**(15): 2907–2910.

Kreitzberg CW, Perkey DJ. 1976. Release of potential instability: Part I. A sequential plume model within a hydrostatic primitive equation model. *Journal of the Atmospheric Sciences* **33**(3): 456–475.

Kristjánsson J, McInnes H. 1999. The impact of Greenland on cyclone evolution in the North Atlantic. *Quarterly Journal of the Royal Meteorological Society* **125**(560): 2819–2834.

Kuo Y, Chao B, Lee L. 1999. A constellation of microsatellites promises to help in a range of geoscience research. *Eos, Transactions American Geophysical Union* **80**(40): 467–471.

Kuo YH, Shapiro M, Donall EG. 1991. The interaction between baroclinic and diabatic processes in a numerical simulation of a rapidly intensifying extratropical marine cyclone. *Monthly Weather Review* **119**(2): 368–384.

Laffineur T, Claud C, Chaboureau JP, Noer G. 2014. Polar lows over the nordic seas: Improved representation in ERA-Interim compared to ERA-40 and the impact on downscaled simulations. *Monthly Weather Review* **142**(6): 2271–2289.

Langford A, Senff C, Alvarez R, Banta R, Hardesty R. 2010. Long-range transport of ozone from the Los Angeles basin: A case study. *Geophysical Research Letters* **37**(6): L06 807, doi: 10.1029/2010GL042507.

Lapeyre G, Held I. 2004. The role of moisture in the dynamics and energetics of turbulent baroclinic eddies. *Journal of the Atmospheric Sciences* **61**(14): 1693–1710.

Lavers DA, Allan RP, Wood EF, Villarini G, Brayshaw DJ, Wade AJ. 2011. Winter floods in Britain are connected to atmospheric rivers. *Geophysical Research Letters* **38**(23): L23 803, doi:10.1029/2011GL049783.

Lavers DA, Villarini G. 2013a. Atmospheric rivers and flooding over the central United States. *Journal of Climate* **26**(20): 7829–7836.

Lavers DA, Villarini G. 2013b. The nexus between atmospheric rivers and extreme precipitation across europe. *Geophysical Research Letters* **40**(12): 3259–3264.

Leckebusch GC, Ulbrich U, Fröhlich L, Pinto JG. 2007. Property loss potentials for European midlatitude storms in a changing climate. *Geophysical Research Letters* **34**(5): L05 703, doi: 10.1029/2006GL027663.

Li Q, Jacob DJ, Park R, Wang Y, Heald CL, Hudman R, Yantosca RM, Martin RV, Evans M. 2005. North American pollution outflow and the trapping of convectively lifted pollution by upper-level anticyclone. *Journal of Geophysical Research* **110**(D10301), doi:10.1029/2004JD005039.

Lindzen R, Farrell B. 1980. A simple approximate result for the maximum growth rate of baroclinic instabilities. *Journal of the Atmospheric Sciences* **37**(7): 1648–1654.

Liu C, Barnes EA. 2015. Extreme moisture transport into the Arctic linked to Rossby wave breaking. *Journal of Geophysical Research* **120**: 3774–3788.

Lock A. 2007. The parameterisation of boundary layer processes. *Unified Model documentation paper* **24**.

Lock A, Brown A, Bush M, Martin G, Smith R. 2000. A new boundary layer mixing scheme. Part I: Scheme description and single column model tests. *Monthly Weather Review* **128**: 3187–3199.

Loughner CP, Allen DJ, Pickering KE, Zhang DL, Shou YX, Dickerson RR. 2011. Impact of fair-weather cumulus clouds and the Chesapeake Bay breeze on pollutant transport and transformation. *Atmospheric Environment* **45**(24): 4060–4072.

Loughner CP, Tzortziou M, Follette-Cook M, Pickering KE, Goldberg D, Satam C, Weinheimer A, Crawford JH, Knapp DJ, Montzka DD, *et al.* 2014. Impact of bay breeze circulations on surface air quality and boundary layer export. *Journal of Applied Meteorology and Climatology* **53**(2014): 1697–1713.

Louis J. 1979. A parametric model of vertical eddy fluxes in the atmosphere. *Boundary layer Meteorology* **17**: 187–202.

Lu R, Turco RP. 1994. Air pollutant transport in a coastal environment. Part I: Two-dimensional simulations of sea-breeze and mountain effects. *Journal of the Atmospheric Sciences* **51**(15): 2285–2308.

Lu R, Turco RP. 1995. Air pollutant transport in a coastal environmentII. Three-dimensional simulations over Los Angeles basin. *Atmospheric Environment* **29**(13): 1499–1518.

Mari C, Jacob DJ, Bechtold P. 2000. Transport and scavenging of soluble gases in a deep convective cloud. *Journal of Geophysical Research: Atmospheres (1984–2012)* **105**(D17): 22 255–22 267.

Martinez JA, Dominguez F. 2014. Sources of atmospheric moisture for the la plata river basin*. *Journal of Climate* **27**(17): 6737–6753.

Martínez-Alvarado O, Joos H, Chagnon J, Boettcher M, Gray S, Plant R, Methven J, Wernli H. 2014. The dichotomous structure of the warm conveyor belt. *Quarterly Journal of the Royal Meteorological Society* **140**(683): 1809–1824.

Martinez-Alvarado O, Madonna E, Gray SL, Joos H. 2015. A route to systematic error in forecasts of rossby waves. *Quarterly Journal of the Royal Meteorological Society* doi:10.1002/qj.2645.

Maryon R. 1998. Determining cross-wind variance for low frequency wind meander. *Atmospheric Environment* **32**(2): 115–121.

Maryon R, Ryall D, Malcolm A. 1999. Met O (PMSR) Turbulence and diffusion note no.262:the NAME 4 dispersion model: Science documentation .

Mass CF, Schultz DM. 1993. The structure and evolution of a simulated midlatitude cyclone over land. *Monthly Weather Review* **121**(4): 889–917.

Masunaga H, L'Ecuyer TS. 2010. The southeast pacific warm band and double ITCZ. *Journal of Climate* **23**(5): 1189–1208.

Matrosov SY. 2013. Characteristics of landfalling atmospheric rivers inferred from satellite observations over the eastern North Pacific ocean. *Monthly Weather Review* **141**(11): 3757–3768.

McDonald JE. 1962. The evaporation precipitation fallacy. *Weather* **17**(5): 168–177.

McNish AG. 1936. Statistical aspects of long-range weather-forecasting. *Eos, Transactions American Geophysical Union* **17**(1): 124–129.

McTaggart-Cowan R, Zadra A. 2015. Representing Richardson number hysteresis in the NWP boundary layer. *Monthly Weather Review* **143**(4): 1232–1258.

Mead DW. 1919. *Hydrology: The fundamental basis of hydraulic engineering*. McGraw-Hill Book Company.

Medeiros B, Hall A, Stevens B. 2005. What controls the mean depth of the PBL? *Journal of Climate* **18**(16): 3157–3172.

Messori G, Czaja A. 2013. On the sporadic nature of meridional heat transport by transient eddies. *Quarterly Journal of the Royal Meteorological Society* **139**(673): 999–1008.

Messori G, Czaja A. 2015. On local and zonal pulses of atmospheric heat transport in reanalysis data. *Quarterly Journal of the Royal Meteorological Society* **141**: 2376–2389.

Meyer AF. 1928. Elements of hydrology. In: *Elements of hydrology*, John Wiley & Sons.

Monin A. 1970. The atmospheric boundary layer. *Annual Review of Fluid Mechanics* **2**(1): 225–250.

Monks P, Granier C, Fuzzi S, Stohl A, Williams M, Akimoto H, Amann M, Baklanov A, Baltensperger U, Bey I, *et al.* 2009. Atmospheric composition change: Global and regional air quality. *Atmospheric Environment* **43**(33): 5268–5350.

Moore N, Rojstaczer S. 2001. Irrigation-induced rainfall and the Great Plains. *Journal of Applied Meteorology* **40**(8): 1297–1309.

Nakamura J, Lall U, Kushnir Y, Robertson AW, Seager R. 2013. Dynamical structure of extreme floods in the US Midwest and the United Kingdom. *Journal of Hydrometeorology* **14**(2): 485–504.

Nakayama Y, Boucher R. 1998. *Introduction to fluid mechanics*. Butterworth-Heinemann.

Neiman PJ, Ralph FM, Wick GA, Kuo YH, Wee TK, Ma Z, Taylor GH, Dettinger MD. 2008a. Diagnosis of an intense atmospheric river impacting the Pacific Northwest: Storm summary and offshore vertical structure observed with COSMIC satellite retrievals. *Monthly Weather Review* **136**(11): 4398–4420.

Neiman PJ, Ralph FM, Wick GA, Lundquist JD, Dettinger MD. 2008b. Meteorological characteristics and overland precipitation impacts of atmospheric rivers affecting the west coast of North America based on eight years of SSM/I satellite observations. *Journal of Hydrometeorology* **9**(1): 22–47.

Neiman PJ, Ralph FM, Wick GA, Lundquist JD, Dettinger MD. 2008c. Meteorological characteristics and overland precipitation impacts of atmospheric rivers affecting the West Coast of north america based on eight years of SSM/I satellite observations. *Journal of Hydrometeorology* **9**(1): 22–47.

Newell RE, Newell NE, Zhu Y, Scott C. 1992. Tropospheric rivers? A pilot study. *Geophysical Research Letters* **19**(24): 2401–2404.

Newell RE, Zhu Y. 1994. Tropospheric rivers: A one-year record and a possible application to ice core data. *Geophysical Research Letters* **21**(2): 113–116.

Newman M, Kiladis GN, Weickmann KM, Ralph FM, Sardeshmukh PD. 2012. Relative contributions of synoptic and low-frequency eddies to time-mean atmospheric moisture transport, including the role of atmospheric rivers. *Journal of Climate* **25**(21): 7341–7361.

Nicholson SE. 2009. A revised picture of the structure of the "monsoon" and land ITCZ over West Africa. *Climate Dynamics* **32**(7-8): 1155–1171.

Nigam S, DeWeaver E. 2003. Stationary waves (orographic and thermally forced) : 2121–2137.

Ninomiya K. 2009. Characteristics of precipitation in the Meiyu-Baiu season in the CMIP3 20th century climate simulations. *Journal of the Meteorological Society of Japan* **87**(4): 829–843.

Nyeki S, Kalberer M, Colbeck Iand De Wekker S, Furger M, Gaggeler H W, Kossmann M, Lugauer M, Steyn D, Weingartner E, Wirth M, Baltensperger U. 2000. Convective boundary layer evolution to 4 km asl over high-alpine terrain: Airborne lidar observations in the alps. *Geophysical Research Letters* **27**: 689–692.

Office M. 1996. *Source book to the forecasters' reference book*. The Met Office.

Oort AH. 1971. The observed annual cycle in the meridional transport of atmospheric energy. *Journal of the Atmospheric Sciences* **28**(3): 325–339.

Oort AH, Rasmusson EM. 1970. On the annual variation of the monthly mean meridional circulation. *Monthly Weather Review* **98**(6): 423–442.

Outten S, Renfrew I, Petersen G. 2009. An easterly tip jet off Cape Farewell, Greenland. II: Simulations and dynamics. *Quarterly Journal of the Royal Meteorological Society* **135**(645): 1934–1949.

Palmén EH, Newton CW, Holopainen EO. 1990. *Extratropical cyclones: The Erik Palmen memorial volume*. American Meteorological Society.

Peake D, Dacre H, Methven J, Coceal O. 2014. Meteorological factors controlling low-level continental pollutant outflow across a coast. *Atmospheric Chemistry and Physics* **14**(23): 13 295–13 312.

Peixoto J, Oort AH. 1996. The climatology of relative humidity in the atmosphere. *Journal of Climate* **9**(12): 3443–3463.

Petoukhov V, Rahmstorf S, Petri S, Schellnhuber HJ. 2013. Quasiresonant amplification of planetary waves and recent northern hemisphere weather extremes. *Proceedings of the National Academy of Sciences* **110**(14): 5336–5341.

Petterson S. 1950. Some aspects of the general circulation. *Centennial Proc. Royal Meteorological Society.* : 120–155.

Petterssen S, Smebye SJ. 1971. On the development of extratropical cyclones. *Quarterly Journal of the Royal Meteorological Society* **97**(414): 457–482.

Pinto JG, Raible CC. 2012. Past and recent changes in the North Atlantic oscillation. *Wiley Interdisciplinary Reviews: Climate Change* **3**(1): 79–90.

Pinto JG, Reyers M, Ulbrich U. 2011. The variable link between PNA and NAO in observations and in multi-century CGCM simulations. *Climate Dynamics* **36**(1-2): 337–354.

Pinto JG, Zacharias S, Fink AH, Leckebusch GC, Ulbrich U. 2008. Factors contributing to the development of extreme North Atlantic cyclones and their relationship with the NAO. *Climate Dynamics* **32**(5): 711–737.

Plant R, Craig GC, Gray S. 2003. On a threefold classification of extratropical cyclogenesis. *Quarterly Journal of the Royal Meteorological Society* **129**(594): 2989–3012.

Polvani LM, Esler J. 2007. Transport and mixing of chemical air masses in idealized baroclinic life cycles. *Journal of Geophysical Research* **112**(D23102), doi:10.1029/2007JD008555.

Pugh T, Cain M, Methven J, Wild O, Arnold S, Real E, Law KS, Emmerson K, Owen S, Pyle J, *et al.* 2012. A lagrangian model of air-mass photochemistry and mixing using a trajectory ensemble: the cambridge tropospheric trajectory model of chemistry and transport (cittycat) version 4.2. *Geoscientific Model Development* **5**(1): 193–221.

Purvis R, Lewis A, Carney R, McQuaid J, Arnold S, Methven J, Barjat H, Dewey K, Kent J, Monks P, *et al.* 2003. Rapid uplift of nonmethane hydrocarbons in a cold front over central Europe. *Journal of Geophysical Research* **108**(D7), doi:10.1029/2002JD002521.

Ralph FM, Neiman PJ, Wick GA. 2004. Satellite and CALJET aircraft observations of atmospheric rivers over the eastern North Pacific ocean during the winter of 1997/98. *Monthly Weather Review* **132**(7): 1721–1745.

Ralph FM, Neiman PJ, Wick GA, Gutman SI, Dettinger MD, Cayan DR, White AB. 2006. Flooding on California's Russian river: Role of atmospheric rivers. *Geophysical Research Letters* **33**(13): L13 801, doi:10.1029/2006GL026689.

Rasmussen E. 1979. The polar low as an extratropical CISK disturbance. *Quarterly Journal of the Royal Meteorological Society* **105**(445): 531–549.

Rasmussen EA, Turner J. 2003. *Polar lows: Mesoscale weather systems in the polar regions*. Cambridge University Press.

Reynolds RW, Smith TM. 1995. A high-resolution global sea surface temperature climatology. *Journal of Climate* **8**(6): 1571–1583.

Rivals H, Cammas JP, Renfrew IA. 1998. Secondary cyclogenesis: The initiation phase of a frontal wave observed over the eastern Atlantic. *Quarterly Journal of the Royal Meteorological Society* **124**(545): 243–268.

Rivera ER, Dominguez F, Castro CL. 2014. Atmospheric rivers and extreme cool season precipitation events in the Verde river basin of Arizona. *Journal of Hydrometeorology* **15**(2): 813–829.

Rossa A, Wernli H, Davies H. 2000. Growth and decay of an extra-tropical cyclone's pv-tower. *Meteorology and Atmospheric Physics* **73**: 139–156.

Rossby C. 1940. Planetary flow patterns in the atmosphere. *Quarterly Journal of the Royal Meteorological Society* **66**(suplement): 66–87.

Rossby C, *et al.* 1939. Relation between variations in the intensity of the zonal circulation of the atmosphere and the displacements of the semi-permanent centers of action. *Journal of Marine Research* **2**(1): 38–55.

Rudeva I, Gulev SK. 2007. Climatology of cyclone size characteristics and their changes during the cyclone life cycle. *Monthly Weather Review* **135**(7): 2568–2587.

Ryall D, Maryon R. 1998. Validation of the UK Met. Offices NAME model against the ETEX dataset. *Atmospheric Environment* **32**(24): 4265–4276.

Sanders F. 1999. A proposed method of surface map analysis. *Monthly weather review* **127**(6): 945–955.

Sansom H. 1951. A study of cold fronts over the British Isles. *Quarterly Journal of the Royal Meteorological Society* **77**(331): 96–120.

Savenije HH. 1995. New definitions for moisture recycling and the relationship with land-use changes in the Sahel. *Journal of Hydrology* **167**(1): 57–78.

Schemm S, Wernli H. 2014. The linkage between the warm and the cold conveyor belts in an idealized extratropical cyclone. *Journal of the Atmospheric Sciences* **71**(4): 1443–1459.

Schemm S, Wernli H, Papritz L. 2013. Warm conveyor belts in idealized moist baroclinic wave simulations. *Journal of the Atmospheric Sciences* **70**(2): 627–652.

Schneider T. 2004. The tropopause and the thermal stratification in the extratropics of a dry atmosphere. *Journal of the Atmospheric Sciences* **61**(12): 1317–1340.

Schultz DM. 2001. Reexamining the cold conveyor belt. *Monthly Weather Review* **129**(9): 2205–2225.

Schultz DM, Keyser D, Bosart LF. 1998. The effect of large-scale flow on low-level frontal structure and evolution in midlatitude cyclones. *Monthly Weather Review* **126**(7): 1767–1791.

Schultz DM, Vaughan G. 2011. Occluded fronts and the occlusion process: A fresh look at conventional wisdom. *Bulletin of the American Meteorological Society* **92**(4): 443–466.

Schwarz E. 1921. The control of climate by lakes. *Geographical Journal* : 166–174.

Segal M, Pan Z, Turner R, Takle E. 1998. On the potential impact of irrigated areas in North America on summer rainfall caused by large-scale systems. *Journal of Applied Meteorology* **37**(3): 325–331.

Semple AT. 2003. A review and unification of conceptual models of cyclogenesis. *Meteorological Applications* **10**(1): 39–59.

Shapiro MA, Keyser DA. 1990. Fronts, jet streams, and the tropopause. *Palmen Memorial Volume, American Met Soc* : 167–191.

Sherwood S, Roca R, Weckwerth T, Andronova N. 2010. Tropospheric water vapor, convection, and climate. *Reviews of Geophysics* **48**(2): RG2001, doi:10.1029/2009RG000301.

Siebesma A, Cuijpers J. 1995. Evaluation of parametric assumptions for shallow cumulus convection. *Journal of the Atmospheric Sciences* **52**(6): 650–666.

Siebesma AP, Bretherton CS, Brown A, Chlond A, Cuxart J, Duynkerke PG, Jiang H, Khairoutdinov M, Lewellen D, Moeng CH, *et al.* 2003. A large eddy simulation intercomparison study of shallow cumulus convection. *Journal of the Atmospheric Sciences* **60**(10): 1201–1219.

Sinclair V. 2008. Boundary layer ventilation by baroclinic lifecycles. PhD thesis, Department of Meteorology, University of Reading.

Sinclair V, Belcher S, Gray S. 2009. Synoptic controls on boundary layer characteristics. *Boundary Layer Meteorology* **134**: 387–409.

Sinclair V, Gray S, Belcher S. 2008. Boundary layer ventilation by baroclinic life cycles. *Quarterly Journal of the Royal Meteorological Society* **134**: 1409–1424.

Sinclair V, Gray SL, Belcher SE. 2010. Controls on boundary layer ventilation: Boundary layer processes and large-scale dynamics. *Journal of Geophysical Research* **115**(D11107), doi:10.1029/2009JD012169.

Smith BL, Yuter SE, Neiman PJ, Kingsmill D. 2010. Water vapor fluxes and orographic precipitation over northern California associated with a landfalling atmospheric river. *Monthly Weather Review* **138**(1): 74–100.

Smith PJ. 2000. The importance of the horizontal distribution of heating during extratropical cyclone development. *Monthly Weather Review* **128**(10): 3692–3694.

Smith R. 1990. A scheme for predicting layer clouds and their water content in a general circulation model. *Quarterly Journal of the Royal Meteorological Society* **116**: 435–460.

Soares P, Miranda P, Siebesma A, Teixeira J. 2004. An eddy-diffusivity/mass-flux parametrization for dry and shallow cumulus convection. *Quarterly Journal of the Royal Meteorological Society* **130**(604): 3365–3383.

Sodemann H, Stohl A. 2013a. Moisture origin and meridional transport in atmospheric rivers and their association with multiple cyclones. *Monthly Weather Review* **141**: 2850–2868.

Sodemann H, Stohl A. 2013b. Moisture origin and meridional transport in atmospheric rivers and their association with multiple cyclones. *Mon.Wea.Rev* **141**: 2850–2868.

Sodemann H, Wernli H, Schwierz C. 2009. Sources of water vapour contributing to the elbe flood in august 2002A tagging study in a mesoscale model. *Quarterly Journal of the Royal Meteorological Society* **135**(638): 205–223.

Stocker T, Qin D, Plattner G, Tignor M, Allen S, Boschung J, Nauels A, Xia Y, Bex B, Midgley B. 2013. IPCC, 2013: climate change 2013: The physical science basis. Contribution of working group I to the fifth assessment report of the Intergovernmental Panel on Climate Change .

Stoelinga MT. 1996. A potential vorticity-based study of the role of diabatic heating and friction in a numerically simulated baroclinic cyclone. *Monthly Weather Review* **124**(5): 849–874.

Stohl A. 2001. A 1-year lagrangian "climatology" of airstreams in the northern hemisphere troposphere and lowermost stratosphere. *Journal of Geophysical Research* **106**(D7): 72637279, doi:10.1029/2000JD900570.

Stohl A, Forster C, Eckhardt S, Spichtinger N, Huntrieser H, Heland J, Schlager H, Wilhelm S, Arnold F, Cooper O. 2003. A backward modeling study of intercontinental pollution transport using aircraft measurements. *Journal of Geophysical Research* **108**(D12): 4370, doi:10.1029/2002JD002862.

Stull RB. 1989. *An introduction to boundary layer meteorology*. Kluwer Academic Publishers.

Su Z, Dorigo W, Fernández-Prieto D, Helvoirt MV, Hungershoefer K, Jeu Rd, Parinussa R, Timmermans J, Roebeling R, Schröder M, *et al.* 2010. Earth observation water cycle multi-mission observation strategy (WACMOS). *Hydrology and Earth System Sciences Discussions* **7**(5): 7899–7956.

Sutcliffe R. 1956. Water balance and the general circulation of the atmosphere. *Quarterly Journal of the Royal Meteorological Society* **82**(354): 385–395.

Swanson KL, Pierrehumbert RT. 1997. Lower-tropospheric heat transport in the Pacific storm track. *Journal of the Atmospheric Sciences* **54**(11): 1533–1543.

Thomson D. 1987. Criteria for the selection of stochastic models of particle trajectories in turbulent flows. *Journal of Fluid Mechanics* **180**: 529–556.

Thorncroft C, Hoskins B, McIntyre M. 1993. Two paradigms of baroclinic-wave life-cycle behaviour. *Quarterly Journal of the Royal Meteorological Society* **119**(509): 17–55.

Thornthwaite C, Holzman B. 1938. A new interpretation of the hydrolcgic cycle. *Eos, Transactions American Geophysical Union* **19**(2): 595–598.

Thorpe AJ, Guymer TH. 1977. The nocturnal jet. *Quarterly Journal of the Royal Meteorological Society* **103**(438): 633–653.

Tiedtke M. 1989. A comprehensive mass flux scheme for cumulus parameterization in large-scale models. *Monthly Weather Review* **117**(8): 1779–1800.

Tiedtke M. 1993. Representation of clouds in large-scale models. *Monthly Weather Review* **121**(11): 3040–3061.

Trenberth KE. 1999. Atmospheric moisture recycling: Role of advection and local evaporation. *Journal of Climate* **12**(5): 1368–1381.

Trenberth KE, Stepaniak DP. 2003. Covariability of components of poleward atmospheric energy transports on seasonal and interannual timescales. *Journal of climate* **16**(22): 3691–3705.

Trenberth KE, Stepaniak DP, Caron JM. 2000. The global monsoon as seen through the divergent atmospheric circulation. *Journal of Climate* **13**(22): 3969–3993.

Trigo IF, Davies TD, Bigg GR. 1999. Objective climatology of cyclones in the Mediterranean region. *Journal of Climate* **12**(6): 1685–1696.

Troen I, Mahrt L. 1986. A simple model of the atmospheric boundary layer; Sensitivity to surface evaporation. *Boundary Layer Meteorology* **37**: 129–148.

Vallis GK. 2006. *Atmospheric and oceanic fluid dynamics: fundamentals and large-scale circulation*. Cambridge University Press.

Van der Ent R, Savenije H. 2011. Length and time scales of atmospheric moisture recycling. *Atmospheric Chemistry and Physics* **11**(5): 1853–1863.

von Engeln A, Teixeira J. 2013. A planetary boundary layer height climatology derived from ECMWF reanalysis data. *Journal of Climate* **26**(17): 6575–6590.

Waliser DE, Gautier C. 1993. A satellite-derived climatology of the ITCZ. *Journal of Climate* **6**(11): 2162–2174.

Wanner H, Brönnimann S, Casty C, Gyalistras D, Luterbacher J, Schmutz C, Stephenson DB, Xoplaki E. 2001. North atlantic oscillation–concepts and studies. *Surveys in Geophysics* **22**(4): 321–381.

Webster H, Thompson D, Morrison N. 2003. New turbulence profiles for NAME **288**.

Weigel AP, Chow FK, Rotach MW. 2007. The effect of mountainous topography on moisture exchange between the surface and the free atmosphere. *Boundary Layer Meteorology* **125**(2): 227–244.

Wernli H, Davies H. 1996. A lagrangian based analysis of extratropical cyclones, I: The method and some applications. *Quarterly Journal of the Royal Meteorological Society* **123**: 467–489.

Wexler H, Namias J. 1938. Mean monthly isentropic charts and their relation to departures of summer rainfall. *Eos, Transactions American Geophysical Union* **19**(1): 164–170.

White GH. 1982. An observational study of the northern hemisphere extratropical summertime general circulation. *Journal of the Atmospheric Sciences* **39**(1): 24–40.

Whittaker L, Horn L. 1984. Northern hemisphere extratropical cyclone activity for four mid-season months. *Journal of Climatology* **4**(3): 297–310.

Willett HC. 1933. *American air mass properties*. Massachusetts Institute of Technology and Woods Hole Oceanographic Institution.

Wilson D, Ballard S. 1999. A microphysically based precipitation scheme for the Meteorological Office Unified Model. *Quarterly Journal of the Royal Meteorological Society* **125**: 1607–1636.

Yihui D, Chan JC. 2005. The East Asian summer monsoon: an overview. *Meteorology and Atmospheric Physics* **89**(1-4): 117–142.

Yin Y, Carslaw K, Feingold G. 2005. Vertical transport and processing of aerosols in a mixed-phase convective cloud and the feedback on cloud development. *Quarterly Journal of the Royal Meteorological Society* **131**(605): 221–245.

Yin Y, Parker D, Carslaw K. 2001. Simulation of trace gas redistribution by convective clouds-liquid phase processes. *Atmospheric Chemistry and Physics* **1**(1): 19–36.

Zappa G, Shaffrey L, Hodges K. 2014. Can polar lows be objectively identified and tracked in the ECMWF operational analysis and the ERA-Interim reanalysis? *Monthly Weather Review* **142**(8): 2596–2608.

Zhang C. 2001. Double ITCZs. *Journal of Geophysical Research* **106**(D11): 11 785–11 792.

Zhang C. 2005. Madden Julian Oscillation. *Reviews of Geophysics* **43**(2): RG2003, doi:10.1029/2004RG000158.

Zhang Y, Dian S, Zhang S. 2013. Trends in planetary boundary layer height over europe. *Journal of Climate* **26**: 10 071–10 076.

Zhu Y, Newell RE. 1998. A proposed algorithm for moisture fluxes from atmospheric rivers. *Monthly Weather Review* **126**(3): 725–735.

Zon R, *et al.* 1927. *Forests and water in the light of scientific investigation*. Govt. print. off.